Technical Report Documentation Page

1. Report No. 1772-1	2. Government Accession No.	3. Recipient's Catalog No.
4. Title and Subtitle CROSS-FRAME AND DIAPHRAGM BEHAVIOR FOR STEEL BRIDGES WITH SKEWED SUPPORTS		5. Report Date July 25, 2003
7. Author(s) Todd A. Helwig and Liqun Wang		6. Performing Organization Code 8. Performing Organization Report No. Research Report 1772-1
9. Performing Organization Name and Address University of Houston 4800 Calhoun, Eng. Bldg. I Rm. N107 Houston, Texas 77204-4003		10. Work Unit No. (TRAIS) 11. Contract or Grant No. Research Study 0-1772
12. Sponsoring Agency Name and Address Texas Department of Transportation Research and Technology Transfer Section/Construction Division P.O. Box 5080 Austin, TX 78763-5080		13. Type of Report and Period Covered Final 14. Sponsoring Agency Code

15. Supplementary Notes
Project conducted in cooperation with the Federal Highway Administration.
Research Study Title: Cross-Frame and Diaphragm Behavior in Skewed Bridges

16. Abstract

Steel bridge girders are prone to buckling from construction loads during casting of the concrete for the composite deck. The buckling capacity of the steel girders can be increased by providing bracing at intermediate locations along the girder length. The intermediate bracing typically takes the form of cross-frames or diaphragms. Skewed supports occur when the supporting abutments for the girders are not normal to the girder line, but are instead offset by a skew angle. The skew angle may be required due to characteristics of intersecting roadways or due to the geological terrain. Fatigue cracks are commonly found around locations of cross-frames and diaphragms during routine maintenance inspections. These cracks form from large stress concentrations in the girder due to cross-frame and diaphragm forces induced by truck traffic on the bridge. This is particularly true for bridges with skewed supports.

The objective of the research outlined in this report is to improve the understanding of the bracing behavior of cross frames and diaphragms in steel bridges with skewed supports. General bracing requirements are developed and new cross-frame and diaphragm details to minimize fatigue problems at bracing locations are proposed.

A variety of parameters were considered in the investigation, including skew angle and girder geometry. The skew angles that were considered varied from 0 degrees (normal supports) to 45 degrees. The geometry of the girder cross-sections ranged from doubly symmetric rolled sections to singly symmetric plate girders. The number of intermediate braces along the girder length was varied as well as the brace orientation relative to the girder axes. Two brace orientations were considered for each skew angle: parallel to the skewed supports and normal to the girder line.

In addition to determining the general bracing requirements, improved bracing details were also considered in the study. Details are proposed that will reduce the brace forces induced from truck traffic. In addition, bracing systems that will reduce the number of cross frames or diaphragms are proposed. Reducing the number of braces will make the bridges easier to inspect since there will be fewer fatigue-prone details.

17. Key Words	18. Distribution Statement
cross-frames, diaphragms, steel bridge, buckling, bracing, fatigue	No restrictions. This document is available to the public through the National Technical Information Service, Springfield, Virginia 22161.

19. Security Classif. (of report)	20. Security Classif. (of this page)	21. No. of pages	22. Price
Unclassified	Unclassified	238	

Form DOT F 1700.7 (8-72) Reproduction of completed page authorized

CROSS-FRAME AND DIAPHRAGM BEHAVIOR FOR STEEL BRIDGES WITH SKEWED SUPPORTS

by

Todd Helwig and Liqun Wang

Research Report Number 1772-1

Research Project 0-1772
Cross-Frame and Diaphragm Behavior in Skewed Bridges

Conducted for the

TEXAS DEPARTMENT OF TRANSPORTATION

in cooperation with the

U.S. DEPARATMENT OF TRANSPORTATION
Federal Highway Administration
by the

UNIVERSITY OF HOUSTON

JULY 2003

DISCLAIMERS

The contents of this report reflect the views of the authors, who are responsible for the facts and the accuracy of the data presented herein. The contents do not necessarily reflect the official views or policies of the Federal Highway Administration or the Texas Department of Transportation. This report does not constitute a standard, specification, or regulation.

There was no invention or discovery conceived or first actually reduced to practice in the course of or under this contract, including any art, method, process, machine, manufacture, design or composition of matter, or any new and useful improvement thereof, or any variety of plant, which is or may be patentable under the patent laws of the United States of America or any foreign country.

NOT INTENDED FOR CONSTRUCTION,
BIDDING, OR PERMIT PURPOSES

Todd A. Helwig
Research Supervisor

ACKNOWLEDGMENTS

The authors would like to thank the project coordinator, J.C. Liu, and the project director, Tim Chase for their cooperation and recommendations during this research study. In addition the authors would like to thank several TxDOT engineers that provided feedback during this project, including John Holt, Jon Holt, Kenny Ozuna and John Vogel.

Research performed in cooperation with the Texas Department of Transportation and the U.S. Department of Transportation, Federal Highway Administration.

SUMMARY

Steel bridge girders are prone to buckling from construction loads during casting of the concrete for the composite deck. The buckling capacity of the steel girders can be increased by providing bracing at intermediate locations along the girder length. The intermediate bracing typically takes the form of cross-frames or diaphragms. Skewed supports occur when the supporting abutments for the girders are not normal to the girder line, but are instead offset by a skew angle. The skew angle may be required due to characteristics of intersecting roadways or due to the geological terrain. Fatigue cracks are commonly found around locations of cross-frames and diaphragms during routine maintenance inspections. These cracks form from large stress concentrations in the girder due to cross-frame and diaphragm forces induced by truck traffic on the bridge. This is particularly true for bridges with skewed supports.

The objective of the research outlined in this report is to improve the understanding of the bracing behavior of cross frames and diaphragms in steel bridges with skewed supports. General bracing requirements are developed and new cross-frame and diaphragm details to minimize fatigue problems at bracing locations are proposed.

A variety of parameters were considered in the investigation, including skew angle and girder geometry. The skew angles that were considered varied from 0 degrees (normal supports) to 45 degrees. The geometry of the girder cross-sections ranged from doubly symmetric rolled sections to singly symmetric plate girders. The number of intermediate braces along the girder length was varied as well as the brace orientation relative to the girder axes. Two brace orientations were considered for each skew angle: parallel to the skewed supports and normal to the girder line.

In addition to determining the general bracing requirements, improved bracing details were also considered in the study. Details are proposed that will reduce the brace forces induced from truck traffic. In addition, bracing systems that will reduce the number of cross frames or diaphragms are proposed. Reducing the number of braces will make the bridges easier to inspect since there will be fewer fatigue-prone details.

Note to Designers

Although the entire report contains important information regarding bracing behavior in steel bridges, bridge designers should pay particular emphasis to Chapters 1, 2, 8, and 9. Two design examples are presented in Chapter 8 that illustrate the recommended bracing provisions for cross-frames and diaphragms.

Table of Contents

List of Figures

List of Tables

Chapter 1
Introduction

1.1 General

The design of steel bridge girders is often controlled by lateral-torsional buckling. The critical stage for buckling of the girders generally occurs during construction of the concrete bridge deck when the steel section must support the entire construction load. The construction load consists of the self-weight of the girders and concrete, the concrete formwork, finishing equipment, as well as the construction personnel. Beam lateral torsional buckling is illustrated in Figure 1.1, which shows that the buckling mode involves a lateral translation of the compression flange accompanied by twisting of the girder cross-section.

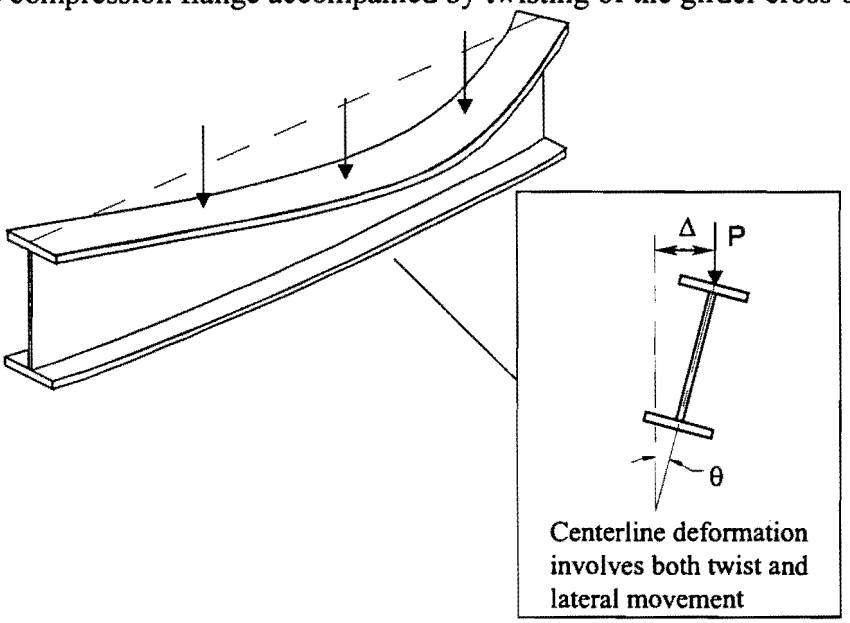

Figure 1.1 Lateral Torsional Buckling

The buckling capacity of the steel girders can be increased by providing bracing at intermediate locations along the girder length. The intermediate bracing typically takes the form of cross-frames or diaphragms. Fig. 1.2 shows a typical steel bridge superstructure consisting of the concrete deck, steel girders and cross-frames for bracing. The braces increase the buckling capacity by controlling the twist of the girder cross-section. In finished bridges, the composite concrete deck provides continuous bracing along the girder length. However, cross-frames and diaphragms provide lateral restraint to the bottom flange against wind load and are still needed in the negative moment region for stability.

Past American Association of State Highway and Transportation Officials specifications [AASHTO 1992] have limited the maximum spacing between cross-frames or diaphragms to 25 feet. The AASHTO Load Resistance Factor Design (LRFD) [1996] removed the 25-feet spacing requirement and instead vaguely requires that the cross-frames or diaphragms be designed by a "rational analysis". The reason for the removal of the

spacing limit in the LRFD specification is to minimize details that are prone to fatigue damage in the bridges. Fatigue cracks are commonly found around locations of cross-frames and diaphragms during routine maintenance inspections. These cracks form due to large stress concentrations in the girder due to cross-frame and diaphragm forces induced by truck traffic on the bridge. This is particularly true when the supporting abutments are not normal to the girder lines but are instead offset by a skew angle.

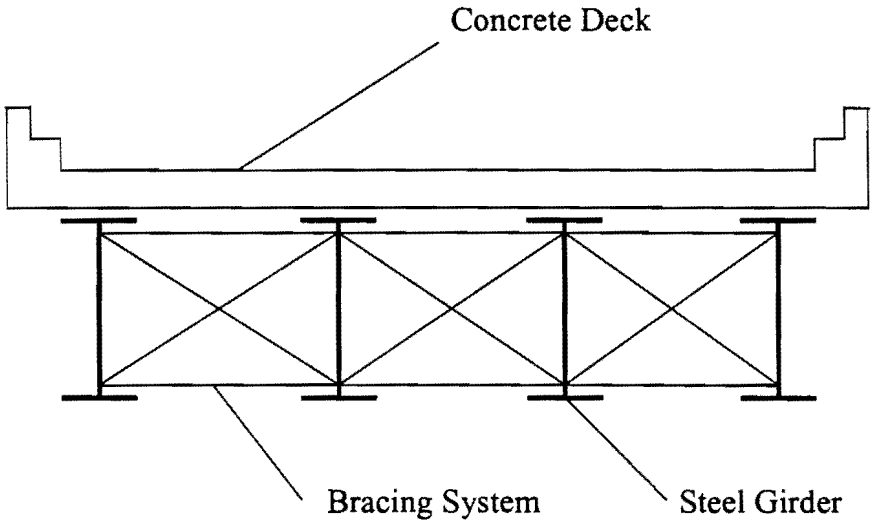

Figure 1.2 Typical Steel Bridge Superstructure

The fatigue problems that occur around brace locations are often aggravated because "typical sizes" and "typical details" are often used for cross-frames and diaphragms instead of designing the braces for the specific application. The "typical sizes" that are used often result in bracing members that are larger than necessary to satisfy the stability requirements. The larger braces attract bigger live load forces due to truck traffic in the finished bridge. The larger live load forces therefore magnify the fatigue problems around the brace locations.

This chapter has been divided into five sections. Following this introduction, typical bracing details currently used in the state of Texas will be presented and discussed. Skewed supports will then be discussed, followed by an outline of previous research efforts pertinent to this investigation. Finally the outline and scope of the research will be presented.

1.2 Standard Size of Cross-frames and Diaphragms

Current AASHTO specifications [1996] do not provide guidelines for the design requirements of bracing for steel girders. In general practice, each state often utilizes its own standard size for cross-frames and diaphragms. Figs. 1.3a and 1.3b illustrate the standard braces currently used in the state of Texas. Fig. 1.3a shows the typical end support diaphragms for plate girders, which depend on the girder web depth. The Type A diaphragms are used for web depths less than or equal to 48 inches. For web depths greater than 48 inches, Type B diaphragms are generally used. Fig. 1.3b shows the intermediate (between supports) diaphragms for straight girders. Type C diaphragms are used for web depths less than or equal to 48 inches, while type D diaphragms are generally used for web depths greater than 48 inches.

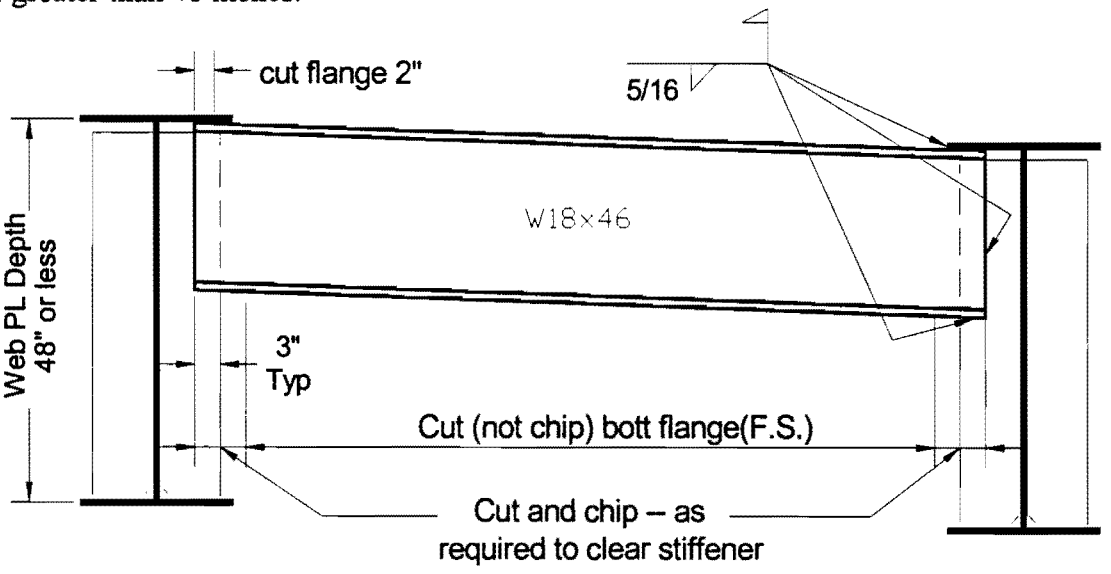

TYPE A END DIAPHRAGM

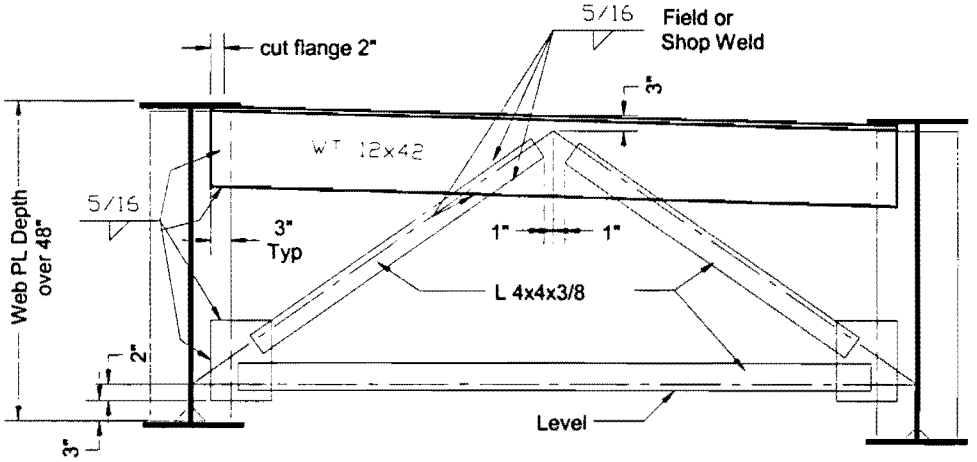

TYPE B END DIAPHRAGMS

Figure 1.3a Standard Sizes of End Diaphragms

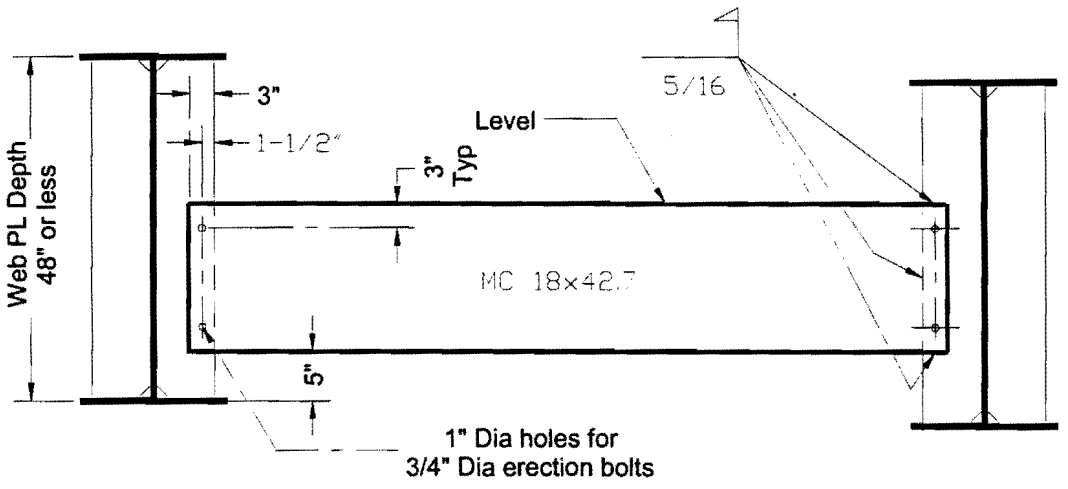

TYPE C INTERIOR DIAPHRAGM FOR STRAIGHT GIRDERS

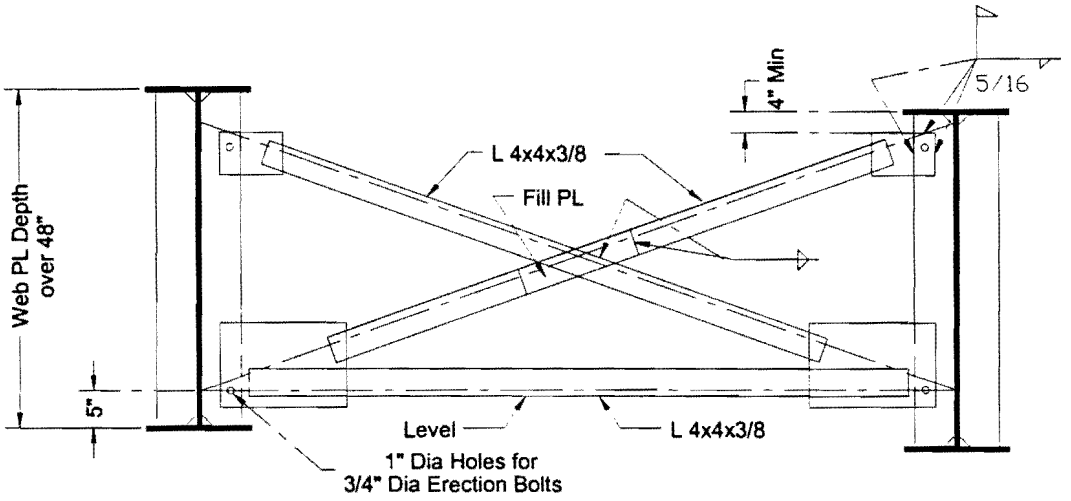

TYPE D INTERIOR DIAPHRAGMS FOR STRAIGHT GIRDERS

Figure 1.3b Standard Sizes of Interior Diaphragms

Locations around cross-frames and diaphragms are often regions of fatigue problems during the bridge service life. Previous studies [Keating and Alan 1992] confirmed that the fatigue cracks found in these regions during annual bridge inspections are often related to the large cross-frame and diaphragm forces developed from truck live loads. Since standard sizes are often employed for cross-frames and diaphragms, these braces are often much stiffer than needed for stability requirements. The stiffer braces develop large localized

forces during truck loading. These large brace forces combined with complex connection details to the girder webs usually lead to large stress concentrations that result in fatigue problems.

Developing fatigue categories for the braces, such as those typically used in evaluating the fatigue behavior of different details is not practical for cross frames and diaphragms since the behavior is sensitive to a wide range of variables. Some of the factors that can effect the fatigue performance of these braces include the relative stiffness of the brace and the girder, the brace spacing, the connection detail between the brace and the girder, as well as the bridge geometry, including the skew angle of the supporting piers.

A more pragmatic approach to mitigating the fatigue problems associated with cross-frames and diaphragms is to develop a comprehensive design approach for these critical braces. Sizing the bracing members for the actual design requirements will often lead to smaller live load forces in the bracing members and therefore minimize fatigue damage. In addition, improved connection details may also minimize these fatigue problems. Reducing the total number of cross-frame and diaphragms on the bridge will also facilitate identifying fatigue damage during periodic bridge inspections.

Therefore this report will focus on investigating the behavior of cross-frame and diaphragms in bridges with skewed supports. A design approach will be developed for the bracing systems as well as recommended bracing details that will minimize the number of brace locations on the bridge as well as reducing brace forces induced by truck loading.

1.3 Bridges with Skewed Supports

Skewed supports occur when the supporting abutments for the girders are not normal to the girder lines, but are instead offset by a skew angle. The skew angle may be required due to characteristics of the intersecting roadways or due to the geological terrain. Fig. 1.4 illustrates a bridge with skewed supports. Most bridges have skewed supports due to increased urban growth and the development of complex intersections with a lack of space in congested areas.

Since skew angles increase the interaction between the steel girders and the braces, the behavior of bridges with skewed supports becomes more complicated than that in bridges with normal supports. The interaction between the girders and braces often results in large live load forces in the cross-frames or diaphragms, which can lead to fatigue problems around the brace locations. The severity of the fatigue problem is dependent on the details that are used for the bracing. If the skew angle is less than 20 degrees, the AASHTO specification [1996] allows the bracing to be parallel to the skew angle. For skew angles greater than 20 degrees, the AASHTO specification requires the bracing to be perpendicular to the longitudinal axis of the girder. Figure 1.5 illustrates the two different orientations of braces for skewed bridges. For braces parallel to the supporting abutments, points A and B

at the ends of the brace will have similar vertical displacements during truck live load. However, when braces are normal to the girder lines, the two ends of the braces will have different vertical displacements during truck loading. This different vertical displacement can result in large brace forces, which can lead to fatigue problems.

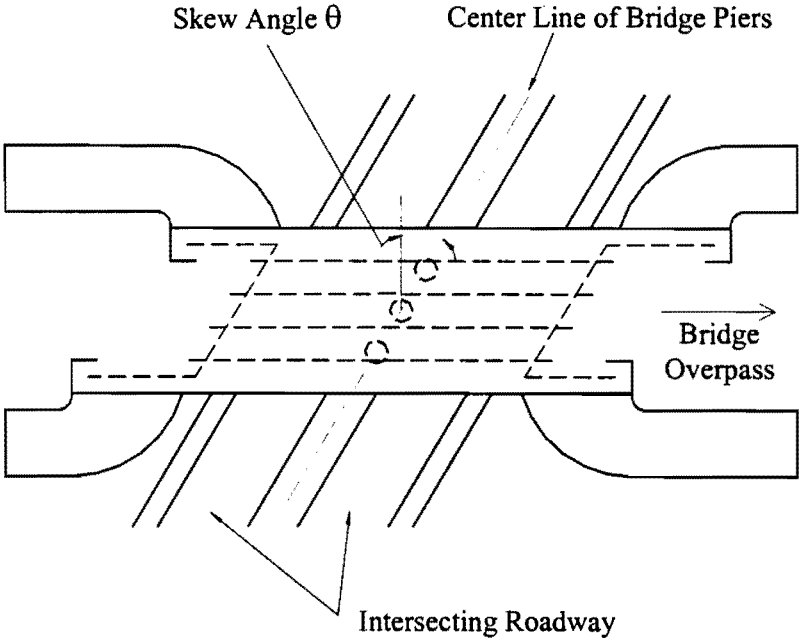

Figure 1.4 Plan View of Bridge with Skewed Supports

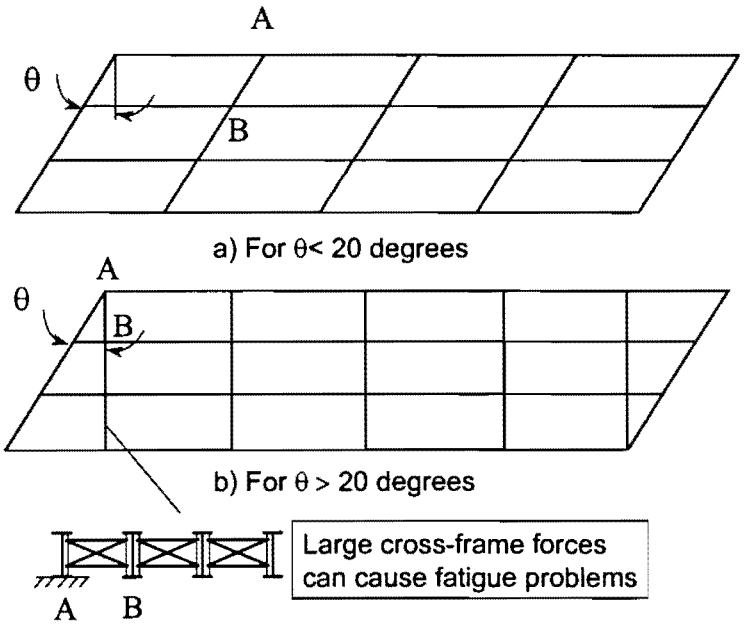

Figure 1.5 Brace Orientations for Bridges with Skewed Supports

1.4 Stability Bracing Requirements

Since much of this report will focus on the stability bracing provided by cross-frames and diaphragms, the fundamental requirements of stability bracing systems should be clearly understood. The basic requirements can be best explained by considering the requirements for a column with lateral braces along the member length. The basic principles established for lateral bracing for a column will also be valid in the later development of the torsional bracing requirements for beams.

An adequate bracing system requires both stiffness and strength [Winter 1958]. Simple brace design formulations, such as designing the brace for 2% of the compressive member force, addresses only the strength criterion. The actual strength requirements of a brace are affected by the shape and magnitude of the initial imperfection and also by the brace stiffness provided.

To study the effect of brace stiffness on the buckling behavior, eigenvalue analyses are often conducted on perfectly straight elastic members. Fig. 1.6 illustrates the flexural buckling behavior of two columns with different lengths and different numbers of lateral braces with stiffness β_L. Column A has a length of $2L_L$ with a single lateral brace at mid-height, while column B has a length of $4L_L$ with three lateral braces. The buckling capacity of column A without bracing is $P_{cr} = \pi^2 EI/(2L_L)^2$. The capacity of column A increases as brace stiffness increases until the maximum strength $P_{cr} = \pi^2 EI/(L_L)^2$ is reached at the non-dimensionalized ideal brace stiffness $N_i = \beta_{Li} L_L/P_E = 2$. Column B also reaches a maximum buckling load of $P_{cr} = \pi^2 EI/(L_L)^2$, however the behavior of the bracing system for column B is quite different from that of column A. The initial capacity of column B is $P_{cr} = \pi^2 EI/(4L_L)^2$, which is 25% of the initial capacity of column A. At low values of the brace stiffness the buckling load increases substantially with a single wave buckled shape until it intersects the curve for column A. The two curves are coincident in shape until column B buckles into three waves and additional brace stiffness becomes less effective. Full bracing occurs at $N_i = 3.41$. Winter presented a simple model for calculating the ideal brace stiffness and showed that N_i varies from 2.0 for one brace to 4.0 for a large number of braces. Yura [1995] recommended the formula $N_i = 4\text{-}2/n_L$ in which n_L is the number of intermediate lateral braces.

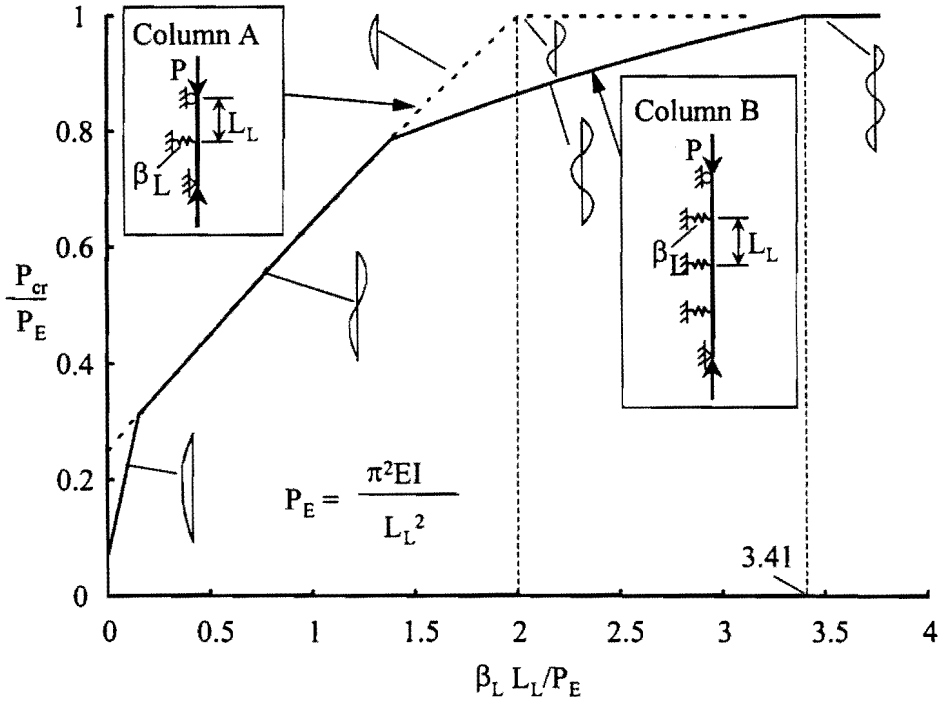

Figure 1.6 Load vs. Lateral Brace Stiffness for Lateral Bracing System

The buckling behavior of columns depicted in Fig. 1.6 demonstrates the bracing requirements for perfectly straight members. In practice all structural members have initial imperfections. For members with initial imperfections, large displacement analyses are conducted to evaluate the brace strength requirements. Winter's simple model demonstrated that imperfections in real columns cause brace stiffness requirements greater than β_{Li}, the ideal brace stiffness, to effectively control lateral deformations and brace forces. The graph of the applied load versus the column lateral displacement illustrated in Fig. 1.7 shows the behavior of an imperfect column with a lateral brace at mid-height. The applied load is normalized by the Euler buckling capacity, P_E, while the total lateral displacement at mid-height, Δ_T, is normalized by the initial imperfection, Δ_0. For columns with initial imperfections, providing the ideal stiffness results in large lateral displacements and large brace forces as the load approaches the buckling load and the Euler buckling capacity, P_E, is actually never reached. On the other hand, providing a lateral brace stiffness with twice the ideal value, results in the maximum column displacement equal to the magnitude of the initial imperfection, Δ_0 at an applied load equal to the Euler buckling capacity, P_E. The magnitude of the brace force is the product of brace stiffness and the lateral displacement. The brace strength requirement can be expressed as $F_{br} = \beta_{Lreq}\Delta_0$, where F_{br} is the brace force, $\beta_{Lreq} \geq 2\beta_{Li}$, and Δ_0 is the magnitude of the initial imperfection. For columns, the initial imperfection is often taken as $L_L/500$ in which L_L is the spacing between braces. The above equation for F_{br} will give conservative estimates of the brace force if a brace stiffness greater than $2\beta_{Li}$ is provided.

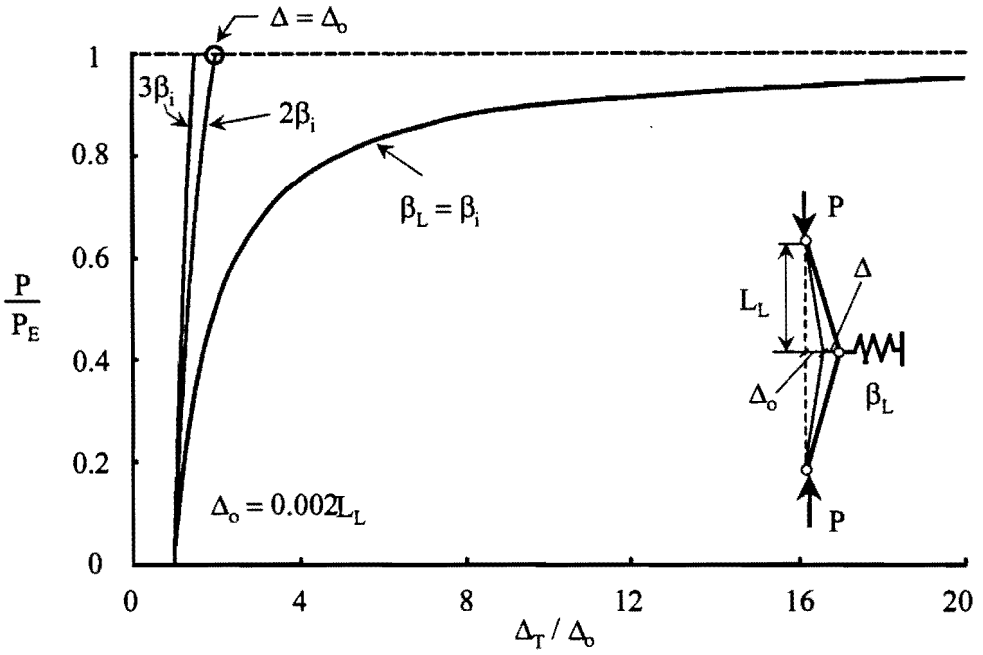

Figure 1.7 Effect of Imperfections on Brace Strength Requirements

Cross frames and diaphragms for beams fit into a category referred to as torsional bracing since they restrain the twist of the member. Although the behavior of torsional bracing systems are generally more complicated than the lateral column bracing discussed above, the basic principles are directly applicable. The bracing must possess adequate strength and stiffness. The research presented in this report will focus on developing general torsional bracing requirements for I-shaped girders.

1.5 Objective and Scope

This report will present results from a study sponsored by the Texas Department of Transportation (TxDOT). The research was a three-year investigation that included both computational and laboratory studies. The objective of this project was to improve the understanding of the bracing behavior of bridges with skewed supports. The purpose of the laboratory studies was to confirm the accuracy of the finite element model that was used to conduct parametrical studies on cross-frame and diaphragm bracing systems. The results from the laboratory studies are discussed by Deaver [2002] and Romero [2002]. This report will focus on the computational studies. A design methodology will be developed for the bracing systems that consider both the skew angle and the brace orientation. Details will be suggested that reduce brace forces induced from truck traffic as well as minimizing the number of fatigue sensitive regions on the bridge.

The computational studies were conducted using the finite element program ANSYS to perform both eigenvalue and large displacement analyses. An eigenvalue buckling analysis generally focuses on the behavior of the straight girder and does not reflect the effects of imperfections. Eigenvalue buckling analyses can be used to investigate the brace stiffness requirements. The stiffness requirements to reach full bracing (buckling between brace points) from such an analysis are usually referred to as the "ideal stiffness requirements".

A large displacement analysis is a nonlinear analysis that considers the effects of imperfections on the girder deformation and the brace forces. Such an analysis can be used to produce the brace strength requirements. Both eigenvalue buckling and large displacement analyses were conducted to determine the stiffness and strength requirements for bridges with skewed supports. The finite element results were compared with the design equations that were developed to reflect the bracing requirements for bridges with skewed supports.

This report has been divided into 9 chapters. Following this introductory chapter, Chapter 2 presents a review of background material. The introductory material will include a review of previous studies on torsional bracing of beams as well as a review of the factors that affect the lateral torsional buckling behavior of beams. Chapter 3 describes the development of the finite element model and the parameters investigated in this research. Chapter 4 focuses on the effects of imperfections on the torsional bracing behavior of steel girders. Finite element results will be presented on twin-girder systems that demonstrate the effects of the shape and magnitude of the initial imperfections. Chapter 5 presents the computational results for bridges with normal supports to verify existing equations and the finite element model. Chapter 6 presents eigenvalue and large displacement analytical results for bridges with braces parallel to the skew angle. The computational results are compared with modified solutions that reflect the parallel bracing requirements for steel girders with skewed supports. Chapter 7 will present computational results of eigenvalue and large displacement analyses for skewed girders with normal braces. The results are compared with the proposed equations that reflect the bracing requirements for skewed girders with normal braces. Chapter 8 will discuss the simplified details for the design and arrangement of cross-frames and diaphragms in bridges with skewed supports to minimize fatigue problems. Analytical results are presented for the steel girders alone as well as truck loading on the composite girders in the completed bridge. Two design examples are presented that illustrate the bracing solutions for cross-frame and diaphragm design for stability requirements during construction. The last chapter of the report will summarize the findings of the research study and also present recommendations for future work.

Although the entire report contains important information regarding the bracing behavior in steel bridges, bridge designers should pay particular emphasis to Chapters 1, 2, 8, and 9.

Chapter 2
Background

2.1 Introduction

Background information is presented in this chapter on lateral torsional buckling as well as an outline of previous research results on torsional bracing systems for beams. The background information that is presented provides a basis for the computational results and design expressions for bridges with skewed supports that will be discussed in later chapters.

2.2 Lateral Torsional Buckling

Beams are structural members that primarily support transverse loads that cause bending in the member. I-shaped sections consisting of two flanges and a web are frequently used for flexural members to maximize the major axis moment of inertia I_x, which results in a large in-plane stiffness. However, due to their low lateral stiffness the I-shaped sections may be susceptible to lateral torsional buckling. The distribution of bending stresses on the beam cross-section produces compression in one of the flanges and tension in the other. The resulting mode of buckling typically involves a lateral translation of the compression flange accompanied by twisting of the whole cross-section, which was shown in Fig. 1.1 in the previous chapter. The buckling capacity can be increased by either increasing the size of the flanges or by providing bracing that prevents twist at intermediate locations along the length. Although bracing can also be achieved by preventing translation of the compression flange, this bracing essentially stops twist of the section, which is the important feature of any effective beam bracing system.

2.3 Doubly Symmetric Section for Constant Moment

Timoshenko [1961] derived a closed-form solution for the buckling capacity of prismatic doubly symmetric beams. Timoshenko's derivation applied to simply supported beams subjected to uniform moment. He assumed that twist was prevented at the ends, however the section was free to warp. The resulting expression is given in the following equation:

$$M_{cr} = \frac{\pi}{L_b}\sqrt{EI_y GJ + \frac{\pi^2 E^2 C_w I_y}{L_b^2}} \tag{2.1}$$

where:

M_{cr} = beam buckling capacity
L_b = unbraced length
E = modulus of elasticity
I_y = weak axis moment of inertia
G = shear modulus
J = St. Venant's torsional constant

C_w = warping constant = $I_y d^2/4$
d = depth of beam

In Timoshenko's original derivation, he also stated that lateral translation was prevented at the ends of the beam, however this assumption was never used. The fact that this assumption is not necessary in the derivation of the solution demonstrates that effective beam bracing need only prevent twist. Therefore, the unbraced length L_b in Eq. 2.1 is the spacing between points with zero twist. Bracing requirements will be discussed in detail later in this chapter. The remainder of this section will focus on section properties that affect the different terms in Eq. 2.1. The torsional stiffness of a member can generally be divided into a uniform torsional component and a non-uniform torsional component. The first term under the radical in Eq. 2.1 is referred to as the St. Venant term and it is related to the uniform torsional stiffness. The second term under the radical is referred as to the warping term and it is related to the non-uniform torsional stiffness. The St. Venant term reflects the ability for a beam to resist the twist of the section and is related to the uniform torsional stiffness of the cross section. The warping term reflects the ability of a beam to resist lateral bending of the flanges and is related to the support conditions of the beam. Solutions such as Eq. 2.1 are based upon the assumption that the ends of the unbraced length are free to warp. For an I-shaped beam, both the St. Venant and warping terms contribute to the beam buckling capacity.

The lateral torsional buckling equation in the American Institute of Steel Construction (AISC) Load & Resistance Factor Design (LRFD) specification [2001] directly employs Timoshenko's equation for the elastic buckling of doubly symmetric I-sections.

2.4 Singly Symmetric Section for Constant Moment

Most bridge designs make use of composite action between the steel girder and the concrete deck. Since the concrete slab contributes to the girder strength in the finished bridge, the top flange of girder is usually smaller than the bottom flange. The resulting steel cross-section has a single plane of symmetry about an axis through the web. Although the concrete contributes to the strength in the finished bridge, during erection and construction the steel section must support the entire construction load. Therefore, lateral torsional buckling of the steel girder is often critical during construction. Eq. 2.1 is only applicable for doubly symmetric sections. The exact solution for singly symmetric sections was presented by Anderson and Trahair [1972] and given in the following expression:

$$M_{cr} = \frac{\pi}{L_b}\sqrt{EI_y GJ}\left(B_1 + \sqrt{1 + \frac{\pi^2 a}{L_b^2} + B_1^2}\right) \tag{2.2}$$

where:

$$a = \sqrt{\frac{EC_w}{GJ}} \tag{2.3}$$

$$B_1 = \frac{\pi}{2}\frac{\beta_x}{L_b}\sqrt{\frac{EI_y}{GJ}} \tag{2.4}$$

$$\beta_x = \frac{1}{I_x}\left(\int_A x^2 y dA + \int_A y^3 dA - 2y_0\right) \tag{2.5}$$

β_x can be evaluated by the following equation:

$$\beta_x = \frac{1}{I_x}\left\{(d-\bar{y})\left[\frac{b_t^3 t_t}{12} + b_t t_t (d-\bar{y})^2 + \frac{(d-\bar{y})^3 t_w}{4}\right] - \bar{y}\left[\frac{b_c^3 t_c}{12} + b_c t_c \bar{y}^2 + \frac{\bar{y}^3 t_w}{4}\right]\right\} - 2y_0 \tag{2.6}$$

The variables in 2.6 are defined in Fig. 2.1.

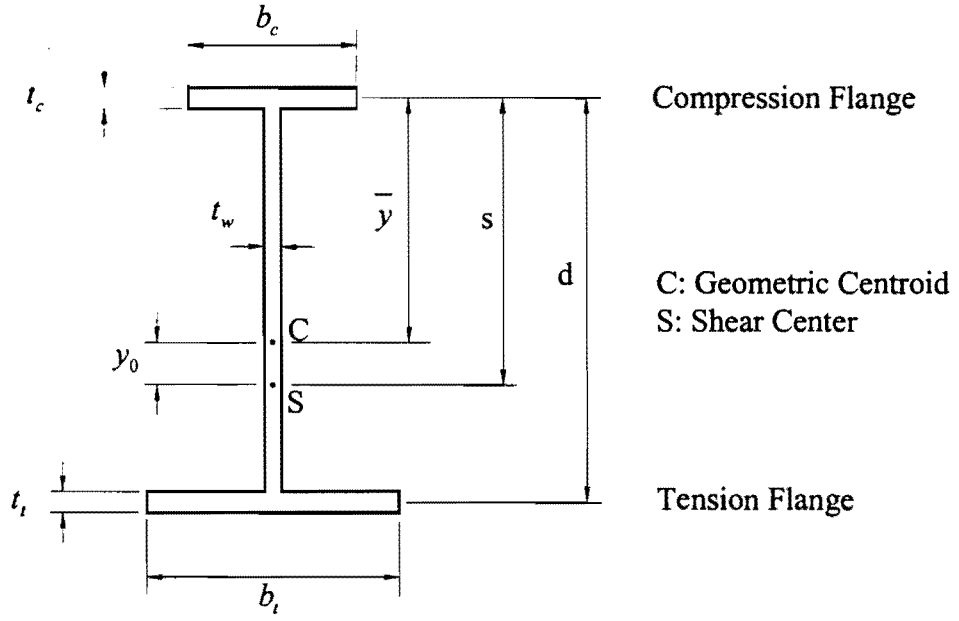

Figure 2.1 Definition of Singly Symmetric Section Variables

Kitipornchai & Trahair [1980] also presented an approximate expression for β_x:

$$\beta_x = 0.9d(2\rho - 1)\left[1 - \left(\frac{I_y}{I_x}\right)^2\right] \tag{2.7}$$

For singly symmetric sections, the warping constant C_w is given by the general expression:

$$C_w = I_y d^2 \rho(1-\rho) \tag{2.8}$$

where:

$$\rho = \frac{I_{yc}}{I_y} \tag{2.9}$$

I_{yc} = moment of inertia of the compression flange about the weak axis.
I_y = moment of inertia of the entire section about the weak axis.
d = distance between centroids of the top and bottom flange.

Depending on the relative sizes of the two flanges, the value of ρ varies from 0 to 1. A tee section with the flange in tension will have ρ = 0 while a tee section with the flange in compression will have ρ = 1.0. For a doubly symmetric section, the flanges are the same size and ρ = 0.5.

The complexity of the exact solution for singly symmetric sections makes these expressions difficult to use and impractical for design. Therefore, most design specifications employ approximate solutions.

The AISC LRFD specification [2001] recommends the approximate expression shown in Eq. 2.10 for elastic buckling of singly symmetric sections. It should be noted that Eqs. 2.10 are slightly different from the equations presented in the specifications because numerical values for π, E=29,000,000 psi, and G=11,200,000 psi have been substituted in the specification's equations. The variables in Eqs. 2.10 to 2.12 have been previously defined.

$$M_{cr} = \frac{\pi}{L_b}\sqrt{EI_y GJ}\left(B_1 + \sqrt{1 + B_2 + B_1^2}\right) \tag{2.10}$$

$$B_1 = 2.25(2\rho - 1)\frac{d}{L_b}\sqrt{\frac{I_y}{J}} \tag{2.11}$$

$$B_2 = 25(1 - \rho)\left(\frac{I_{yc}}{J}\right)\left(\frac{d}{L_b}\right)^2 \tag{2.12}$$

The AASHTO specifications [1996] employ an expression that is very similar to Eq. 2.1 except that I_y has essentially been replaced with $2I_{yc}$. Again, numerical values for π, E, and G have been substituted in the specification equations. The equation is valid for $0.1 \le \rho \le 0.9$ and is given in the following expression:

$$M_{cr} = \pi E\left(\frac{I_{yc}}{L_b}\right)\sqrt{\frac{2G}{E}\left(\frac{J}{I_{yc}}\right) + \pi^2\left(\frac{d}{L_b}\right)^2} \tag{2.13}$$

Sections with ρ values that are outside the range of 0.1 to 0.9 are essentially T-sections and are not permitted for use as bridge girders.

The AASHTO equation is generally conservative if the compression flange is the small flange and slightly unconservative if the compression flange is the large flange. Comparisons of these buckling expressions and finite element results for several singly symmetric sections with different unbraced lengths are presented in Chapter 3.

2.5 Effect of Moment Gradient and Load Height on Buckling Capacity

The equations to estimate the buckling capacity that have been presented in Sections 2.3 and 2.4 were developed for uniform moment loading. However, in most situations the moment varies along the length of the beam. The variable distribution of stress along the beam length may result in a higher buckling capacity than that predicted by the equations developed for uniform moment. To account for the benefits of variable moment, a C_b factor is applied to the expressions developed for uniform moment. Although there are published C_b values for several typical load cases, many specifications provide expressions that can be used to approximate C_b values for general load cases [SSRC 1988]. The AISC LRFD specification [2001] recommends the following expression for estimating the C_b factor:

$$C_b = \frac{12.5M_{\max}}{2.5M_{\max} + 3M_A + 4M_B + 3M_c} \tag{2.14}$$

where:

M_{max} = absolute value of the maximum moment in the unbraced segment
M_A = absolute value of the moment at the quarter point of the unbraced segment
M_B = absolute value of the moment at the midpoint of the unbraced segment
M_C = absolute value of the moment at the three quarter point of the unbraced segment

Eq. 2.14 has also been adopted by the AASHTO LRFD Specifications. For cantilevers or overhangs where the free end is unbraced, Both of the AISC LRFD specifications and AASHTO LRFD specifications conservatively recommend $C_b = 1.0$. Fig. 2.2 shows typical C_b values from Eq. 2.14 for some typical load cases.

The C_b factors that are published and given by Eq. 2.14 are directly applicable for doubly symmetric sections with transverse loads applied at mid-height. Helwig et al. [1997] demonstrated that the C_b factors were also applicable for singly symmetric sections with single curvature bending provided that transverse loads were applied at mid-height. For reverse curvature bending on singly symmetric sections, Helwig et al. found that a modifier of $(0.5 + 2\rho_{Top}^2)$ applied to Eq. 2.14 provided reasonable estimates of the C_b in which $\rho_{Top} = I_{yTop}/I_y$.

The C_b values given by Eq. 2.14 are applicable for transverse loads applied at mid-height of the cross-section. When transverse loads are applied below or above mid-height, the buckling load may be substantially different than that predicted by the buckling equations with the C_b factors. If transverse loads are applied higher on the cross-section, such as at the top flange, the buckling capacity can be significantly lower than for mid-height loading because of an overturning torque that develops at the point of load application when the section twists. A restoring torque develops when loads are applied lower on the cross-section, which increases the buckling capacity relative to mid-height loading.

Effects of load height become more significant with increasing warping stiffness. Since the warping stiffness is an inverse function of the beam span, shorter beams will be more affected by load height effects than longer beams. This is demonstrated in Fig. 2.3 for transverse loads applied at the bottom flange, mid-height and the top flange.

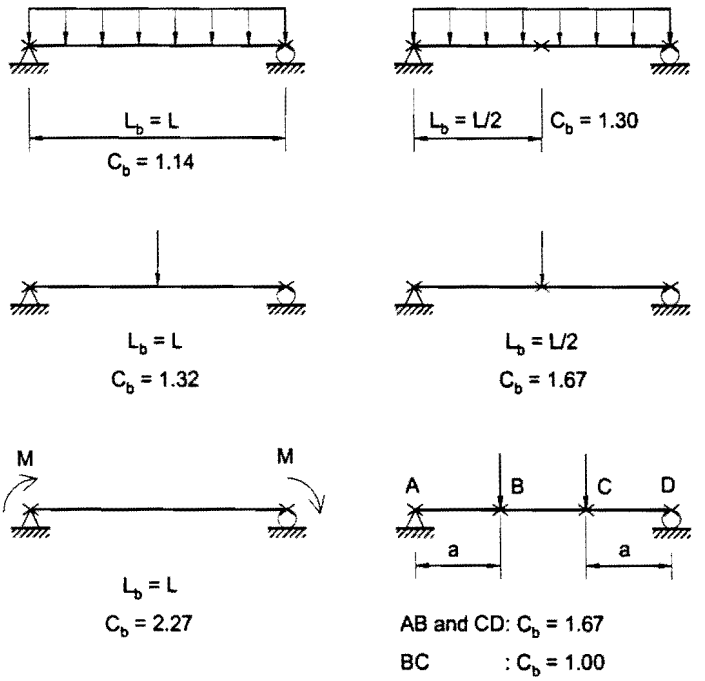

Figure 2.2 C_b factors for Common Load Cases

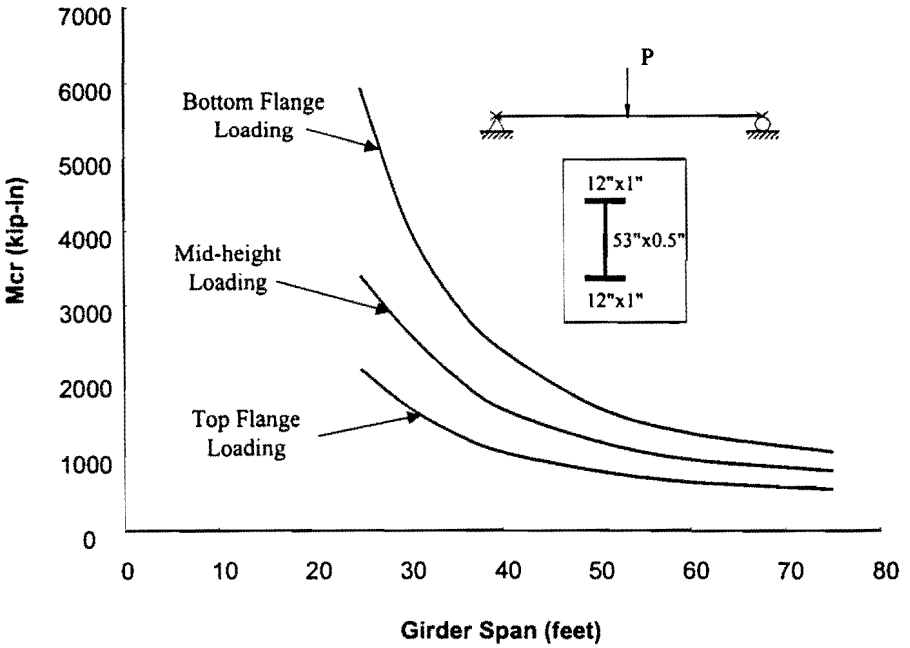

Figure 2.3 Effect of Load Height on Girder Buckling Capacity

Although neither the AASHTO or AISC specifications address the load height issue, solutions are available [SSRC 1988] for estimating the effects of load height. Effects of load height may be approximated with the following solution:

$$C_b^* = C_b(B)^{2y/h} \tag{2.15}$$

where:

C_b^* = the modified moment gradient factor with consideration of load height effect

C_b = the original moment gradient factor without consideration of load height effect

B is defined in the following expressions:

Point Load at Mid-span: $B = 1 - 0.180W^2 + 0.649W$

Uniform Distributed Load: $B = 1 - 0.154W^2 + 0.535W$

W is the beam parameter defined as: $W = \frac{\pi}{L_b}\sqrt{\frac{EC_w}{GJ}}$

y = the distance between point of load application and mid-height. Sign convention is defined as negative if load is applied above mid-height and positive is load is applied below the mid-height

h = depth of beam

Helwig et al. [1997] also found that reasonable estimates of load height could be obtained by simply using B = 1.4. Although the AASHTO and AISC specifications generally neglect the effects of top flange loading, there are a number of mitigating factors that reduce the detrimental effects of top flange loading. The first of these is the presence of intermediate (between supports) bracing such as cross-frames and diaphragms. The effects of top flange loading become less severe with the presence of intermediate bracing. Another mitigating factor is the presence of warping restraint at the ends of the unbraced length that are conservatively neglected in the expressions that are used to estimate the buckling capacity. The sections were generally assumed to be free to warp at the ends of the unbraced length in the derivation of the uniform moment buckling expressions. When the moment varies along the unbraced length, restraints to warping will generally be present at the ends of the unbraced length. Therefore although neglecting top flange loading is unconservative, the mitigating factors reduce the negative effects on the buckling behavior.

2.6 Beam Bracing

Beam bracing can generally be divided into one of two classifications: lateral bracing or torsional bracing. As their names imply, lateral bracing retrains the lateral movement of the girder, whereas torsional bracing restrains twisting of the cross section. Effective beam bracing can be achieved by providing either lateral or torsional bracing. Most bridges make use of cross frames or diaphragms for bracing. These braces fit into the category of torsional braces since they restrain twist of the cross-sections of the two girders that they span between. Cross-frames are truss type systems in which the members resist axial forces.

Diaphragms are beam type systems, in which braces develop bending moments to restrain girder twist.

As outlined in Chapter 1, an adequate bracing system must satisfy both stiffness and strength requirements. The remainder of this section will outline previous research studies on torsional bracing systems.

2.6.1 Beam Bracing Stiffness

Lateral and torsional bracing of simply supported beams was investigated by Flint in the 1940's and 1950's [Flint 1951]. The loading conditions that were considered consisted of both uniform moment and a concentrated load applied at midspan. He considered both lateral and torsional bracing systems. The location of the lateral bracing was varied in the study including midspan bracing located at the top flange, the bottom flange, and at the shear center. He also studied torsional bracing located at mid-span. The beams in Flint's studies were free to warp at the supports. He demonstrated that effective beam bracing could be provided by only restraining twist of the section. Therefore systems such as cross-frames and diaphragms that resist twist are effective bracing systems even though they still allow the cross-section to displace laterally.

Winter investigated the brace stiffness and strength requirements for columns and beams using laboratory experiments as well as simple analytical models. Both discrete and continuous bracing systems were considered. Winter's rigid link column model was discussed briefly in Chapter 1. Winter was the first to demonstrate the dual criteria of both strength and stiffness that is necessary for effective stability bracing. He also demonstrated the effects of initial imperfections on the brace stiffness requirements.

In the 1960's, Taylor and Ojalvo [1966] investigated the behavior of torsional bracing of beams. They considered the effects of both continuous and discrete torsional braces. The loading conditions that were considered consisted of uniform moment, a point load at mid-span and a uniform distributed load. Theoretical equations were derived for uniform moment loading for the beam buckling capacity of doubly-symmetric beams as a function of the continuous brace stiffness. Their study resulted in the following expression:

$$M_{cr} = \sqrt{M_0^2 + \overline{\beta_T} EI_y} \tag{2.16}$$

where M_0 is the beam buckling moment without any bracing, $\overline{\beta_T}$ is the continuous torsional brace stiffness in kip-inch per radian per inch along the beam length.

Mutton and Trahair [1973] studied the stiffness requirements for lateral bracing while studying the buckling behavior of columns and beams with midspan braces. They adapted column-bracing solutions to be applicable for beams with equal and opposite end moments with both translational and rotational restraints. Numerical solutions of the critical buckling loads of elastically restrained beams with central concentrated loads were obtained. Their

study considered the effects of the location of the bracing on the cross-section as well as load height.

Trahair and Nethercot [1982] provided a summary of lateral and torsional bracing requirements for I-shaped beams. Solutions were shown graphically for beams with continuous bracing or discrete bracing for common loading conditions such as uniform moment, a concentrated load at mid-span and a uniformly distributed load. They evaluated the effect of the lateral brace location on the cross section and concluded that the most effective position for lateral bracing was at the compression flange. The brace stiffness requirements considering the effects of load height, web distortion and the connection stiffness were also considered. The following expression was presented to estimate the overall stiffness, α_{kr}:

$$\frac{1}{\alpha_{kr}} = \frac{1}{\alpha_p} + \frac{1}{\alpha_{web}} + \frac{1}{\alpha_j} \tag{2.17}$$

where

α_{kr} = reduced torsional stiffness
α_p = brace stiffness
α_j = connection stiffness
α_{web} = web stiffness = $Et^3/2$

Bishara and Elmir [1990] studied the interaction between cross frames and I-shaped girders in the completed bridge. The authors employed a three-dimensional finite element model to study the forces induced in intermediate and end cross frames of multi-beam composite steel bridges. Four simply supported multi-girder bridges were investigated. One of the four bridges had normal supports while the other three had skewed supports with angles of 20, 40, and 60 degrees. Their results showed that the maximum forces in the cross-frame members were slightly higher in the bridge with a 20° skew angle than those in the bridge with normal supports. With larger skew angles the maximum forces in the cross-frames increased significantly. The study did not address any of the stability requirements for the bracing members.

Yura et al. [1992] conducted a detailed investigation on the lateral and torsional brace requirements for beams. In addition to laboratory tests, a 2-dimensional finite element analytical (FEA) model [BASP 1987] was utilized to study the bracing behavior. The study considered the effects of the type of bracing, brace stiffness, brace location, and the number of braces on the beam buckling behavior. A variety of loading conditions were considered in the study ranging from uniform moment to transverse loading applied at different locations on the cross-section. Torsional braces were placed on the compression flange, the tension flange, as well as at the centroid. Effects of cross-sectional distortion were studied in detail, including unstiffened and stiffened webs (including partial depth stiffeners). The study showed that cross section distortion has a significant effect on the behavior of torsional braces and can be controlled by properly attached stiffeners. They adapted the continuous

bracing expression in Eq. 2.16 from Taylor and Oljavo to include the effects of cross section distortion, top flange loading and moment gradient for beams with normal supports. The resulting expression is given in the following expression:

$$M_{cr} = \sqrt{C_{bu}^2 M_0^2 + \frac{C_{bb}^2 \overline{\beta_T} EI_y}{C_t}} \leq M_s \text{ or } M_y \tag{2.18}$$

where:

M_0 = buckling capacity of unbraced beam with uniform moment loading
C_{bu} = C_b factor corresponding to the unbraced beam
C_{bb} = C_b factor corresponding to the fully braced beam
$\overline{\beta_T}$ = continuous torsional bracing system stiffness
C_t = top flange loading factor = 1.2 (equals to 1.0 for loading at centroid)
M_s = moment corresponding to beam buckling between braces
M_y = beam yield moment

Although Eq. 2.18 was adapted from an expression derived for beams with continuous torsional braces, the expression can also be utilized for discrete braces by using the following expression:

$$\overline{\beta_T} = \frac{n\beta_T}{L} \tag{2.19}$$

where

n = number of intermediate braces
L = span length
β_T = intermediate torsional bracing system stiffness

For the case of a single intermediate torsional brace, Eq. 2.19 provides overly-conservative results. Therefore for the case of a single torsional brace at mid-span, the following equation was recommended:

$$\overline{\beta_T} = \frac{\beta_T}{0.75L} \tag{2.20}$$

For design, the required beam buckling capacity can be obtained by setting Eq. 2.18 equal to the maximum moment and solving for the required brace system stiffness.

For singly-symmetric sections, I_y in Eq. 2.18 should be replaced by I_{eff}, which is given in the following expression:

$$I_{eff} = I_{yc} + \frac{t}{c} I_{yt} \tag{2.21}$$

where

I_{yc} = weak axis moment of inertia of compression flange at weak axis
I_{yt} = weak axis moment of inertia of tension flange at weak axis
c = distance between cross section centroid and centroid of compression flange
t = distance between cross section centroid and centroid of tension flange

Although Eq. 2.18 can be used to solve for the required torsional brace stiffness, the effectiveness of a given brace is affected by a number of factors. Helwig et al. [1993] investigated the stiffness requirements for torsional braces using a three-dimensional finite element model. Their study concluded that the in-plane flexibility of the girders reduces the effectiveness of the torsional braces and therefore the in-plane girder stiffness should be considered when evaluating the system brace stiffness. The effect of the in-plane girder stiffness is demonstrated in Fig. 2.4. When internal moments develop in the torsional brace, vertical shears also develop at the ends of the brace. These shears are transferred to the girders as an upward load on one girder and a downward load on the other girder. These forces cause one of the girders to displace upward while the other girder displaces downward, therefore resulting in a rigid body rotation of the brace. The rotation of the girders reduces the effectiveness of the cross-frame or diaphragm.

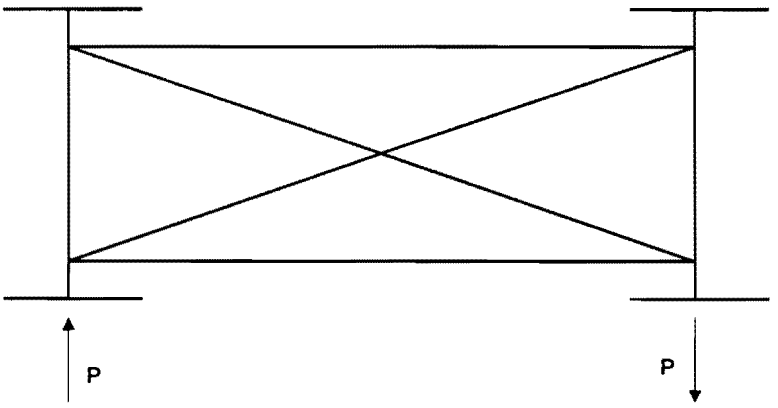

Figure 2.4 Brace Forces Cause Girder Overturning

For a twin-girder system the girder stiffness can be approximated with the following expression:

$$\beta_g = \frac{12S^2EI_x}{L^3} \tag{2.22}$$

where

S = girder spacing
I_x = strong axis moment of inertia of girder
L = girder length

For a system with more than two girders, all of the girders will twist as a unit since they are generally connected across the width of the bridge by cross-frames or diaphragms. The resulting effect on the brace stiffness is substantially less and can be approximated with the following expression [Yura et al. 1992]:

$$\beta_g = \frac{24(n_g - 1)^2}{n_g} \frac{S^2 E I_x}{L^3} \tag{2.23}$$

Where n_g is the number of the girders. The in-plane girder stiffness has much more of an effect on the bracing system stiffness for a twin-girder system than for systems with more than two girders.

Another factor that has a significant effect on β_T is cross section distortion. Web distortion significantly reduces the effectiveness of torsional braces, however properly sized stiffeners can be provided to control the distortion. The required details for the stiffeners depend on the web slenderness of the beam or girder. For rolled sections, Yura and Phillips [1992] recommended that transverse stiffeners extend at least ¾ of the beam depth to effectively control local web distortion. However rolled sections have relatively stocky webs with slenderness values (ratio of web height to thickness) less than 60. The webs of most plate girders have substantially higher values of the web slenderness and the stiffeners often must extend nearly the full depth of the web to adequately control web distortion. Yura and Phillips suggested using the following equations to estimate the cross section stiffness:

$$\frac{1}{\beta_{sec}} = \frac{1}{\beta_c} + \frac{1}{\beta_s} + \frac{1}{\beta_t} \tag{2.24}$$

Where

β_{sec} = cross-section stiffness
β_c = stiffness of web section adjacent to compression flange
β_s = stiffness of web section at stiffener
β_t = stiffness of web section adjacent to tension flange

β_c, β_s, β_t, β_c, β_s, β_t can be determined using the following equation:

$$\beta_j = \frac{3.3E}{h_j} \left(\frac{h}{h_j} \right) \left(\frac{1.5 h_j t_w^3}{12} + \frac{t_s b_s^3}{12} \right) \tag{2.25}$$

where j is c, s or t respectively. The definitions are shown in Fig. 2.5. Design examples are presented in Chapter 7 that demonstrate the use of Eqs. 2.24 and 2.25.

Although determination of the effects of web distortion on the cross sectional stiffness may seem complicated, the concept is relatively simple. The web is separated into stiffened and unstiffened regions and the overall cross sectional stiffness is simply the summation of the individual elements of the cross-section. The equation is given in general terms for completeness, however transverse stiffeners often extend close to the flanges and the whole web can simply be treated as one stiffened region. When a solid diaphragm is used, the portion of the web that coincides with the depth of the diaphragm is extremely stiff and can usually be treated as rigid. For cross-frames the portion of the web within the depth of the cross-frame (h_m in Fig. 2.5) does not affect web distortion since the cross-frames control the relative lateral movement of the flanges. Therefore, a girder with cross-frames near the flanges will not experience significant web distortion.

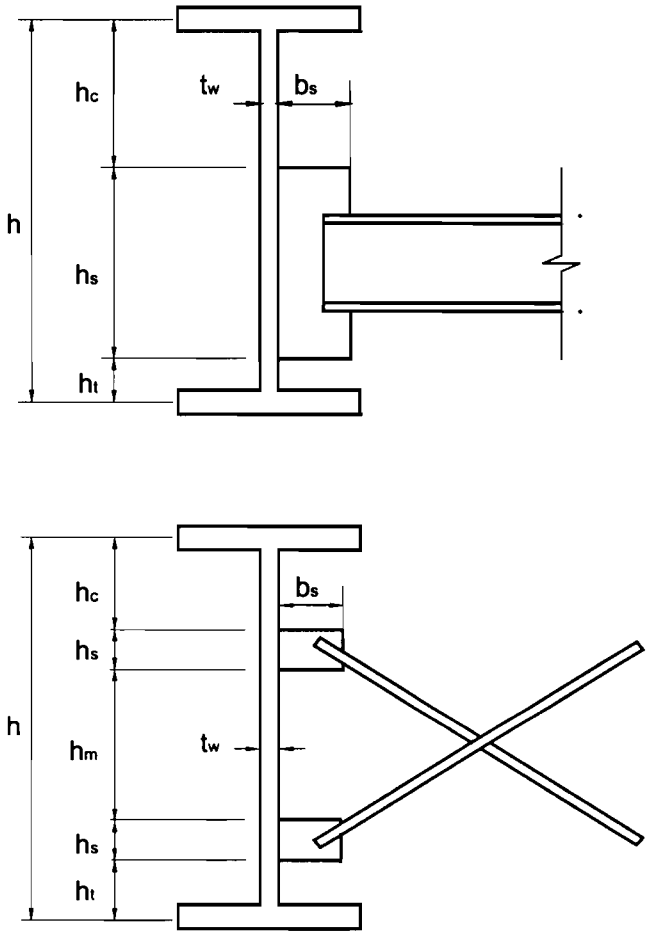

Figure 2.5 Definitions of Web Distortion

The derivation of expressions for evaluating the stiffness of a given cross-frame or diaphragm simply requires a knowledge of the relationship between the moment versus rotation behavior of the brace at the ends. This derivation therefore requires an understanding of how the brace will bend due to girder rotation at the braced location. Fig. 2.6 shows the stiffness formulations for a variety of commonly used torsional bracing systems. The three most common forms of cross frame systems include tension systems, compression systems and k-brace systems.

The bracing requirements of a typical torsional bracing system will often result in equal and opposite moments at the ends of the cross-frame or diaphragm. In a cross-frame with two diagonals, the moment will result in compression in one diagonal and tension in the other. In a tension system, the compression diagonal is conservatively neglected since these members are often relatively slender and may buckle. The tension diagonal will therefore be designed to provide proper strength and stiffness to satisfy the bracing requirements. In a compression system, both diagonals are designed to be effective at resisting the stability moments.

When a diaphragm type brace is used, the brace stiffness depends on the location of the diaphragm on the girder cross-section. If the centroid of the diaphragm is positioned above midheight of the girders (in the positive moment region), the lateral movement of the compression flanges of the two girders will generally be in the same direction and the diaphragm will be subjected to reverse curvature bending thereby resulting in 6EI/S stiffness. If the centroid of the diaphragm is located near the tension flange, such as in the case with a through-girder system, the compression flanges generally translate in opposite directions and the diaphragm will bend in single curvature with 2EI/S stiffness.

The total stiffness of the torsional bracing system is a function of the cross-frame or diaphragm stiffness, the cross-sectional stiffness, as well as the in-plane stiffness of the girder. These individual stiffness components are related by the classic equations for springs in series. Therefore the total system stiffness can be predicted using the following expression:

$$\frac{1}{\beta_T} = \frac{1}{\beta_b} + \frac{1}{\beta_{sec}} + \frac{1}{\beta_g} \tag{2.30}$$

where

β_T = total torsional bracing system stiffness
β_b = brace stiffness
β_{sec} = cross-sectional stiffness
β_g = in-plane girder stiffness

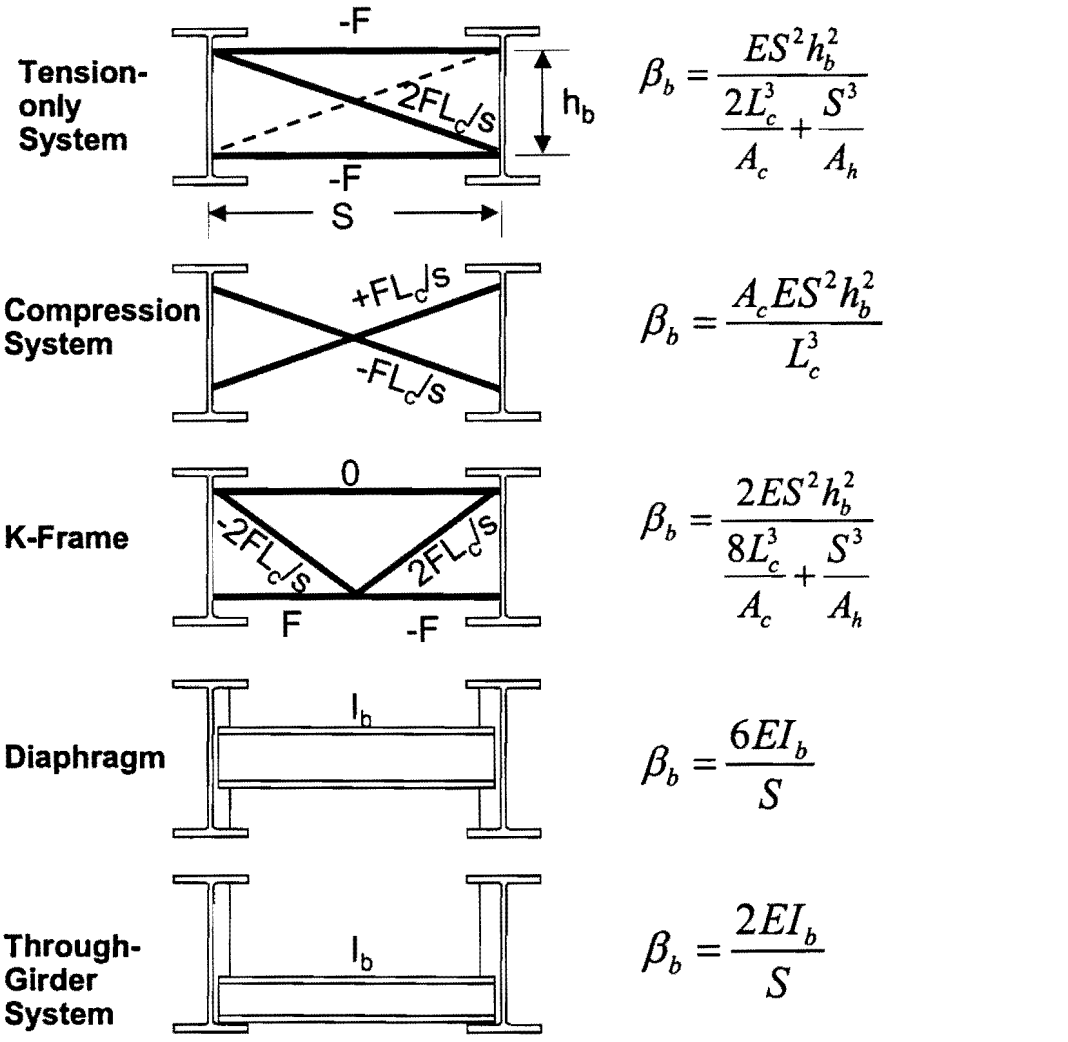

S = Girder Spacing
h_b = Height of Cross Frame
A_h = Area of Horizontal Members
L_c = Length of Diagonal Members
A_c = Area of Diagonal Members
I_b = Diaphragm Moment of Inertia

Brace Forces

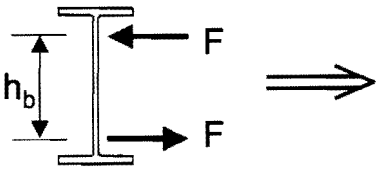

For Cross-Frames:

$$F = \frac{M_{br}}{h_b}$$

Figure 2.6 Brace Forces and Stiffness Formulas for Cross Frames and Diaphragms

Yura et al. [1992] also showed that the location of the torsional bracing on the cross-section did not have a significant effect on the brace stiffness or strength requirements. Therefore, the torsional brace can be placed anywhere on the cross-section with the same effectiveness. The placement of the bracing may affect the cross-sectional stiffness or the brace stiffness (6EI/S or 2EI/S), however these effects can be accounted for using the equations presented in this section.

2.6.2 Beam Brace Strength

Brace strength requirements have been discussed in detail by Yura et al. [1992]. The brace strength requirements are a function of the brace stiffness and the magnitude and shape of the beam initial imperfection. The magnitude of brace moment is a linear function of the magnitude of the initial imperfection. The following expressions can be used to determine the magnitude of the twist at the brace point, ϕ_T, as well as the resulting brace moments, M_{br} (Yura et al. [1992] and Helwig et al. [1993]):

$$\phi_T = \frac{\phi_0}{1 - \frac{\beta_{Ti}}{\beta_T}\frac{M^*}{M_{cr}}} \tag{2.26}$$

$$M_{br} = \beta_T(\phi_T - \phi_0) \tag{2.27}$$

where:

ϕ_o = initial twist angle in radians
β_{Ti} = ideal brace stiffness based on the stiffness requirement, Eqs. 2.18 and 2.19
β_T = actual brace system stiffness
M^* = actual girder moment
M_{cr} =maximum moment corresponding to the girder buckling between brace points

Helwig et al. [1993] presented FEA results to demonstrate the accuracy of the brace strength provisions. A variety of parameters were considered in the study including the number of braces, the brace stiffness, and also the shape and magnitude of initial imperfections. The study concluded that Eqs 2.26 and 2.27 show good correlation with computational results when the initial imperfection has the same basic shape as the final buckled shape. The critical imperfection for beams usually involves a girder twist consisting of a lateral movement of one of the flanges while the other flange remains straight. As a general rule, the shape of the imperfection that produces the largest brace moment usually has one less "wave" than the number of waves in the buckled shape corresponding to buckling between brace points. For example, with one intermediate brace the critical imperfection should be a half sine curve; for two intermediate braces the critical imperfection would be a sine curve, etc.

A review of Eqs. 2.26 and 2.27 shows that the brace moment developed is linearly related to the initial imperfection. These equations use the same concepts presented by Winter [1958] in his rigid link model. Eq. 2.26 shows that if only the ideal stiffness is provided, the total twist angle will increase to infinity when the applied load reaches the critical buckling moment, therefore resulting in very large brace moments. The AISC LRFD Specification [2001] has incorporated the bracing recommendations from Yura et al. [1992] and recommends providing at least twice the ideal stiffness. The design recommendations that are presented in the AISC LRFD Specification are based upon Eqs. 2.18 to 2.27, however the beam unbraced moment capacity in Eq. 2.18 was conservatively neglected, which results in the following expression:

$$\beta_T = \frac{2.4LM_u^2}{\phi n C_{bb}^2 EI_{eff}} \tag{2.28}$$

where M_u is the maximum factored design moment.

For the strength requirement, an initial imperfection of $\theta_0 = L_b/(500d)$ radians was assumed with L_b equal to the spacing between braces and d equal to the beam depth. The resulting brace strength is then given in the expression:

$$M_{br} = \frac{0.024LM_u}{nC_{bb}\, L_b} \tag{2.29}$$

where L is the total beam length.

Eqs. 2.26 to 2.29 are fundamental equations for the strength requirements for beam bracing. While the equations have been developed using finite element models, there has been no experimental testing to verify these strength expressions for torsional bracing systems. Although, as mentioned in Chapter 1, this research study has included experimental testing to measure the brace moments, this report will focus on the FEA results. A difficult aspect of experimental verification of the strength equations presented above revolves around the "worst-case" imperfection that has been assumed in their derivation. As outlined above, the assumed imperfection consisted of a lateral movement of one of the flanges while the other flange remained straight. The imperfections of beams typically encountered in the laboratory will usually have both a sweep and a twist. Comparing the bracing equations with experimental data requires an assessment of the effective imperfection/twist of the test beams. Results will be presented in Chapter 4 that were used to help in the selection of an effective twist of the cross-section.

The remainder of this report will focus on the behavior of torsional bracing systems of bridge girders with both normal and skewed supports. The finite element model will be presented in Chapter 3. Finite element results documenting the effects of a variety of imperfections on the torsional brace forces will be presented in Chapter 4. The brace stiffness and strength equations for girders with normal supports that have been presented in this chapter will be compared with FEA results in Chapter 5. Chapters 6, 7, and 8 will focus

on the behavior of bridges with skewed supports. These chapters will include comparisons between the FEA results and brace stiffness and strength equations modified to account for the skew angle so that general bracing provisions can be developed.

Chapter 3
Finite Element Model

3.1 Introduction

The three-dimensional finite element program ANSYS [1996] was used to perform computational studies on the torsional bracing behavior of steel girders with skewed supports. Both eigenvalue buckling and large displacement analyses were conducted. An eigenvalue buckling analysis is a linear-elastic analysis that can be utilized to study the effects of the brace stiffness on the buckling behavior of a structural system. Since an eigenvalue analysis generally doesn't reflect the effects of imperfections on the buckling behavior, the analysis is used to establish the ideal stiffness requirements for the bracing. To study the effects of imperfections, a large displacement analysis is necessary. A large displacement analysis is a non-linear analysis of an imperfect system that can be used to establish the strength requirements of the bracing. The load is gradually incremented with smaller substeps as the buckling load is approached. Although a variety of solution algorithms are available, Newton-Raphson equilibrium iterations are often used to drive the solution to equilibrium convergence based upon a given tolerance limit at the end of each load increment. Large displacement analyses were used to develop curves of the brace moment versus the applied load for a particular initial imperfection. As discussed in the previous chapter, the critical initial imperfection for beams generally involves an initial twist of the cross-section. Additional FEA analyses directed at the shape and magnitude of the initial imperfection were conducted and the results are presented in Chapter 4.

Although the majority of the analyses were conducted on a twin-girder system, systems with more than two girders were also studied. The girders were I-shaped with torsional braces interconnected between adjacent girders. For beams with skewed supports, there are two possible orientations for the torsional braces: parallel bracing where the braces are parallel to the skew angle, and normal bracing in which the braces are perpendicular to the longitudinal axis of the girders. Results of both eigenvalue and large displacement analyses for girders with normal supports are presented in Chapter 5 to verify existing equations. Results of eigenvalue and large displacement analyses of bridges with skewed supports and parallel bracing are presented in Chapter 6. The FEA results are compared to expressions previously outlined in Chapter 2 with modifications to account for the skew angle. Results of eigenvalue and large displacement analyses of bridges with skewed supports and normal bracing are presented in Chapter 7.

3.2 Finite Element Model

The purpose of the finite element modeling in this study was to investigate the effect of skewed supports on the behavior of the torsional braces. The 3-D finite element model used to study the bracing behavior modeled the construction stage when the steel girders resist the

entire load. Additional features that include the concrete slab in the FEA model to account for the composite bridge behavior are presented in Chapter 7.

A combination of shell, beam, and truss elements was used to model the structural components of the bridge, which included the girders and the cross frames or diaphragms. The cross-section of the girders and the transverse stiffeners were modeled using shell elements. The shell elements used in the model were 8-node quadrilateral shell elements that can model both out-of plane bending and in-plane membrane deformations. The shell elements have a total of 6 degrees of freedom (DOF) at each node, including three linear translations and three rotational DOF's. Displacements are produced at all 8 nodes while stresses are available at the four corner nodes. Input for the shell elements consists of the thickness of the element and the material properties. Two shell elements were used to model the flanges as shown in Fig. 3.1. The number of shell elements in the web varied, however care was taken in selecting the number of elements to avoid aspect ratios much greater than one. In some analyses, shell elements were also used to model solid I-shaped diaphragms framing between adjacent girders.

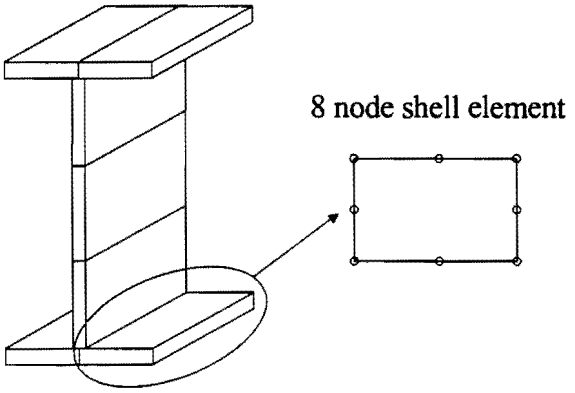

Figure 3.1 Finite Element Model of Girder Cross-Section

Beam elements were used in some analyses to model torsional braces spanning between adjacent girders. These beam elements were used to model the experimental test setup, which consisted of braces that were connected to the top flange of the test beams. The beam elements used in the model were 2-node uniaxial elements with tension, compression, torsion and bending capabilities. Since the element was used to model the beam behavior in three-dimensional space, the general input consists of cross sectional properties such as the area and the moment of inertia about the x-x and y-y axes. The line element that was used does not account for the warping stiffness of thin-walled beams.

Three-dimensional truss elements were used to model cross frames spanning between adjacent girders. These elements have two nodes with three translational degrees of freedom per node. Truss elements cannot model bending or torsional deformation of the individual members. The input for the truss elements simply consisted of the cross sectional area.

Fig. 3.2 illustrates the boundary conditions that were used on a typical twin-girder system with skewed supports and a brace at mid-span. The brace is oriented parallel to the skew angle, and the member was simply supported in-plane. The out-of-plane translation was restrained at the top and bottom of the web at both ends. These out-of-plane restraints prevented girder twist, however the section was free to warp.

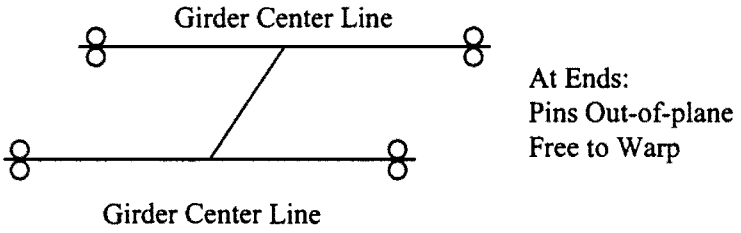

At Ends:
Pins Out-of-plane
Free to Warp

Top View of Twin-Girder System

At Ends:
Simply Supported In-plane

Elevation View of Twin-Girder System

Figure 3.2 Boundary Conditions of FEA Model

Fig. 3.3a shows an illustration of the FEA model of a typical twin-girder system with a cross-frame at midspan. Cross-frames in the study were typically modeled with only three members as shown in the figure. This type of a cross-frame would be typical of a tension-only system in which the compression diagonal is conservatively neglected since the slender members usually have a low buckling strength. Fig. 3.3b shows the model for a twin-girder system with beam elements connected to the top flange of adjacent girders. Analyses were also conducted by modeling the diaphragms and I-shaped beams at the top flange with shell elements. Since identical results were obtained with the line element and shell element models, line element models such as those shown in Figs. 3.3a and 3.3b were mainly used in the study.

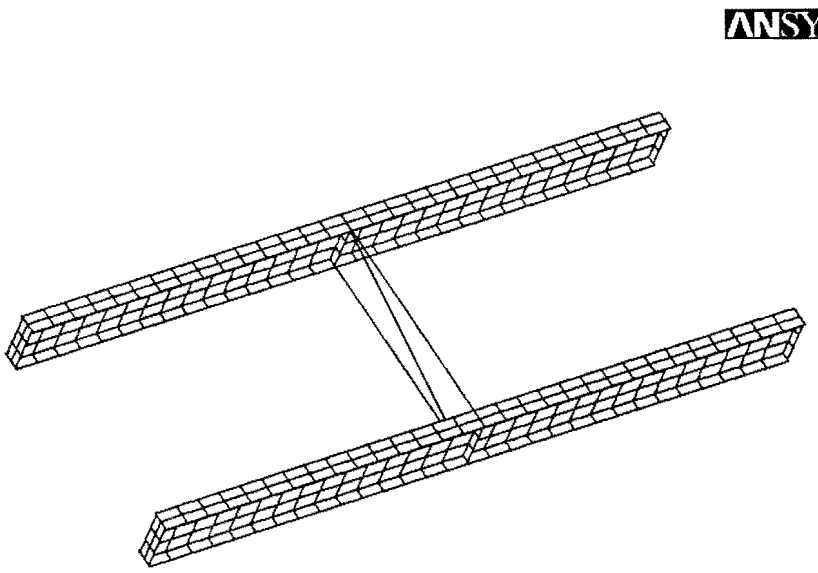

Figure 3.3a Finite Element Model of Twin-Girder System with Tension Only Cross-Frame at Midspan

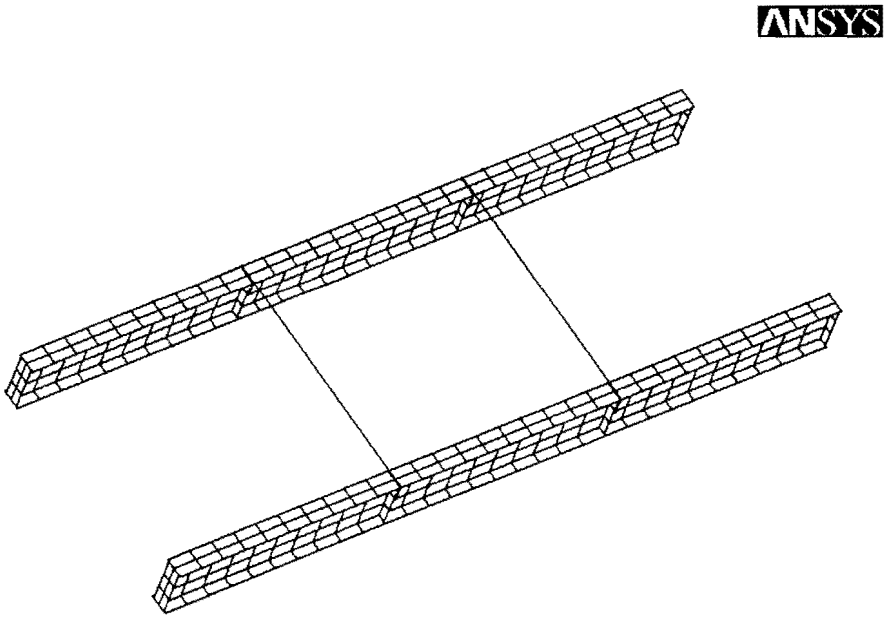

Figure 3.3b Finite Element Model of Twin-Girder System with Top Flange Braces Modeled using Beam Elements

Fig. 3.4 illustrates the two possible buckled shapes from an eigenvalue analysis of a twin-girder system. For brace stiffness as less than "full bracing", the buckled shape corresponded to a half sine curve as shown in Fig. 3.4a. For brace stiffness as greater than or equal to the ideal stiffness, full bracing was achieved and the beam generally buckled between the brace points as shown in Fig. 3.4b. Although the two beams have exactly the same applied load, the buckled shape of the twin-girder system in Fig. 3.4b typically shows that one beam buckles between the brace points and the other beam remains straight. The reason that one girder buckles and the other remains straight is related to the shears that develop at the ends of the braces as equal and opposite bracing moments are developed at the ends of the cross-frame. The end shears are generally equal in magnitude, however they are opposite in direction with one directed upwards and the other directed downwards. This results in a slightly larger load on one of the girders compared to the other, which is why only one girder buckles (the more heavily loaded girder). This effect was explained in Chapter 2 when explaining the effect of the in-plane stiffness of the girder on the brace stiffness requirements.

There were several considerations in the development of the finite element model to ensure the model best represents the actual structure. Details about these considerations are presented in the reminder of this section.

3.2.1 Stiffeners and Cross-Frames

Transverse stiffeners were provided at the brace locations to control cross-sectional distortion. The stiffeners extended from the top of the web to the bottom of the web and generally had the same number of elements as provided through the depth of the girder web. The width of the transverse stiffeners was slightly less than half the width of the flange to avoid the outside stiffener nodes merging with the flange nodes, which would provide extra warping restraint to the beam. The cross-frames were modeled by 3-D truss elements and were framed into the top and bottom of the web. Therefore cross-sectional distortion was not a concern for this bracing system.

3.2.2 I-Shaped Bracing Beams Connected to Top Flanges of Girders

In some instances, details were used with small I-shaped bracing members connected to the top flange of the adjacent girders as shown in Fig. 3.3b. Distortion between the flange and the web was controlled by connecting the transverse stiffener to the flange. Since the stiffener was usually not as wide as the flange, the connection to the web was usually made with an additional corner stiffener as shown in Fig. 3.5.

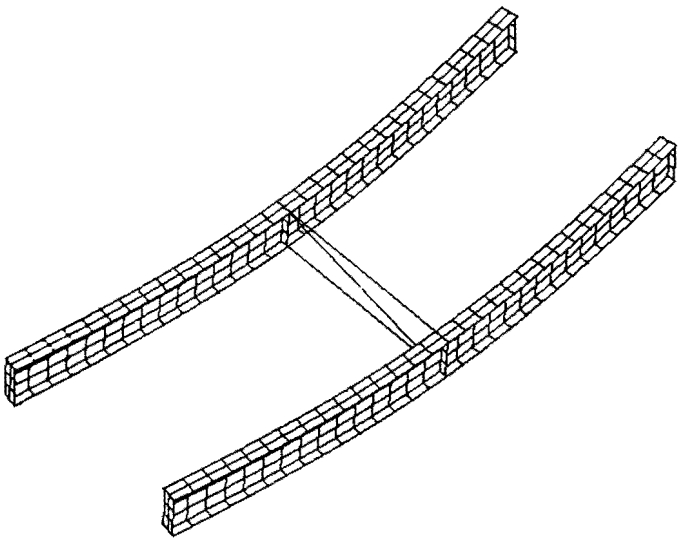

Figure 3.4a Twin-Girder System Buckling Shape with Inadequate Bracing

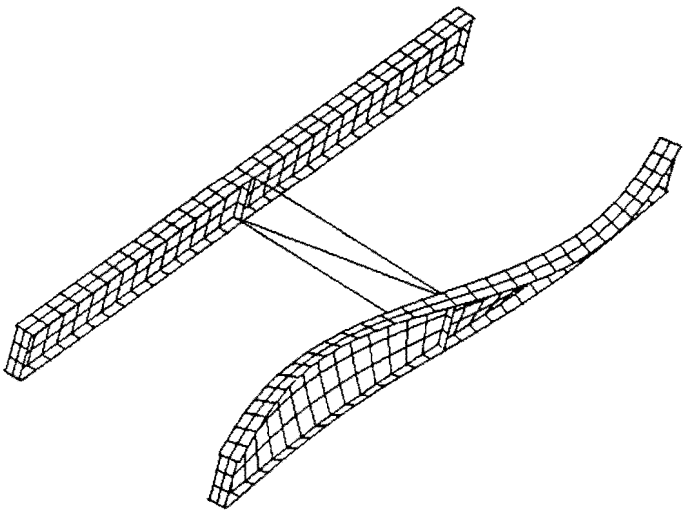

Figure 3.4b Twin-Girder System Buckling Shape with Full Bracing

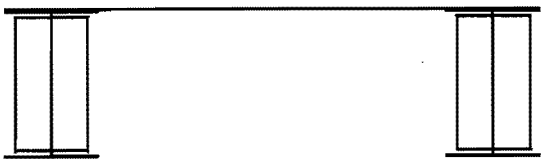

a) Regular Stiffener Modeling

b) Excessive Top Flange Distortion

c) Top Flange Distortion Controlled
by Corner Stiffener

Figure 3.5 Finite Element Modeling Details for Stiffeners

To avoid warping restraint from the top flange braces, the translational DOF's of the flange and brace were rigidly coupled in the vertical and lateral direction at selected nodes. For example, Fig. 3.6a shows a plan view of two buckled girders that demonstrate the warping restraint that may develop due to out-of-plane bending of the brace. Allowing relative moment in the x-direction while rigidly coupling the brace and girder flange nodes in the y and z direction eliminates this warping restraint. Fig. 3.6b illustrates that the nodes at the flange tips were typically coupled in the vertical direction to the corresponding brace nodes, while the node at the middle of the top flange was then coupled to the corresponding brace node in the lateral direction. The corresponding buckled shape is shown in Fig. 3.6c.

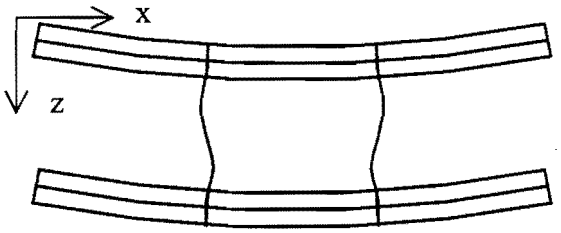

a) Brace Out-of-plane Bending and Twisting

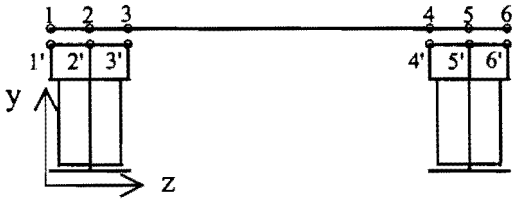

b) Coupling Corresponding Nodes Vertically

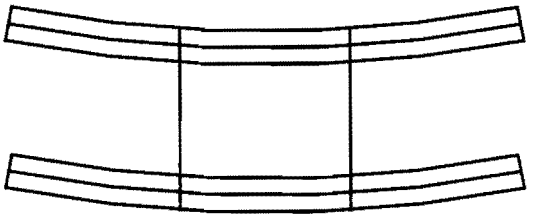

c) Brace without Out-of-plane Bending and Twisting

Figure 3.6 Coupling Details between Braces and Girders of FEA Model

3.2.3 Short Segment Warping Restraint of Bridges with Skewed Supports

When bridges have normal supports the braces can usually be positioned so that the girders have a uniform unbraced length between the cross-frame or diaphragm locations. For bridges with skewed supports and braces perpendicular to the longitudinal axis of the girders, it is often not possible to position the intermediate braces and maintain an equal unbraced length for all of the segments. For the analyses conducted in this study, when the braces were oriented perpendicular to the longitudinal axis of the girders with skewed supports, one end segment was always shorter than the other segments as illustrated in Fig. 3.7. The unbraced segments in Fig. 3.7 are labeled either Segment A and B respectively. The regions labeled Segment A all have the same unbraced length, while the Segment B regions adjacent to the skewed support have shorter unbraced lengths. The buckling capacity of the beam will typically be controlled by one of the Segment A regions.

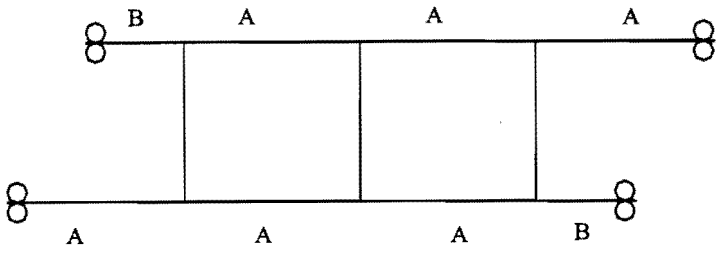

a) Plan View of Skewed Girders with Multiple Braces

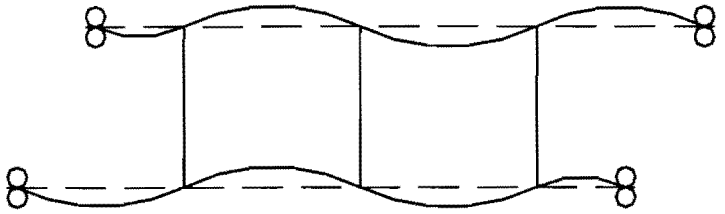

b) Buckling Shape between Brace Points with Full Brace

Figure 3.7 Warping Restraints in FEA Models due to Segments with Smaller Unbraced Lengths

The equations for lateral torsional buckling generally assume the beams are free to warp at ends of the unbraced length. In the FEA model, however, the capacity of the regions labeled Segment B will have a higher buckling capacity than the those labeled Segment A due to the shorter unbraced lengths. The shorter segments will therefore provide some warping restraint to the critical segment A. Depending on the bracing provided, the warping restraint in these cases can lead to higher buckling capacities from the FEA models than those predicted using equations that assume there is no warping restraint. However the amount of bracing necessary to reach the moment levels corresponding to the presence of end warping restraint is very large and is generally not practical for design. Therefore, the stiffness requirements for the bracing are based upon the moment levels neglecting end warping restraint. The presence of end warping restraint will have a small effect for the stiffness requirements, however the benefit is relatively minor and is generally neglected in design. Therefore, for girders with skewed supports, the buckling capacity was defined as the applied moment for the girders to reach a load level corresponding to buckling between brace points using Eqs. 2.1 and 2.2 from Chapter 2. These equations assume no warping restraint at the ends of the unbraced length. The ideal stiffness can be obtained based on this defined buckling capacity. Shi [1997] eliminated the warping stiffness at the ends of the unbraced length in the FEA models by making the compression flange discontinuous at the brace locations. Modifying the model in this manner essentially provided the same buckling capacity that was obtained by defining the load levels by Eqs. 2.1 and 2.2.

3.3 Computational Scope

There were a number of parameters that were considered in the computational study. These parameters include the following:

1) Girder System (two to four girder systems were considered)
2) Girder Span (40 feet to 120 feet)
3) Girder Cross Section (Singly and Doubly Symmetric)
4) Skew Angle (0, 15, 25, 35, and 45 degrees)
5) Brace Orientation (Parallel to Skewed Support or Normal to girders)
6) Loading Condition (Uniform Moment, Concentrated Load, Uniformly distributed Load)
7) Number of intermediate braces

The girder cross sections that were studied are shown in Fig. 3.8. The sections consisted of three doubly-symmetric rolled sections (W14x22, W30x99 and W36x160) and three singly-symmetric plate girders labeled Sections #4, #5, and #6. The degree of monosymmetry of the singly-symmetric sections can be obtained by considering the ratio of I_{yc}/I_y of the sections, in which I_{yc} is the weak axis moment of inertia of the compression flange and I_y is weak axis moment of inertia of the entire girder. The AASHTO Specification requires the ratio for flexural members fall within the following limits:

$$0.1 \leq I_{yc}/I_y \leq 0.9.$$

The respective I_{yc}/I_y ratios for Sections #4, #5, and #6 are: 0.28, 0.27, and 0.18. Doubly-symmetric sections have ratios of I_{yc}/I_y of 0.5.

Although the W14x22 section is relatively small for many bridge applications, this is the section used in the laboratory tests and was consequently included in the finite element modeling. The other five sections were selected from the short span simply supported steel bridge plans recommended by the American Iron and Steel Institute [1994]. Table 3.1 illustrates key parameters for the selected sections such as span, span depth, number of intermediate braces, and maximum unbraced length.

The remainder of this section will focus on comparisons between the FEA results for single girders and predictions from equations outlined in Chapter 2. The results presented are for uniform moment loading on simply supported beams with a variety of unbraced lengths. For doubly symmetrical sections, Timoshenko's solution given in Eq. 2.1 was used in the comparison. For singly symmetrical sections, Eqs. 2.10 and 2.13 were employed as recommended by the AISC LRFD and the AASHTO Specifications.

Tables 3.2 to 3.4 present comparisons of results from Eq. 2.1 and FEA for the doubly-symmetric sections: W14x22, W30x99, and W36x160. The tables show that the buckling

capacities predicted by Eq. 2.1 are generally within 1 to 3% of the FEA solutions. Although the accuracy of Eq. 2.1 does change slightly with increasing unbraced length and varies with the cross-section, the expression provides good estimates of the buckling capacity.

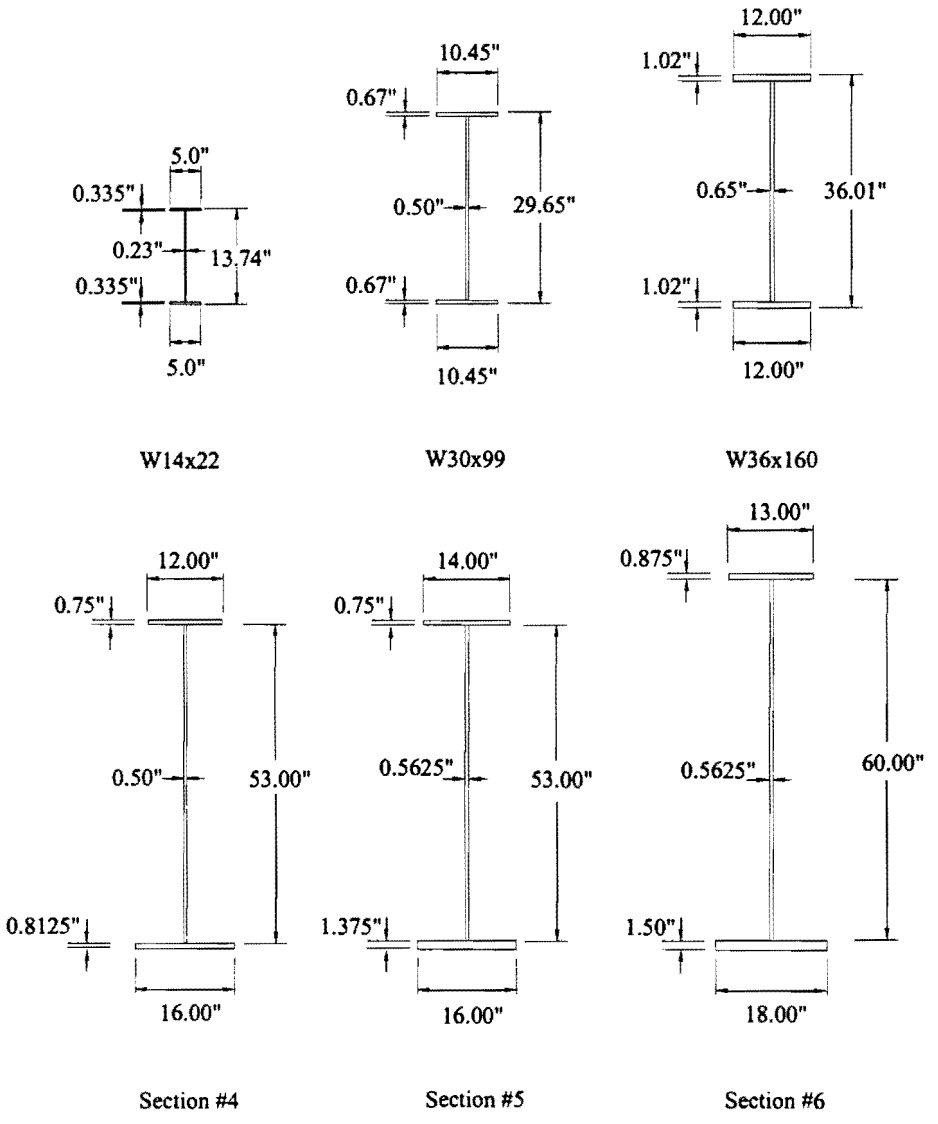

Figure 3.8 Cross Sections Considered in Computational Study

Table 3.1 Parameters for Cross-Sections Studied

Sections	Span (feet)	L/d Ratio	No. of Braces	Unbraced Length (feet)
W14X22	33	28.8	1	16.5
W30X90	40	16.3	1	20
W36X160	60	20	2	20
Section #4	80	18.1	3	20
Section #5	100	22.6	3	25
Section #6	120	24	4	24

Table 3.2 W14X22 Section

Unbraced Length (ft.)	L/d Ratio	Eq. 2.1 (k-ft)	FEM Results (k-ft)	% Difference
10	8.7	89.12	89.55	+0.48%
15	13.1	45.21	44.60	-1.36%
20	17.5	29.28	28.78	-1.72%
25	21.8	21.49	21.09	-1.90%
30	26.2	16.97	16.65	-1.95%

Table 3.3 W30X99 Section

Unbraced Length (ft.)	L/d Ratio	Eq. 2.1 (k-ft)	FEM Results (k-ft)	% Difference
30	12.1	437.12	434.50	-0.60%
40	16.2	280.97	278.59	-0.85%
50	20.2	205.11	203.10	-0.99%
60	24.3	161.33	159.65	-1.05%
70	28.3	133.08	131.68	-1.06%

Table 3.4 W36X160 Section

Unbraced Length (ft.)	L/d Ratio	Eq. 2.1 (k-ft)	FEM Results (k-ft)	% Difference
30	10.0	1219.28	1193.31	-2.18%
40	13.3	784.15	764.40	-2.58%
50	16.7	572.68	557.25	-2.77%
60	20.0	450.57	438.27	-2.81%
70	23.3	371.75	361.75	-2.76%

Tables 3.5 to 3.7 show comparisons of the buckling capacities from the FEA result and the expressions in the AISC LRFD and AASHTO specifications for the singly-symmetric sections #4, #5, and #6. Within each cell in the third and fourth column, the value on the top line is the prediction using the AISC or AASHTO expression, while the value on the second line is the percent difference with respect to the FEA results. A positive value of the percent difference indicates that the equation was conservative with respect to the FEA solution.

Table 3.5 Singly-Symmetric Section #4

Unbraced Length (ft.)	L/d Ratio	AISC LRFD Eq. 2.10	AASHTO Eq. 2.13	FEM Results
40	9.1	733.66 k-ft (+0.27%)	708.92 k-ft (+3.63%)	735.64 k-ft
50	11.3	508.43 k-ft (+0.33%)	488.20 k-ft (+4.30%)	510.11 k-ft
60	13.6	384.35 k-ft (+0.30%)	366.18 k-ft (+5.02%)	385.53 k-ft
70	15.8	308.01 k-ft (+0.28%)	290.85 k-ft (+5.84%)	308.88 k-ft
80	18.1	257.14 k-ft (+0.26%)	240.52 k-ft (+6.70%)	257.79 k-ft

Table 3.6 Singly-Symmetric Sectic #5				
Unbraced Length (ft.)	**L/d Ratio**	**AISC LRFD Eq. 2.10**	**AASHTO Eq. 2.13**	**FEM Results**
40	9.1	1300.03 k-ft (-2.71%)	1245.07 k-ft (+1.63%)	1265.76 k-ft
50	11.3	933.57 k-ft (-3.07%)	883.10 k-ft (+2.50%)	905.75 k-ft
60	13.6	728.12 k-ft (-3.16%)	679.34 k-ft (+3.75%)	705.78 k-ft
70	15.8	598.97 k-ft (-3.48%)	550.99 k-ft (+4.81%)	578.81 k-ft
80	18.1	510.86 k-ft (-3.49%)	463.48 k-ft (+6.11%)	493.64 k-ft

Table 3.7 Singly-Symmetric Section #6				
Unbraced Length (ft.)	**L/d Ratio**	**AISC LRFD Eq. 2.10**	**AASHTO Eq. 2.13**	**FEM Results**
50	10	1071.37 k-ft (-2.95%)	975.19 k-ft (+6.29%)	1040.68 k-ft
60	12	849.31 k-ft (-3.32%)	755.59 k-ft (+8.08%)	822.03 k-ft
70	14	709.14 k-ft (-3.54%)	616.29 k-ft (+10.01%)	684.87 k-ft
80	16	612.95 k-ft (-3.87%)	520.66 k-ft (+11.76%)	590.08 k-ft
90	18	542.69 k-ft (-4.06%)	451.13 k-ft (+13.49%)	521.49 k-ft

The results shown in Tables 3.5 through 3.7 show that the lateral torsional buckling equation in the AASHTO Specification provides reasonable estimates of the buckling capacity of the steel girders, though it is somewhat conservative for the plate girders studied. Although the LRFD expression shows closer agreement with the FEA solution, this expression is substantially more complex than the AASHTO expression.

In addition to the finite element analyses of the steel sections, three dimensional FEA studies of the completed bridges were also conducted. The FEA model of the completed bridge is discussed in Section 7.4.1. The FEA results of the completed bridge are presented in Chapter 7.

Chapter 4
Effects of Imperfections on Stability Brace Forces

4.1 Introduction

Although there are a number of factors that affect the magnitude and distribution of stability brace forces, the two primary factors are the brace stiffness and the magnitude and shape of the initial imperfection. Providing a brace stiffness equal to twice the ideal stiffness is generally recommended to control brace forces and deformations. By providing twice the ideal stiffness, deformations at the brace are generally limited to a value approximately equal to the initial imperfection. The critical imperfection for beams involves a twist of the cross-section that is often denoted as ϕ_o. Therefore if at least twice the ideal stiffness is provided, the maximum brace moment can be estimated using the following expression:

$$M_{br} = \beta_T \phi_o \tag{4.1}$$

where β_T is the provided brace system stiffness and ϕ_0 is the initial imperfection.

Equation 4.1 shows that the brace moment is directly related to the magnitude of the initial imperfection. Therefore, if the initial imperfection is doubled then the brace moment is also doubled. A key aspect of developing bracing provisions is to establish a recommended value of the initial imperfection, ϕ_o. In addition, to appropriately conduct studies on the bracing behavior of torsional bracing systems, the shape of the critical initial imperfection must also be established. The following section will present FEA results that established the critical imperfections used in the bracing studies presented in this dissertation, and results are summarized in Chapter 4.3.

4.2 Critical Imperfections for Torsional Bracing of Beams

As outlined in Chapter 3, this study included both eigenvalue buckling and large displacement analyses to study the behavior of torsional bracing systems. The large displacement analyses were conducted on imperfect systems to determine the strength requirements for the braces. To conduct such an analysis, the critical imperfection must first be determined. The critical imperfection is an initial out-of-straightness and/or twist that can reasonably occur in practice and will generally result in the maximum brace forces. Establishing the critical imperfection for torsional bracing systems requires appropriate selection of the magnitude and distribution of the initial imperfection, which can be a complicated problem. The complexity of selecting an imperfection occurs in determining how the cross-section should be twisted as well as how the twist should vary along the girder length. The determination of how the imperfection should be distributed along the girder length is often complicated by systems with multiple intermediate braces and moment gradient. The critical imperfection will be established in this chapter by first considering

systems with only one intermediate brace followed by systems with multiple intermediate braces.

Finite element results on the W14x22 section that was studied in the laboratory investigations were used to help define the critical twist on the cross-section. The initial imperfection of the two beams used in the twin girder experimental setup varied slightly from one another. One beam essentially had a pure lateral sweep of both flanges in a half sine curve shape of equal magnitude along the length. The second beam also had an imperfection with both flanges swept laterally in the same direction, however the top flange had a larger lateral sweep than the bottom flange. The maximum sweep for both beams was approximately 0.25 in. Although pure lateral sweep of the cross-section is generally not as critical as imperfections with twist, the sweep of the section can still produce significant brace moments. In these cases the girder essentially behaves like a "curved girder" with a relatively large radius of curvature. However, the difficulty associated with beams such as those in the experimental study that have such a pure sweep is trying to determine the "effective initial twist," ϕ_o, for use in an expression such as Eq. 4.1. A beam with a pure sweep does not have an initial twist. The problem is further complicated because the two beams of a twin girder system usually have different imperfections as was the case in the experimental studies conducted during this project. The purpose of the experimental program was to investigate the behavior of steel beams with skewed supports and also to validate design expressions established in the FEA studies. Although an equivalent twist was derived or back calculated from the experimental test data, FEA studies were also conducted on the test beams focusing on variations in the initial imperfection and the effect on the brace moment.

The W14x22 beams had a span of 33 ft. and were simply supported with twist prevented at the supports. A midspan point load was applied at the top flange. A torsional brace with a stiffness approximately equal to twice the ideal value was provided at midspan of the beams. Figure 4.1 shows graphs of the brace moment versus the applied load from the FEA analyses. A variety of initial imperfections were considered to evaluate the effects on the brace moment with the different imperfections labeled in the figure as Cases A-G.

The graph shows brace moments are relatively sensitive to the imperfection that is input to the analysis. The largest brace moment occurred with the Case A imperfection, in which the top flange was displaced an amount equal to 0.25 in. in one direction while the bottom flange had an initial out-of-straightness of 0.08 in. in the opposite direction. In Case B, the top flange had an initial out-of-straightness of 0.25 in. while the bottom flange was straight. The resulting brace moment is smaller than that observed for Case A, however the reason for this is probably because the Case A imperfection has a larger initial twist. For Case C the initial twist is the same as in Case B, however the flanges are displaced in opposite directions similar to Case A. The resulting brace moments in Case C are slightly smaller than those obtained in Case B. The similar behavior of the two cases labeled B and C indicates that the brace moment response is the most sensitive to the magnitude of the

initial twist. Case G shows the resulting brace moments for a section with a pure lateral sweep. The brace moments are substantially smaller than those from Cases A, B, and C. Cases D, E, and F were conducted to try to establish an equivalent twist for the laboratory tests by comparing the measured brace moments to those from the FEA analyses. The Case D imperfection produced brace moments that were very close the measured values.

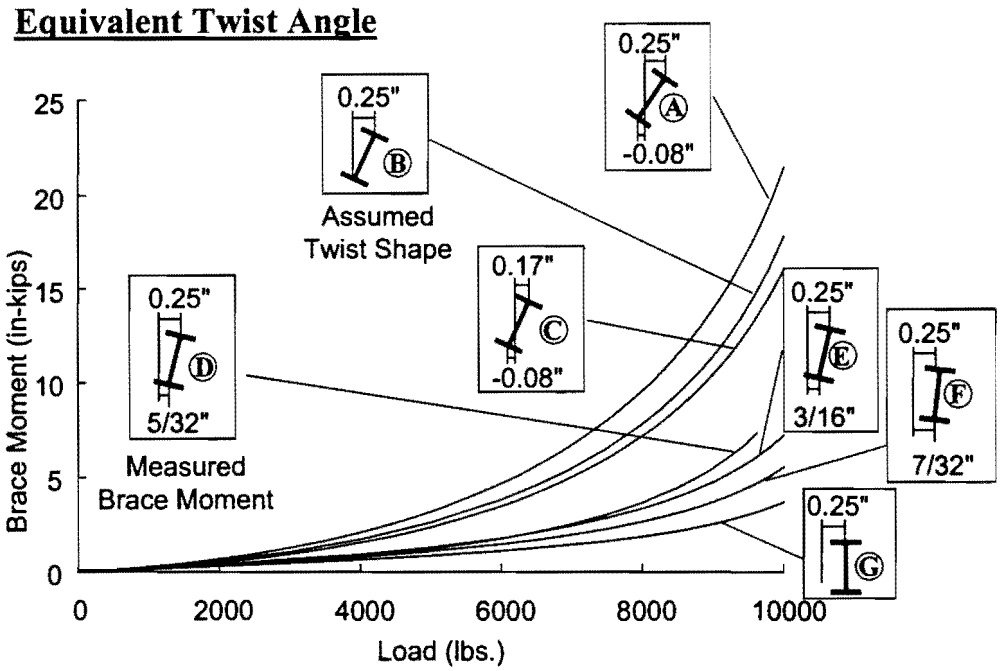

Figure 4.1: Effects of Imperfections on Brace Moments

Although the maximum sweep in the test beams was measured at 0.25 in., for design it is important to select an initial twist magnitude that is practical for the variety of imperfections that may be encountered in practice. The provisions in the AISC LRFD Specifications (2001) are based upon an initial imperfection such as that shown in Fig. 4.2, where L_b is the spacing between brace points. The top flange has an initial sweep of $L_b/500$ while the bottom flange is straight as in the Case B imperfection in Fig. 4.1. The $L_b/500$ lateral sweep of the top flange is consistent with the sweep tolerances for rolled beams. Utilizing the sweep tolerance of $L_b/500$, based upon the results shown in Fig. 4.1, the worst-case scenario with regard to the maximum brace moments would probably occur if both flanges had initial sweeps of $L_b/500$ in opposite directions. However, the likelihood of both flanges sweeping in opposite directions by magnitudes equal to the maximum sweep tolerances is relatively unlikely. Therefore the initial imperfection that will be assumed in this study will take the form of that shown in Fig. 4.2.

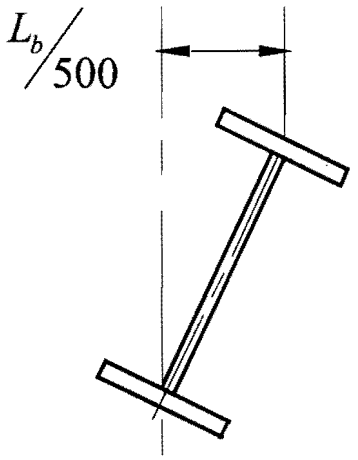

Figure 4.2: Assumed Initial Imperfection

Another concern with regard to the brace strength requirements from a large displacement analysis is the distribution of the initial imperfection along the girder length. This is particularly true for cases with multiple intermediate braces. Previous studies [Helwig et al. 1993] have demonstrated that the shape of the initial imperfection should generally contain one less wave than the buckled shape between brace points to produce the largest possible brace moment. Therefore for the W14x22 section with one intermediate brace as discussed above the shape of the critical imperfection would be similar to that of a half sine curve with the maximum twist occurring at midspan where the bending moment is the largest. However, for cases with more than one intermediate brace the shape of the critical imperfection can be somewhat more complicated since it isn't clear where the maximum twist should occur to produce the largest brace moment.

Figure 4.3 shows graphs of the brace moments from the FEA results for a W36x160 with two intermediate braces and a maximum unbraced length of 20 ft. The value of $L_b/500$ for the beam is therefore equal to 0.48 in. In the finite element model the bottom flange was kept straight while the top flange was displaced to twist the section along the girder length. The girders have zero twist at the supports and initial imperfections with four different distributions of twist along the length were analyzed. Results are shown for three different loading conditions in Figures 4.3a, 4.3b, and 4.3c for the respective cases of uniform moment loading, a distributed load applied at the top flange, and a midspan point load applied at the top flange. For all three load cases, twisting the section so that the maximum initial twist occurred at one of the brace points while the initial twist at the other brace was zero produced the worst case with regards to maximizing the brace forces. The graphs show the brace moment on the vertical axis versus the moment applied on beams on the horizontal axis for the different distributions of twist. The brace moment has been normalized by the maximum brace moment corresponding to the critical moment applied on the beam for the initial imperfection of Case 1, while the applied beam moment has been normalized by the beam buckling capacity that corresponds to the beam buckling between the brace points.

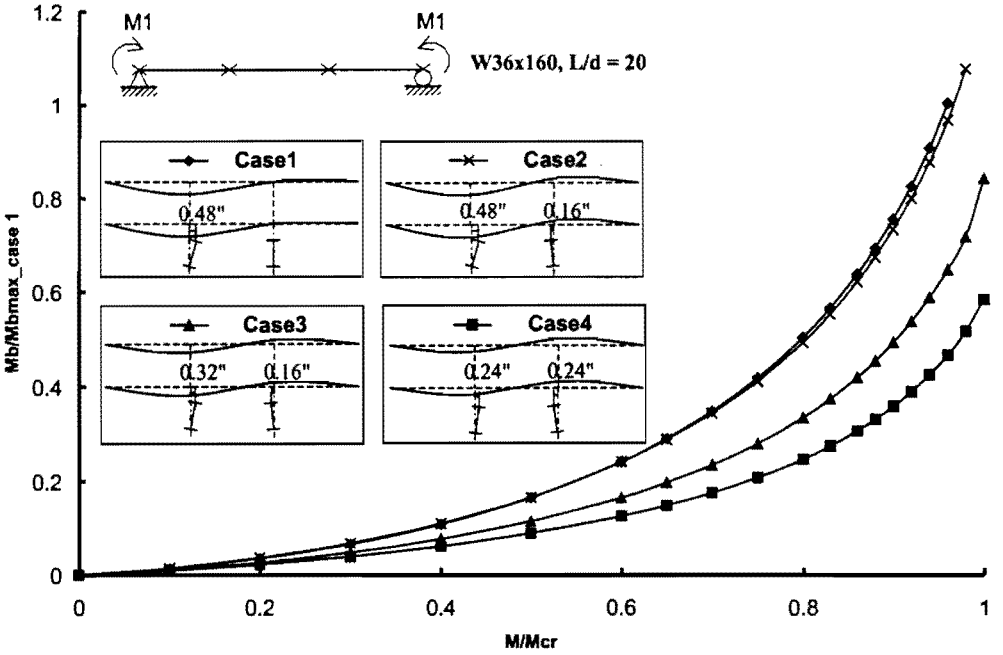

Figure 4.3 (a) Brace Moment versus Applied Moment for W36x160 with Uniform Moment – Effect of Shape of Imperfection

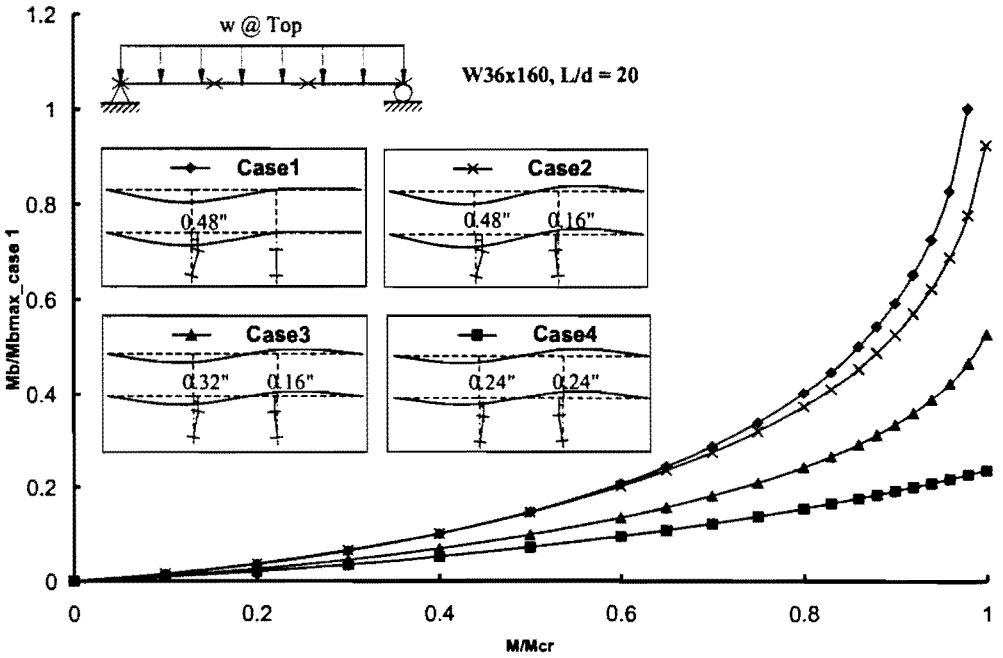

Figure 4.3 (b) Brace Moment versus Applied Moment for W36x160 with Uniform Distributed Load – Effect of Shape of Imperfection

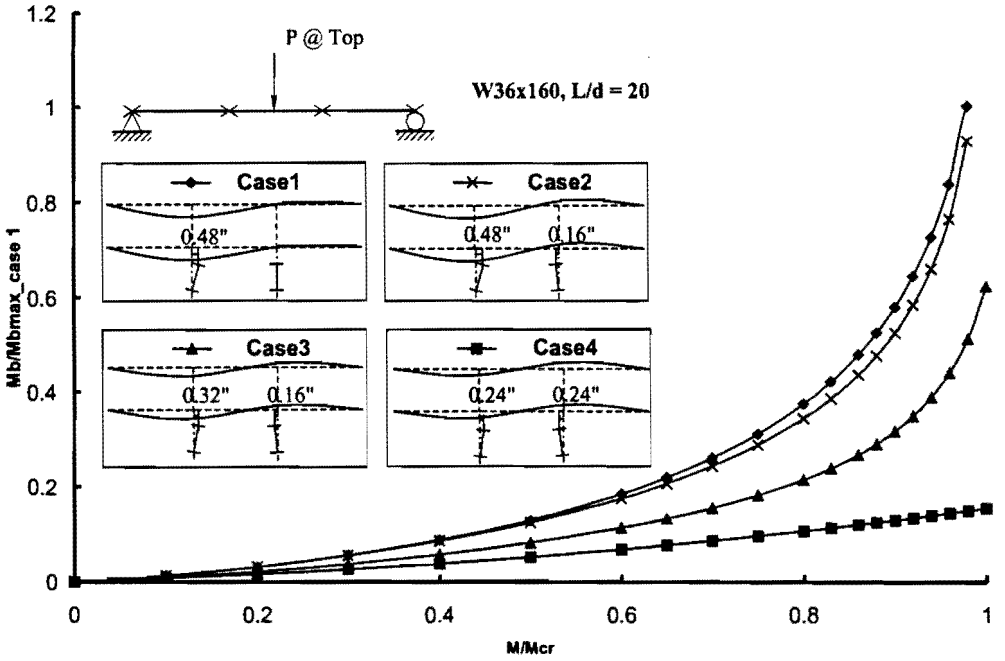

Figure 4.3 (c) Brace Moment versus Applied Moment for W36x160 with Point Load at Midspan – Effect of Shape of Imperfection

Results from the FEA analysis indicate that the maximum twist generally occurred at the brace closest to the point of maximum bending moment on the beam. The change in twist between the brace point nearest the point of maximum bending moment and the adjacent braces should be equal to ϕ_o, which is given in the following expression:

$$\phi_o = \frac{L_b}{500d} \tag{4.2}$$

where: d is the depth of the section, and L_b is the spacing between brace points.

A number of girder cross-sections with a variety of geometrical layouts that were considered in this study. The number of intermediate brace locations was varied from one to five with several different bracing orientations. Figure 4.4 shows the critical imperfections that were used for the variety of twin girder systems. The maximum twists of all of the beams were established using Eq. 4.2. The magnitudes of the twist at the adjacent cross-frames were essentially zero. The imperfections shown in Fig. 4.4 were used throughout the majority of the studies that will be presented in Chapters 5 and 6. The imperfections that were used in Chapter 7 differed slightly, since the braces in these cases were oriented perpendicular to the longitudinal axis of the girders with skewed supports. In these

instances, for girders with only one intermediate brace, the unbraced lengths of the beam sections adjacent to the brace are different. The initial twist used in these cases was based on the value given by Eq. 4.2 with the largest L_b. Results will be presented in Chapter 8 for a four-girder bridge. The imperfections that were used for these girders will be discussed in that chapter.

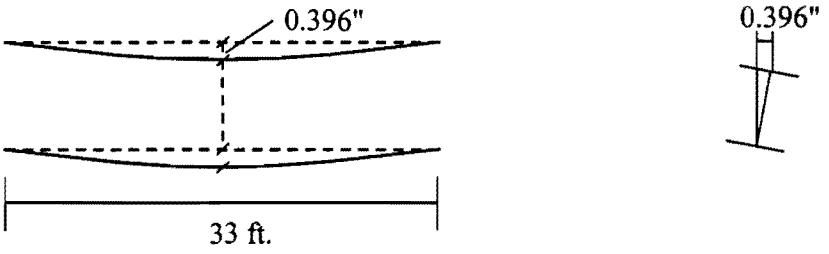

(a) W14x22 section

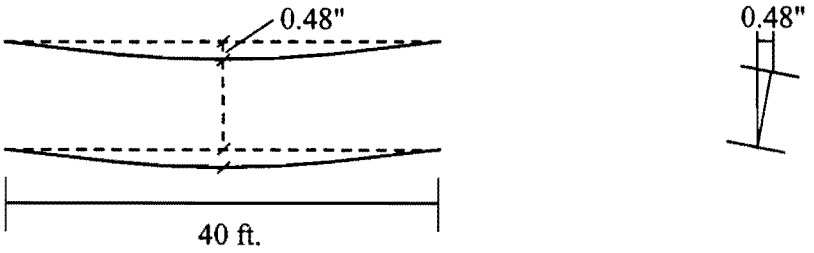

(b) W30x99 section

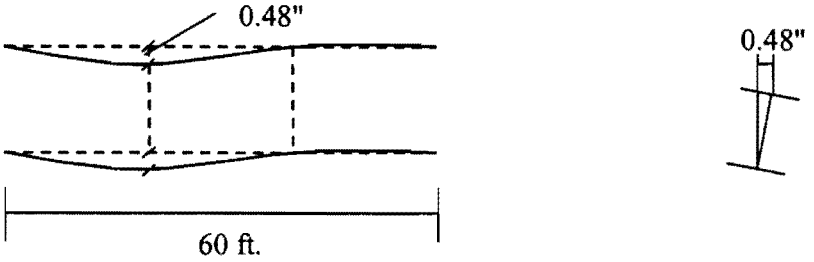

(c) W36x160 section

Figure 4.4 Shape and Magnitude of the Imperfections in FEA Studies

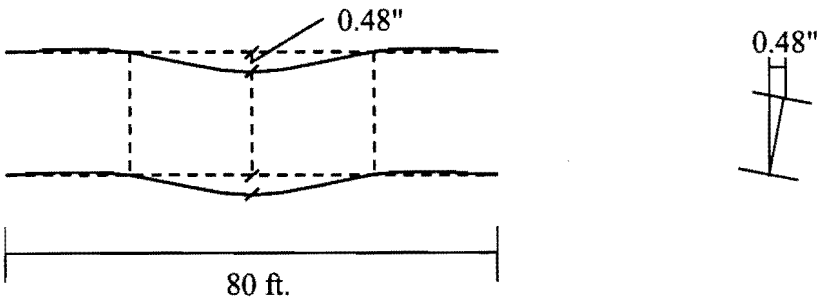

(d) Section #4

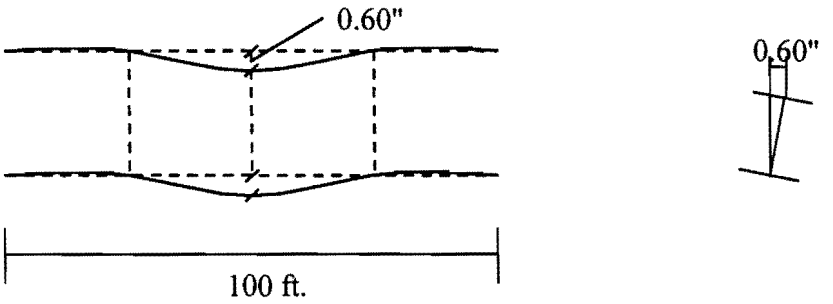

(e) Section #5

Figure 4.4 Shape and Magnitude of Imperfections in FEA Studies - continued

4.3 Summary

This chapter has focused on the selection of critical imperfections for torsional bracing systems. The critical imperfection that can be reasonably expected to occur in practice generally consists of a cross-sectional twist resulting from a lateral displacement of one flange while the other flange remains straight. A practical value for the maximum lateral flange displacement for both plate girders and rolled sections can be obtained using a value of $L_b/500$. This maximum lateral displacement is consistent with the sweep tolerances for rolled sections and results in the same imperfection that is assumed in the torsional bracing provisions in the AISC LRFD (2001) Specifications. Several different distributions of the twist were investigated. To maximize the brace forces, the maximum initial twist should generally occur near the brace closest to the point of maximum beam moment with zero twist at adjacent brace points.

Chapter 5
Bracing Requirements for Bridges with Normal Supports

5.1 Introduction

The lateral torsional buckling behavior of girders with normal supports was reviewed in Chapter 2 and equations were discussed for the brace stiffness and strength requirements. Finite element results are presented in this chapter for girders with normal supports. The different loading conditions that were considered in the analyses include uniform moment, a uniformly distributed load applied at the top flange, and a concentrated top flange load at mid-span. The FEA results are compared with the solutions previously outlined in Chapter 2. Results are shown for both the rolled beam sections and singly symmetric girder sections that were shown in Fig. 3.7. Analyses were conducted on two, three, and four-girder systems.

Results from eigenvalue buckling analyses of twin-girder systems are compared with the brace stiffness requirements in Section 5.2. The girder span-to-depth ratios studied varied from 16 to 29 with one or multiple braces. Tension-only cross frames were used for the braces. Finite element results from the large displacement analyses of twin-girder systems will be presented in Section 5.3. These results will be compared to the strength requirements previously outlined in Chapter 2. The strength solutions are also shown with a slight modification to improve the prediction of the brace strength for a variety of moment levels. Eigenvalue and large displacement analytical results for three and four girder systems are presented in Section 5.4. Finally, the computational results for the bracing behavior of girders with normal supports are summarized in Section 5.5.

For many of the girder cross-sections that were considered in this investigation, comparisons between the FEA results and the equations showed similar trends. In these cases, representative results are presented and discussed, while redundant results for sections with similar behavior are presented in the appendix.

5.2 Comparison of Normal Girder Stiffness Requirements with FEA Results

The equations for the normal girder brace stiffness requirements were presented in Chapter 2. The solution presented included the effects of moment gradient and load height on the bracing behavior. In this section, results for twin-girder systems with single or multiple braces are presented. A variety of loading cases were considered in the analyses, including uniform moment, uniformly distributed loads and concentrated loads at mid-span. All transverse loads were applied at the top flange. Moment gradient factors for hand calculations were evaluated using the formula from the AISC and AASHTO LRFD specifications that was given in Eq. 2.15. Since full-depth cross-frames were used in the FEA models, the bracing members framed into the girders at the top and bottom flange locations, and cross sectional distortion had no effect on the overall bracing stiffness. The

equation for bracing stiffness for the systems considered can therefore be simplified to the following expression:

$$\frac{1}{\beta_T} = \frac{1}{\beta_g} + \frac{1}{\beta_b} \tag{5.1}$$

where: β_T is the bracing system stiffness, β_g is the girder in-plane stiffness, and β_b is the brace stiffness.

Figure 5.1 shows a comparison of results from the equations presented in Chapter 2 with the FEA results for a W14x22 section. The two members in the twin-girder system were spaced 78 inches apart and had a span of 33 feet. Since one midspan brace was used, the unbraced length was 16.5 feet. Figures 5.1 (a), (b) and (c) illustrate the respective systems under loading conditions of uniform moment, uniformly distributed loads applied at the top flange, and a concentrated top-flange load at midspan. The beam buckling capacity is graphed on the vertical axis while the brace stiffness is graphed on the horizontal axis. The buckling moment has been normalized by the moment corresponding to buckling between the brace points. The brace stiffness has been normalized by the ideal brace stiffness calculated from Eqs. 2.18 and 2.19. Each of the figures shows a profile of the girders and depicts the type of loading and the layout of the intermediate braces. A plan view is also shown that clearly shows the orientation of the bracing. Since the girders presented in this chapter all had normal supports, the braces were perpendicular to the longitudinal axis of the girders. In Chapters 6, 7, and 8, which focus on bridges with skewed supports, these plan views will help indicate the orientation and layout of the braces relative to the skew angle.

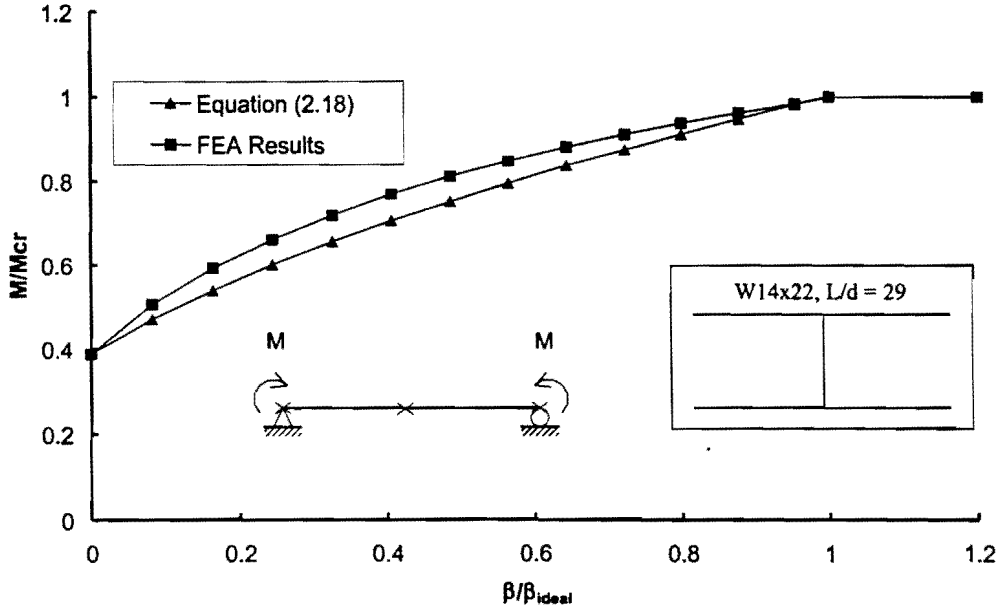

Figure 5.1 (a) M/M_{cr} versus β/β_{ideal} for a W14x22 Section with Uniform Moment

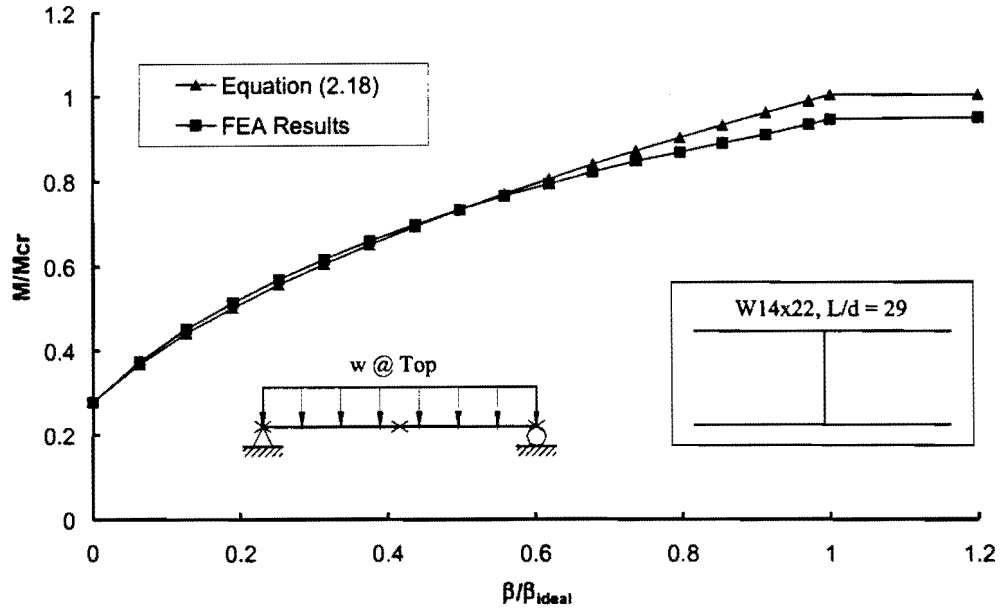

Figure 5.1 (b) M/M_{cr} versus β/β_{ideal} for a W14x22 Section with Distributed Load on Top Flange

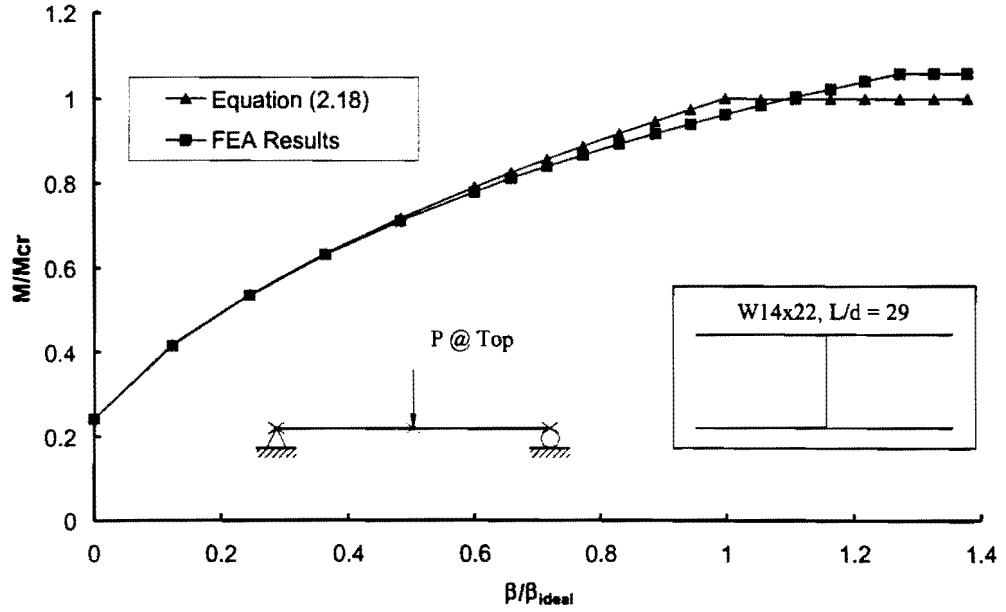

Figure 5.1 (c) M/M_{cr} versus β/β_{ideal} for a W14x22 Section with Concentrated Top-flange Loads at Midspan

The graphs show good agreement between the computational results and the equations introduced in Chapter 2 in prediction of the ideal brace stiffness. The equations are the most accurate at predicting the ideal stiffness for the case with uniform moment loading which makes sense since they were developed for this loading case. For the cases with transverse loads applied at the top flange, the equation results are slightly unconservative with respect to the FEA results. The primary source for this difference between the equation and the FEA results is due to load height effects. Although the factor C_t is used in Eq. 2.18 to account for top flange loading, the C_b factors don't reflect effects of top flange loading on the buckling capacity. As a result, for distributed loads at the top flange shown in Fig. 5.1(b), the equation overestimates the buckling capacity by about 6% compared to the FEA results. For the case with a midspan point load at the top flange, load height has very little effect on the buckling capacity since the point loads are applied directly at the brace location. The difference between the FEA solution and equations in Fig. 5.1(c) is due to the value of the C_{bb} factor that results from using Eq. 2.14, which often provides conservative estimates of the C_b factors. As outlined in Chapter 2, the bracing expressions are often a function of the moment gradient factor corresponding to buckling between brace points, which is denoted by C_{bb}. Although constant C_b values are often used for particular load cases, the actual C_b values are a function of the warping stiffness of a section. For example, the estimated value of C_{bb} = 1.67 for the case in Fig. 5.1c differs from the actual value of C_{bb} = 1.76 for the W14x22 with a ratio of L/d of 29. The actual value of C_{bb} = 1.76 was determined from an FEA analysis. The C_b factor is used to evaluate both M_{cr} and β_{ideal}.

Eigenvalue buckling analyses were also performed on a W30x99 section, which had a 40 ft. span (L/d =16) and a girder spacing of 100 in. With one brace at midspan, the unbraced length was 20 feet. The comparison of the FEA results and equation results for the W30x99 section is very similar to that of the W14x22 section and is shown in Appendix A.

Figure 5.2 shows the comparison of the results from the equations and the FEA analysis for the W36x160 section. This twin-girder system had a 60 ft. span and a girder spacing of 120 inches. Intermediate braces were placed at the third points to provide an unbraced length of 20 feet. Figures 5.2 (a), (b), and (c) illustrate the system under loading conditions of uniform moment, uniformly distributed loads applied at the top flange, and a concentrated top-flange load at midspan, respectively.

The graphs show that the computational results have good agreement with the equations, particularly for the case of uniform moment loading. For cases of uniformly distributed loads and midspan point loads, the equations generally provide conservative estimates of moment with respect to the FEA solutions for most β/β_{ideal} ratios. The primary reason for the large difference between the two solutions is because the equation conservatively neglects the warping restraint provided to the middle third of the beam by the exterior thirds. For lower values of the brace stiffness, some of the conservative nature of the equations with respect to the FEA results is probably due to the relatively stocky nature of the W36x160.

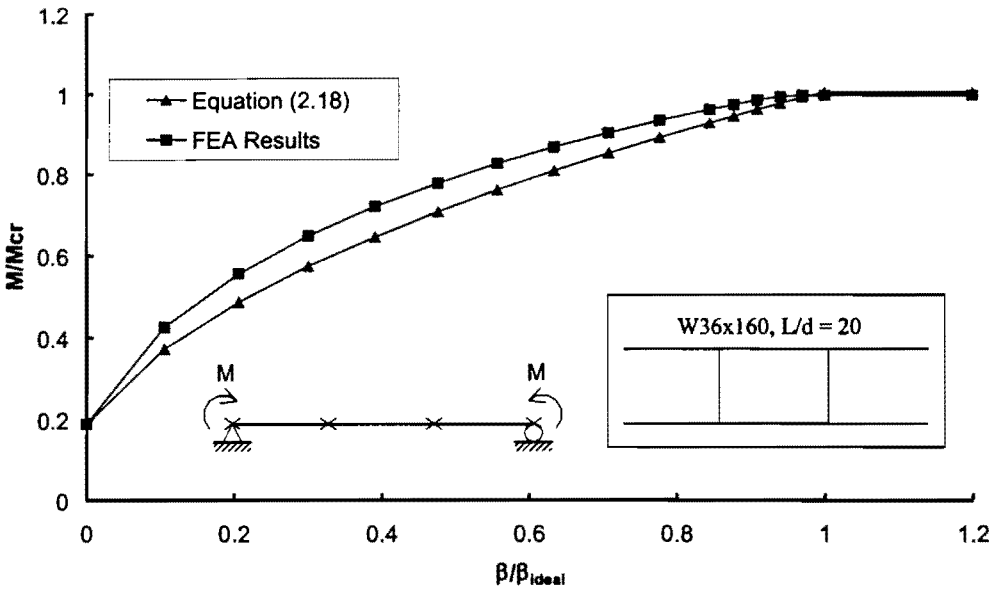

Figure 5.2 (a) M/M_{cr} versus β/β_{ideal} for a W36x160 Section with Uniform Moment

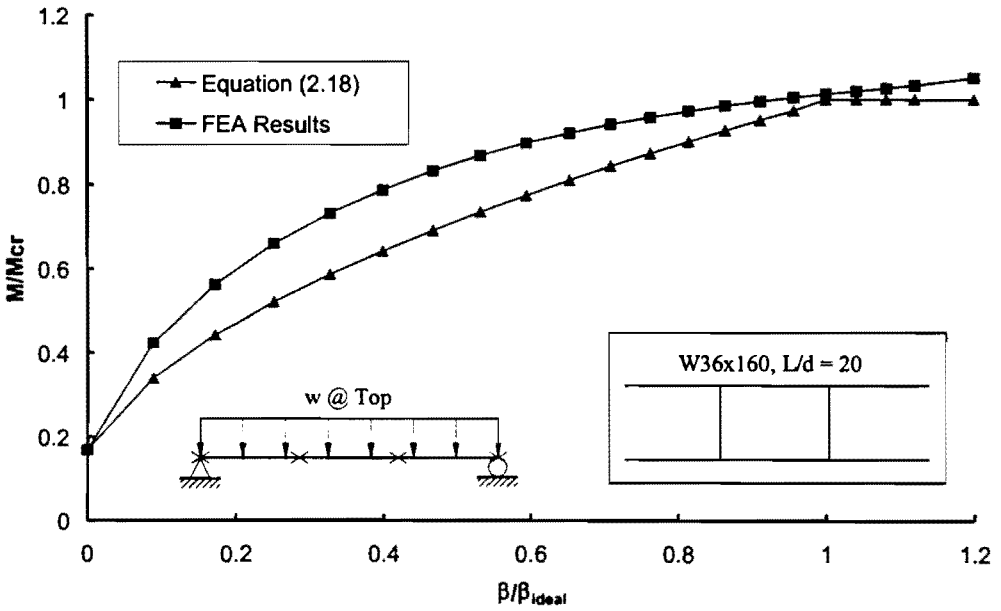

Figure 5.2 (b) M/M_{cr} versus β/β_{ideal} for a W36x160 Section with Distributed Load on Top Flange

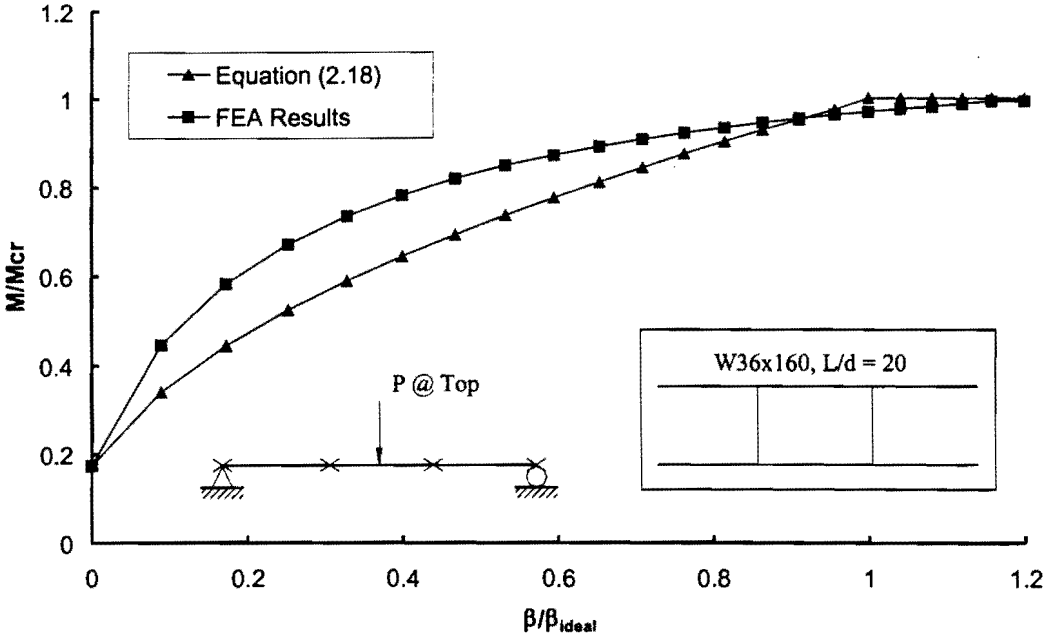

Figure 5.2 (c) M/M_{cr} versus β/β_{ideal} for a W36x160 Section with Concentrated Load on Top Flange at Midspan

Effects of top flange loading are not as significant with two intermediate braces when compared to cases with only one intermediate brace. This is demonstrated in Fig. 5.2b by the relatively small difference between the equations and the FEA results for $\beta/\beta_{ideal} > 1.0$ compared to the respective case shown previously in Fig. 5.1b. Load height effects for the case with a top flange point load at midspan shown in Fig. 5.2c are noticeable since the equation slightly overestimates the capacity relative to the FEA results (for $\beta/\beta_{ideal} > 1.0$), however the effects are less than was observed in Fig. 5.1c.

Figure 5.3 shows the comparison of results from the equations and the FEA solutions for the singly-symmetric Section #4. The twin-girder system had a span of 80 feet and a girder spacing of 120 inches. Three intermediate braces were employed to give an unbraced length of 20 feet. Figures 5.3 (a), (b) and (c) illustrate the system under loading conditions of uniform moment, uniformly distributed loads applied at the top flange, and concentrated top-flange loads at midspan, respectively.

The graphs show good agreement between the computational results and the equations, particularly for the uniform moment loading case. The AISC LRFD equation for singly-symmetric sections (Eq. 2.10) was used to estimate the critical capacity for buckling between brace points. The equation overestimates the buckling capacity by approximately 3% with respect to the FEA results when the girder buckles between the brace points. Use of the AASHTO expression for lateral torsional buckling would lead to additional conservatism

since the compression flange (top flange) of the singly-symmetric sections is the smaller flange, however the amount of conservatism would generally be less than 10%.

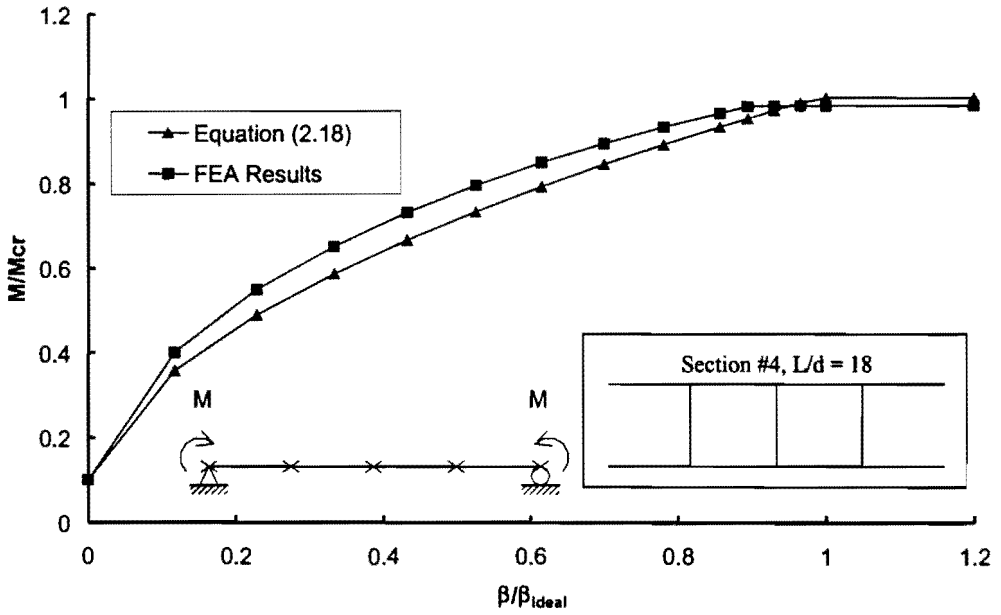

Figure 5.3 (a) M/M_{cr} versus β/β_{ideal} for Section #4 with Uniform Moment

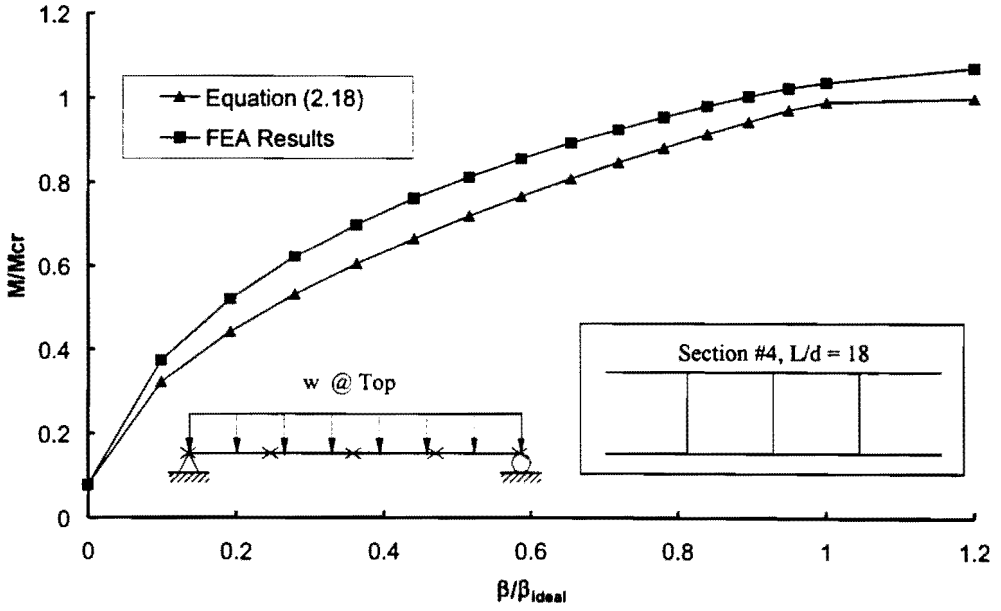

Figure 5.3 (b) M/M_{cr} versus β/β_{ideal} for Section #4 with Distributed Loads on Top Flange

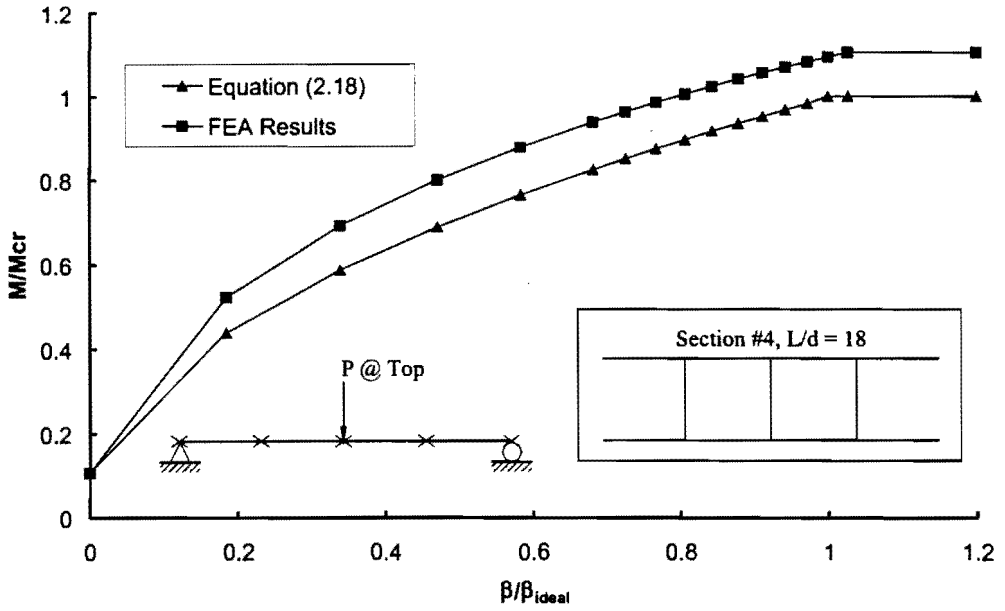

Figure 5.3 (c) M/M_{cr} versus β/β_{ideal} for Section #4 with Concentrated Top-flange Loads at Midspan

As discussed for the graphs previously shown in Figs. 5.2b and 5.2c, the cases with a moment gradient, the buckling capacity from the FEA results are approximately 10% higher than the equations due to the warping restraint provided by the outside quarters of the beams. With three intermediate braces, the effects of load height have a minimal effect on the buckling capacity. The results for the other singly-symmetric Sections #5 and #6 are similar to the results of Section #4 and are presented in Appendix A.

Overall, Figs. 5.1 to 5.3 (as well as the corresponding results shown in the Appendix) show that the solutions presented in Chapter 2 provide good estimates of the ideal brace stiffness. Most of the differences between the graphs of the FEA solution and the equations were primarily caused by differences in evaluating the buckling capacity of the girder once full bracing was achieved and the beam buckled between brace points. These differences were mainly due to either warping restraint or load height effects, both of which are usually neglected in hand solutions.

For the cases with moment gradient and multiple braces along the girder length, the middle segment is usually more critical than the segments close to the ends. When the girder buckles between the brace points, the outside segments provide extra warping restraint to the middle segment, which results in a higher buckling capacity. The warping restraint is generally neglected in hand calculations, which leads to conservative estimates of the buckling capacity and brace stiffness requirements. Top flange loading has an effect on the critical buckling capacity for the systems, however these effects were most predominant with

only one intermediate brace at midspan. Load height effects become less significant for systems with more than one intermediate brace.

5.3 Comparison of Normal Girder Strength Requirements with FEA Results

The equations for the brace strength requirements for girders with normal supports were presented in Chapter 2. This section will present and compare results on the brace strength requirements from FEA analyses and the previously presented equations. As mentioned in Chapter 3, large displacement analyses are required to investigate the brace strength requirements. The magnitudes of the brace forces are directly related to the shape and magnitude of the initial imperfection as discussed in the previously chapter. Therefore, the critical imperfection discussed in Chapter 4 was utilized to maximize the potential brace forces.

The brace strength requirements presented in Chapter 2 use the following equation to predict the total twist angle for a beam with an initial twist angle, ϕ_0.

$$\phi_T = \frac{\phi_0}{1 - \frac{\beta_{Ti}}{\beta_T}\frac{M^*}{M_{cr}}} \tag{5.2}$$

where: β_{Ti} is the ideal torsional brace stiffness, β_T is the brace stiffness provided, M^* is the maximum applied moment, and M_{cr} is the critical moment corresponding to buckling between braces. The brace moment can then be estimated using Hooke's law:

$$M_{br} = \beta_T(\phi_T - \phi_0) \tag{5.3}$$

The total twist angle ϕ_T that results from Eq. 5.2 for a beam with an initial imperfection ϕ_o and a brace stiffness of twice the ideal value is equal to twice the initial twist angle at a moment level of M_{cr}. Equations 5.2 and 5.3 were developed in previous studies [Yura and Phillips 1992] on torsional bracing behavior for beams. A comparison of results from the solution and FEA analyses is illustrated in Fig. 5.4 for a W14x22 section. The solution is conservative for loads less than approximately 90% of the critical load. However, the solution shows good agreement with the FEA results for loads at or near the critical load, albeit slightly unconservative for the case shown. The slight unconservative nature of the solution comes from the assumption that the total twist is equal to twice the initial twist, ϕ_o, when a stiffness of twice the ideal value is provided. In reality, the twist is slightly larger than twice the initial imperfection, however the difference is not too significant.

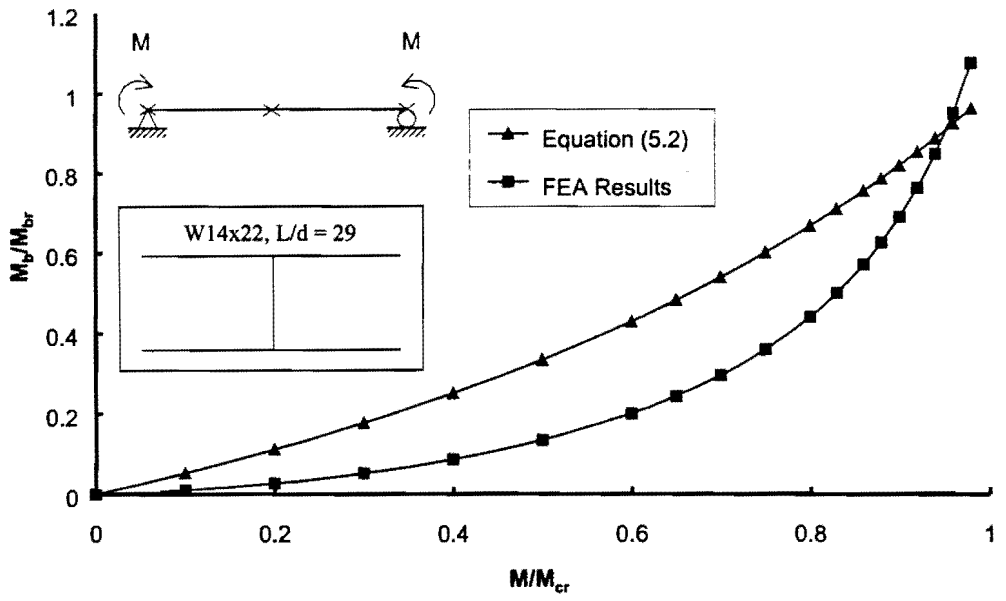

Figure 5.4 M_b/M_{br} versus M/M_{cr} for a W14x22 Section with Uniform Moment

Based upon the FEA results in this study, Eq. 5.2 was modified as shown in Eq. 5.4 to provide better estimates of the brace moments. The change consists of simply squaring the moment term.

$$\phi_T = \frac{\phi_0}{1 - \frac{\beta_{Ti}}{\beta_T}\left(\frac{M^*}{M_{cr}}\right)^2} \tag{5.4}$$

Figure 5.5 shows a comparison between the FEA results and the predicted brace moment utilizing Eq. 5.4 for ϕ_T in Eq. 5.3 for the W14x22 section with uniform moment loading. The accuracy of the prediction for the W14x22 section with uniform moment loading is substantially better for all brace moments than that previously shown in Fig. 5.4.

Figures 5.6a, b, and c show good agreement was also obtained with Section #5 for the respective load cases of uniform moment, uniform distributed loads at the top flange, and a midspan point load applied at the top flange. Graphs for the other sections also showed good agreement between the predicted brace moment and the FEA analyses and are presented in the Appendix.

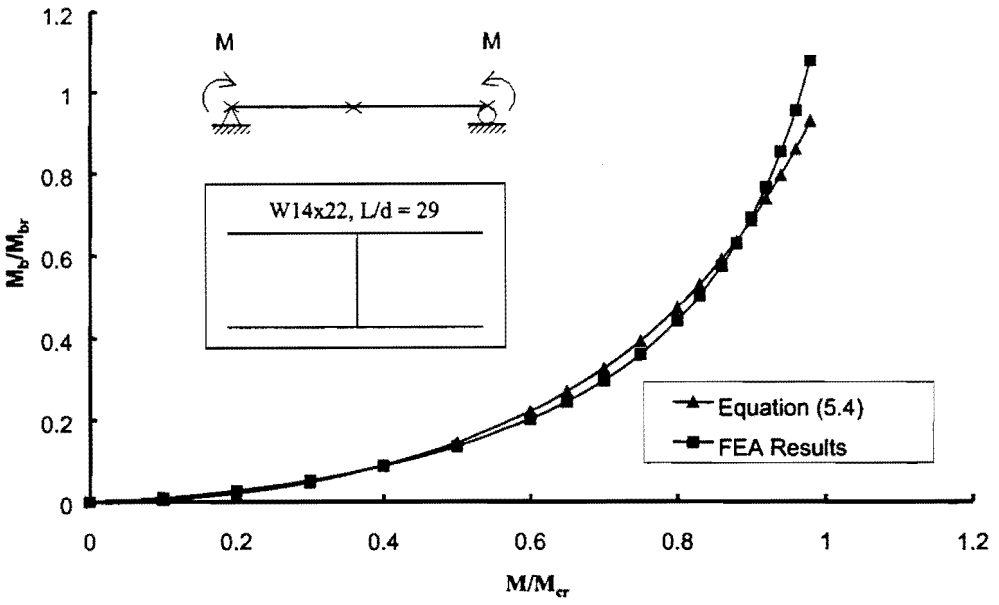

Figure 5.5 M_b/M_{br} versus M/M_{cr} for a W14x22 Section with Uniform Moment

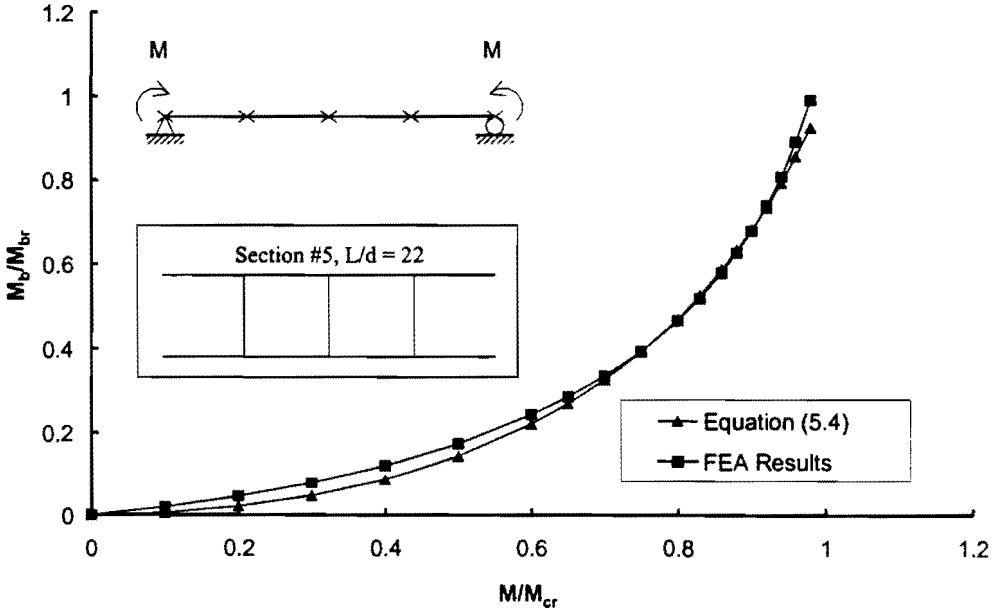

Figure 5.6 (a) M_b/M_{br} versus M/M_{cr} for Section #5 with Uniform Moment

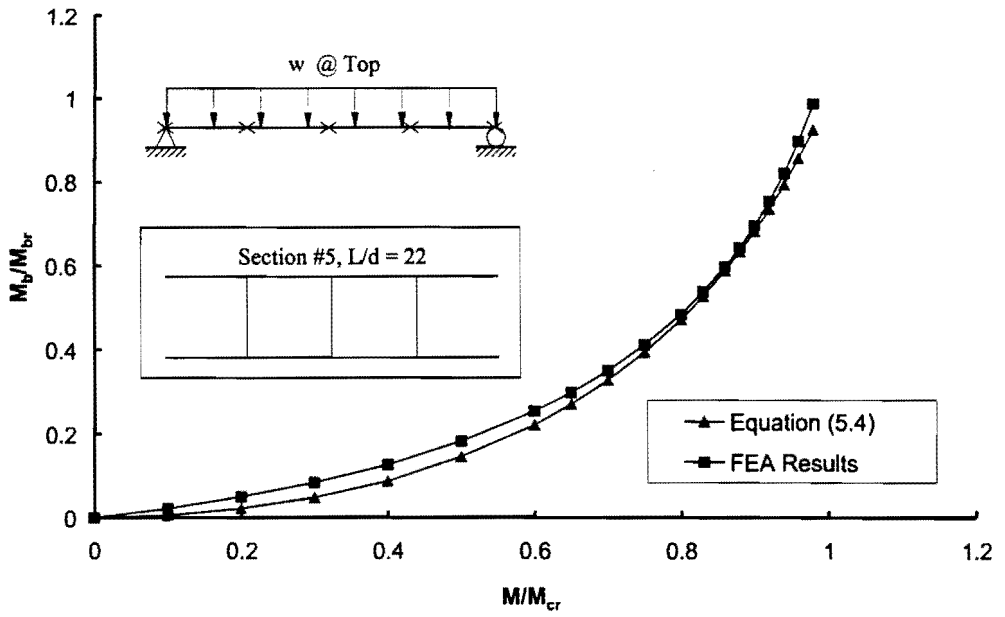

Figure 5.6 (b) M_b/M_{br} versus M/M_{cr} for Section #5 with Distributed Loads on Top Flange

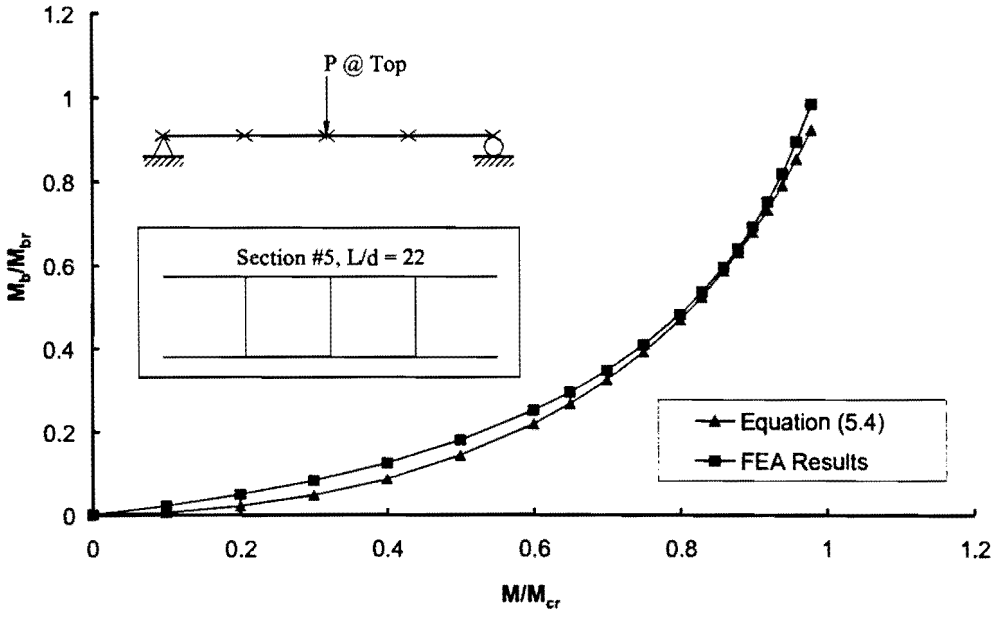

Figure 5.6 (c) M_b/M_{br} versus M/M_{cr} for Section #5 with Concentrated Loads on Top Flange at Midspan

The behavior of the W36x160 differed from the other four sections because the maximum moment occurred between brace points instead of directly at a brace. The twin girder system had two intermediate braces located at the third points. Figure 5.7 shows the comparison of Eq. 5.4 with the FEA results for the W36x160 section. The graphs show that Eq. 5.4 has good agreement with the FEA results for uniform moment loading (Fig. 5.7a). However, for cases with a moment gradient, the solution is relatively conservative with respect to the FEA results. The conservative nature of the equations for cases with moment gradient is due to the location of the maximum applied moment relative to the brace location. The maximum applied moment occurs at midspan, while the intermediate braces are located at the third points. When the maximum moment occurs between brace points, adjacent braces share the brace moment instead of a single brace providing the majority of the restraint, which is the case when the maximum moment occurs at the brace location. Although the equations were conservative for the W36x160, the graphs shown in this section as well as in the appendix demonstrate that the equations do a reasonable job of predicting the brace moments.

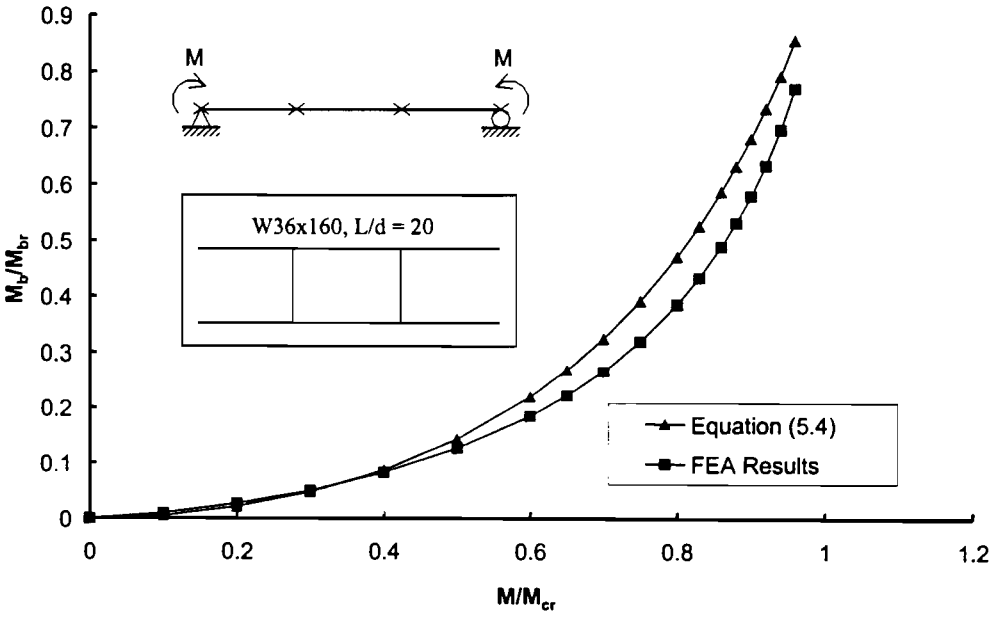

Figure 5.7 (a) M_b/M_{br} versus M/M_{cr} for W36x160 Section with Uniform Moment

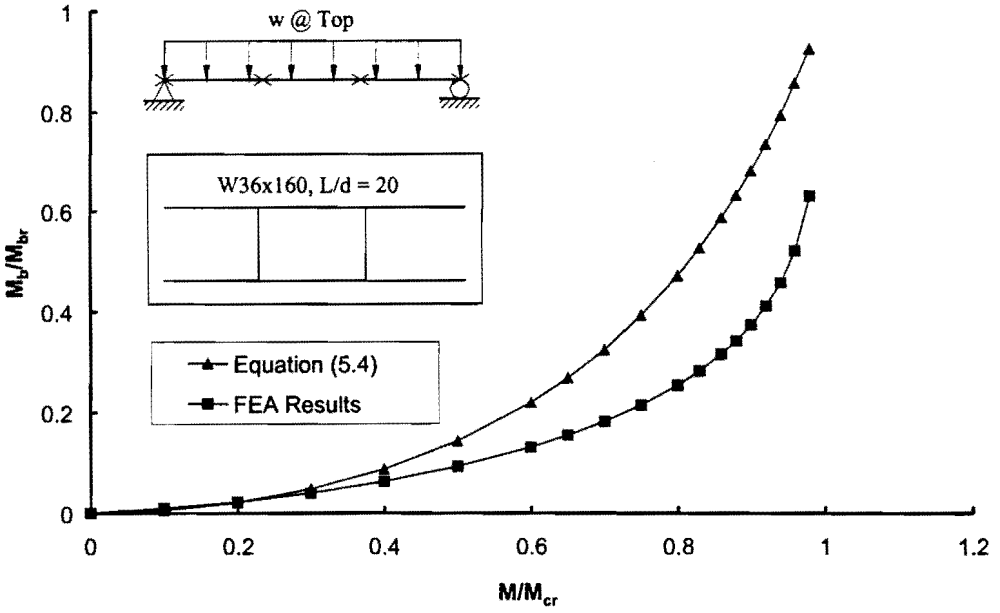

Figure 5.7 (b) M_b/M_{br} versus M/M_{cr} for W36x160 Section with Distributed Load on Top Flange

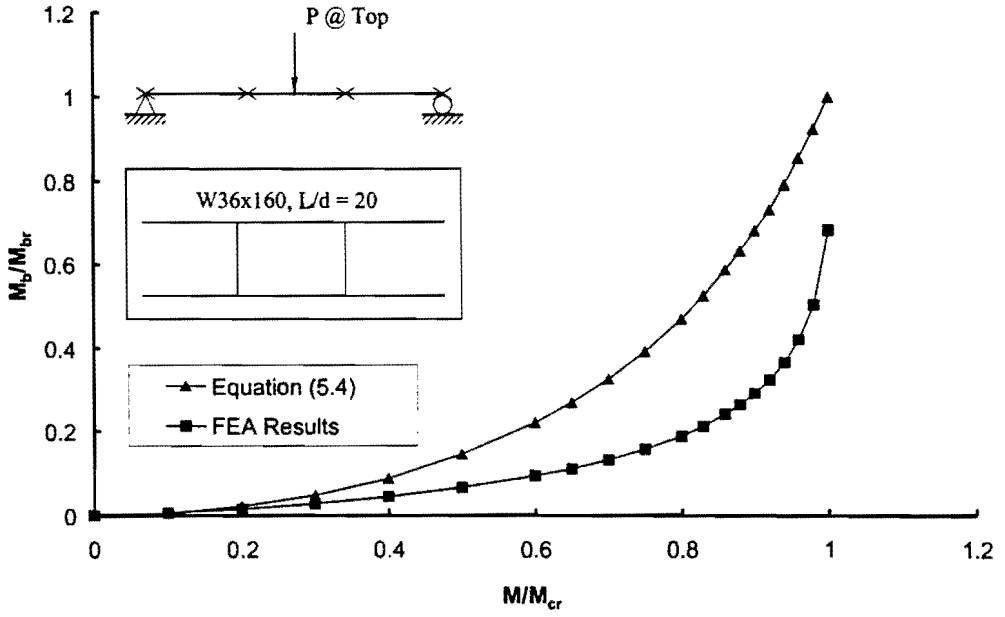

Figure 5.7 (c) M_b/M_{br} versus M/M_{cr} for W36x160 Section with Midspan Concentrated Loads on Top Flange

5.4 Brace Stiffness and Strength Requirements for Systems with Several Girders

The results presented thus far have focused on twin girder systems. Since most systems consist of several girders through the width of the bridge, three- and four- girder systems were also considered to study the effect of girder interaction. Little research has been published on the brace stiffness requirements for systems with more than two-girders. One of the major differences in bracing behavior in systems with several girders is the effect of the in-plane girder stiffness, since the girders are often tied together through the width of the bridge. The original development of the brace stiffness component of the in-plane stiffness by Helwig et al. [1993] considered a twin girder system. Yura [1994] modified this twin-girder solution to yield the following expression:

$$\beta_g = \frac{24(n_g - 1)^2}{n_g} \frac{S^2 E I_x}{L^3} \tag{5.6}$$

where:

S = girder spacing
I_x = moment of inertia of girder at strong axis
L = girder length
n_g = the number of the girders

For systems with several girders, the in-plane girder stiffness becomes relatively large and has significantly less effect on the overall brace stiffness than was observed with twin-girder systems.

The equations for the brace stiffness requirements for three- and four-girder systems are presented in this section and are compared with results from the FEA solutions. The equations used to calculate the total stiffness for each individual brace are presented in Chapter 2. The expression to convert the discrete torsional brace stiffness to the equivalent continuous torsional brace stiffness were modified using the following equation:

$$\overline{\beta_T} = \frac{2 n_i n_c \beta_T}{\alpha n_g L} \tag{5.7}$$

where $\alpha = 0.75$ for a single torsional brace at midspan; $\alpha = 1.0$ for cases with more than one intermediate brace; n_i is the number of intermediate brace locations along the girder length; n_c is the number of braces at a single brace location (across the width of the bridge); and n_g is the number of the girders. For example, $n_c = 2$ for a 3-girder system and $n_c = 3$ for a 4-girder system.

Although FEA analyses were performed on three- and four-girder systems with all five sections shown previously in Fig. 3.7, the sections exhibited similar behavior with respect to the bracing equations. Therefore, typical results for a few of the sections are shown in this

section, while the remainder of the results are presented in the Appendix. Equations 5.6 and 5.7 were used to evaluate the brace stiffness requirements. Figures 5.8 and 5.9 show the respective results for a three-girder system with W30x99 sections and a four-girder system using Section #5. The comparisons between the equations and the FEA results that are presented in this chapter are similar to the results for the other sections presented in the Appendix.

The graphs show that Eq. 5.7 does a good job of estimating the ideal brace stiffness for three- and four-girder systems, particularly for the uniform moment loading. For cases with moment gradient the results are either conservative or unconservative, depending on which case is considered. For example, in Fig. 5.8, the equations are approximately 8% unconservative with respect to the FEA results for the W30x99 section. The unconservative nature of the predicted results is primarily due to the effects of load height as outlined previously. For cases with multiple braces and moment gradient, warping restraints in segments with lower moment levels and these restraints lead to conservative estimates of the buckling behavior. This effect is demonstrated in Figs. 5.9b and c for Section #5. The FEA results are approximately 10 % higher than the equations due to the warping restraint provided by the outside segments of the beams.

The remainder of this section will present FEA large displacement analysis results for multi-girder system. The comparison of the FEA results with results from the bracing equations are shown in Fig. 5.10 and Figure 5.11. The graphs show that good agreement between the equation and the FEA results for multi-girder system.

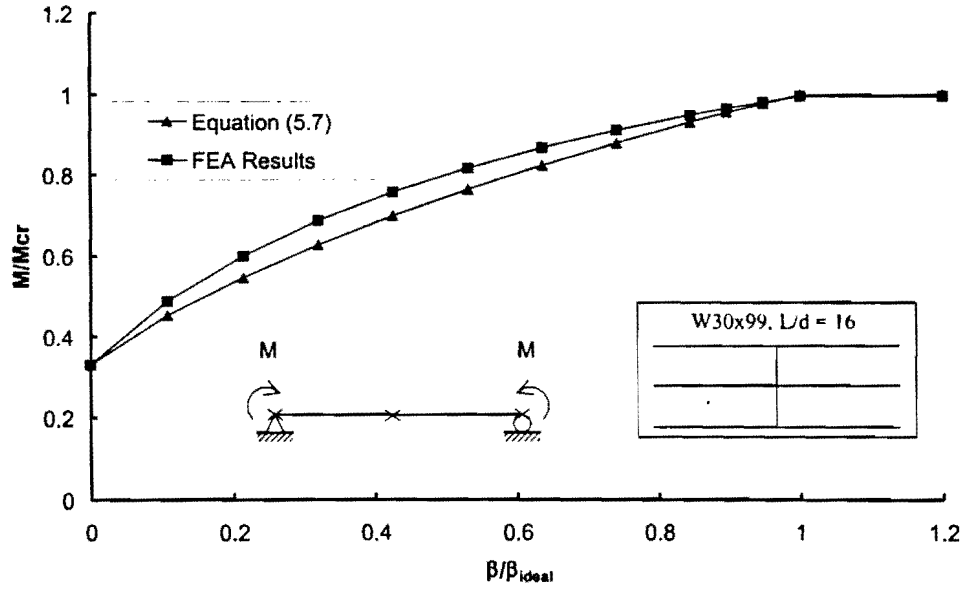

Figure 5.8 (a) M/M_{cr} versus β/β_{ideal} for a W30x99 Section 3-girder System with Uniform Moment

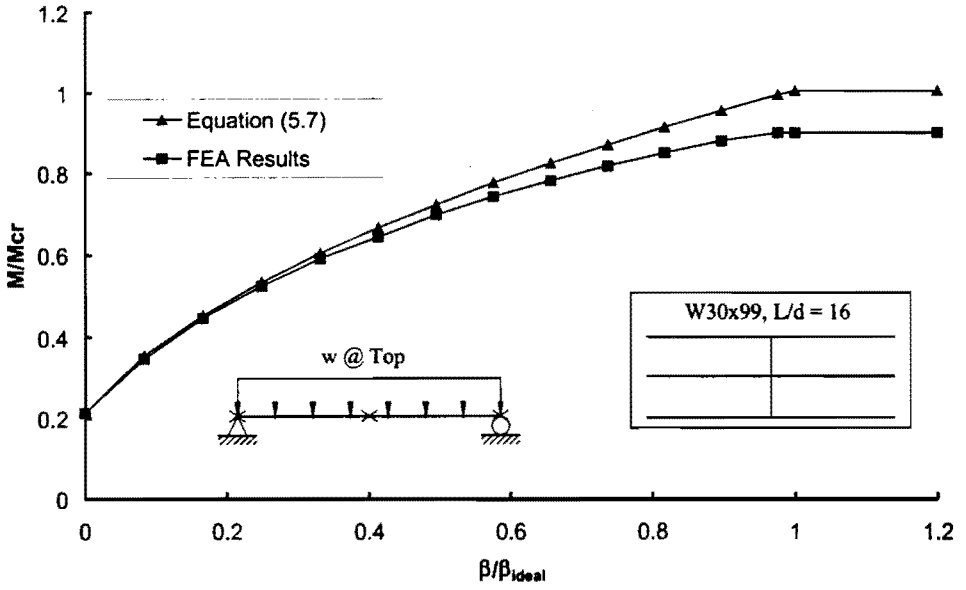

Figure 5.8 (b) M/M_{cr} versus β/β_{ideal} for a W30x99 Section 3-girder System with Distributed Loads on Top Flange

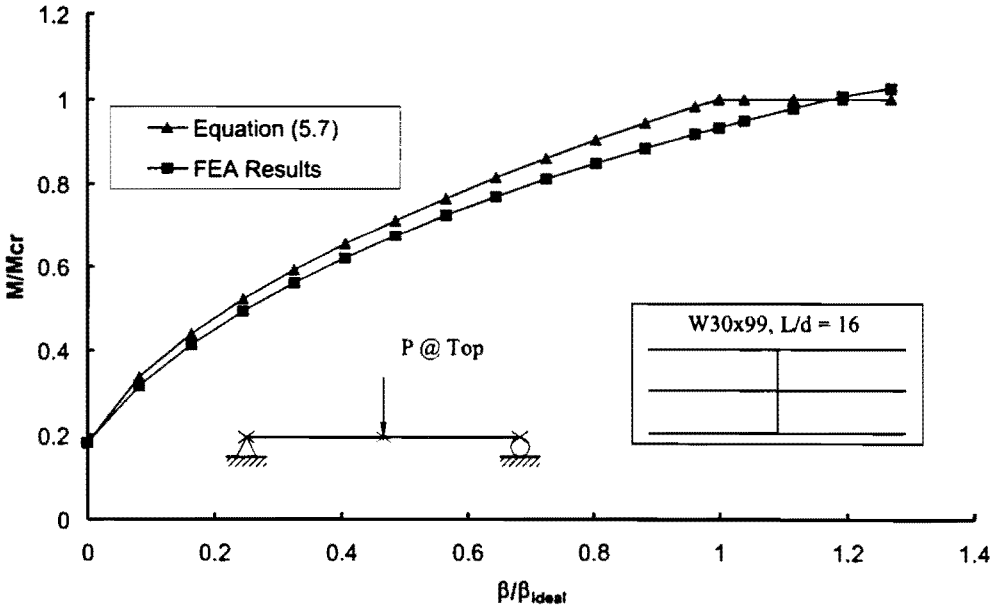

Figure 5.8 (c) M/M_{cr} versus β/β_{ideal} for a W30x90 Section 3-girder System with Midspan Concentrated Loads on Top Flange

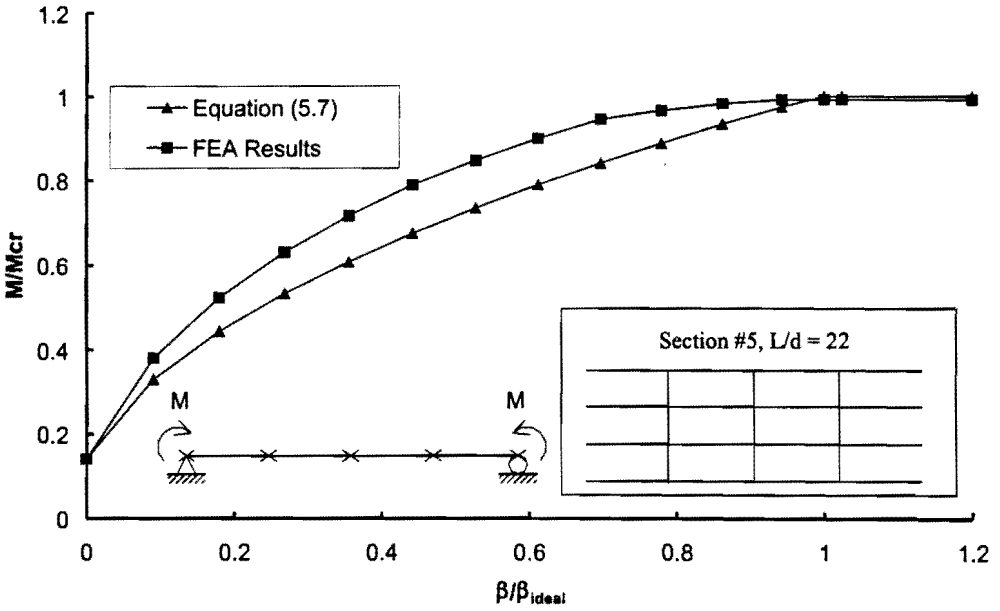

Figure 5.9 (a) M/M_{cr} versus β/β_{ideal} for Section #5 4-girder System with Uniform Moment

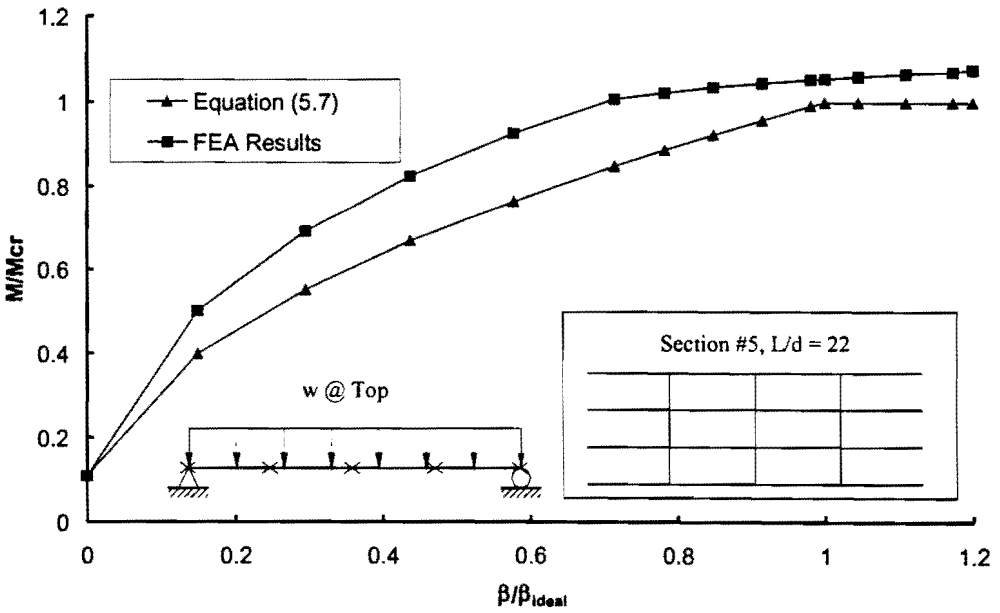

Figure 5.9 (b) M/M_{cr} versus β/β_{ideal} for Section #5 4-girder System with Distributed Load on Top Flange

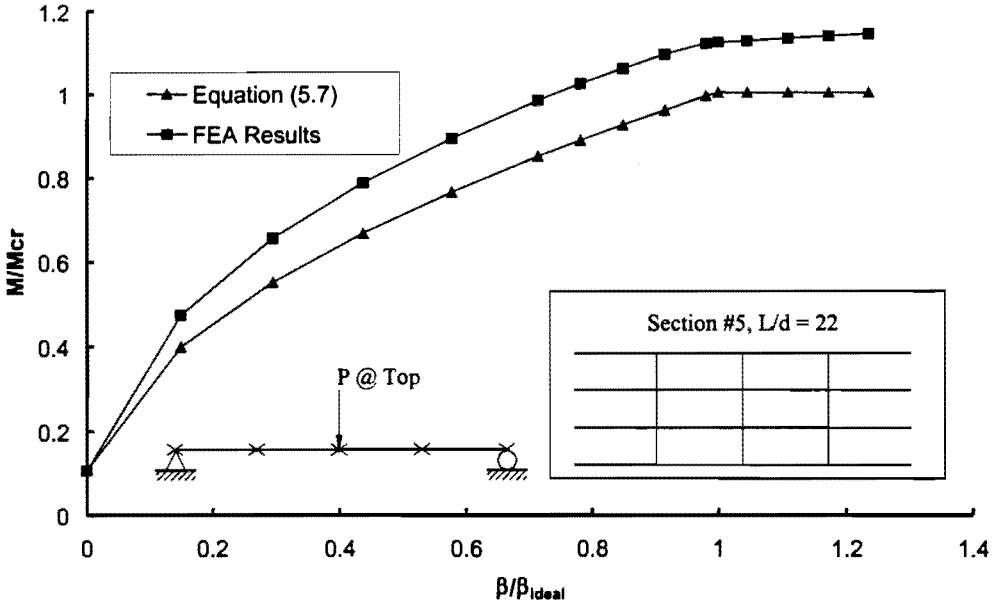

Figure 5.9 (c) M/M_{cr} versus β/β_{ideal} for Section #5 4-girder System with Midspan Concentrated Load on Top Flange

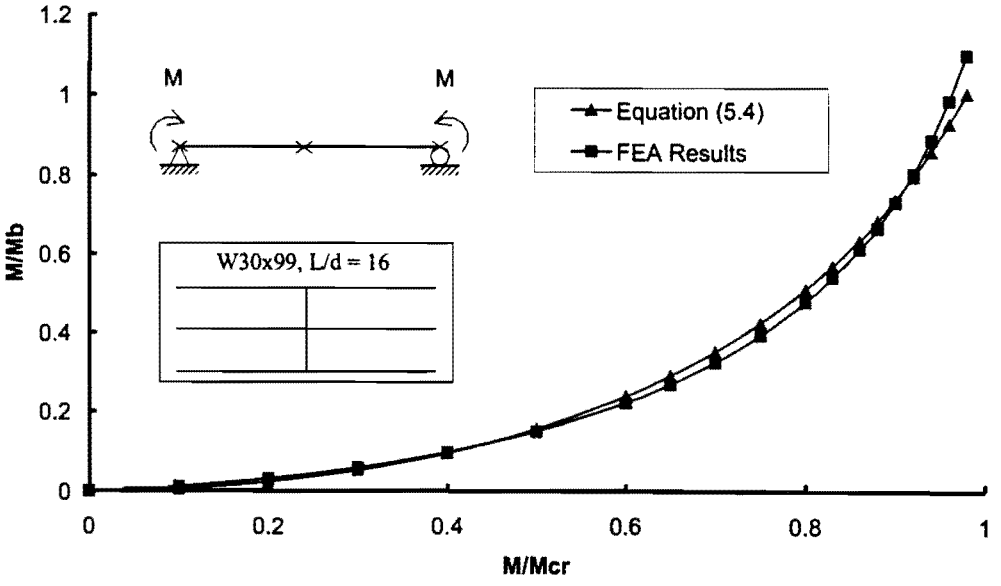

Figure 5.10 (a) M_b/M_{br} versus M/M_{cr} for 3-girder System of W30x99 Section with Uniform Moment

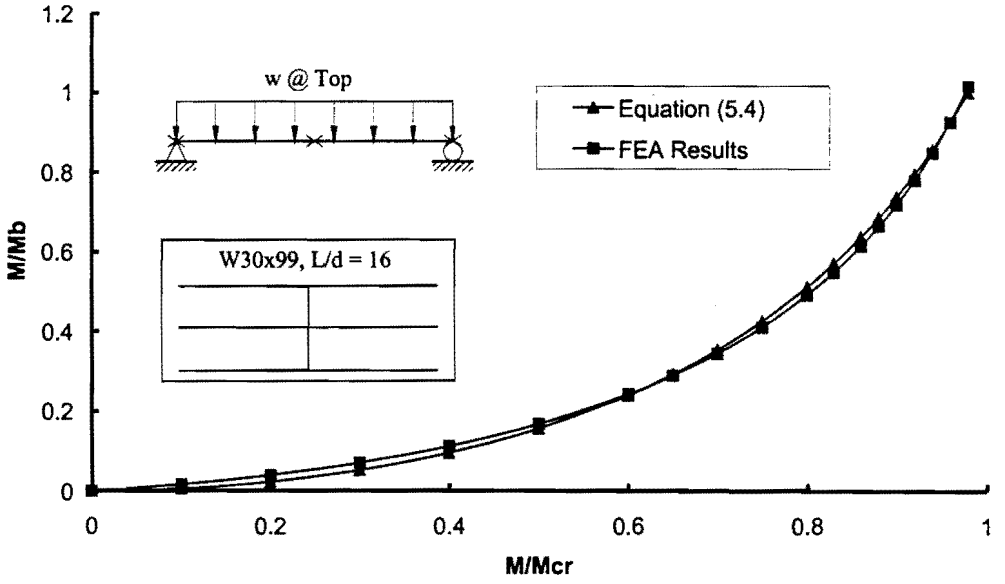

Figure 5.10 (b) M_b/M_{br} versus M/M_{cr} for a 3-girder System of W30x99 Section with Distributed Load on Top Flange

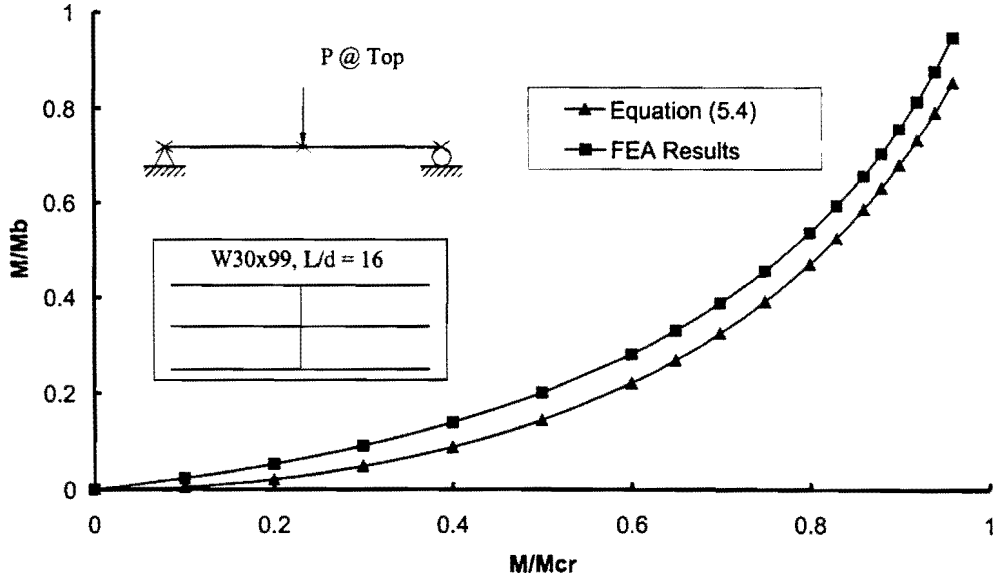

Figure 5.10 (c) M_b/M_{br} versus M/M_{cr} for a 3-girder System of W30x99 Section with Midspan Concentrated Loads at Top Flange

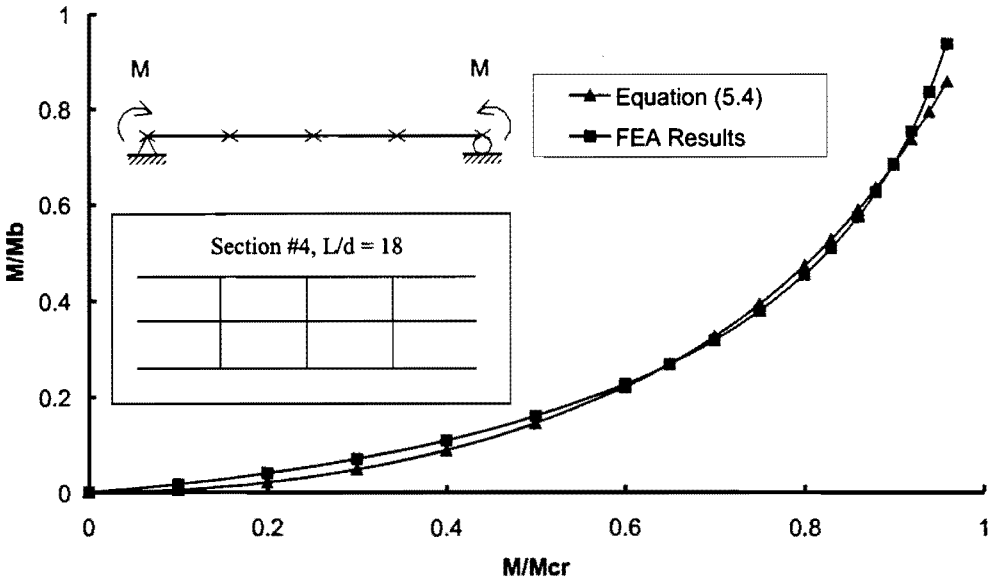

Figure 5.11 (a) M_b/M_{br} versus M/M_{cr} for a 4-girder system of Section #4 with Uniform Moment

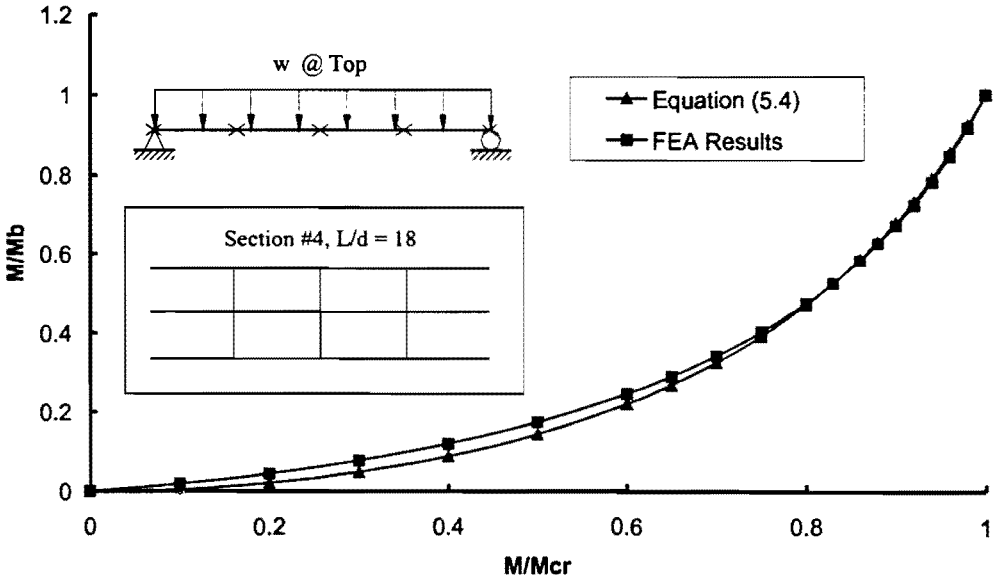

Figure 5.11 (b) M_b/M_{br} versus M/M_{cr} for a 4-girder System of Section #4 with Distributed Loads on Top Flange

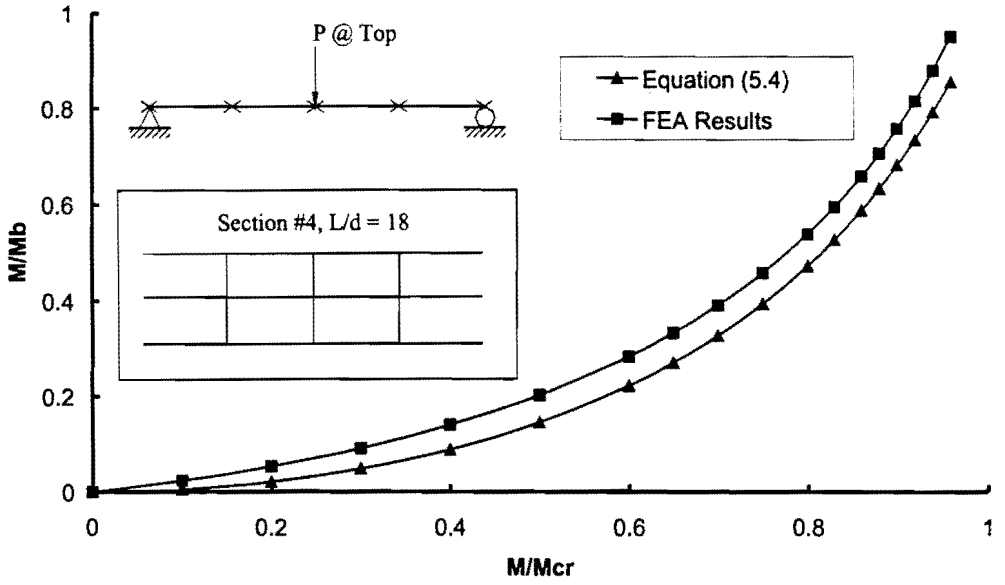

Figure 5.11 (c) M_b/M_{br} versus M/M_{cr} for a 4-girder System of Section #4 with Concentrated Loads on Top Flange at Midspan

5.5 Summary

This chapter has presented finite element results for several different sections with a variety of loading conditions. The results have demonstrated the torsional bracing behavior of two-, three-, and four-girder systems.

Equations for the brace stiffness requirements presented in Chapter 2 show good agreement with the FEA results. The modified Eq. 5.4 together with Eq. 5.3 can be used to estimate strength requirements that show good comparison with the large displacement analysis results.

For the multi-girder systems, Eq. 5.7 can be used to estimate the total brace stiffness, which is a function of the number of girders and the number of braces per brace location. The results show a good agreement with the FEA results.

Chapter 6
Bracing Requirements for Bridges with Skewed Supports and Parallel Braces

6.1 Introduction

The brace stiffness and strength requirements for normal girders were discussed in Chapter 5. This chapter will focus on bridges with skewed supports and braces that are parallel to the skew angle. Both stiffness and strength requirements for the braces were investigated. The five cross sections outlined in Chapter 3 were utilized in the FEA studies with a variety of loading conditions including: uniform moment, uniformly distributed loads applied at the top flange, and midspan concentrated loads applied at the top flange. Comparisons are made in this chapter between the FEA results and expressions for the brace stiffness and strength requirements. The brace requirements for girders with skewed supports have been obtained by modifying the previous solutions that were developed for girders with normal supports. Two-, three, and four-girder systems were considered with skew angles ranging from 10° to 45°.

Following this introductory subsection, the stiffness requirements for braces parallel to the skew angle are presented in Section 6.2. The bracing system utilized in the FEA analytical results presented in this chapter consisted of tension-only cross frames. The skew angles that were considered were 10, 20, 30 and 45 degrees. Although the results presented in the main text focus on selected skew angles, such as 20 and 45 degrees, in many situations results for the other skew angles that were considered will be presented in the Appendix. Brace strength requirements for bridges with braces parallel to the skew angle will be presented in Section 6.3. The girder systems considered in sections 6.2 and 6.3 consist of two-, three-, and four-girder bridges. The results will be summarized in Section 6.4.

Similarities were observed between many of the comparisons of the FEA analyses and the modified solutions for the variety of girder systems that were studied. In these instances, representative results will be presented and discussed in this chapter while graphs of the other sections will be presented in the Appendix.

6.2 Brace Stiffness Requirements for Girders with Skewed Supports and Parallel Braces

When a brace is oriented parallel to the skewed supports, the effectiveness of the brace can be significantly reduced by a reduction in the stiffness component that resists girder twist. The stiffness reduction is due to the fact that the full stiffness of the brace is not engaged in resisting twist of the girder cross-section due to the angled orientation of the brace. Figure 6.1 illustrates the derivation of the stiffness of a tension-only system for a parallel brace. The component stiffness of the parallel brace that resists girder twist can be derived by utilizing the geometrical dimensions in the skewed orientation (i.e. the member

lengths will be longer in the skewed orientation) and can be expressed by the following expression:

$$\beta_{bskew} = \beta_b \cos^2\theta \tag{6.1}$$

where: β_b is the brace stiffness given by the expressions shown previously in Fig. 2.7 and θ is the skew angle. The $\cos^2\theta$ term in Eq. 6.1 accounts for the reduction in brace stiffness when the brace is oriented parallel to the skew angle. Expressions for the cross-section distortion and the in-plane girder stiffness are the same as given in Chapter 2. For a given stiffness of parallel brace, β_{bskew}, the following expression can be used to estimate the total stiffness of the bracing system:

$$\frac{1}{\beta_T} = \frac{1}{\beta_{bskew}} + \frac{1}{\beta_{sec}} + \frac{1}{\beta_g} \tag{6.2}$$

The overall stiffness behavior of the parallel brace decreases significantly with the skew angle since the $\cos^2\theta$ term reduces the stiffness. The effectiveness of the brace for a given member area is also reduced due to the increase in brace length due to the orientation of the brace.

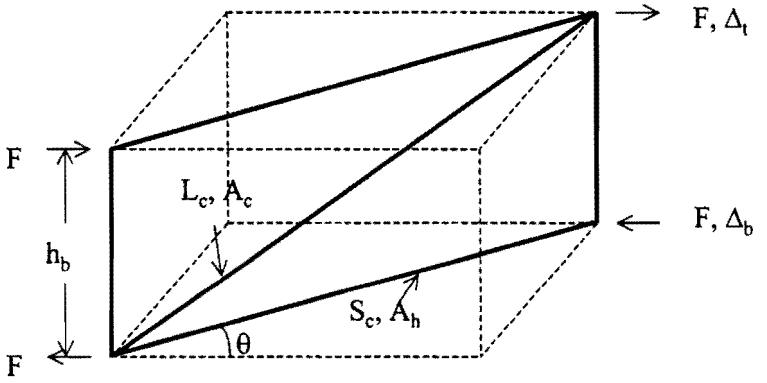

$$\theta = \frac{\Delta_t + \Delta_b}{h_b} \qquad M = Fh_b$$

$$\Delta_t = \frac{1}{EA_c}\frac{2FL_c^3}{S_c^2\cos^2\theta} \qquad \Delta_b = \frac{1}{EA_h}\frac{FS_c}{\cos^2\theta}$$

$$\beta_{bskew} = \frac{M}{\theta} = \cos^2\theta \frac{Eh_b^2 S_c^2}{\frac{2L_c^3}{A_c} + \frac{S_c^3}{A_b}} = \beta_b \cos^2\theta$$

Figure 6.1 Derivation of Brace Stiffness for Parallel Brace

Figures 6.2, 6.3, and 6.4 show comparisons of Eqs. 6.1 and 6.2 with FEA results for a W14x22 section. The results are from an eigenvalue buckling analysis for a twin-girder system with a 33-foot span and a single brace at midspan. Results are shown for skew angles of 26.5° and 45°, which are the angles that were used for the test beam supports in the experimental study. Figs 6.2, 6.3, and 6.4 illustrate the systems under the respective loading conditions of uniform moment, uniformly distributed loads applied at the top flange, and concentrated top-flange loads at midspan. The beam buckling capacity is graphed on the vertical axis while the brace stiffness is graphed on the horizontal axis. The buckling moment has been normalized by the moment corresponding to girders buckling between the brace points. The brace stiffness has been normalized by the ideal brace stiffness calculated from Eqs. 6.1 and 6.2. The results graphed in Fig. 6.2 show good agreement between the equations and the FEA results for the W14x22 beams with uniform moment loading. Graphs are shown for skew angles of 26.5° and 45° in the separate figures labeled a and b, respectively. Figs. 6.3 and 6.4 show the skewed twin-girder system for the respective cases of a uniformly distributed load and a concentrated load applied at the top flange. The graphs show that for the uniform moment loading case, Eqs. 6.1 and 6.2 have good agreement with the FEA results. For cases with moment gradient, the equations are slightly unconservative for stiffness at or near the ideal value, however, this is due to effects of load height and underestimating the actual C_b factor as discussed in Chapter 5.

Eigenvalue buckling analyses were also performed on a W30x99 section, which had a 40 ft. span (span to depth ratio, L/d =16) and a single parallel brace at midspan. Skew angles of 10° and 30° were considered for these the beams. The comparisons of the FEA and equation results for the W30x99 section are similar to that of the W14x22 section and are presented in Appendix B.

Figs. 6.5, 6.6, and 6.7 show the comparisons of the results from the equations and the FEA analyses for the W36x160 section. The twin-girder system had a 60 ft. span (L/d = 20) and a girder spacing of 120 inches. Skew angles of 20° or 45° were considered. Parallel intermediate braces were placed at the third points to provide an unbraced length of 20 feet. Figs. 6.5, 6.6, and 6.7 illustrate the system under the respective loading conditions of uniform moment, uniformly distributed loads applied at the top flange, and concentrated top-flange loads at midspan. The graphs show that Eqs. 6.1 and 6.2 have good agreement with the FEA results, particularly for the uniform loading case. For cases with moment gradient, the equations provide conservative estimates with respect to the FEA solutions, however, this is because the hand calculations conservatively neglect the warping restraint provided to the middle third of the beam by the exterior thirds as was discussed in Chapter 5. This warping restraint as well as the presence of intermediate bracing tends to negate the effects of top flange loading.

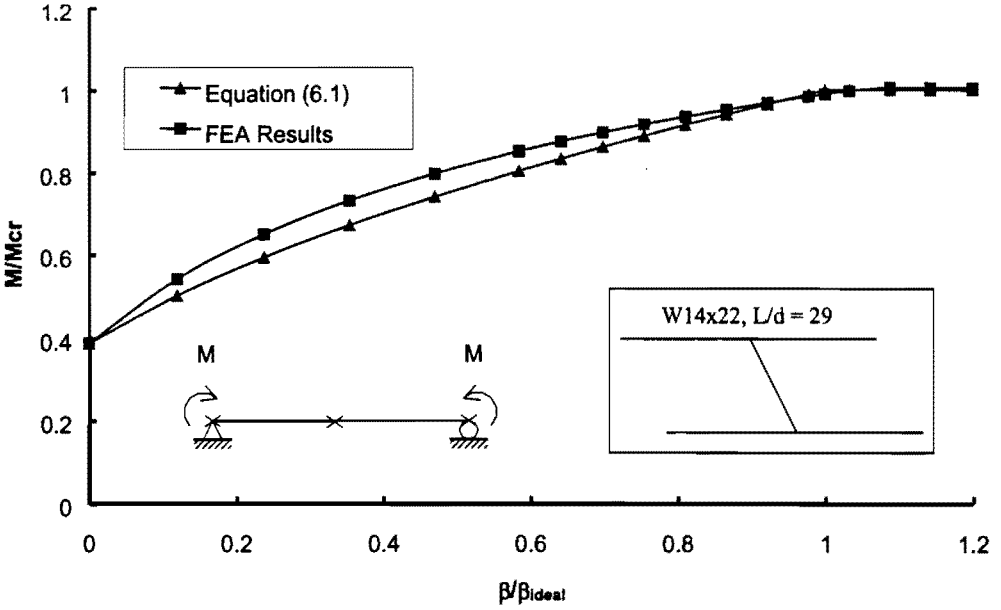

(a) skew angle =26.5°

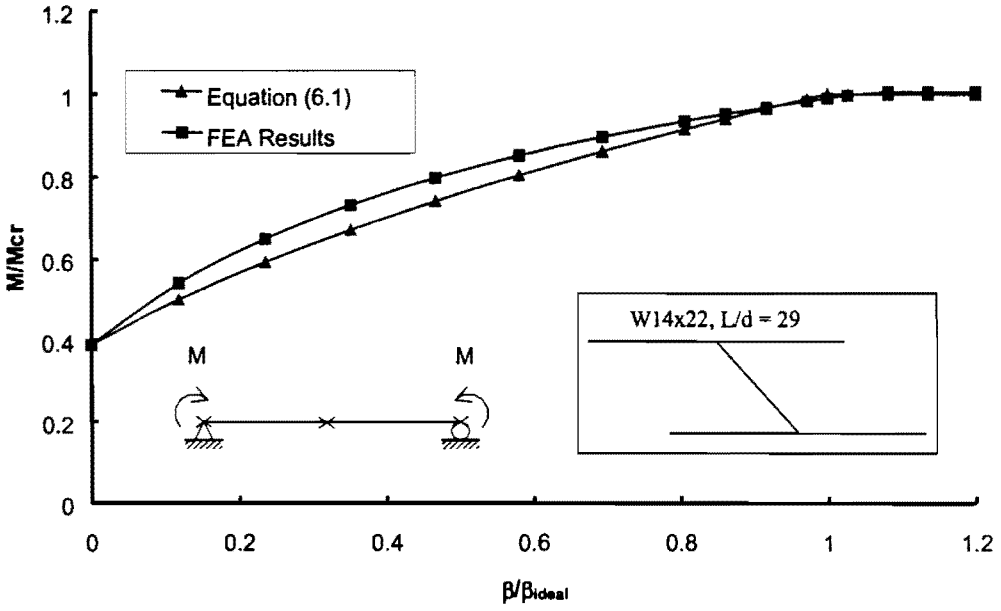

(b) skew angle = 45°

Figure 6.2 M/M_{cr} versus β/β_{ideal} for a W14x22 Section with Uniform Moment

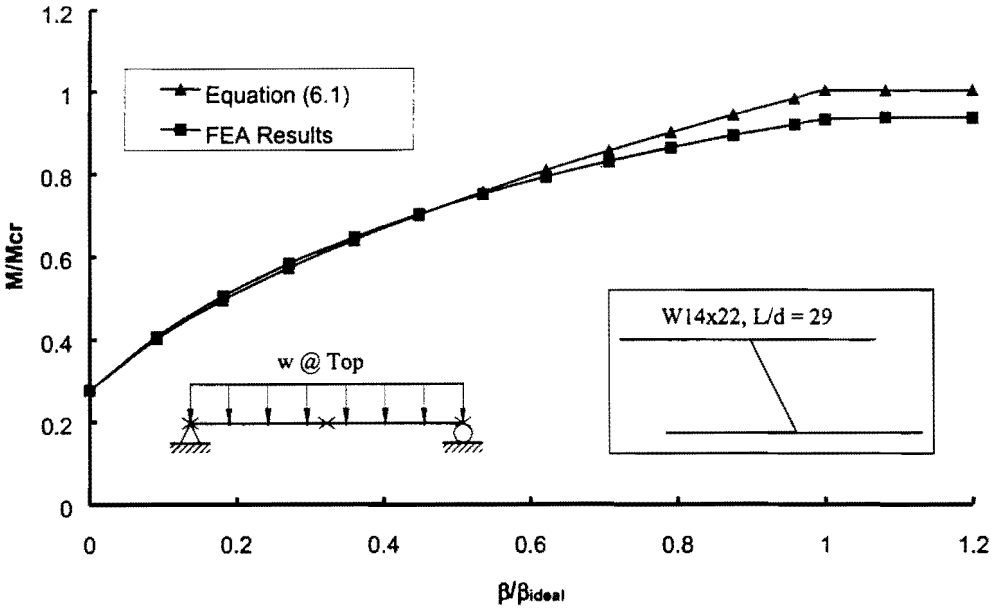

(a) skew angle =26.5°

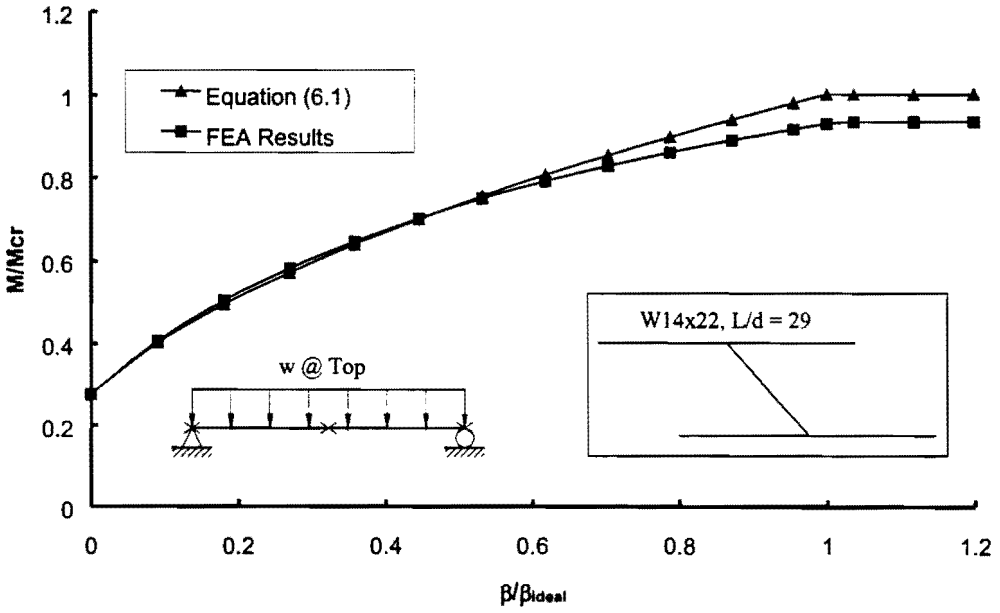

(b) skew angle = 45°

Figure 6.3 M/M_{cr} versus β/β_{ideal} for a W14x22 Section with Distributed Loads on Top Flange

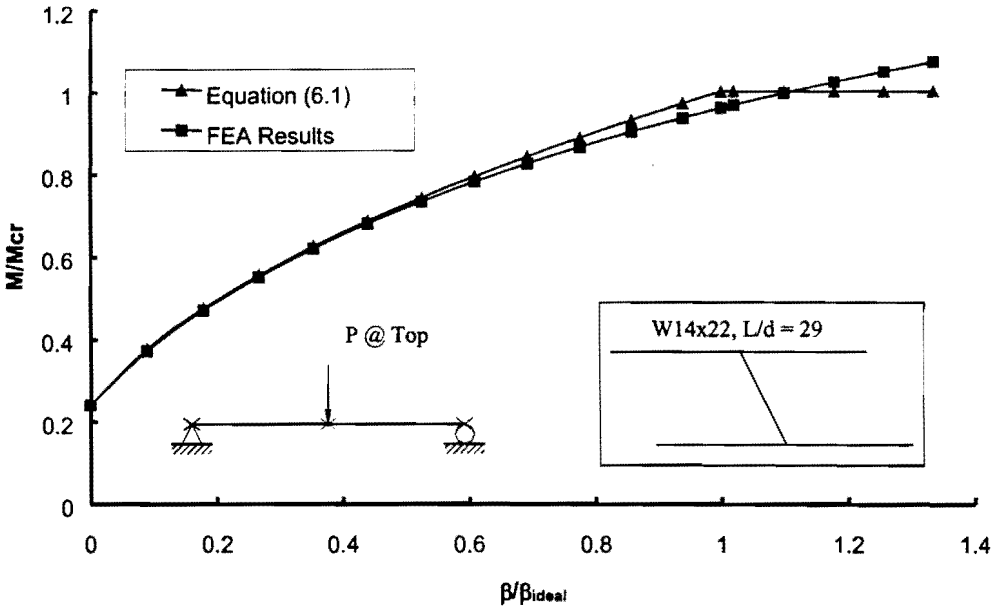

(a) skew angle =26.5°

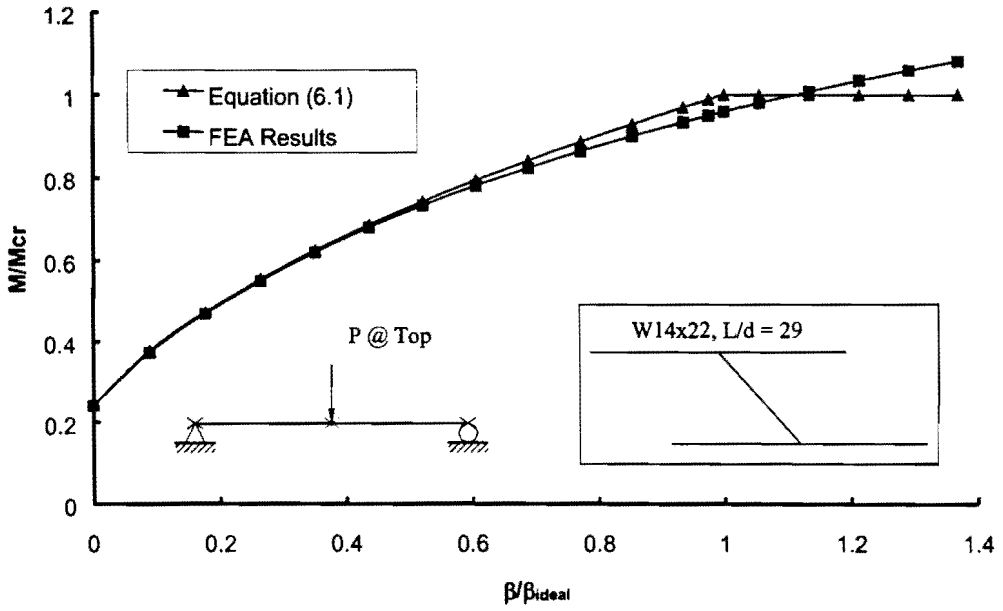

(b) skew angle = 45°

Figure 6.4 M/M_{cr} versus β/β_{ideal} for a W14x22 Section with Midspan Concentrated Load on Top Flange

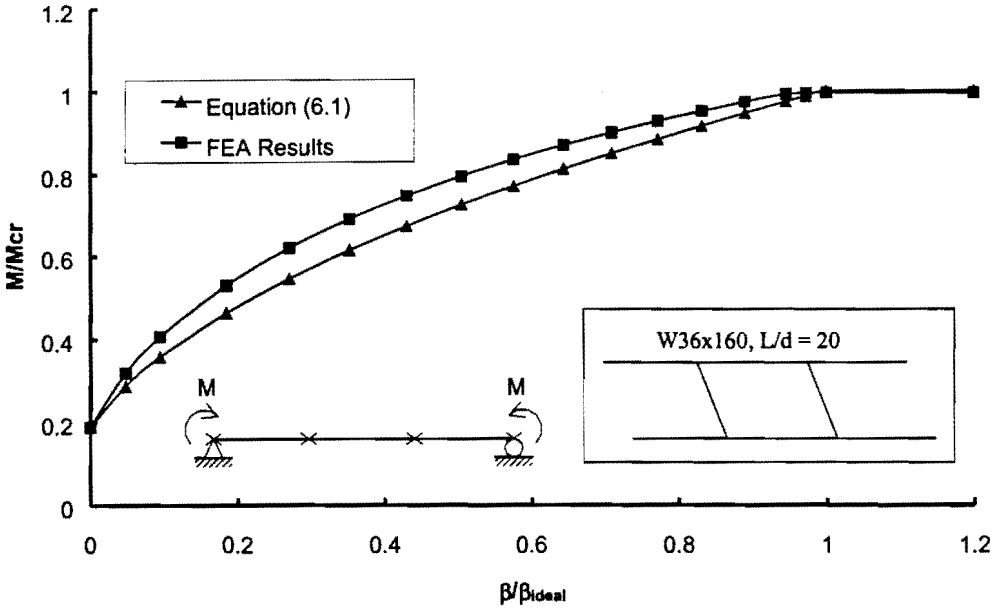

(a) skew angle =20°

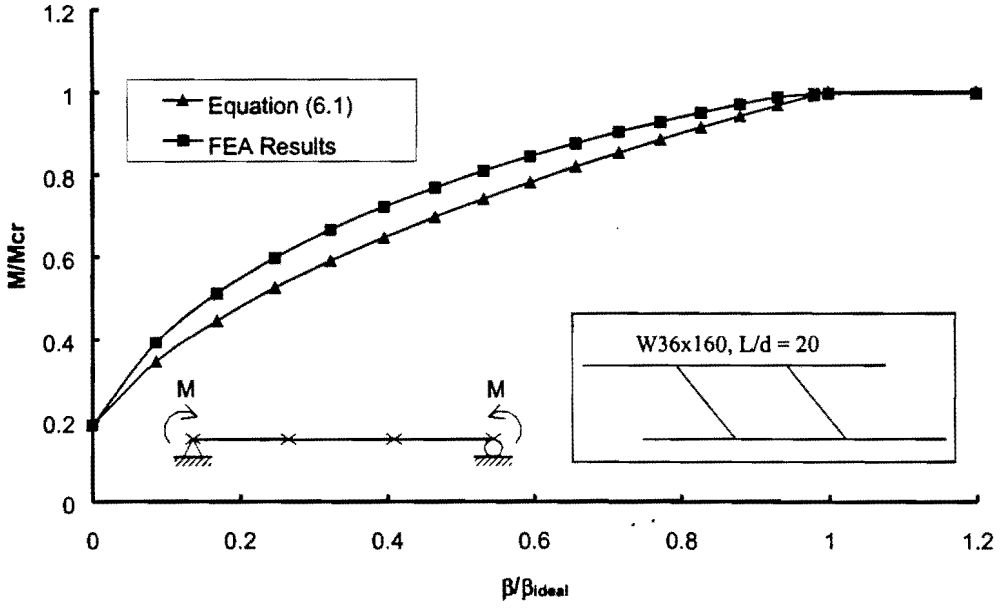

(b) skew angle = 45°

Figure 6.5 M/M_{cr} versus β/β_{ideal} for a W36x160 Section with Uniform Moment

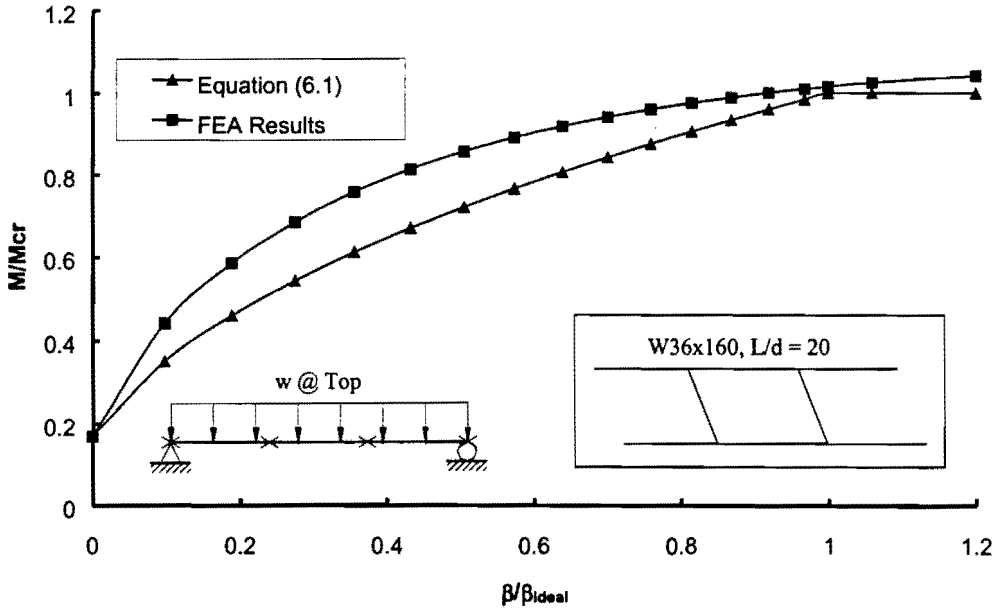

(a) skew angle =20°

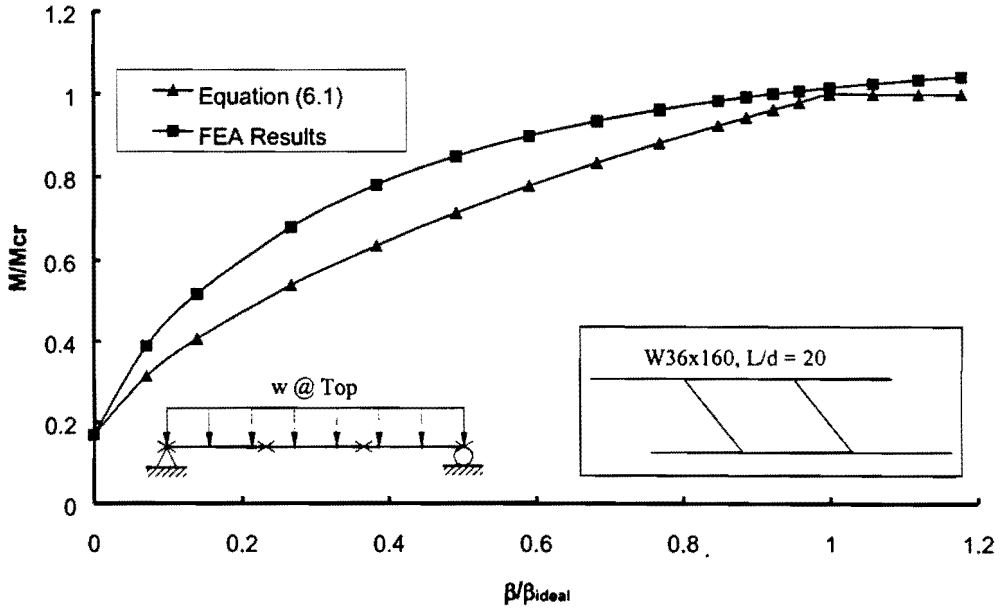

(b) skew angle = 45°

Figure 6.6 M/M_{cr} versus β/β_{ideal} for a W36x160 Section with Distributed Loads on Top Flange

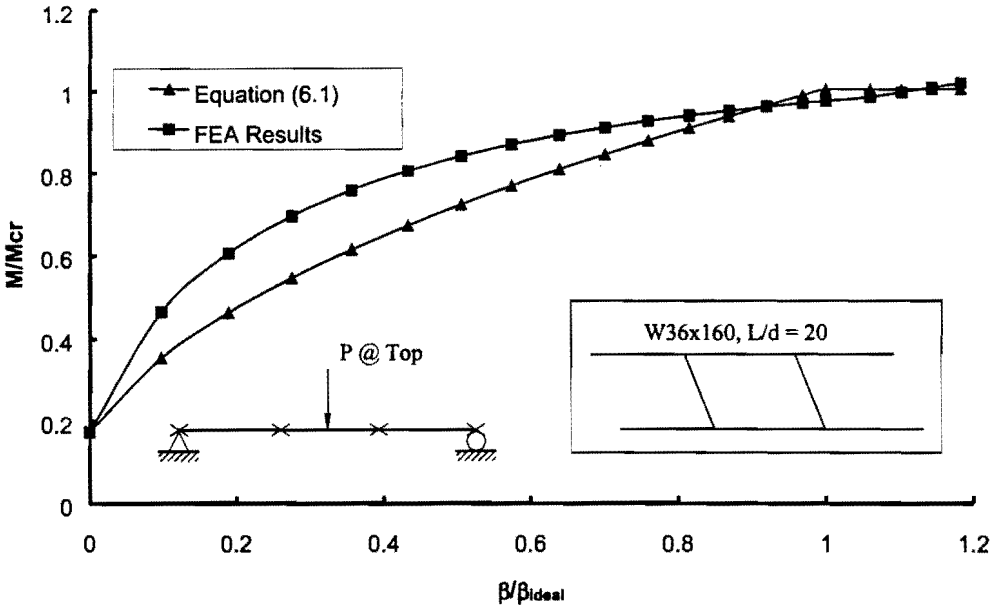

(a) skew angle =20°

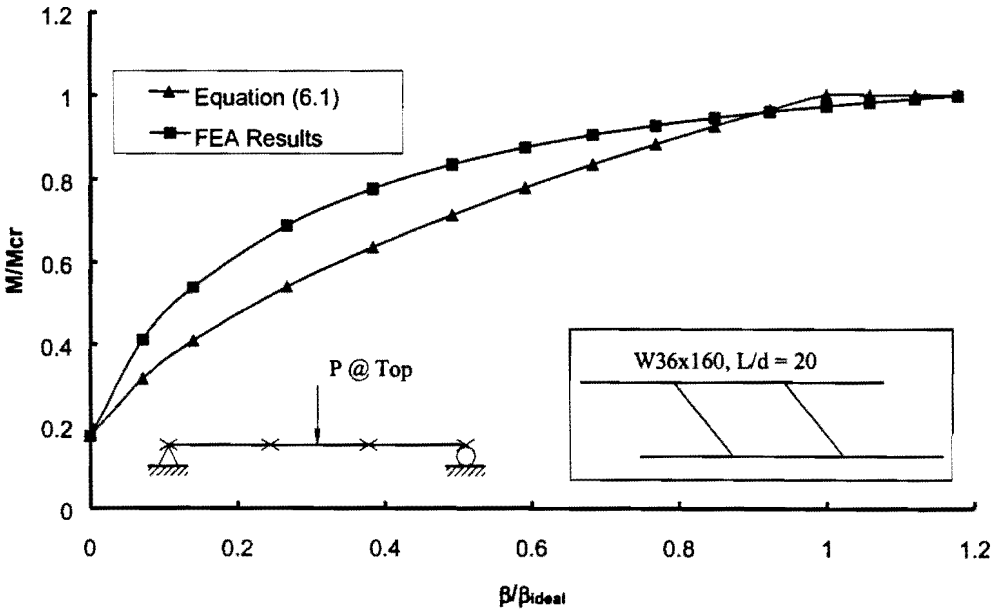

(b) skew angle = 45°

Figure 6.7 M/M_{cr} versus β/β_{ideal} for a W36x160 Section with Midspan Concentrated Loads on Top Flange

Figures 6.8, 6.9, and 6.10 show the comparisons of the equation and FEA results for the singly-symmetric Section #5. The twin-girder system had a span of 100 feet and a girder spacing of 120 inches. Skew angles of 20° and 45° were considered. Three intermediate parallel braces were employed yielding an unbraced length of 25 feet. Figs 6.8, 6.9, and 6.10 illustrate the system under the respective loading conditions of uniform moment, uniformly distributed loads applied at the top flange, and concentrated top-flange loads at midspan. The graphs show good agreement between the computational results and the equations, particularly for the uniform moment loading case. For cases with moment gradient, the buckling capacities from the FEA results are approximately 10% higher than the Eqs. 6.1 and 6.2 due to the warping restraint provided by the outside quarters of the beams as discussed in Chapter 5. The effects of load height have a minimal effect on the buckling capacity with three intermediate braces.

Results for the other singly-symmetric section #4 are similar to results of section #5 and are presented in Appendix B. The twin-girder system had an 80 ft span (L/d = 18) and a girder spacing of 120 inches with skew angles of 20° or 30°. Three intermediate braces were employed to give an unbraced length of 20 feet.

The graphical comparisons of the FEA results and Eqs. 6.1 and 6.2 presented in this section and the Appendix show that the expressions provide good estimates of the brace stiffness requirements for girders with braces parallel to skewed supports. The expressions are the most accurate for the cases with uniform moment loading. Although the solutions had good agreement with the FEA results for cases with moment gradient, the expressions were either slightly conservative or unconservative depending on the distribution of bracing along the girder length. These slight differences between the analytical results and the predicted solutions were due to either load height effects or warping restraints that are generally neglected in the hand calculations.

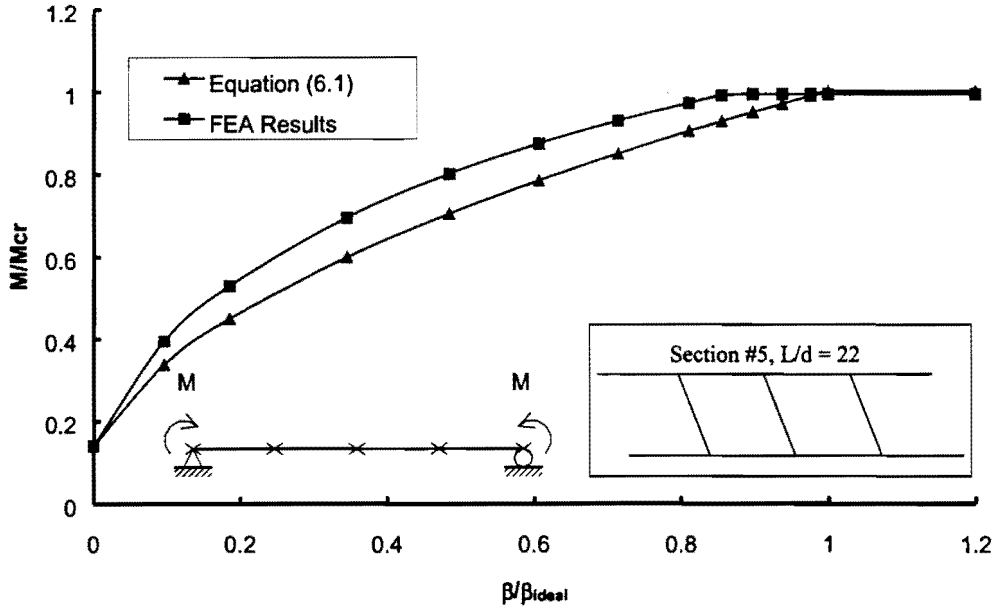

(a) skew angle =20°

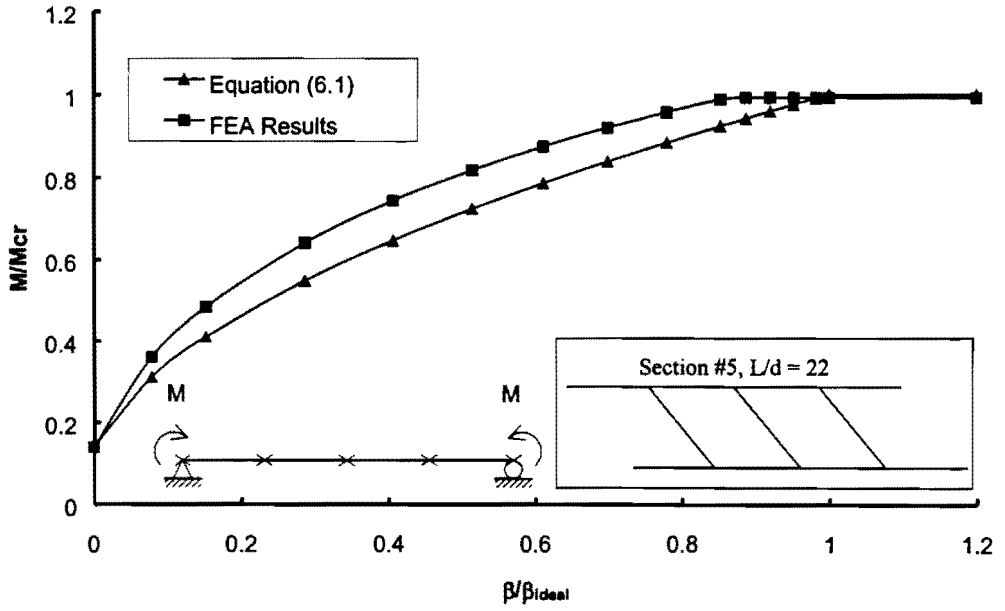

(b) skew angle = 45°

Figure 6.8 M/M_{cr} versus β/β_{ideal} for Section #5 with Uniform Moment

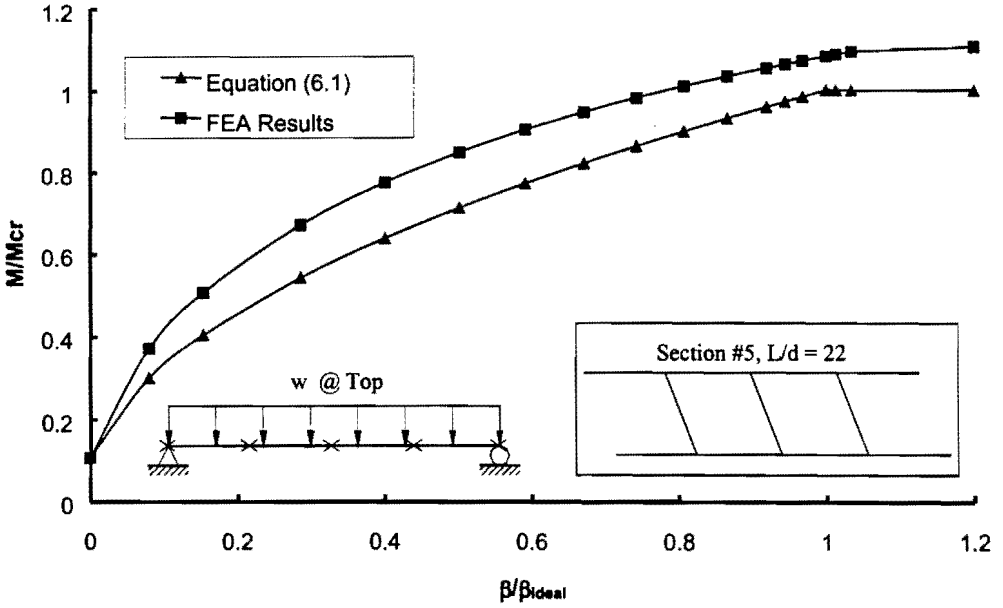

(a) skew angle =20°

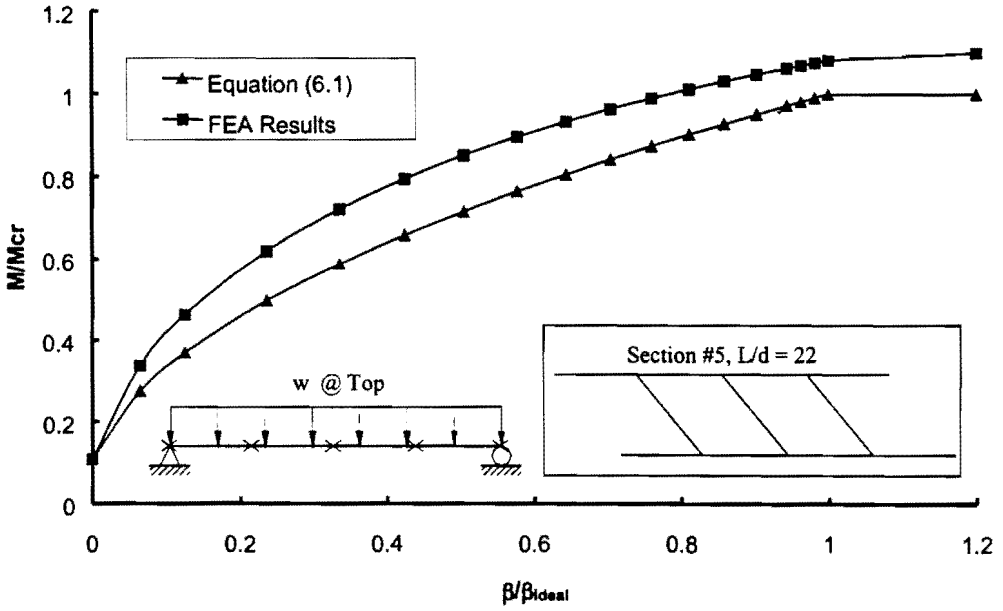

(b) skew angle = 45°

Figure 6.9 M/M_{cr} versus β/β_{ideal} for Section #5 with Distributed Loads on Top Flange

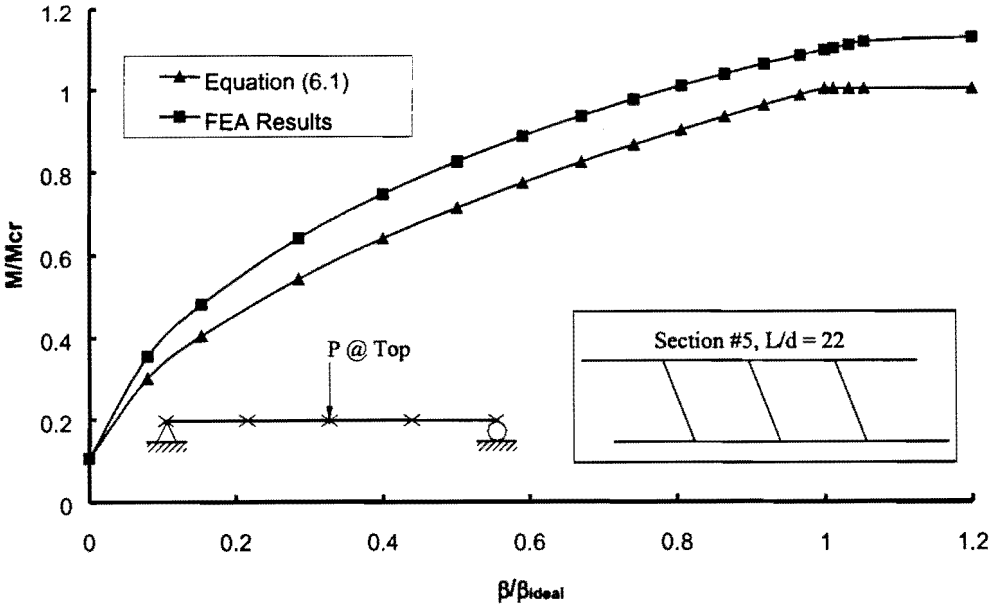

(a) skew angle =20°

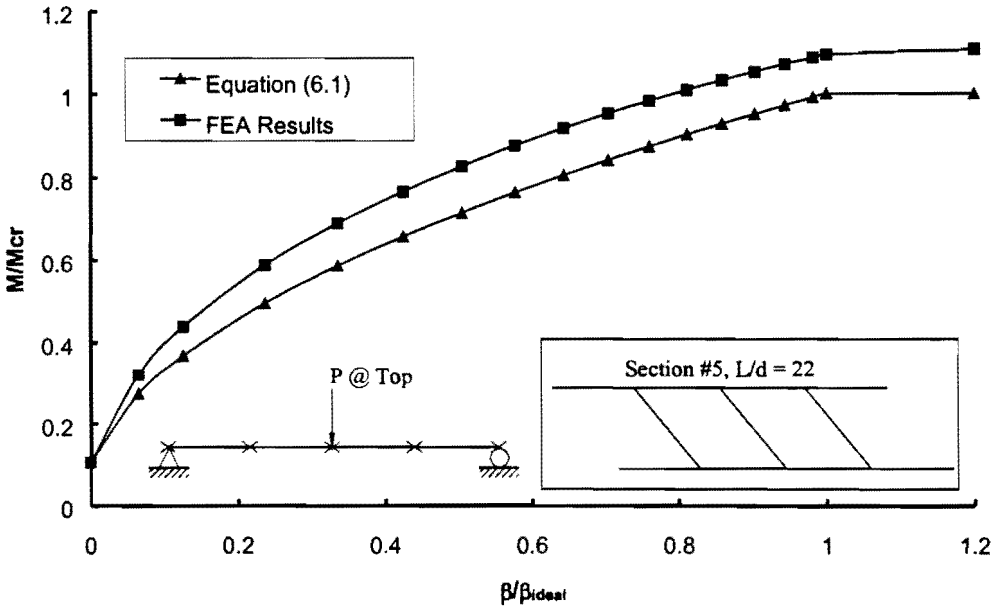

(b) skew angle = 45°

Figure 6.10 M/M_{cr} versus β/β_{ideal} for Section #5 with Midspan Concentrated Loads on Top Flange

6.3 Brace Strength Requirements for Girders with Skewed Supports and Parallel Braces

In addition to altering the effectiveness of the braces from a stiffness perspective, the parallel brace orientation also affects the forces that develop in the braces. The strength requirements for the parallel braces can be simply modified by the following expression:

$$M_{brskew} = \frac{M_{br}}{\cos\theta} \tag{6.3}$$

where: M_{br} is the recommended value of the brace moment for girders with normal supports, and θ is the skew angle.

The strength requirements for the braces were determined using large displacement analyses. The accuracy of Eq. 6.3 was checked with a variety of values of the brace stiffness relative to the ideal value. As outlined in Chapter 2, the magnitudes of the brace moments are a function of the brace stiffness that is provided. Although a brace stiffness of twice the ideal value is often recommended, the strength requirements can be adjusted to account for cases in which larger or smaller stiffness are provided. Figs. 6.11, 6.12, and 6.13 show comparisons of the FEA results and the equations for the W14x22 section with values of the brace stiffness of $\beta_T = 1.5\beta_{ideal}$, $\beta_T = 2\beta_{ideal}$, and $\beta_T = 3\beta_{ideal}$,. Large displacement analyses were conducted on this twin girder system, which had a 33 ft. span and a girder spacing of 78 inches with a 26.5° skew angle. The loading cases included uniform moment, uniformly distributed loads and concentrated loads at midspan. The transverse loads were applied at the top flange. The graphs show the brace moment on the vertical axis versus the moment applied on the beams on the horizontal axis. The brace moment has been normalized by the maximum brace moment corresponding to the critical moment applied on the beam, while the applied beam moment has been normalized by the beam buckling capacity that corresponds to the beam buckling between the brace points. The graphs show that the strength equations with the modification to account for the skew angle (Eq. 6.3) have good agreement with the FEA results along the entire range of loading. The expressions are slightly unconservative for a few cases as the applied moment approaches the load corresponding to buckling between the brace points. The slight unconservative nature of the solution comes from the assumption that the total twist is equal to twice the initial twist, ϕ_o, when a stiffness of twice the ideal value is provided. In reality, the twist is slightly larger than twice the initial imperfection, however the assumption provides reasonable estimates of the brace moments. Results for the singly-symmetric section #4 are similar to the results of the W14x22 section and are presented in Appendix B. The twin-girder system had an 80 ft span (L/d = 18) and a girder spacing of 120 inches with 30° skew angle. Three intermediate parallel braces were employed to give an unbraced length of 20 feet.

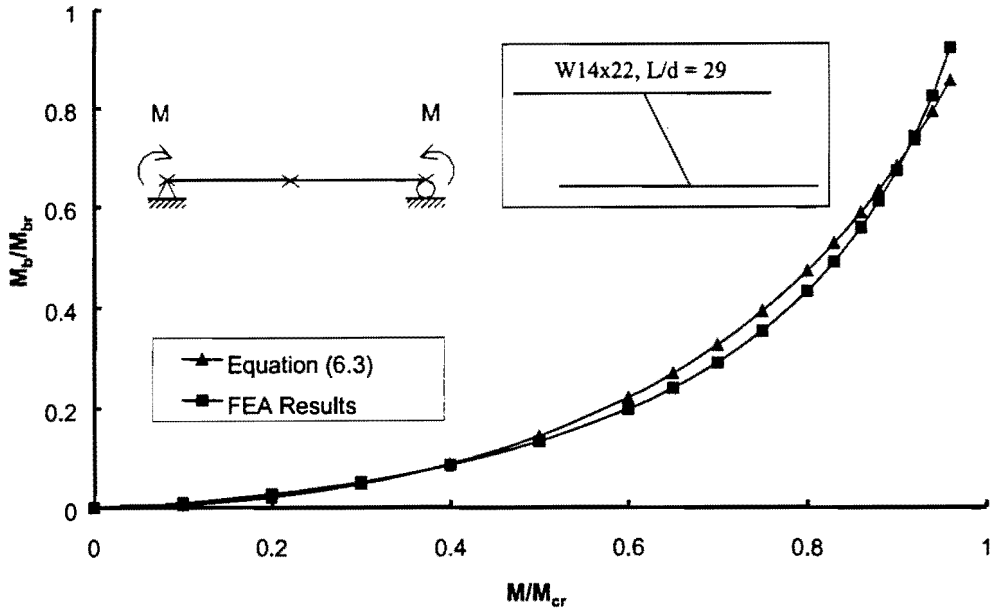

Figure 6.11 (a) M_b/M_{br} versus M/M_{cr} for a W14x22 Section with Uniform Moment, $\beta_T=2\beta_{ideal}$

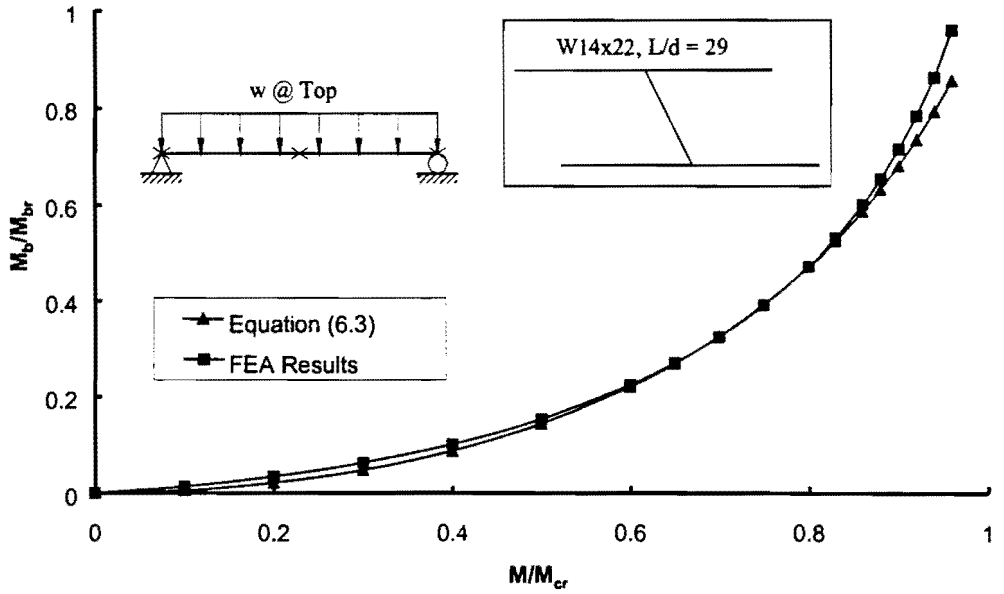

Figure 6.11 (b) M_b/M_{br} versus M/M_{cr} for a W14x22 Section with Distributed Loads on Top Flange, $\beta_T=2\beta_{ideal}$

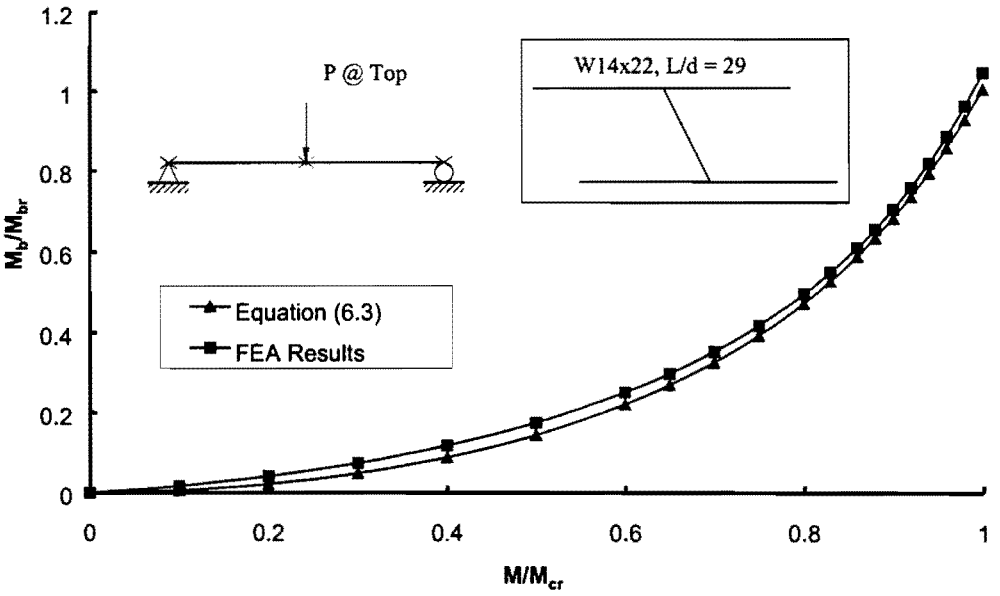

Figure 6.11 (c) M_b/M_{br} versus M/M_{cr} for a W14x22 Section with Top Flange Concentrated Loads at Midspan, $\beta_T=2\beta_{ideal}$

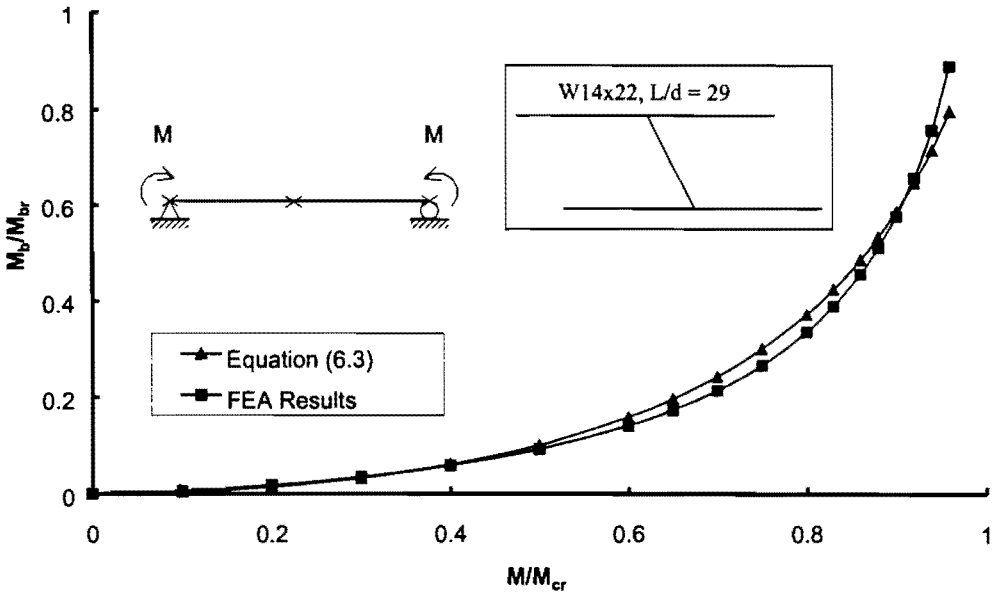

Figure 6.12 (a) M_b/M_{br} versus M/M_{cr} for a W14x22 Section with Uniform Moment, $\beta_T=1.5\beta_{ideal}$

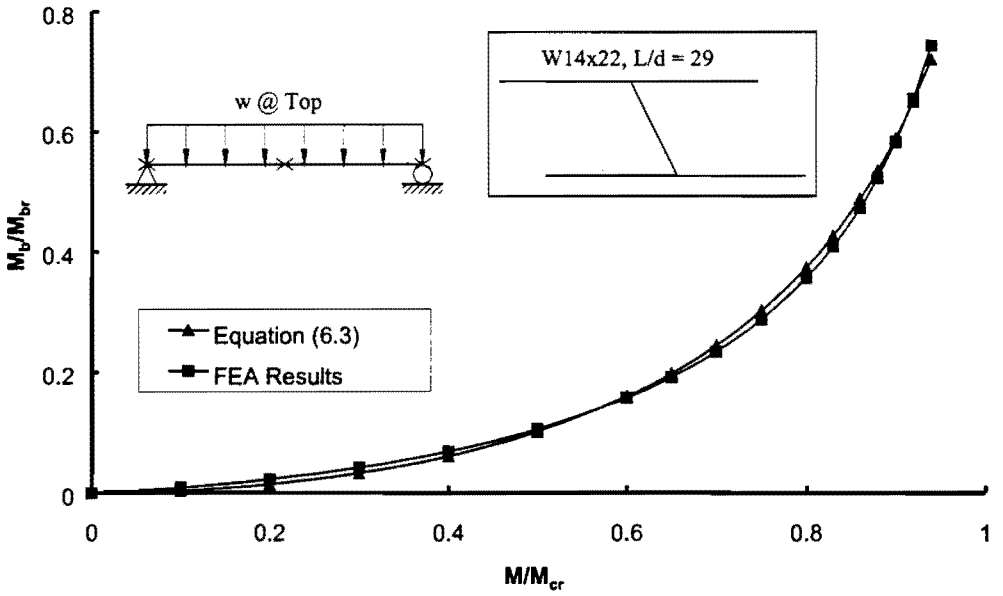

Figure 6.12(b) M_b/M_{br} versus M/M_{cr} for a W14x22 Section with Distributed Loads on Top Flange, $\beta_T=1.5\beta_{ideal}$

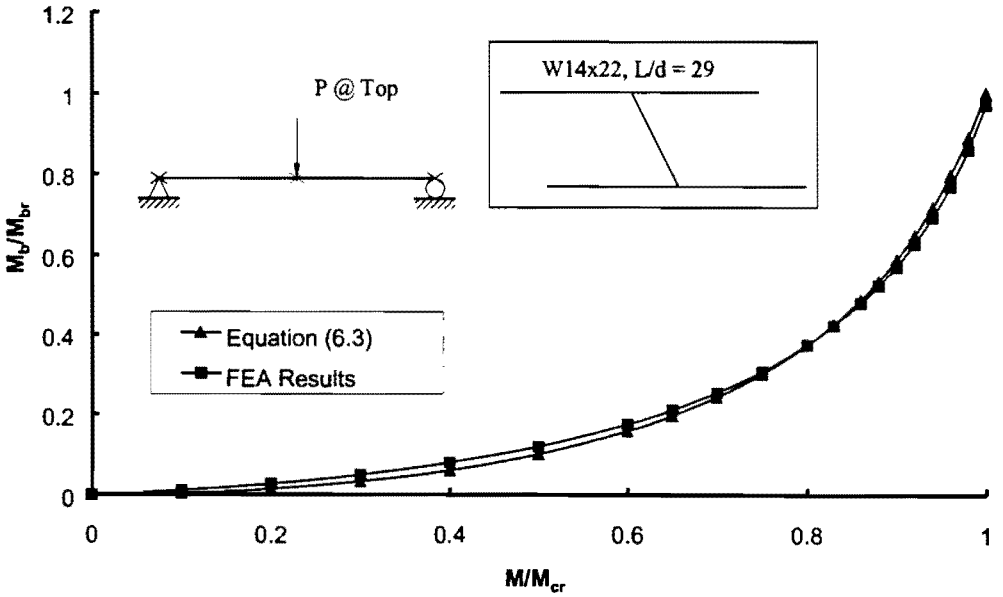

Figure 6.12 (c) M_b/M_{br} versus M/M_{cr} for a W14x22 Section with Top Flange Concentrated Loads at Midspan, $\beta_T=1.5\beta_{ideal}$

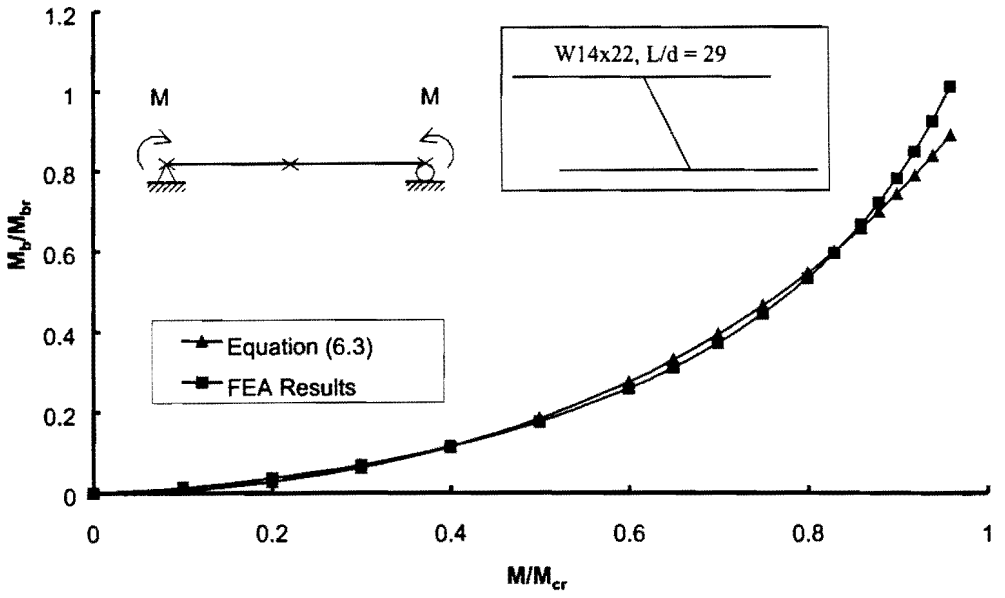

Figure 6.13 (a) M_b/M_{br} versus M/M_{cr} for a W14x22 Section with Uniform Moment, $\beta_T=3\beta_{ideal}$

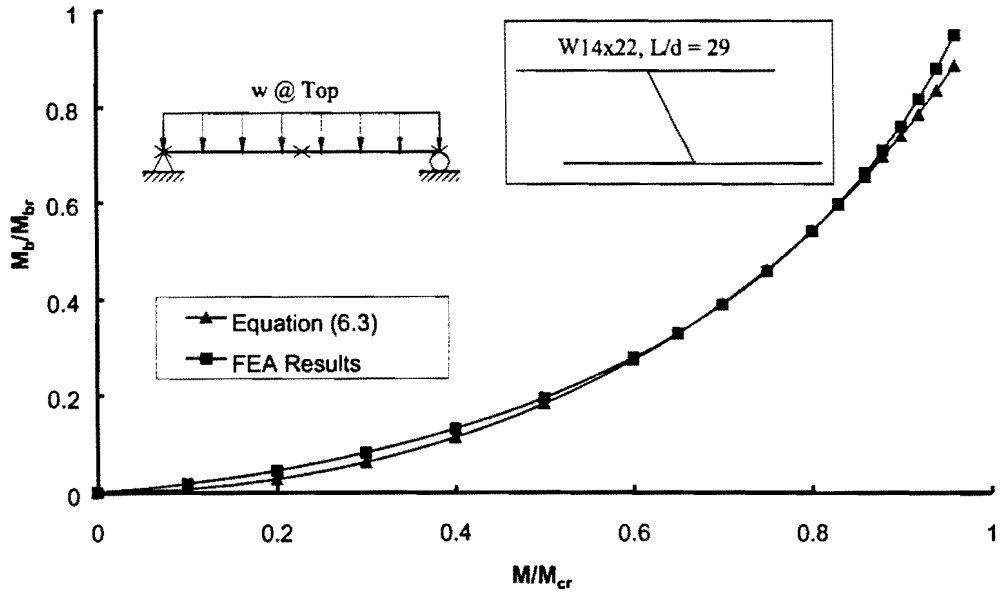

Figure 6.13(b) M_b/M_{br} versus M/M_{cr} for a W14x22 Section with Distributed Loads on Top Flange, $\beta_T=3\beta_{ideal}$

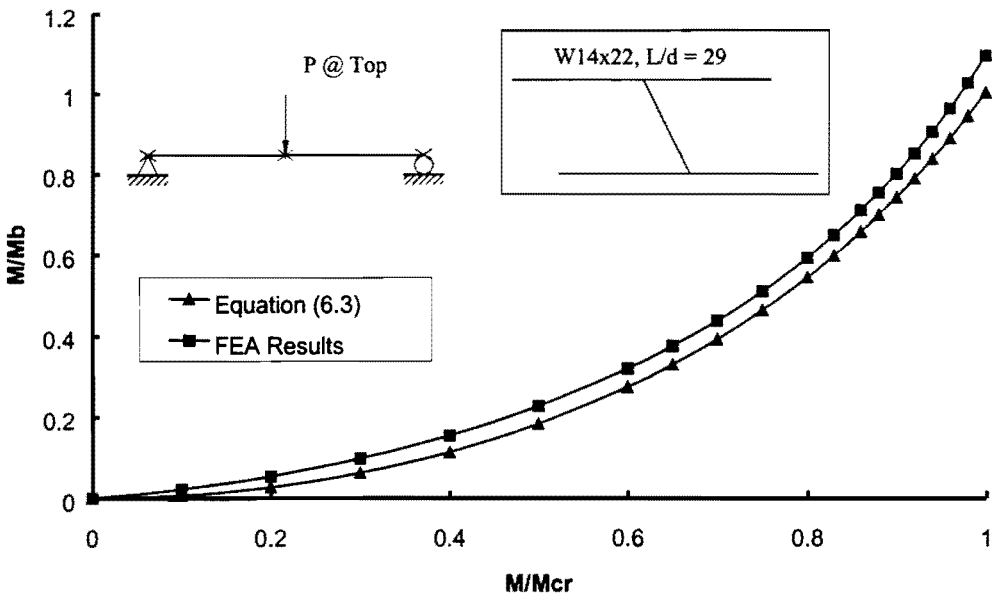

Figure 6.13 (c) M_b/M_{br} versus M/M_{cr} for a W14x22 Section with Top Flange Concentrated Loads at Midspan, $\beta_T=3\beta_{ideal}$

6.4 Summary

Comparisons between the FEA results and expression for the strength and stiffness requirements of braces parallel to the skew angle have been presented in this chapter. A variety of parameters were considered in the study including skew angle, loading conditions, and the cross-sectional shape. The expressions that were modified to account for the skew angle had good agreement with the FEA results in estimating both the strength and stiffness requirements of torsional braces.

Chapter 7
Bracing Requirements for Bridges with Skewed Supports and Normal Braces

7.1 Introduction

The bracing requirements for normal girders and skewed girders with parallel braces were discussed in Chapters 5 and 6. When the skew angle is greater than 20° the AASHTO Specifications require braces to be oriented normal to the girder lines. This chapter will investigate the bracing requirements for bridges with skewed supports and braces that are normal to the longitudinal axis of the girders (normal braces). The solutions for bracing requirements in girders with skewed supports and normal braces will be investigated and compared with FEA results. The girder systems studied only include twin-girder systems. The skew angles of the bridges that were studied range from 10° to 45°. Similar to the loading conditions studied in the previous chapters, load cases consisting of uniform moment, uniformly distributed loads applied at the top flange, and concentrated top flange loads at mid-span were considered. The chapter is divided into four sub-sections. Following this introduction, the brace stiffness requirements for bridges with skewed supports and normal braces are discussed in Section 7.2. The effect of the skew angle on the brace stiffness requirements was investigated. The bracing systems utilized in the FEA analysis for the results presented in this chapter consisted of tension-only cross frames. Brace strength requirements for bridges with skewed supports and normal braces are discussed in Section 7.3. Finally, the results are summarized in Section 7.4.

As mentioned in the previous chapters, in many situations, comparisons of the FEA results and the equations were similar for a variety of the girder cross-sections and the skew angles that were considered. In these cases, representative results are presented and discussed in this chapter, while redundant results for sections with similar behavior are presented in the Appendix.

7.2 Brace Stiffness Requirements for Girders with Skewed Supports and Normal Braces

When a brace is oriented normal to the girder line for bridges with skewed supports, the skew angle can affect the bracing behavior, however the effect on the stiffness is not as significant as was observed for braces oriented parallel to skewed supports. Figure 7.1 illustrates the effect of the skew angle on the brace stiffness for girders with skewed supports and normal braces. Skew angles of 0°, 20°, and 30° were considered. The girders were subjected to uniform moment loading. Figure 7.1a shows the comparison of FEA results for a twin girder system with W30x99 girders and a 40-foot span. There is only one intermediate brace between the supports. With one intermediate brace, changes in the skew angle affect the unbraced length of the longer beam segment. The unbraced length of the longer beam segment ranged from 20 ft. with normal supports to 22.5 ft. with a 30° skew.

The longer unbraced length for the beams with the larger skew angles leads to lower buckling capacities corresponding to full bracing (buckling between the brace points).

The buckling capacity is graphed on the vertical axis versus the area of the cross frame members on the horizontal axis. For all three skew angles, the buckling capacity of the girders has been normalized by the moment, $M_{cr\_0°skew}$, corresponding to buckling between the brace points for the case with zero skew (normal supports). Therefore, the ratios of $M/M_{cr\_0°skew}$ corresponding to buckling between the braced points (full bracing) for the cases with 20° and 30° skew angles are less than 1.0 since the girders in these cases have a larger unbraced length than the case with normal supports.

In addition to a lower buckling capacity corresponding to full bracing, the bracing is also less effective for beams with skewed supports compared to the cases with normal supports. This is reflected by the lower buckling moment for a given brace stiffness for the cases with skewed supports in Fig. 7.1a. Therefore the expressions used for determining the stiffness required should be modified to account for this effect.

The expressions for the torsional brace stiffness required that was presented in Chapters 2 and 5 were based upon an equivalent "continuous brace stiffness" given in the following expression:

$$\overline{\beta_T} = \frac{n\beta_T}{L} \tag{7.1}$$

where: n is the number of intermediate brace locations along bridge length.

For beams with only one intermediate brace, it was recommended to divide β_T by 0.75L in Eq. 7.1. Results presented in Chapter 5 showed good agreement between the FEA results and the equations for this recommendation. However to avoid unconservative estimates of the bracing required for beams with skewed supports and normal supports, it is recommended to use Eq. 7.1 (with the full L) for all beams regardless of the number of intermediate braces. Doing so will generally be conservative for beams with skewed supports and normal supports; subsequent graphs presented in this chapter will show good agreement for members with skewed supports and only a single brace.

Figure 7.1b shows the corresponding graph for the singly-symmetric Section #4 with an 80 ft. span. Three intermediate cross-frames were provided. For the three cases considered, the largest unbraced lengths ranged from 20 feet for normal supports to 21.5 feet for a skew angle of 30°. The vertical axis of the graph has again been normalized by the buckling capacity, $M_{cr\_0°skew}$, corresponding to full bracing for the case with normal supports. Although the buckling capacity corresponding to full bracing does differ for the three different skew angles (due to the larger unbraced length for the cases with skewed supports) the curves nearly coincident for much of the graph. This indicates that for multiple intermediate braces that are perpendicular to the longitudinal axis of the girders, the skew

angle does not affect the bracing requirements. Therefore, the definition for $\overline{\beta_T}$ given in Eq. 7.1 is recommended for all beams, regardless of the number of intermediate braces.

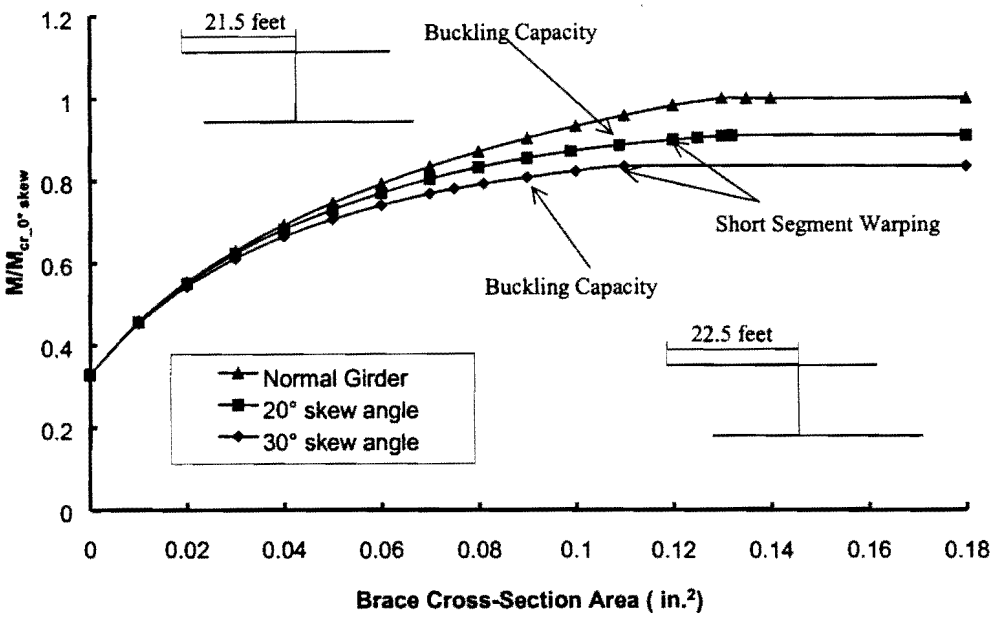

(a) $M/M_{cr\_0°skew}$ vs. Brace Area for W30x99 with One Normal Brace and 40 ft. Span

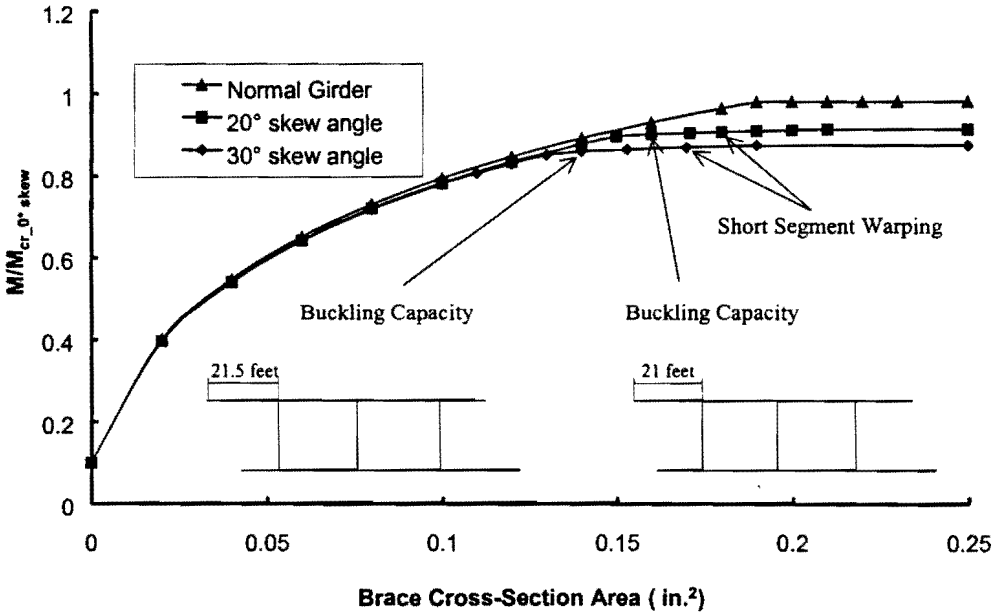

(b) $M/M_{cr\_0°skew}$ vs. Brace Area for Section #4 with Three Normal Braces and 80 ft. Span

Figure 7.1 Effect of Skew Angle on Brace Stiffness

The expressions for cross-section distortion, and in-plane girder stiffness are not changed, and the system stiffness is given by the following expression:

$$\frac{1}{\beta_T} = \frac{1}{\beta_b} + \frac{1}{\beta_{sec}} + \frac{1}{\beta_g} \tag{7.2}$$

where: β_T is the system stiffness
β_b is the stiffness of the brace
β_{sec} is the effect of cross-sectional distortion
β_g is the effect of the in-plane stiffness

The parameters in Eq. 7.2 were discussed in Chapter 2.

Figures 7.2, 7.3 and 7.4 show the comparisons of Eqs. 7.1 and 7.2 and the FEA results from eigenvalue buckling analyses for a W14x22 section. The results shown are for a twin-girder system with a 33 ft. span and a single normal brace close to midspan. Figs. 7.2, 7.3 and 7.4 illustrate the respective systems under loading conditions of uniform moment, uniformly distributed loads applied at the top flange, and concentrated top-flange loads at midspan. Graphs are shown for skew angles of 26.5° and 45° in the separate figures labeled (a) and (b), respectively. The graphs show that for the uniform moment case, Eqs. 7.1 and 7.2 have good agreement with the FEA results. For the cases with moment gradient, the equations are slightly unconservative for stiffness at or near the ideal value, however, this is due to effects of load height and underestimating the actual C_b factor as was discussed in Chapter 5.

Eigenvalue buckling analyses were also performed on a W30x99 section, which had a 40 ft. span (L/d =16) and a 100 in. girder spacing with 10° and 30° skew angles and a single normal brace close to midspan. The comparison of the FEA results and the equation results for the W30x99 section were very similar to that of the W14x22 section and are presented in Appendix C.

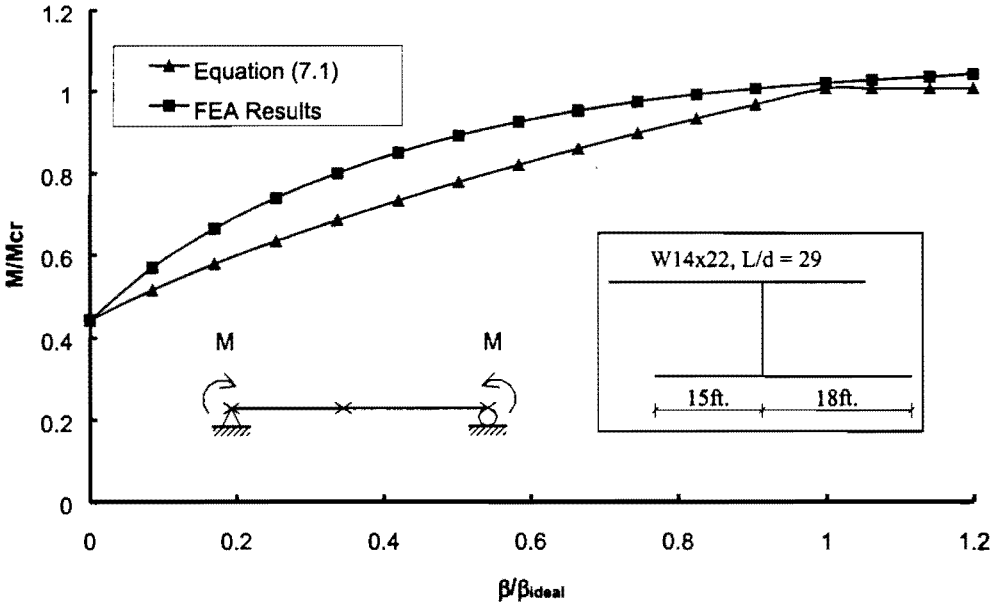

(a) skew angle =26.5°

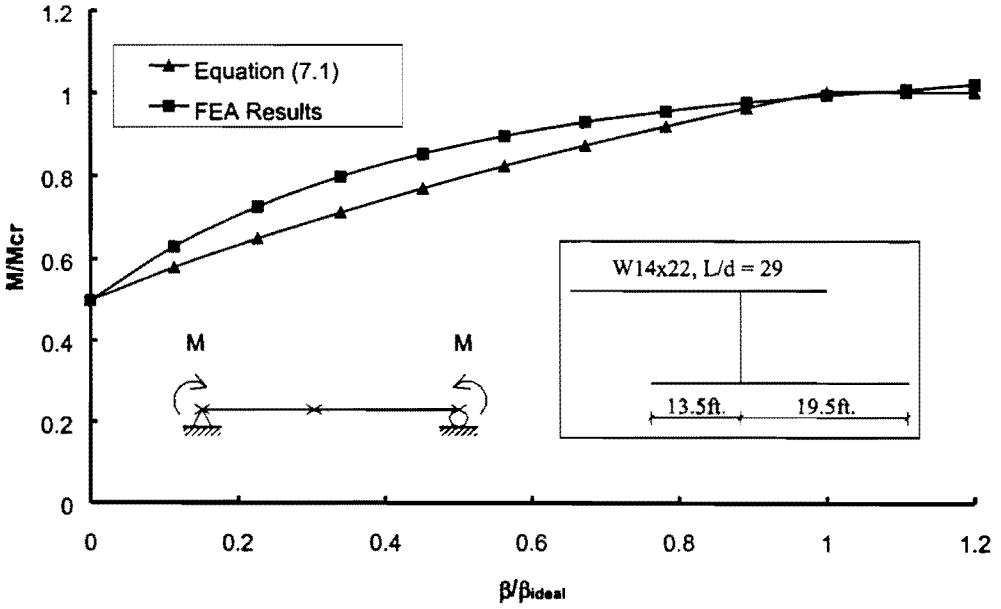

(b) skew angle = 45°

Figure 7.2 M/M_{cr} versus β/β_{ideal} for a W14x22 Section with Uniform Moment

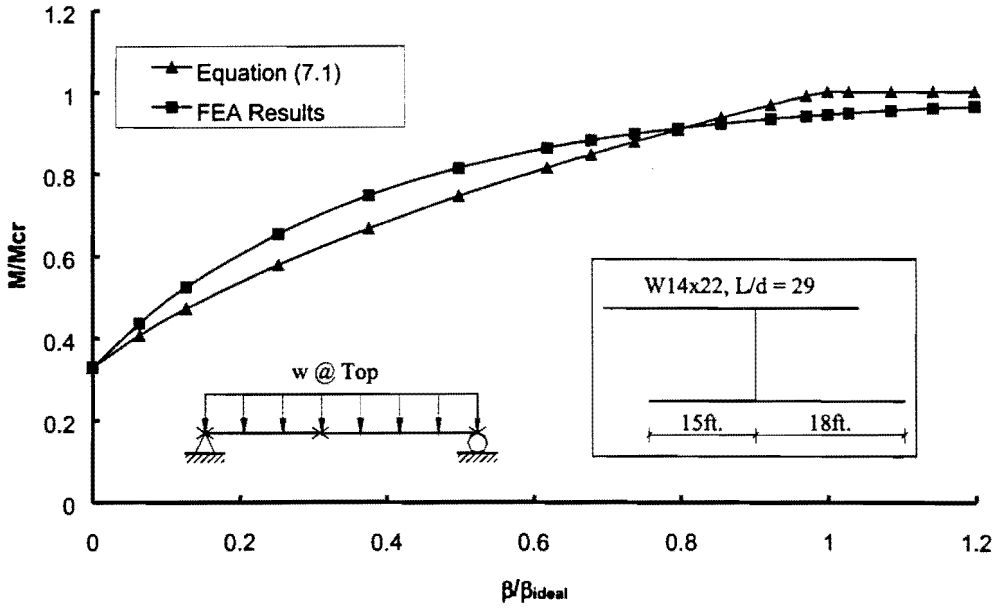

(a) skew angle =26.5°

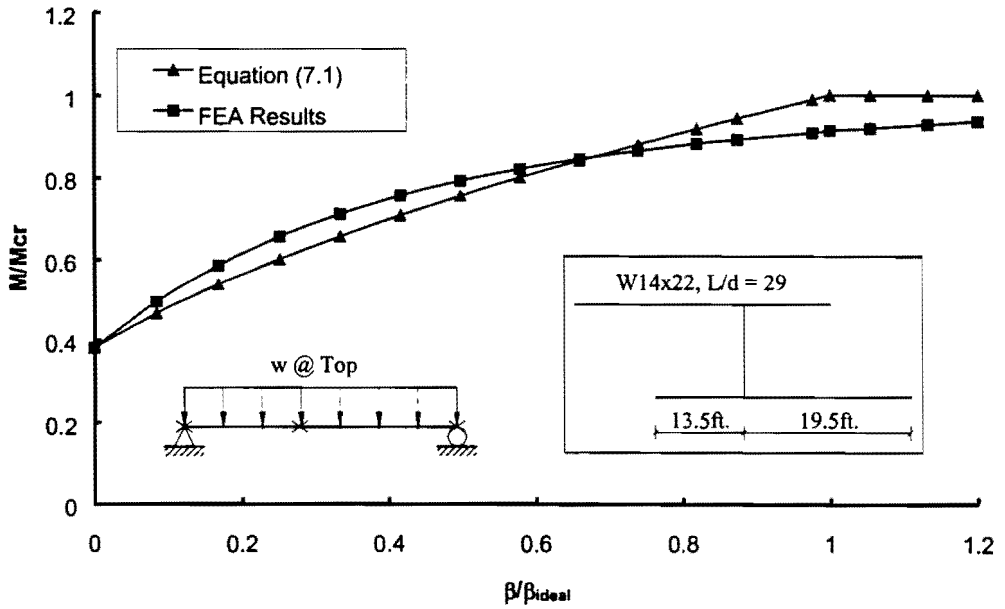

(b) skew angle = 45°

Figure 7.3 M/M_{cr} versus β/β_{ideal} for a W14x22 Section with Distributed Loads on Top Flange

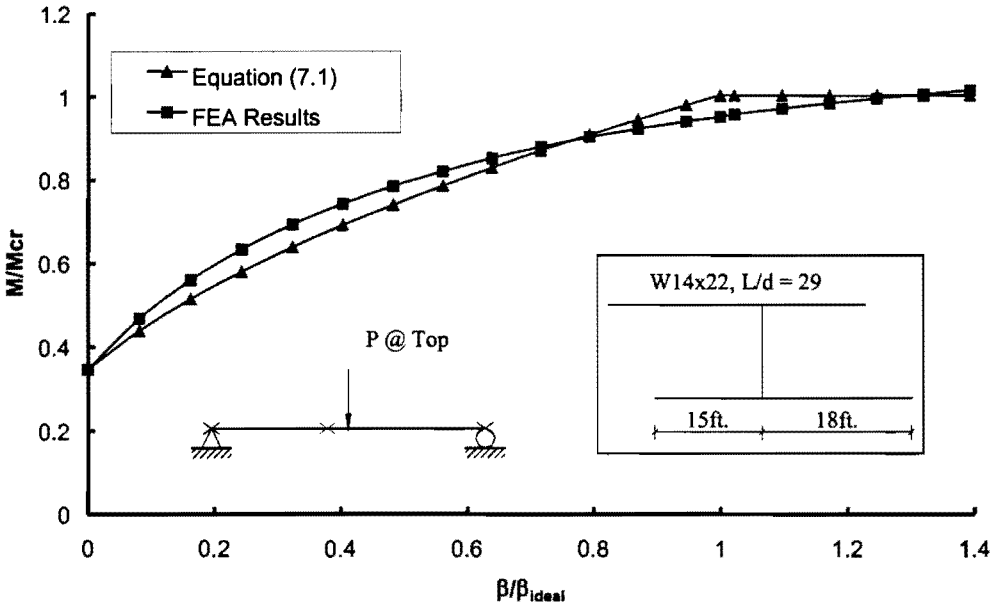

(a) skew angle =26.5°

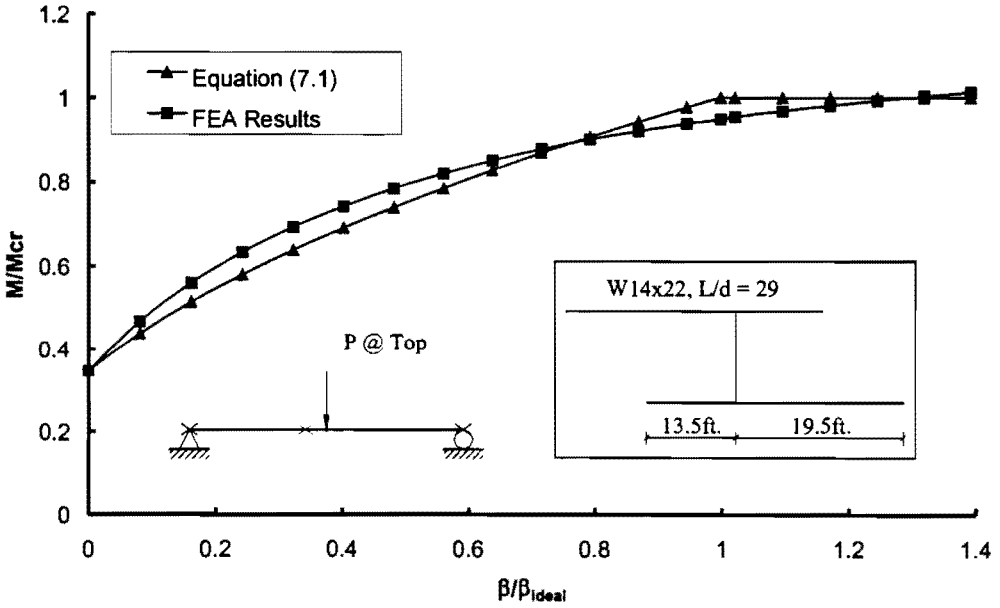

(b) skew angle = 45°

Figure 7.4 M/M_{cr} versus β/β_{ideal} for a W14x22 Section with Midspan Concentrated Load on Top Flange

Figures 7.5, 7.6, and 7.7 show the comparisons of the results from Eqs. 7.1 and 7.2 and the FEA analyses for the W36x160 section for the respective load cases of uniform moment, a distributed load applied at the top flange, and a midspan point load applied at the top flange. The twin-girder system had a 60 ft. span and a girder spacing of 120 inches with 20° and 45° skew angles. Two intermediate braces were placed normal to the girder longitudinal axis. The graphs show good agreement between Eqs. 7.1 and 7.2 and the FEA results, particularly for the uniform moment case. For cases with moment gradient, the equations provide conservative estimates with respect to the FEA solutions. As was discussed in previous chapters, the slight conservatism in the equations is caused by neglecting the warping restraint provided to the middle third of the beam by the exterior thirds of the beam. Effects of top flange loading on the buckling capacity are not as significant with two intermediate braces as was observed with a single intermediate brace.

A comparison of the FEA results and Eqs. 7.1 and 7.2 for the singly-symmetric Section #4 are shown in Figs. 7.8, 7.9, and 7.10 for the respective loading cases of uniform moment, a distributed load applied at the top flange, and a midspan point load applied at the top flange. The twin-girder system had an 80 ft. span and a girder spacing of 120 inches with skew angles of 20° and 30°. Three intermediate parallel braces were employed normal to the longitudinal axes of the girders. The graphs show good agreement between computational results and the equations, particularly for the uniform moment loading case. For cases with moment gradient, the buckling capacity from the FEA results are approximately 10% higher compared to the equations due to the warping restraint provided by the outside quarters of the beams as was discussed in Chapter 5. As discussed earlier, for beams with multiple intermediate braces load height does not have too significant of an effect on the buckling capacity. Results for the singly-symmetric Section #5 are similar to results for Section #4 and are presented in Appendix C.

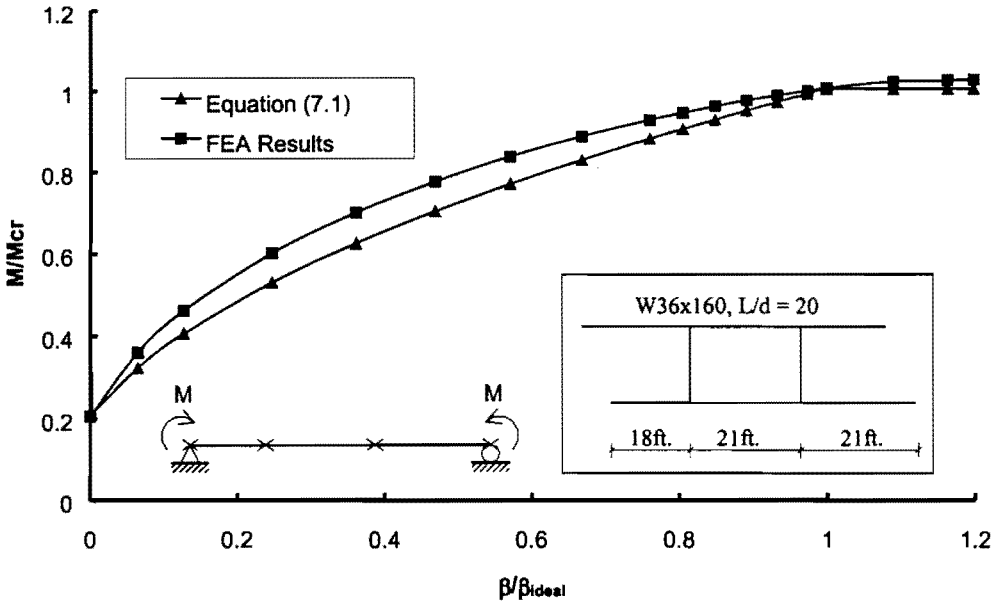

(a) skew angle =20°

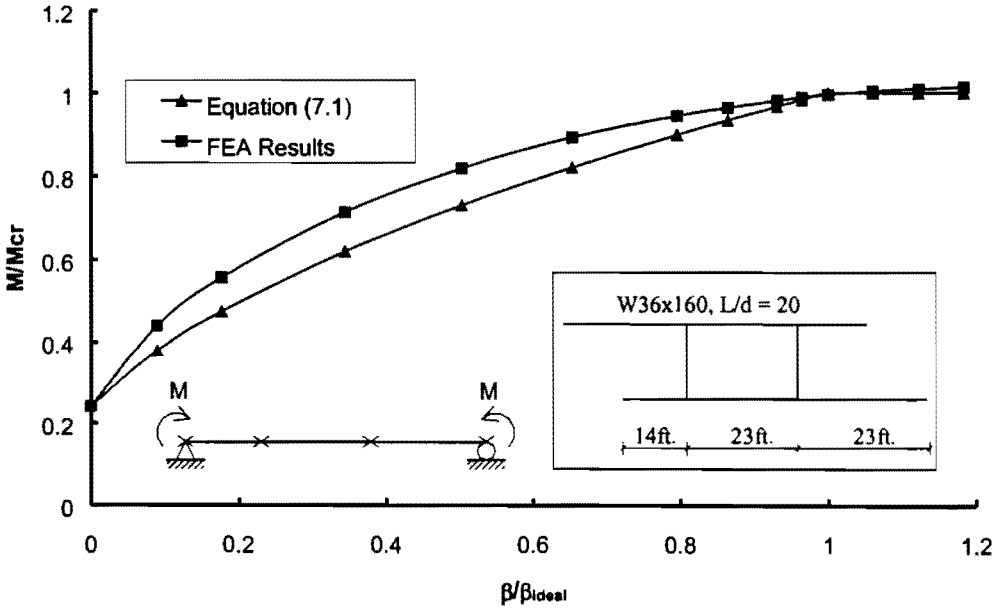

(b) skew angle = 45°

Figure 7.5 M/M_{cr} versus β/β_{ideal} for a W36x160 Section with Uniform Moment

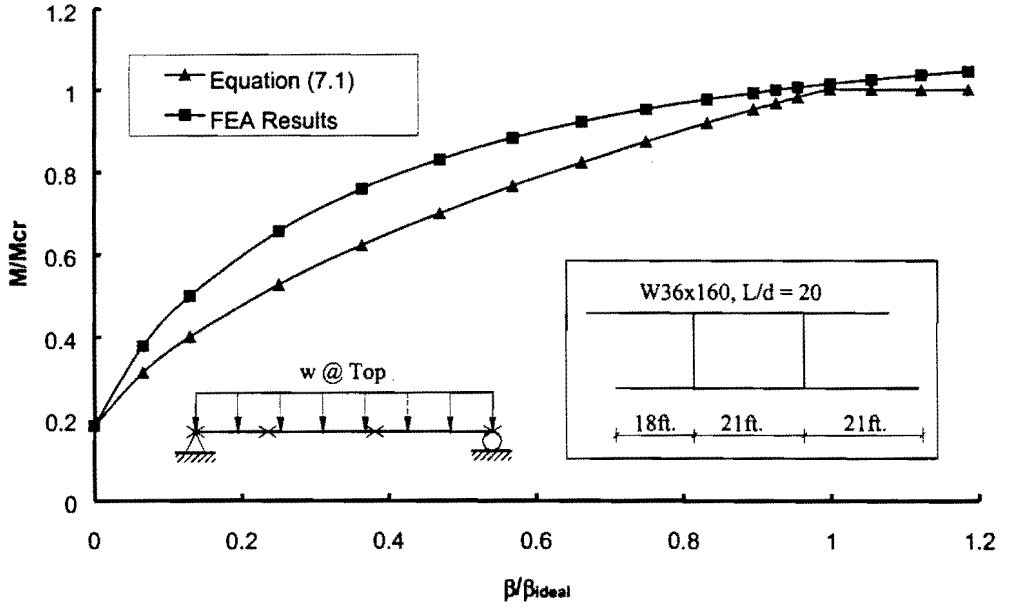

(a) skew angle =20°

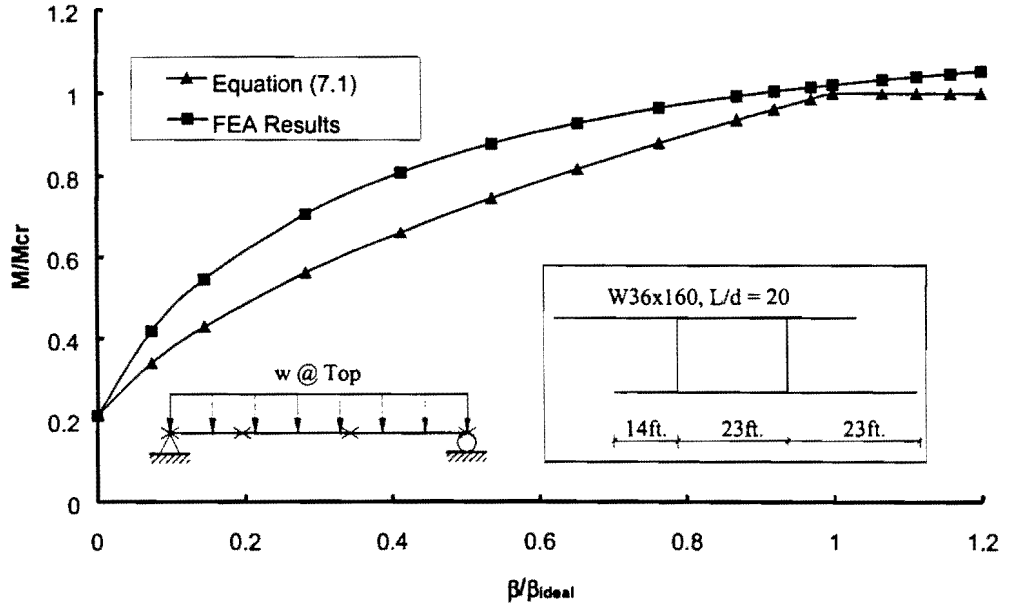

(b) skew angle = 45°

Figure 7.6 M/M_{cr} versus β/β_{ideal} for a W36x160 Section with Distributed Loads on Top Flange

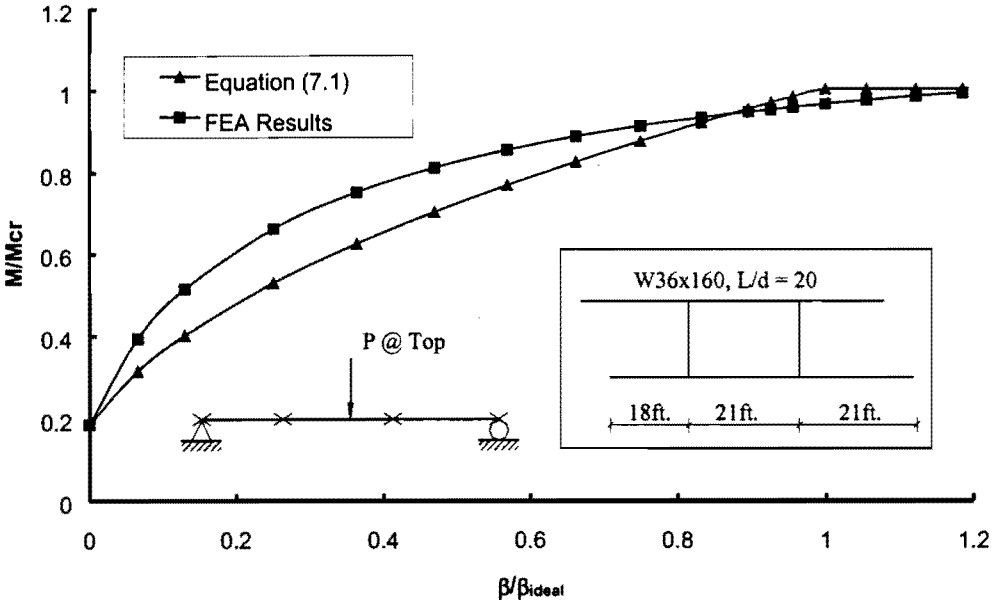

(a) skew angle =20°

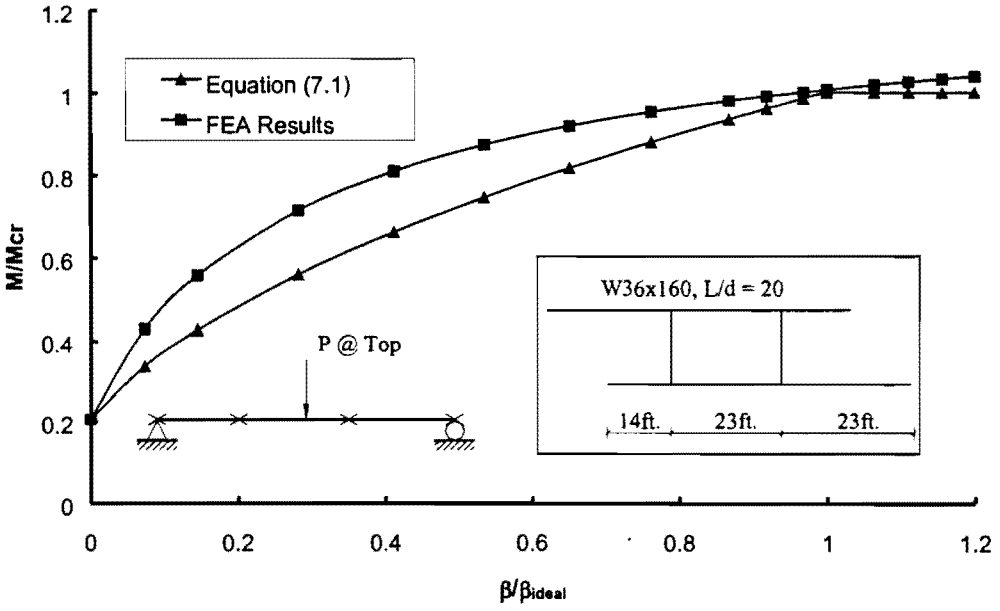

(b) skew angle = 45°

Figure 7.7 M/M_{cr} versus β/β_{ideal} for a W36x160 Section with Midspan Concentrated Load on Top Flange

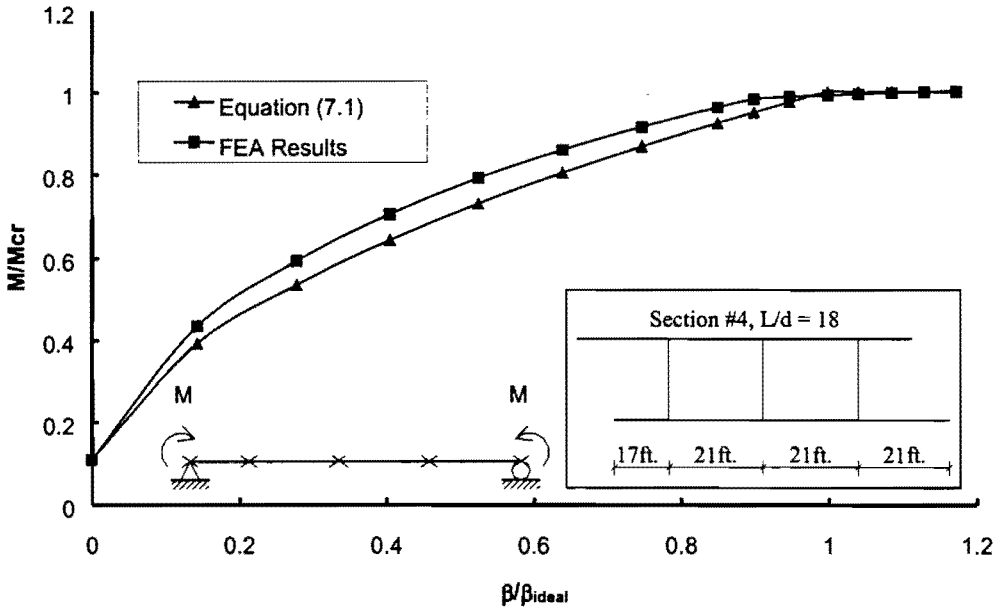

(a) skew angle =20°

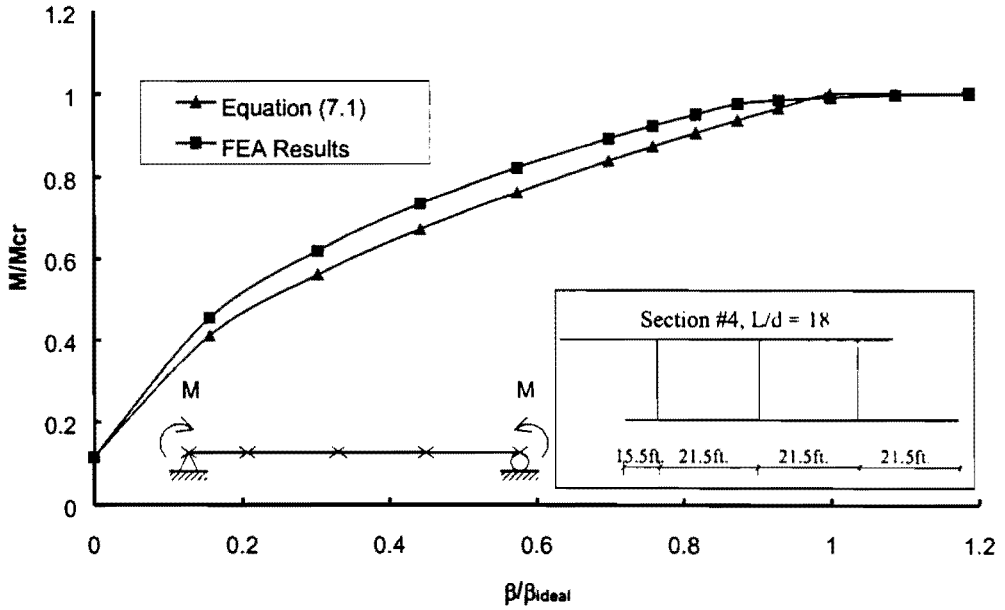

(b) skew angle = 30°

Figure 7.8 M/M_{cr} versus β/β_{ideal} for Section #4 with Uniform Moment

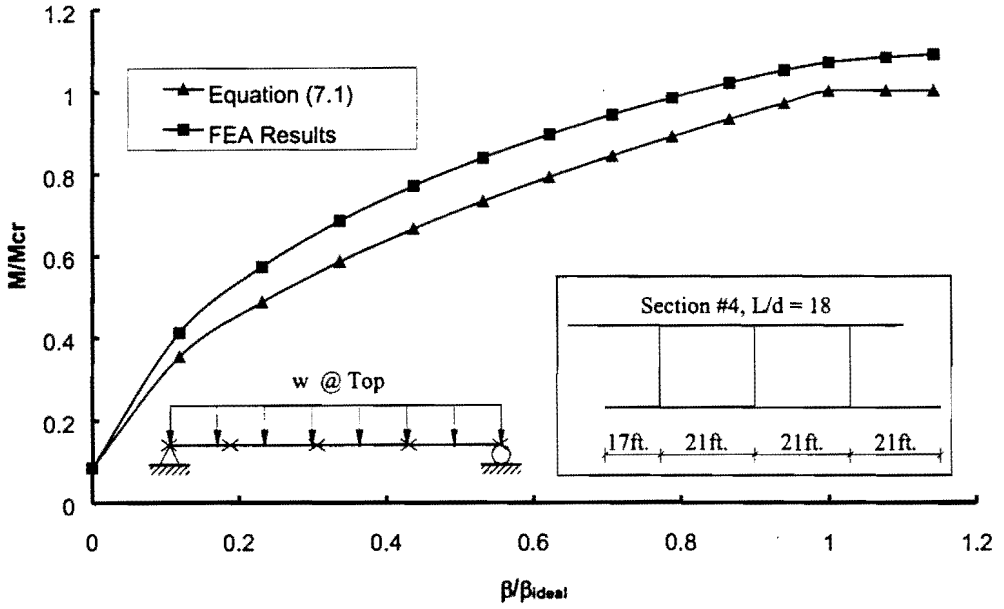

(a) skew angle =20°

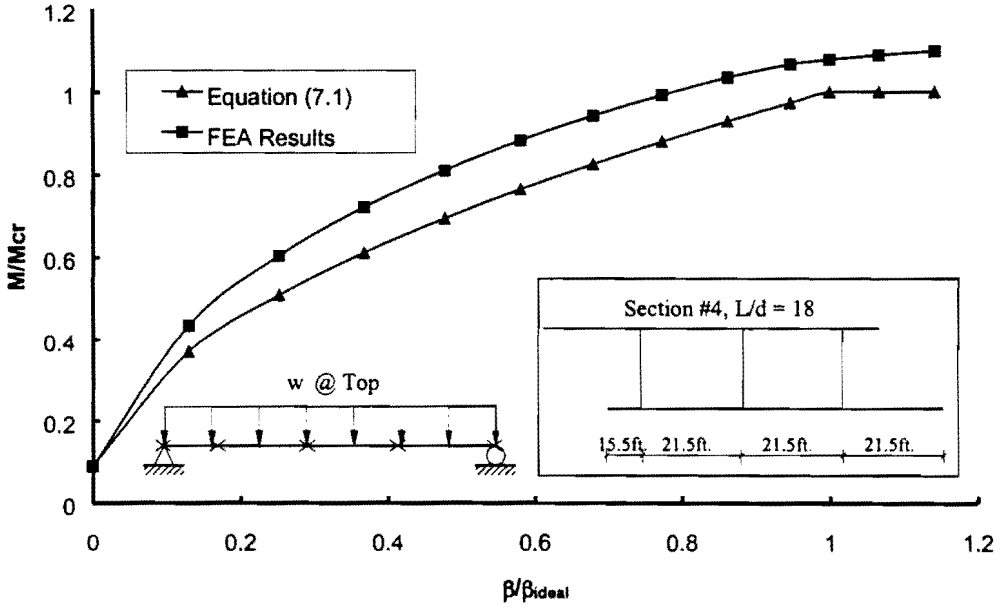

(b) skew angle = 30°

Figure 7.9 M/M_{cr} versus β/β_{ideal} for Section #4 with Distributed Loads on Top Flange

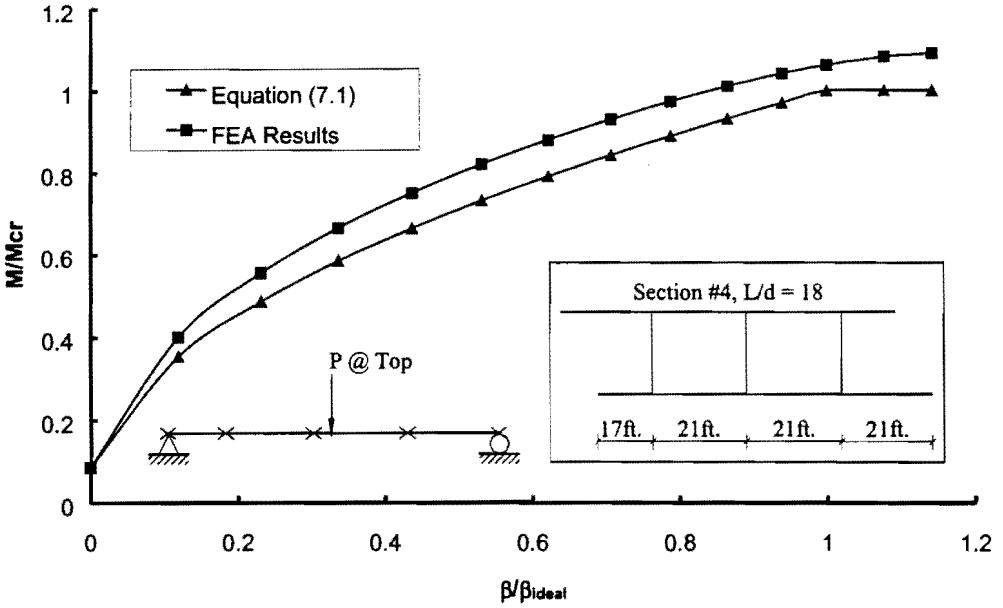

(a) skew angle =20°

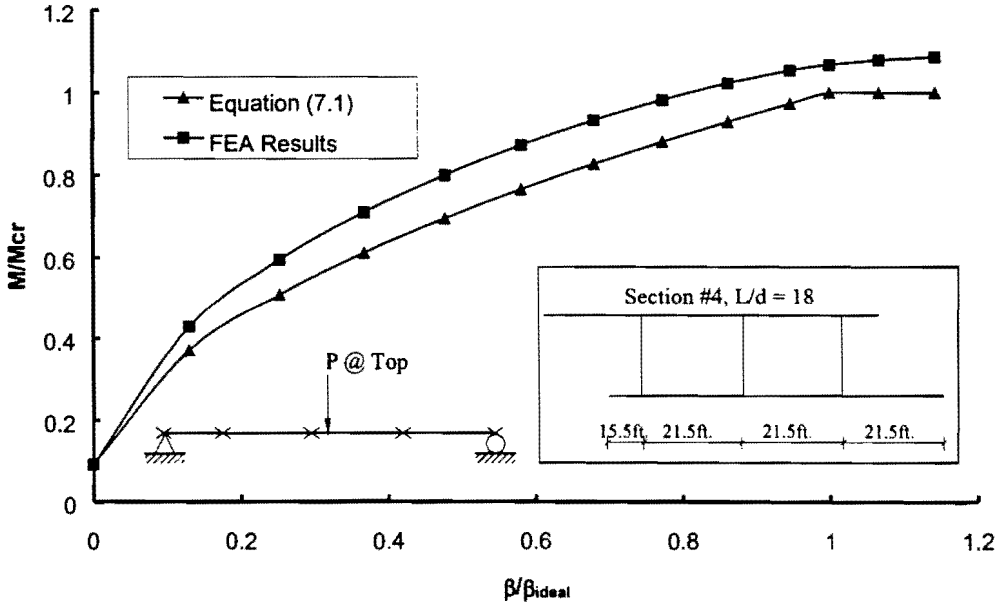

(b) skew angle = 30°

Figure 7.10 M/M_{cr} versus β/β_{ideal} for Section #4 with Midspan Concentrated Load on Top Flange

The results presented in Figures 7.2 to 7.10, as well as those presented in the Appendix, show that the equations provide good estimates of brace stiffness requirements for girders with braces oriented perpendicular to the skewed supports. Equations 7.1 and 7.2 provide good estimates of the brace stiffness requirements for cases with both uniform moment loading as well as cases with moment gradient. For the cases with moment gradient, the solutions provide slightly unconservative or conservative estimates for the girders depending on the number of intermediate braces. For cases with a single intermediate brace, the solutions were slightly unconservative due to effects of load height that are generally not considered in hand solutions. Although beams with multiple intermediate braces are also affected by load height, these effects are not as significant as for the case with a single intermediate brace. However, beams with multiple intermediate braces do conservatively neglect the warping restraint provided to the critical unbraced length by the other beam segments that have smaller moments and/or smaller unbraced lengths. As a result, the stiffness equations are slightly conservative with respect to the FEA results.

7.3 Brace Strength Requirements for Girders with Skewed Supports and Normal Braces

When the skewed bridges have braces oriented normal to the girder line, the skew angle has less of an effect on the brace moment than it did on the cases observed in Chapter 6 with braces parallel to the skew angle. Consequently, the basic strength requirements discussed in Chapters 2 and 5 can be applied directly to the cases with bracing oriented normal to the girder lines.

Comparisons of equations with the FEA large displacement analysis results are presented for several of the girder cross-sections that were studied. Graphs are presented for the girders with different skew angles for the different loading conditions that were considered. For the sections W14x22, W30x99, Section #4, and Section #5 the maximum moment occurred at or close to the middle cross-frame and the comparisons between the brace moment predicted by the equations and the FEA results were very similar. Therefore results for one section, Section #5, are presented in this chapter as a representative sample while the graphs for the other sections are provided in Appendix C. Figures 7.11, 7.12, and 7.13 show the graphs of the equations and the FEA results for Section #5 with the three load cases that were considered. The brace moment is graphed on the vertical axis while the applied moment is on the horizontal axis. The brace moment has been normalized by the maximum brace moment, while the applied moment has been normalized by the moment corresponding to buckling between the brace points.

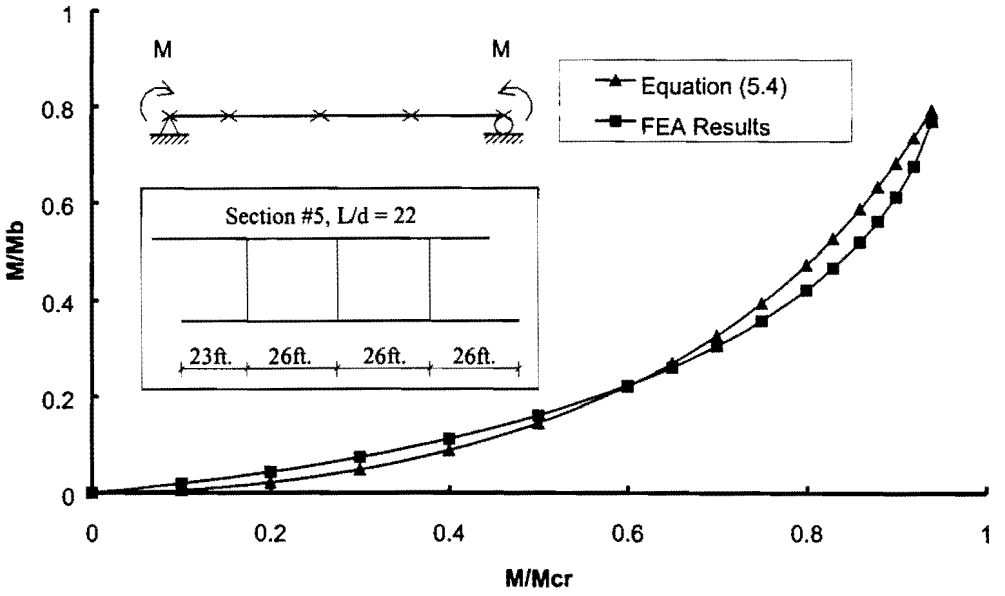

(a) skew angle =20°

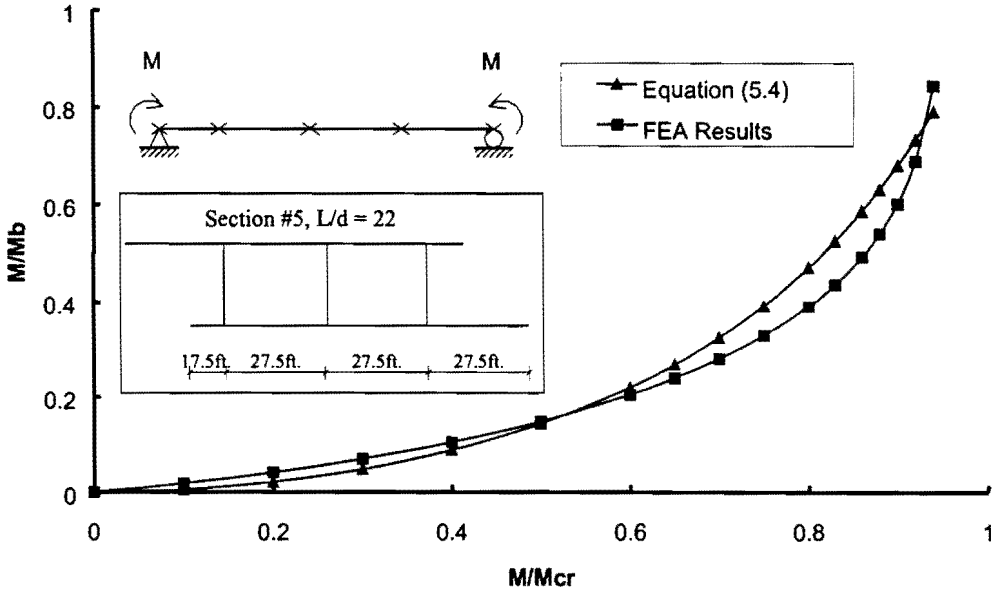

(b) skew angle = 45°

Figure 7.11 M_b/M_{br} versus M/M_{cr} for Section #5 with Uniform Moment and $\beta_T = 2\beta_{ideal}$

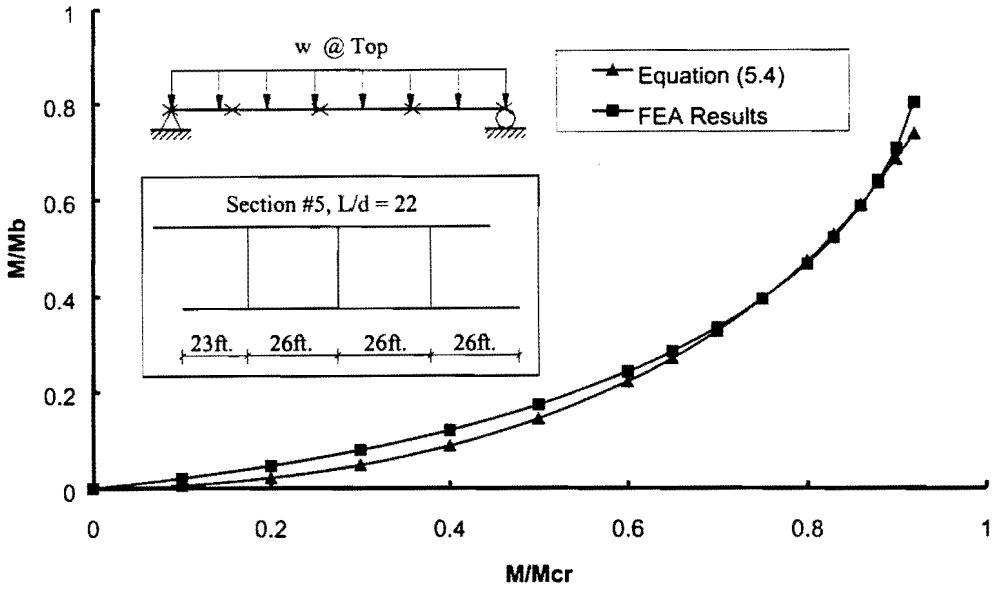

(a) skew angle =20°

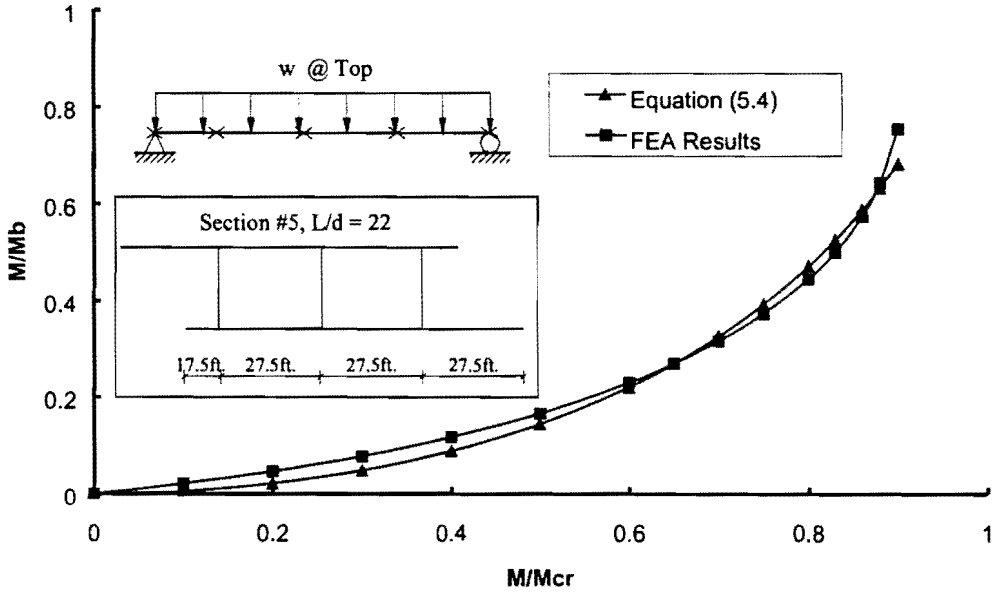

(b) skew angle = 45°

Figure 7.12 M_b/M_{br} versus M/M_{cr} for Section #5 with Distributed Loads on Top flange and $\beta_T = 2\beta_{ideal}$

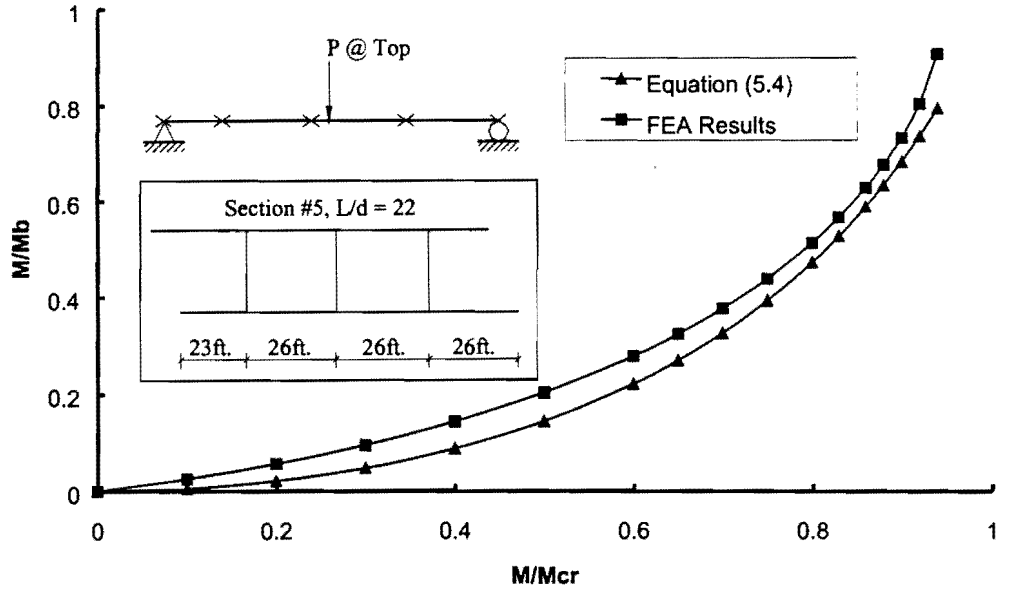

(a) skew angle =20°

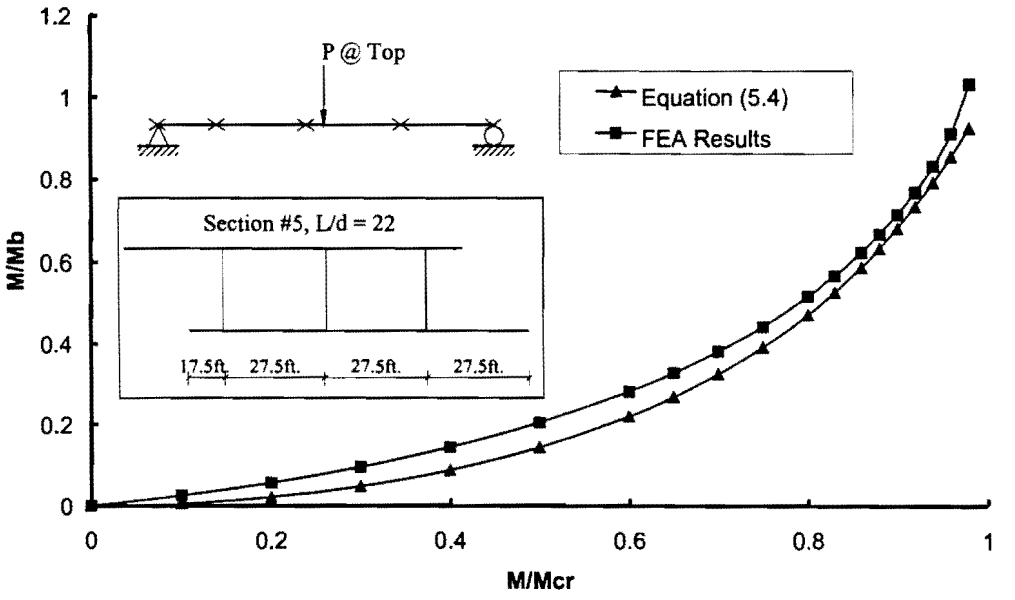

(b) skew angle = 45°

Figure 7.13 M_b/M_{br} versus M/M_{cr} for Section #5 with Concentrated Loads on Top Flange at Midspan and $\beta_T = 2\beta_{ideal}$

The behavior of the W36x160 differed from the other four sections due to differences in the distribution of the moments and the intermediate cross-frame locations. Comparisons of the equations and FEA results are shown in Figs. 7.14, 7.15, and 7.16 for the three different load cases that were considered. Results are shown for skew angles of 20° and 45°. Reasonable agreement between the equations and the FEA solution was obtained for the case with uniform moment loading as shown in Fig. 7.14. However for the cases with moment gradient shown in Figs. 7.15 and 7.16, the equations were relatively conservative with respect to the FEA solutions. The conservative nature of the equations for cases with moment gradient is because the maximum applied moment occurs at midspan, while the intermediate braces are located at the third points. When the maximum moment occurs between brace points, adjacent braces share the brace moment instead of a single brace providing the majority of the restraint, which is the case when the maximum moment occurs at the brace location. Although the equations were conservative for the W36x160, the graphs shown in this section as well as in the appendix demonstrate that the equations do a reasonable job of predicting the brace moments.

7.4 Summary

This chapter has presented finite element results for girders with skewed supports and normal braces. The analyses are conducted on several different sections with different skew angles and a variety of loading conditions. The results have demonstrated the normal bracing behavior of twin-girder systems .

The previous recommendation of using 0.75L in Eq. 7.1 for girders with only one intermediate brace was generally found to be unconservative for girders with skewed supports. Simply using the full girder length, L, in Eq. 7.1 had good agreement with the FEA results in obtaining the ideal stiffness. For skewed girders with more than one normal brace, the equations presented in Chapter 5 show good agreement with the FEA results in predicting the ideal stiffness, and these solutions can therefore be directly applied to girders with skewed supports provided the braces are oriented normal to the girder lines. The equations to estimate the strength requirement presented in Chapter 5 can be directly used to estimate the brace moment for skewed girders with normal braces.

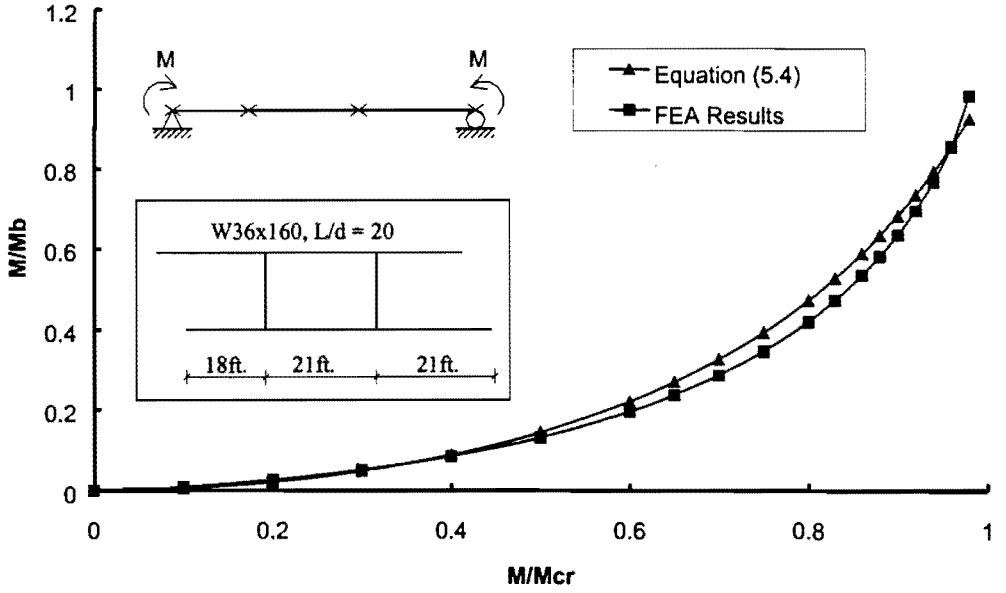

(a) skew angle =20°

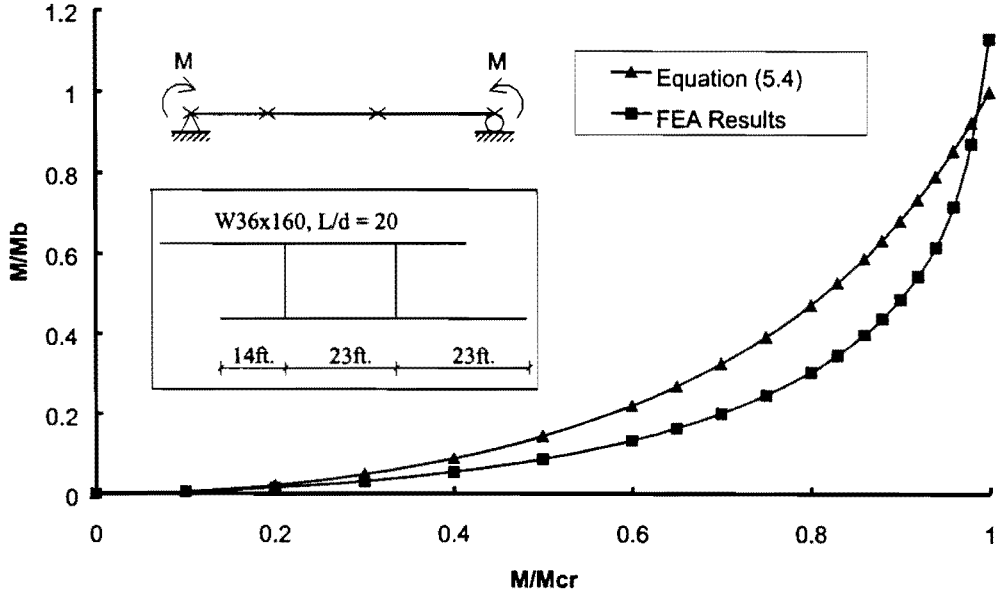

(b) skew angle = 45°

Figure 7.14 M_b/M_{br} versus M/M_{cr} for a W36X160 Section with Uniform Moment and $\beta_T = 2\beta_{ideal}$

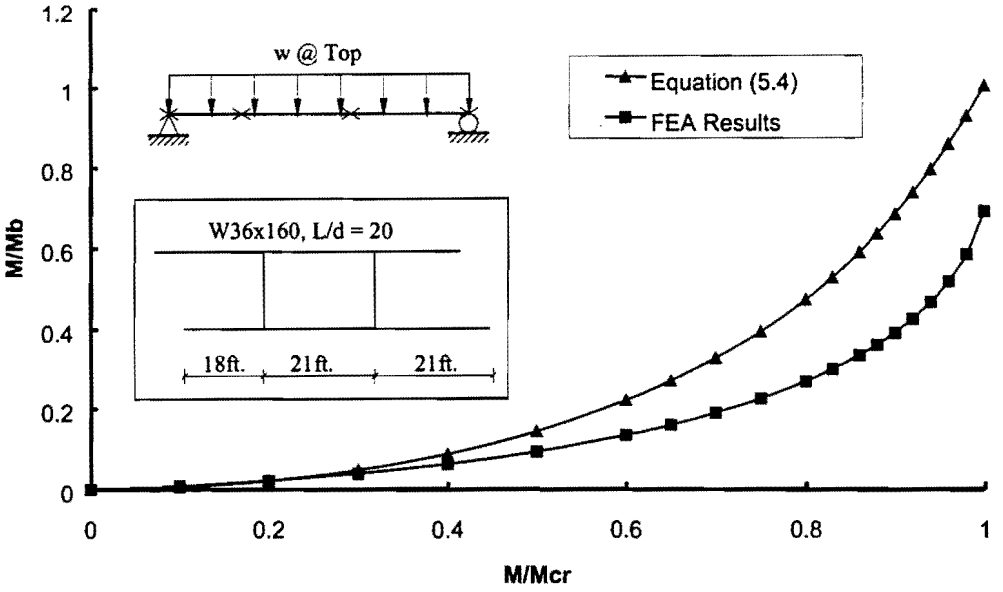

(a) skew angle =20°

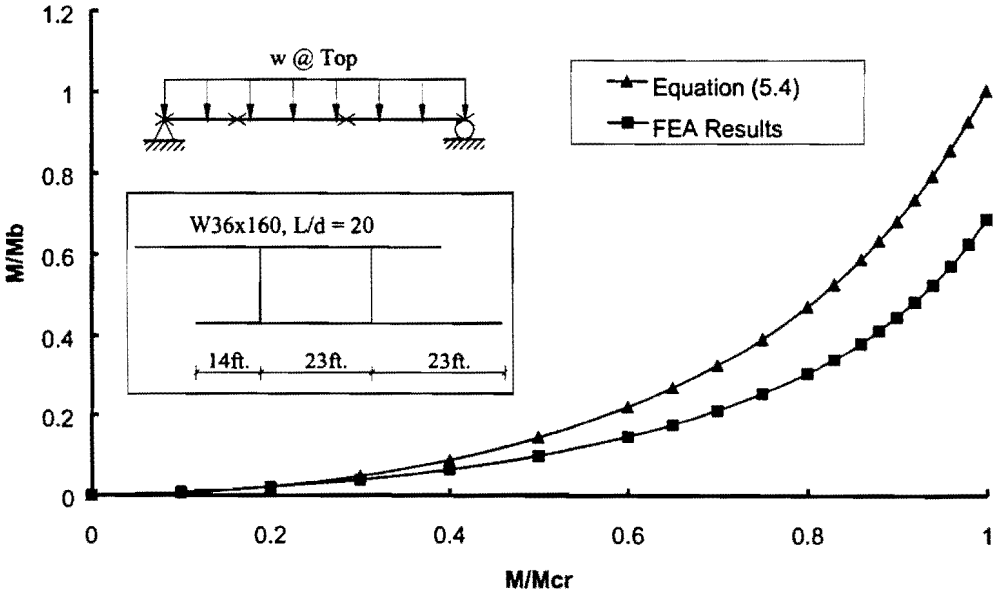

(b) skew angle = 45°

Figure 7.15 M_b/M_{br} versus M/M_{cr} for a W36x160 Section with Distributed Loads on Top Flange and $\beta_T = 2\beta_{ideal}$

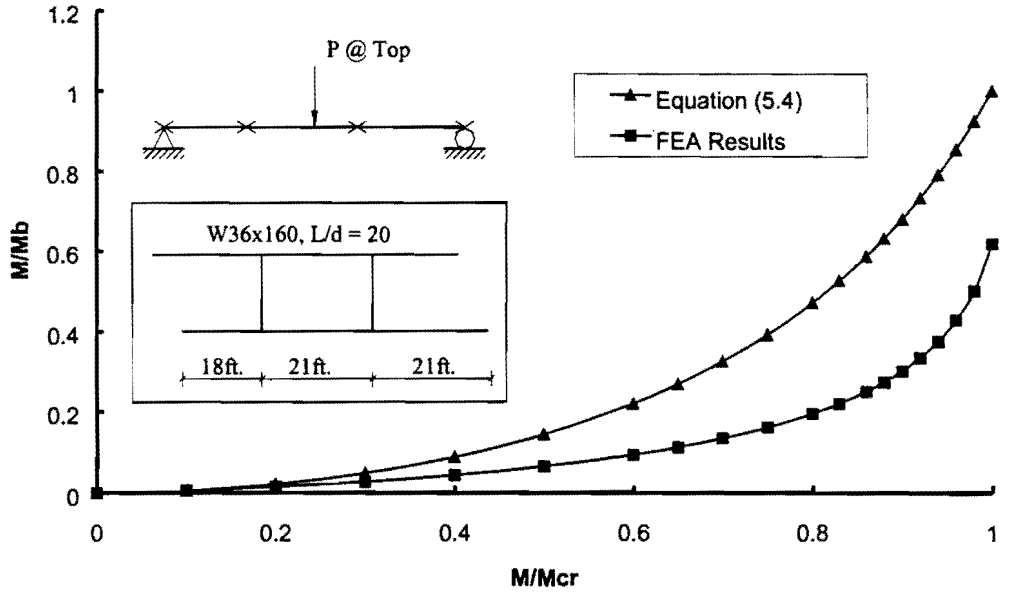

(a) skew angle =20°

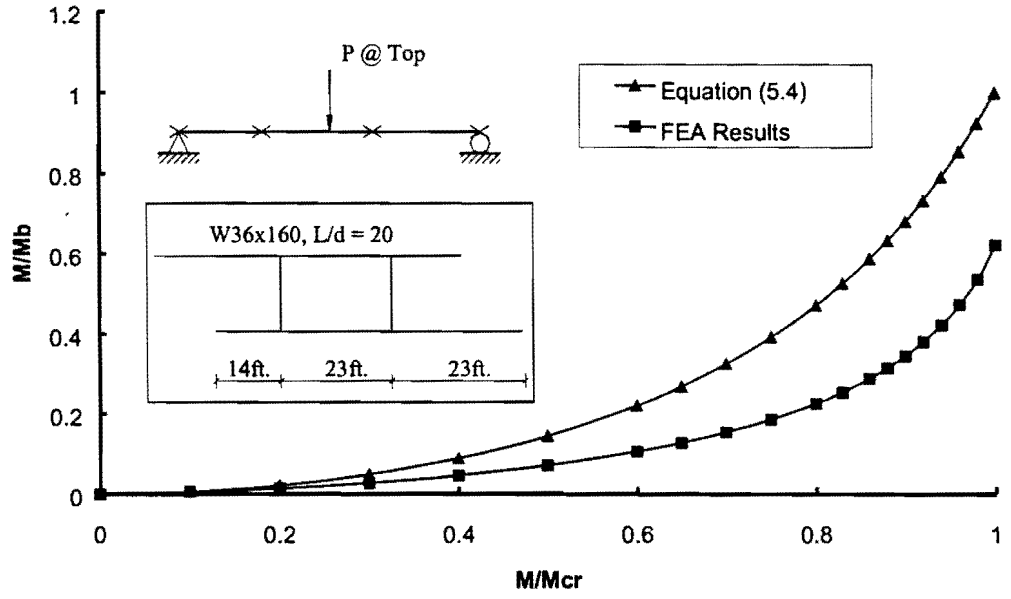

(b) skew angle = 45°

Figure 7.16 M_b/M_{br} versus M/M_{cr} for a W36x160 Section with Concentrated Loads on Top Flange at Midspan and $\beta_T = 2\beta_{ideal}$

Chapter 8
Bracing Details for Bridges with Skewed Supports

8.1 Introduction

The bracing requirements for steel girders with skewed supports were discussed in Chapters 6 and 7, which presented the respective results for brace orientations that were parallel to the skewed supports and normal to the longitudinal axes of the girders. The analyses that were presented in these previous chapters mainly focused on twin-girder systems. This chapter will investigate the bracing behavior for steel bridge systems with four girders that have skewed supports. A number of different bracing details were investigated in these analyses. As outlined in Chapter 1, in addition to developing bracing requirements for bridges with skewed supports, a primary goal of this research is to develop new details to reduce the fatigue sensitivity of the cross-frame and diaphragm regions as well as to reduce the total number of braces on the bridge. Since many of the typical details that are currently employed are often stiffer and stronger than necessary, a number of cross-frames could potentially be eliminated by employing lateral struts positioned near the top and bottom flanges and leaning several girders on a single brace. The braces can therefore be positioned to minimize the brace forces that would be induced by truck traffic, thereby reducing the sensitivity of these brace regions to fatigue damage. In addition, with fewer braces the bridge may be easier to inspect for potential fatigue damage since it can be difficult to locate fatigue cracks in the regions around cross-frames and diaphragms.

This chapter has been divided into five subsections. Following the introductory material presented in this section, analytical results for a four-girder bridge with cross-frames extending across the full width of the bridge will be presented in Section 8.2. Both eigenvalue buckling and large displacement analyses were performed, and the FEA results are compared to the equations discussed in the previous chapters. In Section 8.3, results are presented in which braces are removed and several girders across the width of the bridge lean on a single cross-frame. The analytical results presented in Sections 8.2 and 8.3 focus on the behavior of the non-composite steel girder with top flange loading. In Section 8.4, the forces induced in the cross frames due to truck loading on the composite girders in the finished bridge are studied. The FEA model of the steel girders and the concrete bridge deck are discussed in Section 8.4, along with the model of the truck loading. FEA results are compared using both existing and proposed bracing details. Finally, the results are summarized in Section 8.5.

8.2 Bracing Behavior for a Four-Girder Bridge with Skewed Supports

Finite element results are presented in this section demonstrating the bracing behavior of the cross-frames in a four-girder bridge with skewed supports. A plan view of the four-girder bridge system is shown in Fig. 8.1. The bridge has a 124 ft. span with five intermediate cross-frame lines, which produces an unbraced length of 24 ft. At each brace

location, cross frames extend across the entire width of the bridge and are numbered from 1 to 15. The cross-frames numbered 3 and 13 frame into the fascia girder 4 feet from the skewed support. Many current details for such a condition often have the bracing framing directly into the support. Doing so however results in relatively large live load forces induced in the braces when the truck traffic passes over the bridge. This will be demonstrated later in this chapter. Much better behavior is achieved by offsetting the bracing from the support by a relatively small amount such as the 4 ft. offset shown for this particular bridge.

The singly symmetric girder labeled Section #6 from the sections presented in Fig. 3.8 was used in the analyses. The bridge modeled has a skew angle of 33.7° and uniformly distributed loads applied at the top flange to simulate the construction loads.

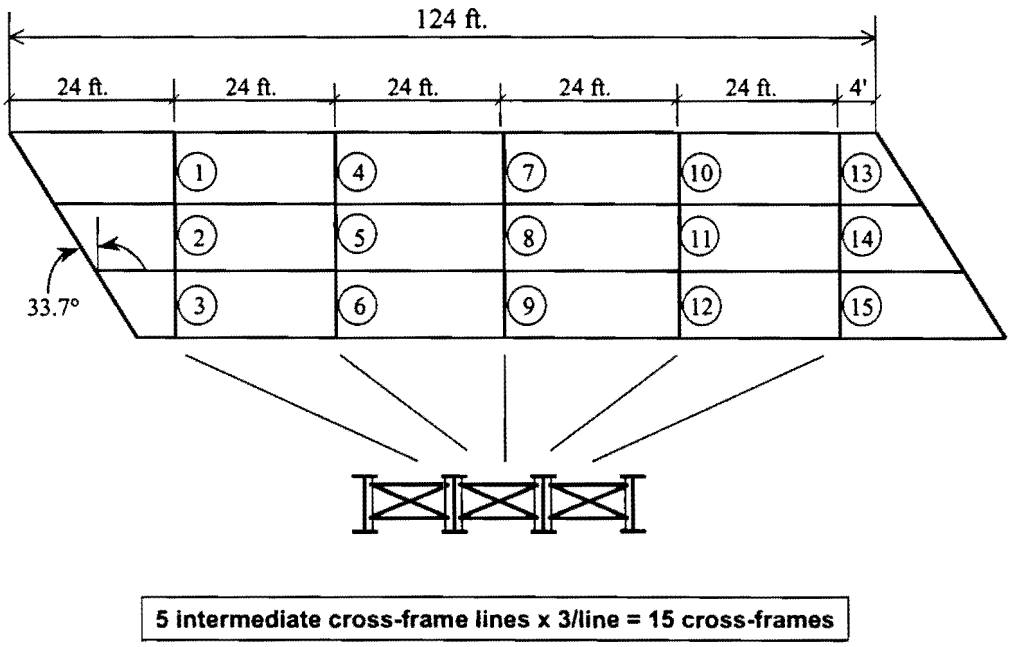

Figure 8.1 Four-Girder Bridge Layout

Figure 8.2 shows a comparison of the results from the eigenvalue buckling analyses and the equations presented in Chapters 5 and 7. The graph shows good agreement between the equation results and the FEA results in obtaining the ideal stiffness and are approximately 5% conservative at the point of full bracing.

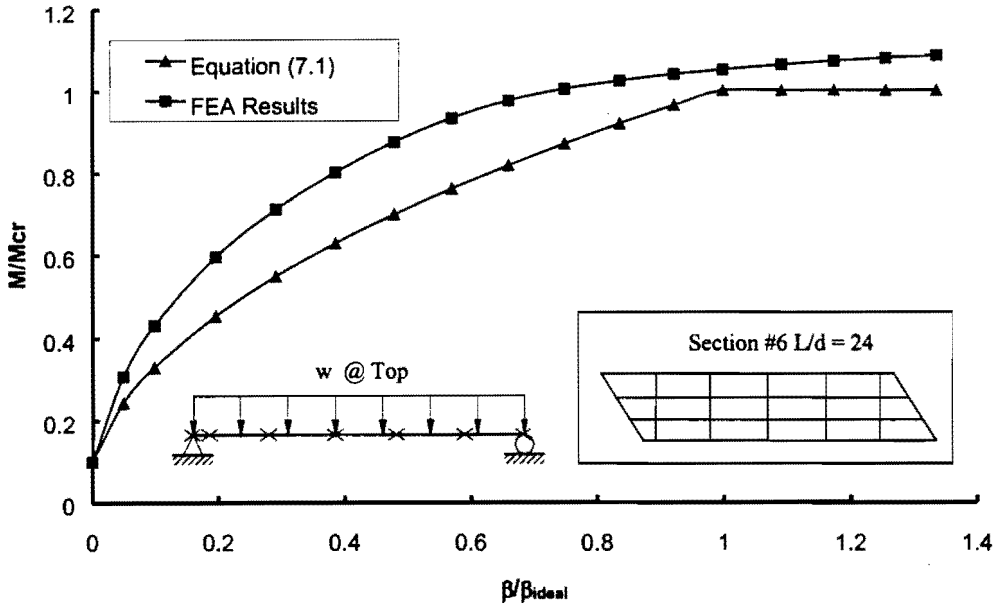

Figure 8.2 M/M_{cr} versus β/β_{ideal} for Section #6 Four-Girder System with Distributed Loads on Top Flange

The process for selecting the critical imperfections that were utilized in the FEA studies on the brace strength requirements for Chapters 5, 6, and 7 were outlined in Chapter 4. Similar criteria were utilized in the selection of the imperfection for the 4-girder system shown in Fig. 8.1. The resulting imperfection is shown in Fig. 8.3. The maximum lateral displacement in the imperfection of the top flange was 0.576 inches, which corresponds to $L_b/500$. The bottom flange was straight.

A graph of the FEA results and the equation results for the brace moment is given in Fig. 8.4. The brace moment is graphed on the vertical axis versus the applied beam moment. The brace moments have been normalized by the maximum moment predicted by the strength equations, while the applied beam moment has been normalized by the maximum moment. A brace stiffness corresponding to twice the ideal value was used. The brace force that is graphed corresponds to the moment in cross-frame number 9, which was the maximum brace moment that was encountered throughout the bridge. The graph shows that the equations have good agreement with the FEA results, although the equation prediction is slightly conservative as the applied loads approach the buckling capacity. The reason for the conservative estimates is due to the interaction between the cross-frames at the brace line. Each brace line has three cross-frames which connect the four girders together. When all the girders displace laterally and twist, the middle two girders will experience more restraint than the two edge girders. Considering the brace line located near midspan of the bridge, the middle cross-frame (cross frame #8 in Fig. 8.1) will generally have less force than the cross-frames located near the edges (cross-frames #7 and #9). Therefore, the resulting maximum force in the cross-frame is lower than would be predicted using the brace strength

requirements, which assume all the cross-frames are equally critical. In addition, since the braces across the bridge width do not all frame into the girders at the exact same point along the bridge length, the girder moments at the ends of the cross-frames are different. Results will be presented later in this chapter that will show that the forces in braces that are not at the point of maximum moment are often substantially lower than those positioned at or near the region of maximum bending moment.

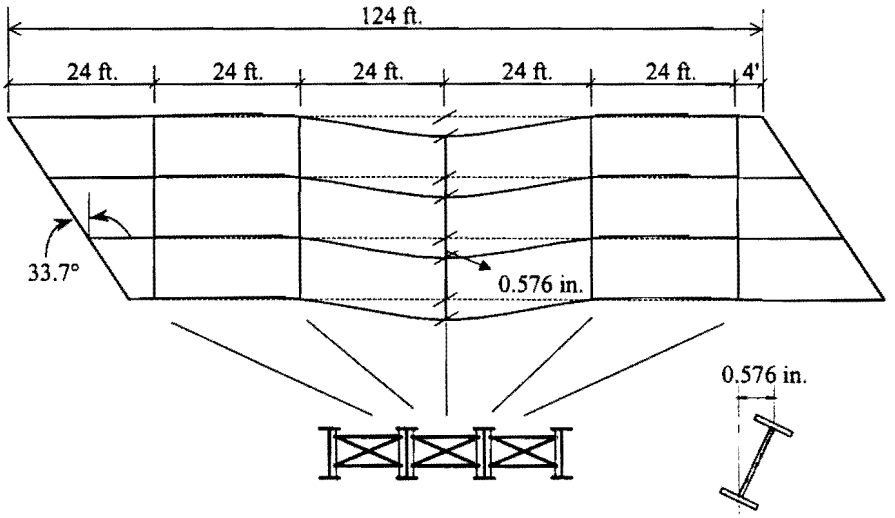

Figure 8.3 Critical Imperfection Utilized in Four Girder Bridge

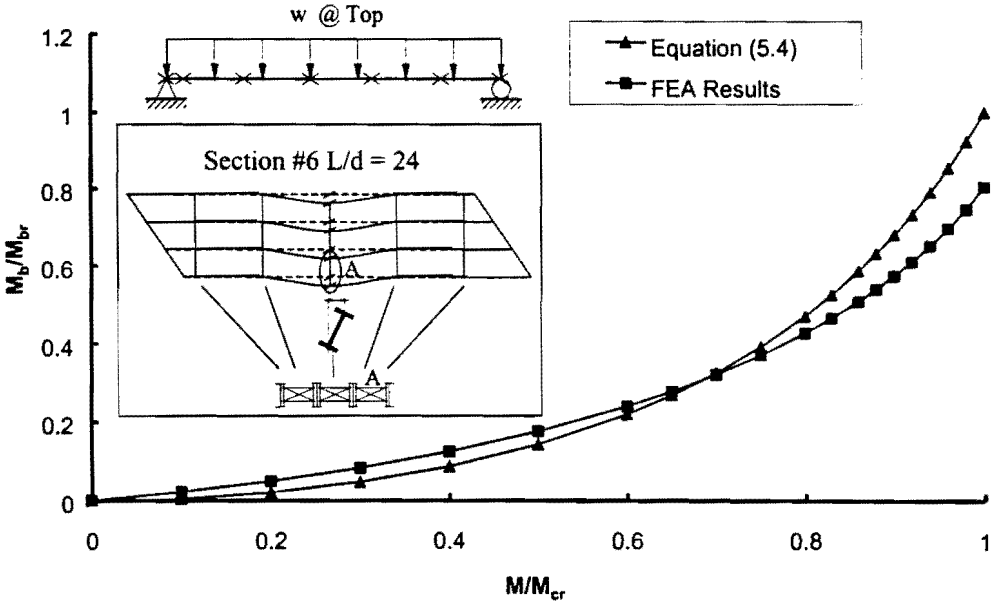

Figure 8.4 M_b/M_{br} versus M/M_{cr} for Section #6 with Distributed Loads on Top Flange (Cross-Frame A)

Equation 2.18 that was given in Chapter 2 can be slightly modified and used to solve for the required brace stiffness. Equation 2.18 is based upon the ideal stiffness and is given in the following expression:

$$M_{cr} = \sqrt{C_{bu}^2 M_0^2 + \frac{C_{bb}^2 \overline{\beta_T} E I_y}{C_t}} \leq M_s \text{ or } M_y \tag{8.1}$$

The first term under the radical in Eq. 8.1 is the buckling capacity of the girder with no intermediate bracing while the second term accounts for the contribution of the bracing. Following the simplification applied in the AISC LRFD (2001) Specification, the initial capacity of the girder can be conservatively neglected. Equation 8.1 can then be set equal to the maximum design moment and reorganized to solve for the ideal brace stiffness. Assuming top flange loading with a $C_t = 1.2$, Eq. 8.1 reduces to the following expression:

$$\beta_{Ti} = \frac{1.2 L M_u^2}{C_{bb}^2 n E I_y} \tag{8.2}$$

As mentioned earlier, the ideal stiffness should be doubled to control initial imperfections and brace forces. If the allowable stress design (ASD) method is used, a factor of safety of 2.0 should be used on the stiffness requirement. Doubling the ideal stiffness and applying the factor of safety therefore yields the following expression:

$$\text{Service Load (Allowable Stress Design): } \beta_{T\,Req'd} = 2(2\beta_{Ti}) = \frac{4.8 L M_u^2}{C_{bb}^2 n E I_y} \tag{8.3}$$

If ultimate strength design approaches such as the Load Factor Design (LFD) or the Load and Resistance Factor Design (LRFD) methods are used, a resistance factor of 0.75 should be used on the stiffness. Doubling the ideal stiffness and applying the resistance factor to the denominator therefore leads to the following expression for the required brace stiffness:

$$\text{Ultimate Strength (LFD or LRFD): } \beta_{T\,Req'd} = \frac{2\beta_{Ti}}{0.75} = \frac{3.2 L M_u^2}{C_{bb}^2 n E I_y} \tag{8.4}$$

Equation 8.4 is essentially identical to the expression in the AISC LRFD Specification (2001). For an initial twist $\phi_o = L_b/(500h)$, where L_b is the girder unbraced length and h is the girder depth, the strength requirements be obtained by multiplying twice the ideal stiffness by the initial twist, ϕ_o. This therefore results in the following expression:

$$M_{br} = 2\beta_{Ti}\phi_0 = \frac{2.4 L M_u^2}{C_{bb}^2 n E I_y} \times \frac{L_b}{500h} \tag{8.5}$$

For a design based upon ASD, M_u in Eqs. 8.3 and 8.5 is the maximum moment from service loads; while the maximum moment from factored loads is used in either LFD or LFRD based designs in Eqs. 8.4 and 8.5. In checking the strength of a bracing member using Eq. 8.5, the appropriate ASD, LFD, or LFRD strength equation (with factors of safety or resistance factors) will apply. M_{br} is the brace moment based upon the provided brace stiffness equal to the required brace stiffness, $\beta_{T\ Req'd}$, which equals to twice the ideal stiffness. For cases where the provided brace stiffness, β_{act}, is larger than the required brace stiffness, the brace moment can be reduced by the following expression:

$$M_{act} = M_{br}\left[\frac{\left(\frac{M_u}{M_{cr}}\right)^2}{2-\frac{\beta_{T\,Req'd}}{\beta_{act}}\left(\frac{M_u}{M_{cr}}\right)^2}\right] \tag{8.6}$$

A derivation of Eq. 8.6 is presented in Appendix D.

The example presented in Fig. 8.5 for the design of the bridge girders shown previously in Fig. 8.1 demonstrates the application of the brace stiffness and strength requirements that were outlined in Chapters 2 and 6.

TORSIONAL BRACING EXAMPLE - CROSSFRAMES

Girder Properties

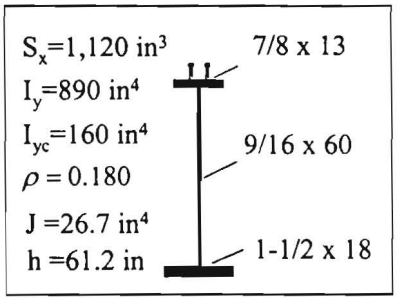

Span = 124 ft.; 8 in. concrete slab; 4 girders @ 10 ft spacing, Gr 50 steel. Design a torsional bracing cross-frame system to stabilize the girders during the deck cast.

Figure 8.5 Cross-Frame Torsional Bracing Design Example (1/4)

Use a Load Factor = 1.3 for the construction condition

Steel girder: A = 72.1 in^2 , wt = 240 lb/ft

Concrete slab: 10' x 8/12 x 150 lb/ft^3 = 1000 lb/ft

w=1,240 lb/ft = 1.24 k/ft

$C_b = 1.0$

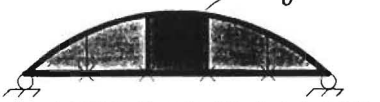

$M_u = 1.3\ (1.24^{k/ft})\ (124^{ft})^2\ /8 = 3{,}100$ k-ft

Check Lateral Buckling – use 24 ft unbraced length (AASHTO 10.48.4 10-103c)

$$M_{cr} = 91{,}000 \times \frac{160}{24 \times 12}\sqrt{0.772 \times \frac{26.7}{160} + 9.87\left(\frac{61.2}{24 \times 12}\right)^2}$$

= 38,300 k-in = 3,190 k-ft > 3,100 k-ft

Note: Eqn. in AISC-LRFD Table A-F1.1 yields:
M_{cr} = 3,370 K-ft

CROSS FRAME LAYOUT

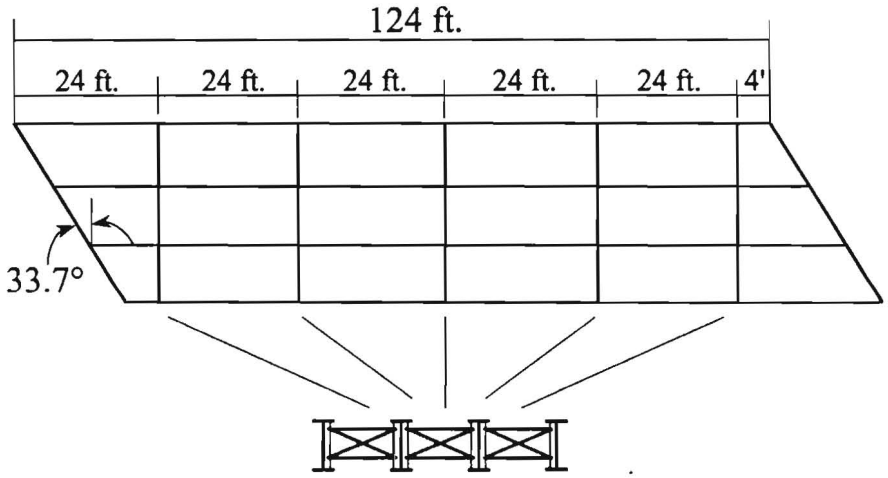

5 intermediate cross-frame lines x 3/line = 15 cross-frames

Figure 8.5 Cross-Frame Torsional Bracing Design Example (2/4)

TORSIONAL BRACE DESIGN – STIFFNESS

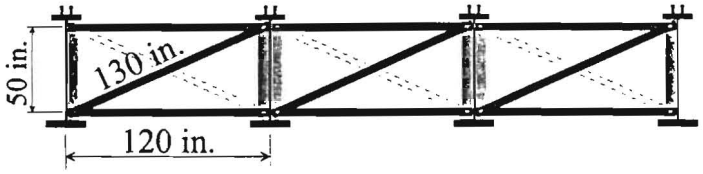

Girder Properties:

h=61.2 in c=37.2 in t = 22.8 in

I_x=41,650 in^4 I_y=890 in^4 I_{yc}=160 in^4

I_{eff}=609 in^4 J =26.7 in^4

Three cross-frames stabilize the four girders. Use a tension-only cross-frame system with one size of single angle members. A 1/2x6 in. stiffener from top to bottom flange is used to control web distortion – the stiffener should be welded to both flanges.

Girder Stiffness: Eqn. 2.23

$$\beta_g = \frac{24(4-1)^2 29{,}000 \times 120^2 \times 41{,}650}{4(124\times 12)^3} = 285{,}000\, in-k/rad$$

Cross-section Stiffness: Eqn. 2.25

$$\beta_{sec} = \frac{1}{2}\frac{3.3(29{,}000)}{5}\left(\frac{60}{5}\right)^2\left(\frac{1.5\times 5\times 0.5625^3}{12}+\frac{0.5\times 6^3}{12}\right) = 12{,}560{,}000\ \ in-k/rad$$

Brace Stiffness: See Fig. 2.6

$$\beta_b = \frac{ES^2 h_b^2 A_b}{2L_c^3 + S^3} = \frac{29{,}000\times 120^2 \times 50^2 A_b}{2(130)^3 + (120)^3} = 170{,}500 A_b\, in-k/rad$$

Eqn. 8.2 (Ideal Torsional Stiffness):

$$\beta_{Ti} = \frac{1.2LM_u^2}{nC_{bb}^2 EI_{eff}} = \frac{1.2\times 124\times 12\times (3{,}100\times 12)^2}{5\times 1.0^2\times 29{,}000\times 609} = 28{,}100\, in-k/rad$$

Eqn. 8.4 (LFD Design):

$$\beta_{T\,Req'd} = \frac{2\beta_{Ti}}{0.75} = \frac{2(28{,}100)}{0.75} = 74{,}900\, in-k/rad$$

Eqn. 2.30

$$\frac{1}{\beta_{T\,Req'd}} = \frac{1}{\beta_b}+\frac{1}{\beta_g}+\frac{1}{\beta_{sec}} \qquad \frac{1}{74{,}900} = \frac{1}{\beta_b}+\frac{1}{285{,}000}+\frac{1}{12{,}560{,}000}$$

$$\beta_b = 102{,}400 = 170{,}500 A_b\, in-k/rad \Longrightarrow \boxed{A_b = 0.60\ \text{in}^2}$$

This corresponds to twice the ideal stiffness

Figure 8.5 Cross-Frame Torsional Bracing Design Example (3/4)

TORSIONAL BRACE DESIGN – STRENGTH

Assumed Initial Twist: $\phi_0 = \frac{L_b}{500h} = \frac{24\times12}{500\times61.2} = 0.0094\ rad$

$$M_{br} = F_{br}\times 50 = 2\beta_{Ti}\times\phi_0 = 2(28{,}100)\times 0.0094 = 528\ in-k$$

$F_{br} = 10.6\ kips$ See Fig. 2.6 for member forces

→ Max. Horz. Force = 10.6 kips (compression)

Max. Diagonal Force $= \frac{2FL_c}{s} = \frac{2(10.6)130}{120} = 22.9$ kips (tension)

Try an L 3x3x 5/16 : A = 1.78 in^2. > 0.60 in^2 (stiffness requirement) ,
r_z = 0.589 in. , I_z = 0.617 in^4.

Strength : Tension - $P_n = 0.9(36)1.78 = 57.6$ kips > 22.9 kips

Compression: (AASHTO LFD 10-154)

$$\frac{KL_c}{r_z} = \frac{1.0\times10\times12}{0.589} = 204 > \sqrt{\frac{2\pi^2E}{F_y}} = \sqrt{\frac{2\times3.14^2\times29{,}000}{36}} = 126$$

(AASHTO LFD 10-153)

$$F_{cr} = \frac{\pi^2\times E}{(KL_c/r_z)^2} = 6.89ksi \longrightarrow P_n = 0.85AF_{cr} = 10.4kips < 10.6kips$$

Very close

Although the above capacity seems very close to the force, since the **L 3x3x5/16** provides a stiffness larger than the required brace stiffness the design brace moment can be reduced as follows:

A=1.78 in^2 $\beta_b = 170{,}500A_b = 303{,}500$ in-k/rad

$$\frac{1}{\beta_{act}} = \frac{1}{\beta_b} + \frac{1}{\beta_g} + \frac{1}{\beta_{sec}} \qquad \frac{1}{\beta_{act}} = \frac{1}{303{,}500} + \frac{1}{285{,}000} + \frac{1}{12{,}560{,}000}$$

$$\beta_{act} = 145{,}300\ in-k/rad = 1.42\beta_{TReq'd}$$

$$M_{act} = M_{br}\times\frac{1}{2-\frac{\beta_{TReq'd}}{\beta_{act}}} = 528\times\frac{1}{2-\frac{1}{1.42}} = 407\ in-k$$

$F_{br} = 8.1\ kips < 10.4\ kips$ OK

Cross-frames and Lateral Struts
Final Size : L3x3x5/16 Angle

Figure 8.5 Cross-Frame Torsional Bracing Design Example (4/4)

8.3 Bracing Behavior for Girders with Skewed Supports and Lean-On Cross-Frames

As shown in the design example in the previous section, the cross section area of 0.60 in^2 that was required based on the stiffness requirements for the cross-frame members is relatively small. The strength requirements controlled the design and an L3x3x5/16 was required, which has a cross sectional area of 1.78 in^2. As a result, the provided stiffness is larger than twice the ideal stiffness value and the required design forces would actually be reduced from 10.6 kips to 8.1 kips as shown in the calculations at the end of the example problem. The strength requirements were reworked to account for the larger stiffness, which results in a lower design force. In practice, "typical sizes" are usually used for the cross-frame members. As shown in the details depicted in Chapter 1 the typical size for cross-frame members in the state of Texas often consist of an L4x4x3/8 angle, which has a cross sectional area of 2.86 in^2.

Since the typical sizes of the cross-frames are often larger than required for strength and stiffness, it may be possible in several instances to eliminate a number of cross-frames throughout the bridge. In doing so, the top and bottom struts would be provided to "lean" several girders on a single cross-frame. An attractive feature of eliminating selected cross-frames is that braces that are more likely to result in potential future fatigue problems can be eliminated. A possible bracing layout is illustrated in Fig. 8.6 in which a number of cross-frames have been eliminated. The five intermediate brace lines have been labeled A, B, C, D, and E. The cross-frames near the skewed supports have been eliminated because the relative difference of the vertical displacement between adjacent girders is larger in those locations. Larger relative vertical displacements generally lead to larger forces being developed in the brace members during truck loading. In addition to minimizing the live load induced forces in the braces, the layout of the cross-frames over the length of the bridge have been arranged so as to tie the four girders together across the width of the bridge. Tying all four girders together in this way provides better integrity to the bracing system as well as increasing the in-plane girder stiffness.

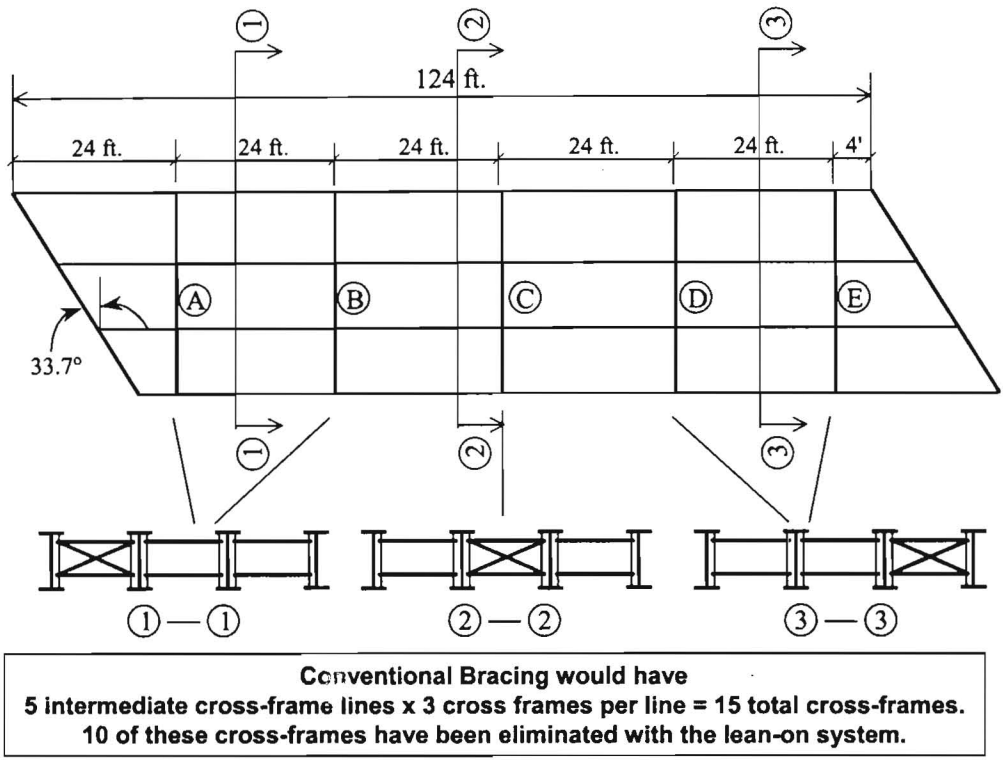

Figure 8.6 Proposed Cross-frame Layout to Minimize Fatigue Damage

Since several girders lean on a single cross-frame, the cross-frame stiffness and strength requirements need to be modified to account for the increased demand on the braces. Figures 8.7 and 8.8 illustrate the lean-on brace forces and deformations when the cross-frames are located at the edge of the girders and in the middle of the girders, respectively. Derivations of the general brace stiffness and strength requirements are presented in Appendix D. The stiffness derivation is based upon the "critical girder" based upon the maximum deformations. Although placing the cross-frame in the middle of the girders would generally result in an increased stiffness from the deformational perspective, locating the bracing near one edge at locations near the supports will probably lead to better fatigue behavior since this placement gets the brace further away from the skewed support. The derivations assume that the same size members will be used for all of the horizontal struts. For strength considerations, the horizontal struts need to be checked for buckling based upon the maximum compression force (ie. –3F for the case in Fig. 8.7).

BRACE FORCES AND DEFORMATIONS

Brace Forces:

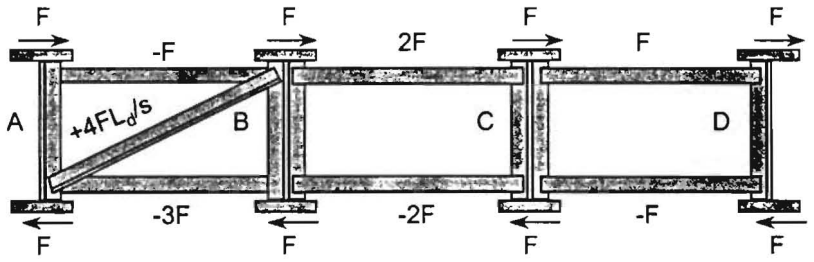

Brace Deformations:

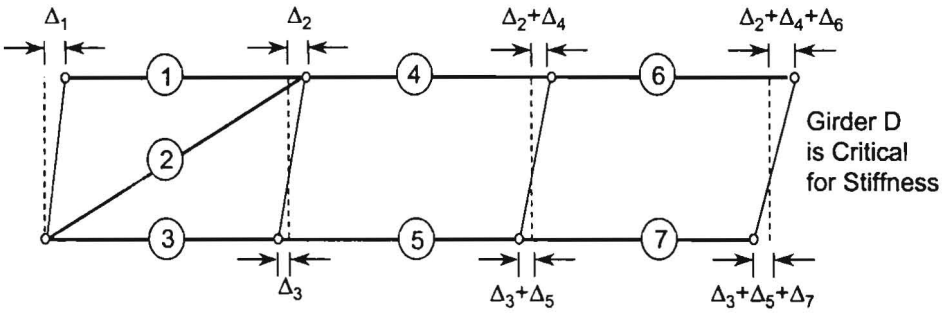

CROSS-FRAME STIFFNESS AND STRENGTH REQUIREMENTS

Define n_{gc} as the number of girders per cross-frame.

Brace Strength:

$$F_d = \frac{n_{gc} F L_d}{S}$$

$$F_s = (n_{gc} - 1)F$$

$$F = M_{br} / h_b$$

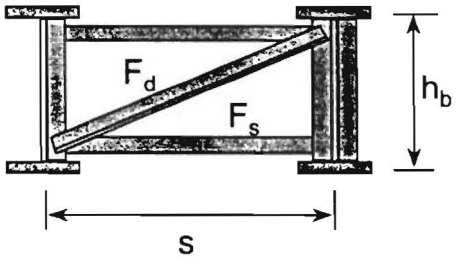

Brace Stiffness:

$$\beta_b = \frac{E S^2 h_b^2}{\frac{n_{gc} L_d^3}{A_d} + \frac{S^3}{A_c}(n_{gc} - 1)^2}$$

Figure 8.7 Equations for Stiffness and Strength Requirements for Lean-On Braces - Cross-Frame Located at Edge of Bridge

BRACE FORCES AND DEFORMATIONS

Brace Forces:

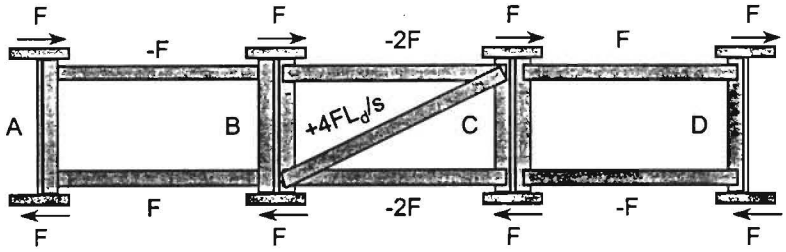

Brace Deformations:

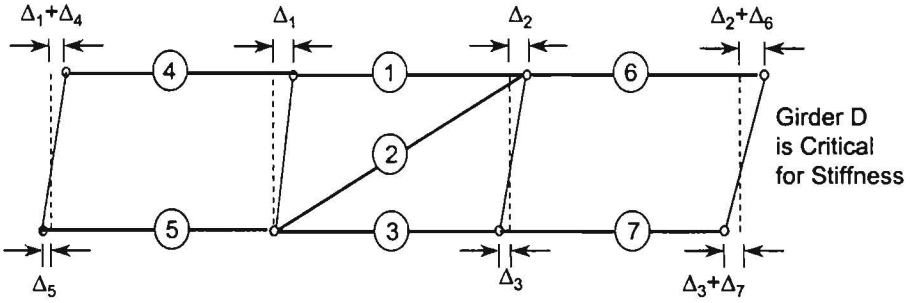

CROSS-FRAME STIFFNESS AND STRENGTH REQUIREMENTS

Define n_{gc} as the number of girders per cross-frame.

Brace Strength:

$$F_d = \frac{n_{gc} F L_d}{S}$$

$$F_s = (n_{gc}/2)F$$

$$F = M_{br}/h_b$$

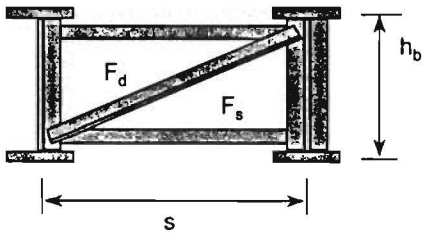

Brace Stiffness:

$$\beta_b = \frac{ES^2 h_b^2}{\frac{n_{gc} L_d^3}{A_d} + \frac{S^3}{A_c}(n_{gc}/2)^2}$$

Figure 8.8 Equations for Stiffness and Strength Requirements for Lean-On Braces - Cross-Frame Located at Middle of Bridge

The stiffness of a cross-frame with n_{gc} girders leaning on the cross frame is given by the following expression:

$$\beta_b = \frac{ES^2 h_b^2}{\frac{n_{gc} L_d^3}{A_d} + \frac{S^3}{A_c}(n_{gc}-1)^2} \tag{8.7}$$

The stiffness of a diaphragm with n_{gc} girders leaning on the diaphragms is given by the following expression:

$$\beta_b = \frac{E}{\frac{(2n_{gc}-3)S}{6I_b} + \frac{S}{A_c h_b^2}(n_{gc}-1)(n_{gc}-2)} \tag{8.8}$$

Derivations of Eqs. 8.5 and 8.6 are provided in Appendix D.

The terms in Eqs. 8.5 and 8.6 have been previously defined in Chapter 2. When lean-on bracing is used with the cross-frames, the effect of the in-plane stiffness of the girders needs to be reevaluated. The following expression for evaluating the in-plane stiffness of the girders was given in Chapter 2:

$$\beta_g = \frac{24(n_g-1)^2}{n_g}\frac{S^2 EI_x}{L^3} \tag{8.9}$$

For a twin-girder system ($n_g = 2$), the above expression reduces to the following:

$$\beta_g = \frac{12S^2 EI_x}{L^3} \tag{8.10}$$

For a four-girder system with cross-frames extending across the full bridge width at each brace line, Eq. 8.9 would produce,

$$\beta_g = \frac{54S^2 EI_x}{L^3} \tag{8.11}$$

which is 4.5 times the twin-girder stiffness. When the lean-on braces are provided as shown in Figure 8.6, the effect on the in-plane girder stiffness is not clear. The actual in-plane girder stiffness would probably be between the case of a twin girder system and the case where braces are used across the full bridge width. Comparisons with FEA solutions showed that simply reducing the expression in Eq. 8.9 by 50% provides reasonable estimates of the girder in-plane stiffness component when lean-on bracing is utilized. This leads to the following expression for systems with lean-on bracing:

$$\beta_g = \frac{12(n_g-1)^2}{n_g}\frac{S^2 EI_x}{L^3} \tag{8.12}$$

For the four-girder system in this chapter this leads to the following expression for the in-plane girder component:

$$\beta_g = \frac{27S^2 EI_x}{L^3} \tag{8.13}$$

A comparison of the results of the eigenvalue analyses and the equations for the bridge with lean-on braces is shown in Fig. 8.9. The graph shows that although Eqs. 8.5 and 8.11 are conservative with respect to the FEA results, the expressions provide reasonable estimates of the ideal stiffness requirements. The conservative nature of the equations may result from a number of possible sources. One of these sources may be the expression used for the in-plane stiffness of the girders. Other possible sources for the conservatism are that the cross-frame near midspan of the bridge has a higher stiffness than the other cross-frames near the edge of the bridge, however the design equations assume that all of the cross-frames have the same stiffness. The other potential source is that when deriving Eq. 8.5 as shown in Fig. 8.7, girder D is the most critical with respect to the required stiffness. However, when the girders buckle in the FEA studies, they all buckle at the same time. Therefore, there may be an interaction between the girders through the width of the bridge thereby raising the effectiveness of the bracing.

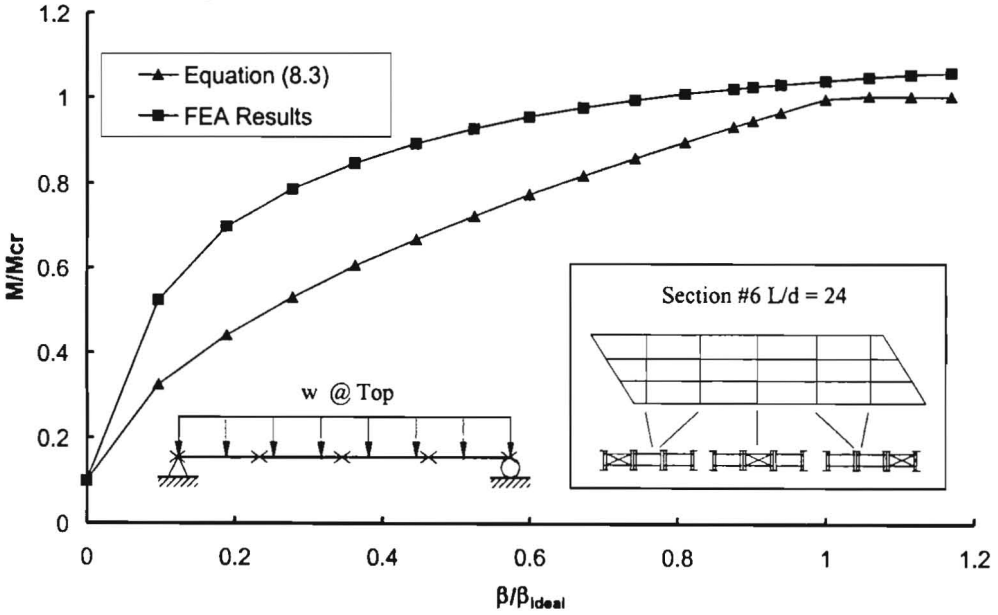

Figure 8.9 M/M_{cr} versus β/β_{ideal} for Section #6 Four-Girder System with Lean-On Braces and Distributed Loads on Top Flange

Figure 8.10 illustrates the shape and the magnitude of the initial imperfections used in the FEA large displacement analyses to determine the strength requirements. The imperfection is identical to that shown in Fig. 8.3. The analysis results confirm that the behavior of the bracing members is very close to that using when deriving the stiffness equation shown in Figure 8.8. The horizontal members of the two outside lean-on cross-frames have a positive and a negative force F. The horizontal members of the middle cross-frame have forces 2F in compression and the diagonal member has a tensile force equal to $\frac{4FL_d}{S}$, where L_d is the length of the diagonal member and S is the girder spacing.

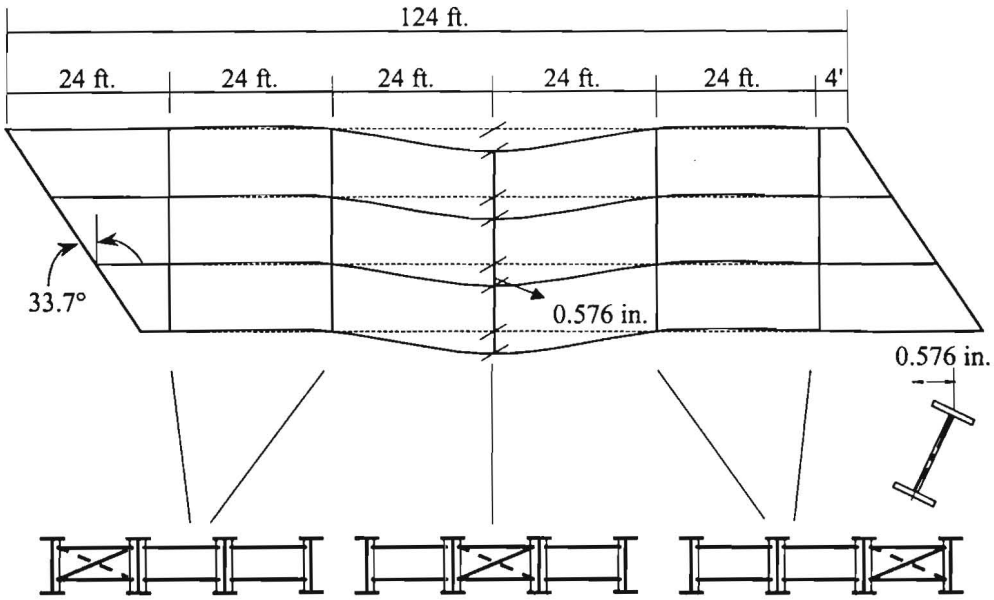

Figure 8.10 Imperfections for the Four-Girder Bridge with Lean-On Braces

The same equations presented in Chapter 5 were used to predict the brace moments. Figure 8.11 illustrates the comparison of the FEA results and the equation results for the 4-girder bridge with lean-on braces. The graph shows good agreement between the equation and the FEA results, although the equations predict slightly unconservative results when the applied loads approach the critical load. A design example for a lean on cross-frame system is illustrated in Fig. 8.12.

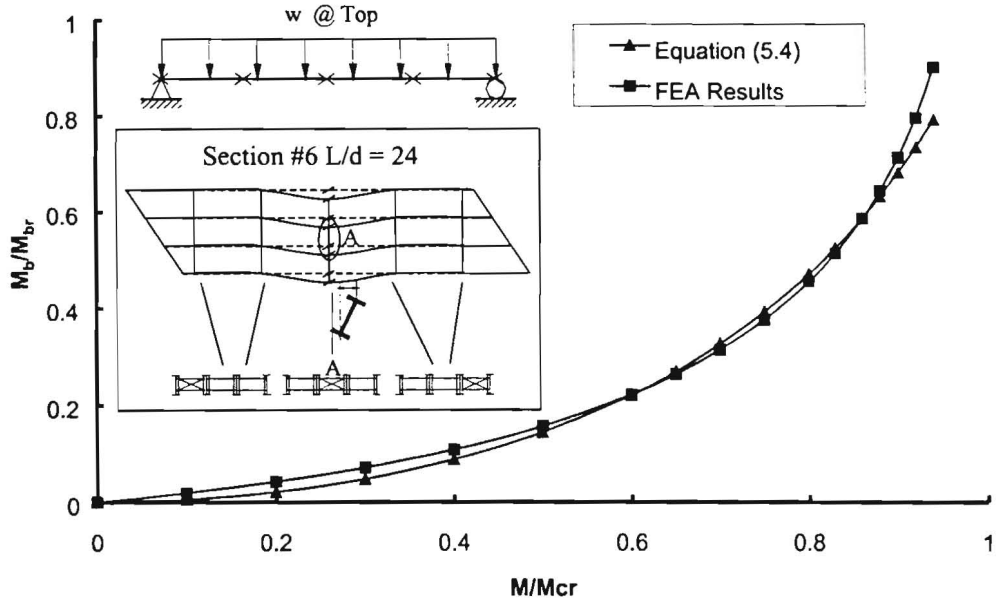

Figure 8.11 M_b/M_{br} versus M/M_{cr} for Section #6 Four-Girder System with Lean-On Braces and Distributed Loads on Top Flange

TORSIONAL BRACING EXAMPLE – LEAN-ON SYSTEM

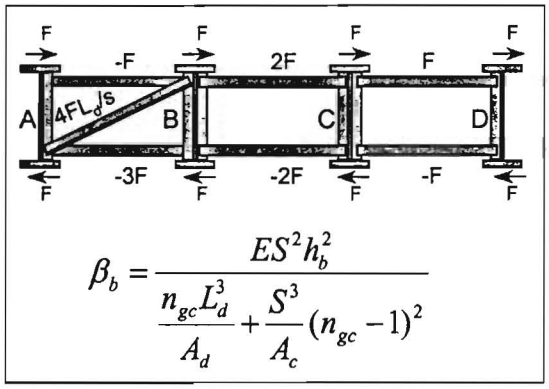

$$\beta_b = \frac{ES^2h_b^2}{\frac{n_{gc}L_d^3}{A_d} + \frac{S^3}{A_c}(n_{gc}-1)^2}$$

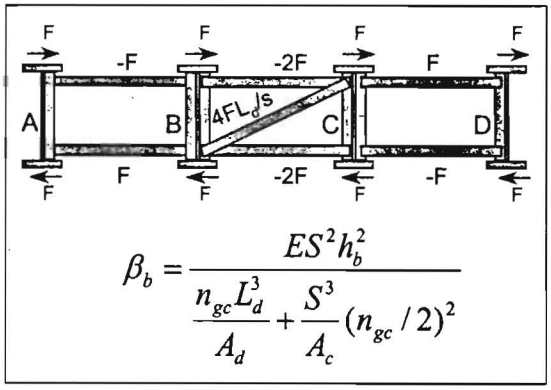

$$\beta_b = \frac{ES^2h_b^2}{\frac{n_{gc}L_d^3}{A_d} + \frac{S^3}{A_c}(n_{gc}/2)^2}$$

Same problem as cross-frame example previously shown in Fig. 8.5, except A lean-on bracing system is used to stabilize the four girders.

Girder Stiffness: $\beta_g = \frac{12(4-1)^2 29{,}000\times 120^2\times 41{,}650}{4(124\times 12)^3} = 142{,}500 \ \ in-k/rad$

Cross-section Stiffness:

$$\beta_{sec} = \frac{1}{2}\frac{3.3(29{,}000)}{5}\left(\frac{60}{5}\right)^2\left(\frac{1.5\times 5\times 0.5625^3}{12} + \frac{0.5\times 6^3}{12}\right) = 12{,}560{,}000 \ \ in-k/rad$$

TORSIONAL BRACE DESIGN – STIFFNESS

Brace Stiffness: (conservatively)

$$\beta_b = \frac{ES^2h_b^2}{\frac{n_{gc}L_d^3}{A_d} + \frac{S^3}{A_c}(n_{gc}-1)^2} = \frac{29{,}000\times 120^2\times 50^2 A_b}{4(130)^3 + 9(120)^3} = 42{,}890A_b \ \ in-k/rad$$

From the cross-frame example: Fig.8.5 (3/4) $\boxed{\beta_{TReq'd} = 74{,}900 \ \ in-k/rad}$

$$\frac{1}{\beta_{TReq'd}} = \frac{1}{\beta_b} + \frac{1}{\beta_g} + \frac{1}{\beta_{sec}} \qquad \frac{1}{74{,}900} = \frac{1}{\beta_b} + \frac{1}{142{,}500} + \frac{1}{12{,}560{,}000}$$

$$\beta_b = 159{,}900 = 42{,}890A_b \ \ in-k/rad \Longrightarrow \boxed{A_b = 3.73 \ \ in^2}$$

Corresponds to twice the ideal stiffness

Figure 8.12 Torsional Bracing Design Example – Lean on System (1/2)

TORSIONAL BRACE DESIGN – STRENGTH

Assumed Initial Twist: $\phi_0 = \frac{L_b}{500h} = 0.0094\ rad$

$M_{br} = F_{br} \times 50 = \beta_T \times \phi_0 = 74{,}900 \times 0.0094 = 704\ in-k$ $\quad F_{br} = 14.1\ kips$

Max. Diagonal Force $= \frac{4FL_c}{s} = \frac{4(14.1)130}{120} = 61.0$ kips (tension)

Max. Horz. Force = 2x14.1 =28.2 kips (compression)

Try an L 4x4x 1/2 : $r_z = 0.776$ in., $A = 3.75$ in^2. > 3.73 in^2 (stiffness)

Strength : Tension - $P_n = 0.9(36)3.75 = 121.5$ kips > 61.0 kips

Compression: (AASHTO LFD 10-154) $L_c = s$

$$\frac{KL_c}{r_z} = \frac{1.0 \times 10 \times 12}{0.776} = 155 > \sqrt{\frac{2\pi^2 E}{F_y}} = \sqrt{\frac{2 \times 3.14^2 \times 29{,}000}{36}} = 126$$

(AASHTO LFD 10-153)

OK

$$F_{cr} = \frac{\pi^2 \times E}{(KL_c/r_z)^2} = 11.9ksi \longrightarrow P_n = 0.85AF_{cr} = 38.0kips > 28.2kips$$

Cross-frames and Lateral Struts
Final Size : L4x4x1/2 Angle

Figure 8.12 Torsional Bracing Design Example – Lean on System (2/2)

When the cross-frame is located at the middle of the line of girders, the maximum compression force, which generally controls the design, is equal to 2F as shown in Fig. 8.8. However, when the cross-frame is located at the edge of the girders shown in Fig. 8.7, the maximum compression force increases to 3F, where F is related to the maximum brace moments developed at the individual brace line ($F=M_{br}/h$).

For practicality, most designers will use the same size cross-frames throughout the bridge. Therefore the engineer will generally select the cross-frame that results in the largest forces due to the applied loading. In instances where a number of girders may lean on a single cross-frame, identifying the critical brace can sometimes be difficult due to the distribution of brace forces. For example, in Fig. 8.6 brace line C is located at the maximum moment region when the distributed loads are applied on the girders, which is generally the region where the largest brace moment will be developed. However, since the cross-frame is located in the middle, only 2F compression forces are generated in the top and bottom cross-frame struts. Brace lines B and D, on the other hand, are located in regions with applied moments that are lower than the maximum midspan moment. However, since the cross-frames along these lines are located at the edge of the bridge, a compression force of 3F is developed and may create larger compression forces that may control the design. An additional FEA analysis was therefore conducted to locate the critical brace member for design.

Figure 8.13 illustrates the shape and the magnitude of the imperfection used to maximize the brace moment at the brace line B. The imperfection is very similar to that shown in Fig. 8.10, however the maximum twist occurs at line B instead of line C.

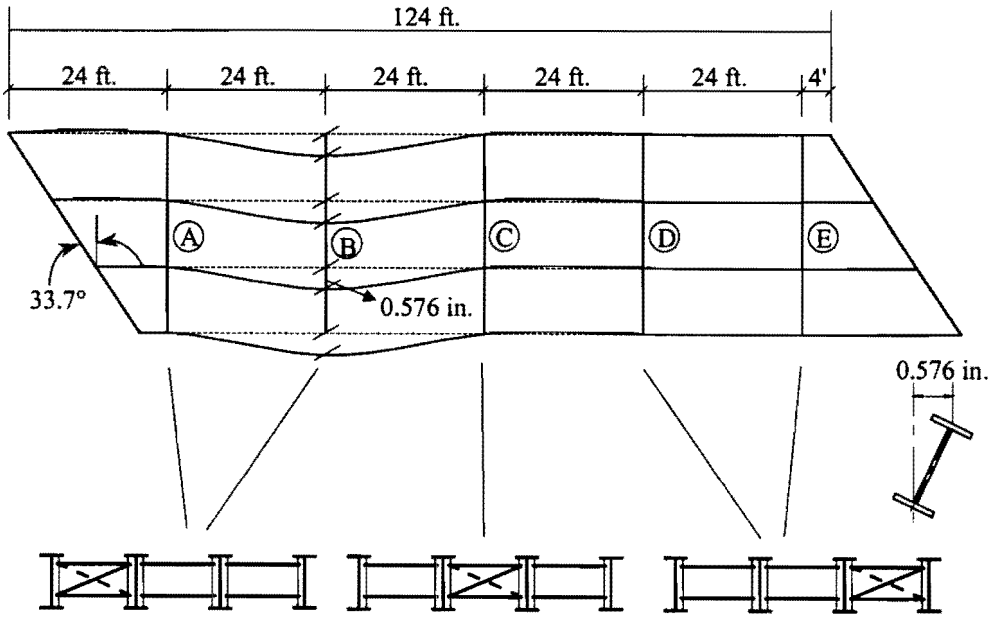

Figure 8.13 Imperfections for the Four-Girder Bridge with Lean-On Braces

Figure 8.14 illustrates the comparison of the FEA and equation results. The graph shows that the equation is very conservative with respect to the FEA results. The reason for the conservatism is that brace line B is not located at the maximum applied moment region (midspan). The brace moment developed for this case is significantly smaller than that generated by the cross-frame located at midspan, for which there was very good agreement between the FEA and equation solutions shown previously in Fig. 8.11. Similar situations

were previously observed in Figs. 5.7b and 5.7c. In most situations, the cross-frame located nearest the maximum girder moment will result in the largest brace forces, regardless of the cross-frame location along the bridge width.

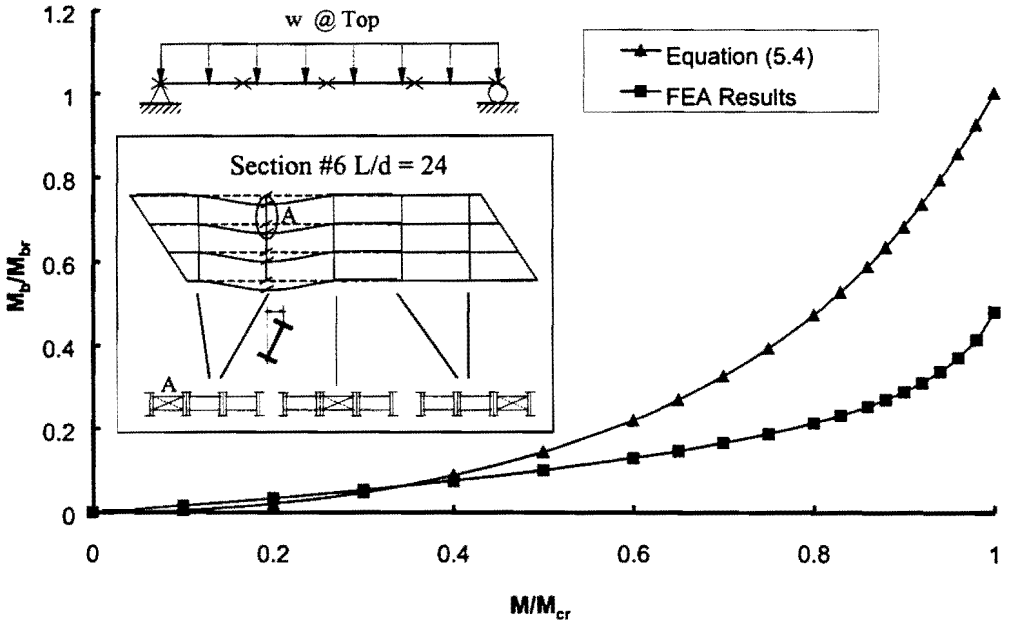

Figure 8.14 M_b/M_{br} Versus M/M_{cr} for Section #6 with Distributed Loads on the Top Flange

8.4 Analyses for the Completed Bridge with the Concrete Deck

Several FEA analyses were performed on the bridge with the completed concrete deck. Once the concrete hardens, the deck provides continuous lateral and torsional restraint to the top flange along the bridge length. The bracing from the concrete bridge deck is generally substantial enough so as to provide full bracing to the top flange along the bridge length. Therefore, in the positive moment region, the intermediate cross-frames are essentially unnecessary for stability bracing once the concrete deck hardens. However, the braces do help to distribute the lateral wind load up to the concrete bridge deck as well as providing stability in the negative moment region.

The FEA model of the steel girders is essentially identical to the models discussed in Chapter 3, however in the completed bridge the concrete bridge deck must also be modeled. Direct approaches for modeling the slab can employ brick elements such as isotropic eight-node brick elements shown in Fig. 8.15a, however utilizing brick elements leads to extremely large numbers of degrees of freedom [Tarhini and Frederick 1992]. Shell elements have also been proposed to model the concrete slab. The difficulty of this method, however is to deal with the eccentricity between the deck and steel girder top flanges. Idealizing the concrete deck by shell elements comprises a 2-D surface in the FEA model that would typically be

located at the middle of the thickness of the slab. The location of this surface relative to the steel girder must be accurately reflected in the FEA model so as to correctly model the in-plane stiffness of the composite girder. The resulting model will generally have an eccentricity between the plane of shell elements and the top flange of the steel girder. Therefore it is necessary to provide a structural link between the two structural components that will maintain compatibility and accurately model the composite stiffness. One method that has been employed is to provide rigid links between the girder flanges and the slab [Brockenbrough 1987, Tabsh and Sahajwani 1997]. The slab nodes are connected to the girder by the rigid links, which are typically beam elements with a very large stiffness (Fig. 8.15b). This method is effective in modeling the bending behavior in the girder in the longitudinal direction, however the shear capacity of the cross-section may be overestimated. Many FEA programs also provide the capacity of coupling the degrees of freedom for separated nodes without physical modeling the constraints. The coupled nodes are essentially connected by a link with infinite stiffness in the coupled degrees of freedom, however this requires assumptions about the constraints and compatibility between the slab and the girders that can be difficult to formulate.

A method proposed by Fan [1999] that utilized a combination of shell and brick elements for the slab model was employed in this study. In this method, 8-node quadrilateral shell elements are used to model the concrete slab as well as the steel girders. The shell elements for the concrete slab are located at the mid-thickness of the slab. A 20-node brick element was then used to connect the top flange of the steel girder and the concrete slab. Fig. 8.15c illustrates the modeling technique. There is no pre-assumed coupling condition introduced in the method. The top and bottom surfaces of the brick element overlap the shell elements for the slab and the top girder flange thereby providing a direct connection by shared nodes.

Elastic analyses were performed on the completed bridge to investigate the forces induced in the cross-frames due to truck loading. The purpose of these analyses was to compare and investigate the behavior of different bracing layouts in an effort to reduce potential fatigue damage from in-service loading due to truck traffic. Comparisons were made of the cross-frame forces induced for different bracing details consisting of conventional bracing layouts in which the cross frames are located continuously across the bracing lines versus systems in which several girders lean on a single cross-frame. The area of the diagonal and the struts of the cross-frame were 1.88 in^2, which corresponds to an L3x3x3/8 angle. This area provided a stiffness that was equal to twice the ideal stiffness for the lean on system. The truck loading that was employed consisted of the HS20-44 truck live load. The HS20-44 truck is shown in Figure 8.16. The two back wheels of the design truck have a variable spacing ranging from 14 feet to 30 feet. To produce the maximum stresses in the analysis a spacing of 14 feet was utilized.

Once the concrete deck cures, forces in the top horizontals of the cross-frames are generally small from truck traffic due to the relatively large stiffness of the cured concrete

that joins adjacent girders. However large forces can still be induced in the bottom horizontal member and the diagonal member of the cross-frame due to the truck traffic.

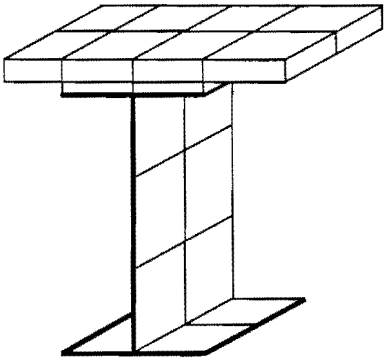

(a) Brick Element for Slab

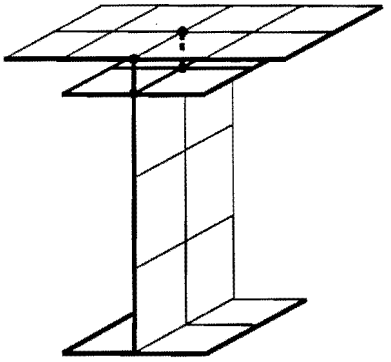

(b) Shell Element for Slab and Rigid Link

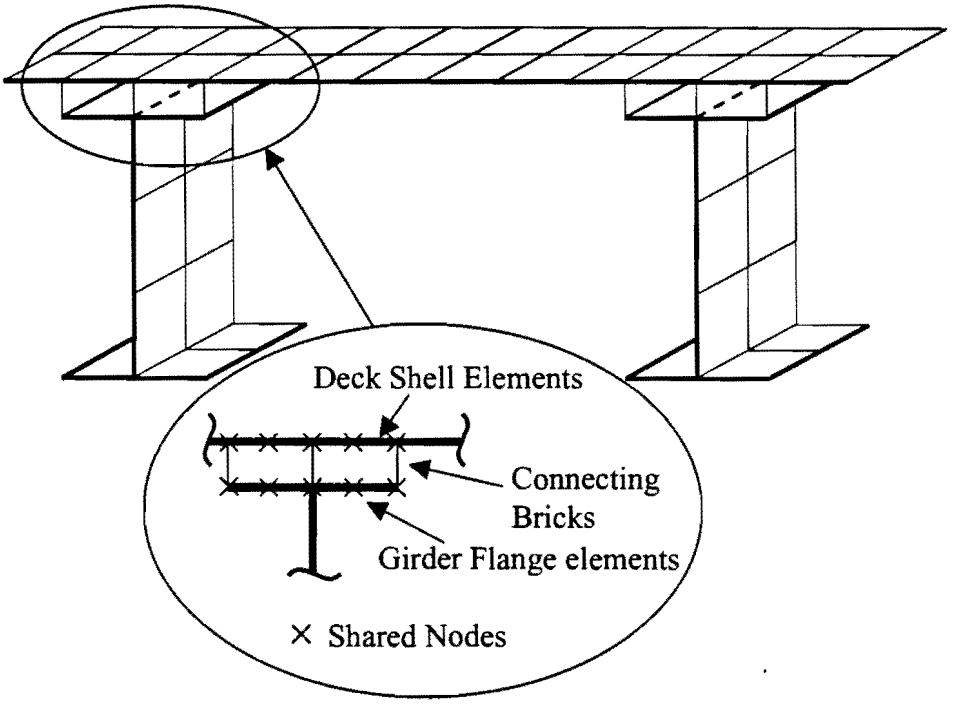

(c) Shell Element for Slab and Brick Element Connection

Figure 8.15 FEA Model for Completed Bridges

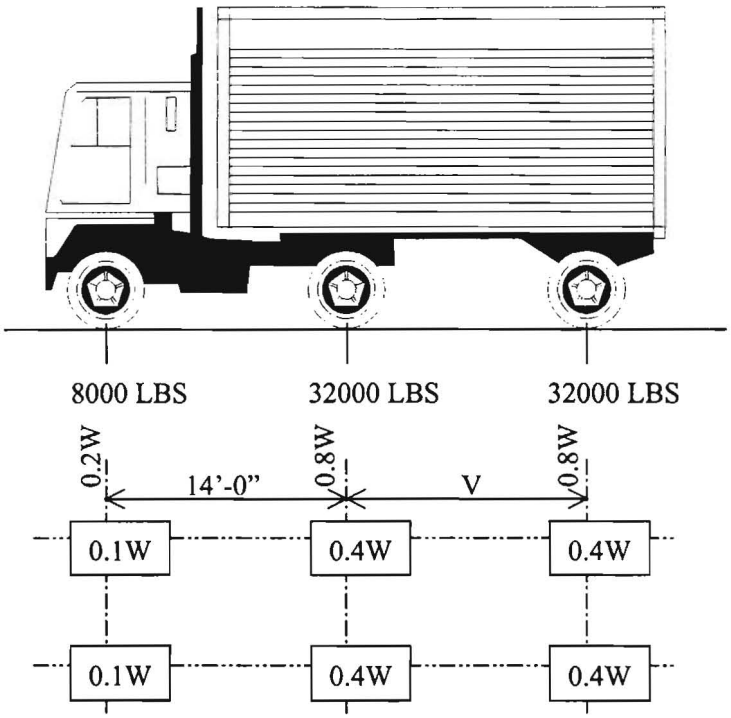

W = COMBINED WEIGHT ON THE FIRST TWO AXLES WHICH IS THE SAME AS FOR THE CORRESPONDING H TRUCK.

V = VARIABLE SPACING– 14 FEET TO 30 FEET INCLUSIVE. SPACING TO BE USED IS THAT WHICH PRODUCES MAXIMUM STRESSES.

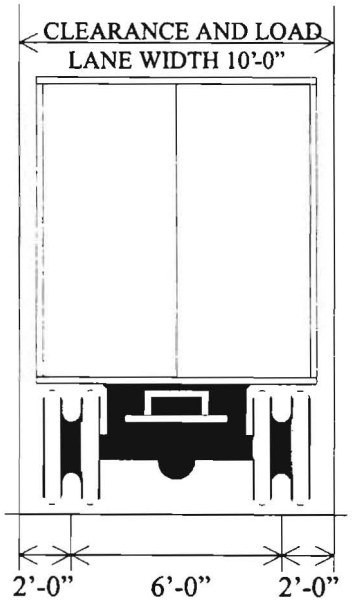

Figure 8.16 HS20-44 Truck

Figure 8.1 showed the locations of the braces labeled from No.1 to No. 15 that will be used in the following discussion. Conventional bracing details in bridges with skewed supports often have the cross-frame lines framing directly into the skewed support such as the case depicted in the plan view of a bridge in Fig. 8.17. One end of cross-frame #3 in this figure frames directly into the support region. For the first series of analyses the lateral position of the truck was as shown in Fig. 8.17. The truck was then incrementally moved across the bridge and the cross-frame forces were recorded for each truck position.

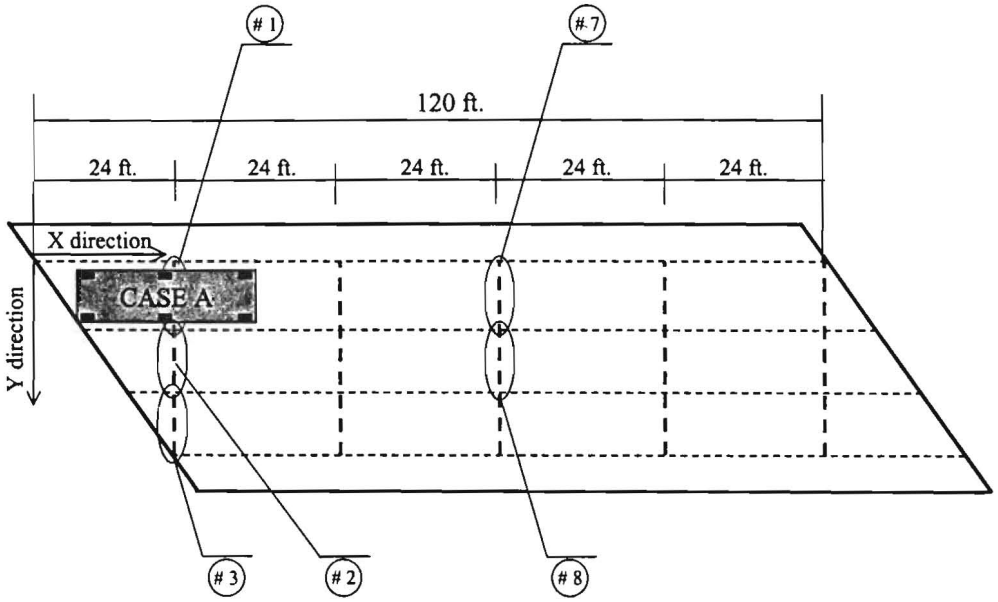

Figure 8.17 Truck Live Loading – Case A

Figures 8.18a, 8.18b, and 8.18c show comparisons of the FEA results of the brace forces induced from the HS-20-44 truck at different brace locations for the cases with cross-frames across the entire bridge width (herein referred to as the "conventional bracing detail") and lean-on cross-frames. The force induced in the respective cross-frame members is graphed on the vertical axis versus the longitudinal truck location on the bridge. The position of the truck is indicated on the figures. Figure 8.18a shows the forces in the cross-frame #1 members and demonstrates that there is essentially no difference in the magnitudes of the cross-frame forces between the lean-on and conventional bracing layout. Both the diagonals and the bottom horizontals of the cross frames have maximum member forces of approximately 3000 lbs. for both bracing layouts. As mentioned above, the forces in the top horizontals were relatively small due to the large stiffness of the concrete deck and therefore forces in the top members are not graphed.

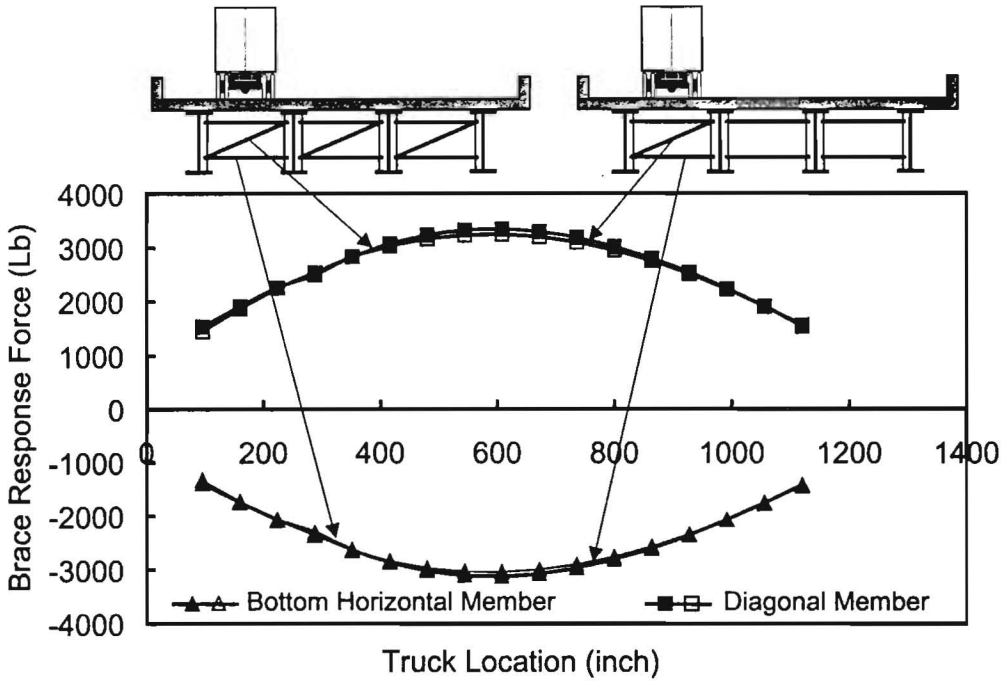

Figure 8.18 (a) Brace Force Response Envelope at Brace Location #1 with Edge Truck Loading - Conventional vs. Lean On Bracing

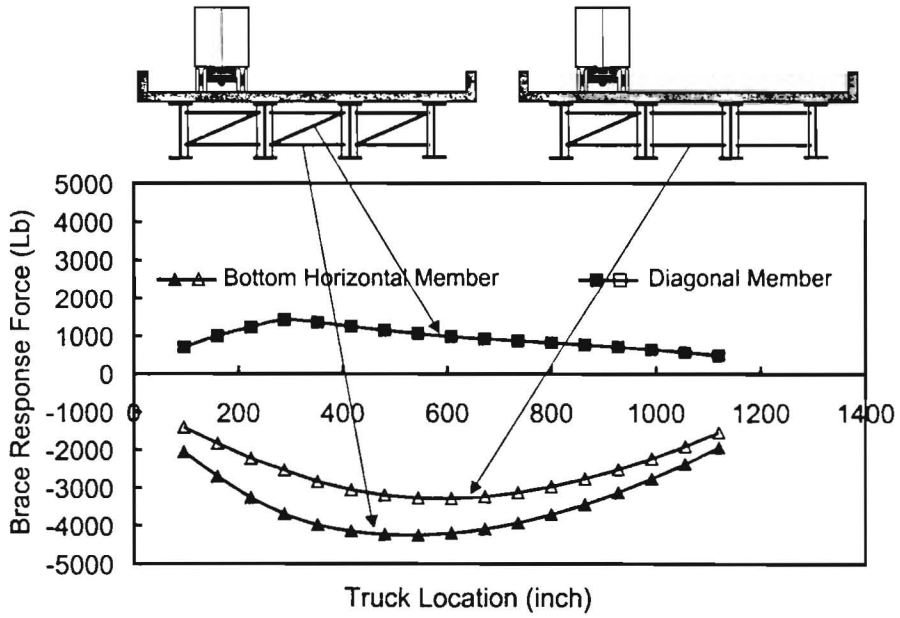

Figure 8.18 (b) Brace Force Response Envelope at Brace Location #2 with Edge Truck Loading - Conventional vs. Lean On Bracing

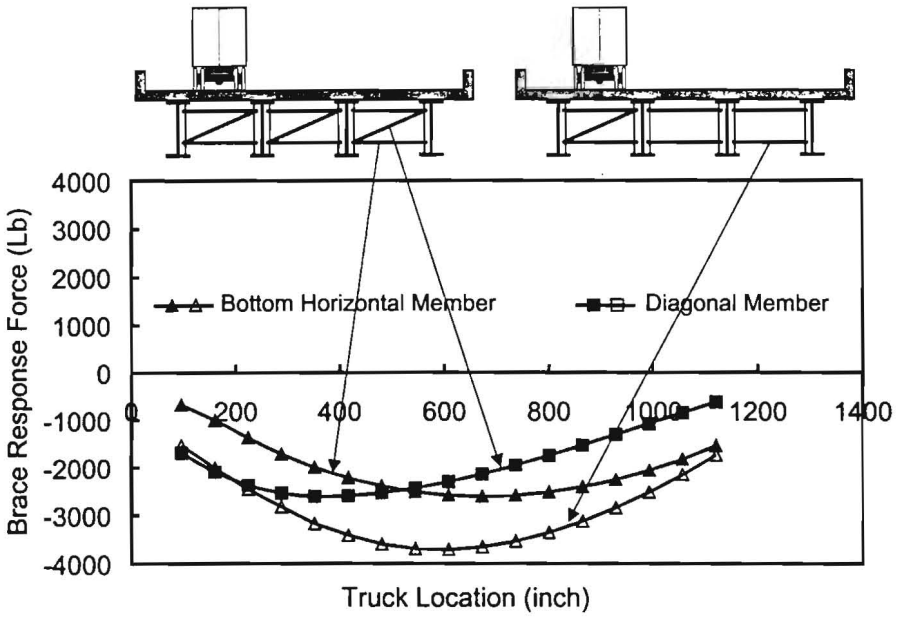

Figure 8.18 (c) Brace Force Response Envelope at Brace Location #3 with Edge Truck Loading - Conventional vs. Lean On Bracing

Although the lean-on system did show a benefit over the conventional bracing layout for member forces for cross-frame #2, the revised layout actually resulted in larger forces in the bottom horizontal for cross-frame #3. These trends are shown in Figs. 8.18b and 8.18c. The reason that there was very little benefit in the induced forces for the lean-on bracing system versus the conventional layout shown in Fig. 8.18a, 8.18b, and 8.18c is because the horizontal members frame directly into the support. The rigid support restrains the adjacent girders from relative horizontal deflections, which therefore leads to large member forces.

In an attempt to reduce the magnitude of the brace forces, analyses were conducted in which the cross-frame lines did not frame directly into the supports, but instead were slightly offset. Figure 8.19 shows the plan view of one such layout. The bridge is essentially identical to that shown in Fig. 8.17, however the total length is 4 feet longer so as to keep the geometry of the braces essentially the same. These bridges have the same basic geometry and cross-frame layouts that were considered earlier in the chapter for stability bracing of the steel section. Comparing the layout to that previously shown in Fig. 8.17, the two bridges have the same maximum spacing between cross-frames of 24 feet, however the cross-frame lines near the supports in Fig. 8.19 frame into the fascia girders at cross-frames #3 and #13 locations at a distance of 4 feet from the support. Two different truck locations are also indicated in the figure, Case A and Case B. The Case A location is the same truck location that was presented for the bridge in Fig. 8.17. The Case B location consisted of a truck line passing down the middle of the bridge.

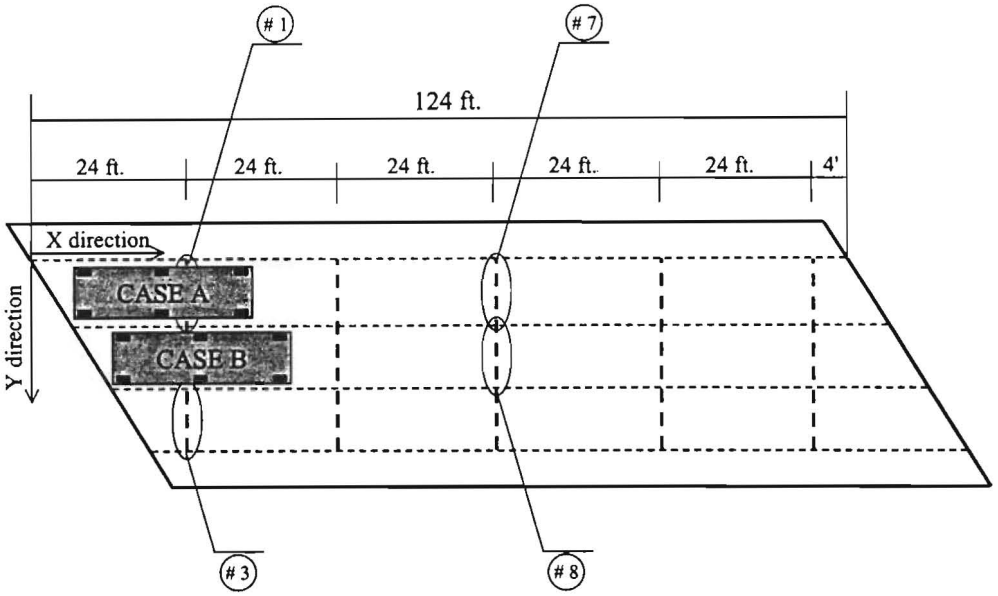

Figure 8.19 Truck Live Loading Cases

Figures 8.20a, 8.20b, and 8.20c show comparisons of some of the resulting cross-frame member forces for the two bracing orientations with the Case A truck position. Figure 8.20a shows the resulting forces in Cross-frame #1 for the two bracing layouts. Comparing the cross-frame forces between Fig. 8.18a and 8.20a for the conventional bracing layout, the maximum member forces for both bridge geometries were approximately 3000 lbs. Although there was very little change in the member forces for the conventional bracing layout for the two bridge geometries, the lean-on bracing performed much better than previously observed in Fig. 8.18a. The magnitudes of the diagonal and bottom chord forces for the lean-on bracing were approximately half the values when the cross-frames extended the full width of the bridge.

Figure 8.20b shows the member forces in Cross-frame #3 for the two bracing layouts. The force in the bottom horizontal is significantly lower than was previously observed in Fig. 8.18c. Figure 8.20c shows the resulting force in Cross-frame #8, which is located near the middle of the bridge. The comparison between the two different bracing layouts is similar to that observed for Cross-frame #1 with the member forces in the lean-on system approximately half of those from the conventional bracing layout. The forces in the lean-on system in the line of bracing labeled 13, 14, and 15 were somewhat larger than observed in the first line (1, 2, and 3). Figure 8.20d shows the forces in Cross-frame #15. With the exception of the last line of cross-frames (13, 14, and 15), the forces in the lean-on bracing system were substantially lower than those in the conventional bracing layout with the edge truck loading. The response envelopes for all of the cross-frames are presented in App. D.

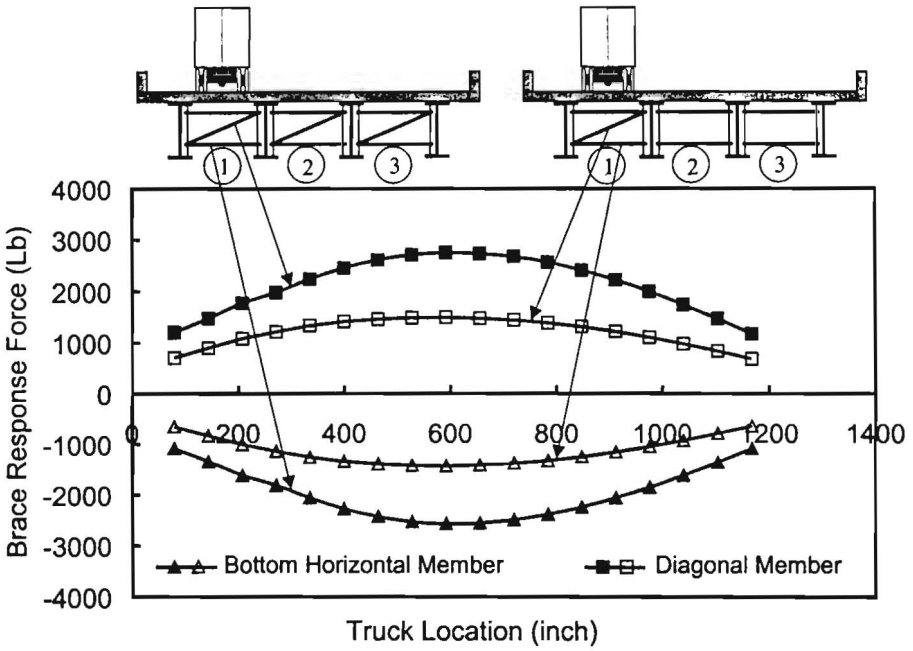

Figure 8.20 (a) Brace Force Response Envelope at Brace Location #1 with Edge Truck Loading - Conventional vs. Lean On Bracing

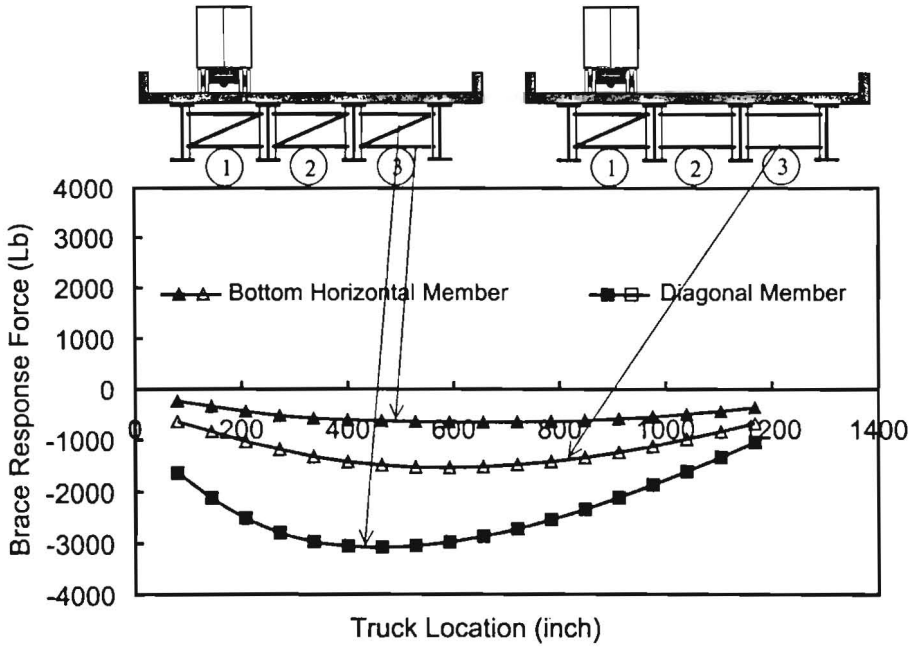

Figure 8.20 (b) Brace Force Response Envelope at Brace Location #3 with Edge Truck Loading - Conventional vs. Lean On Bracing

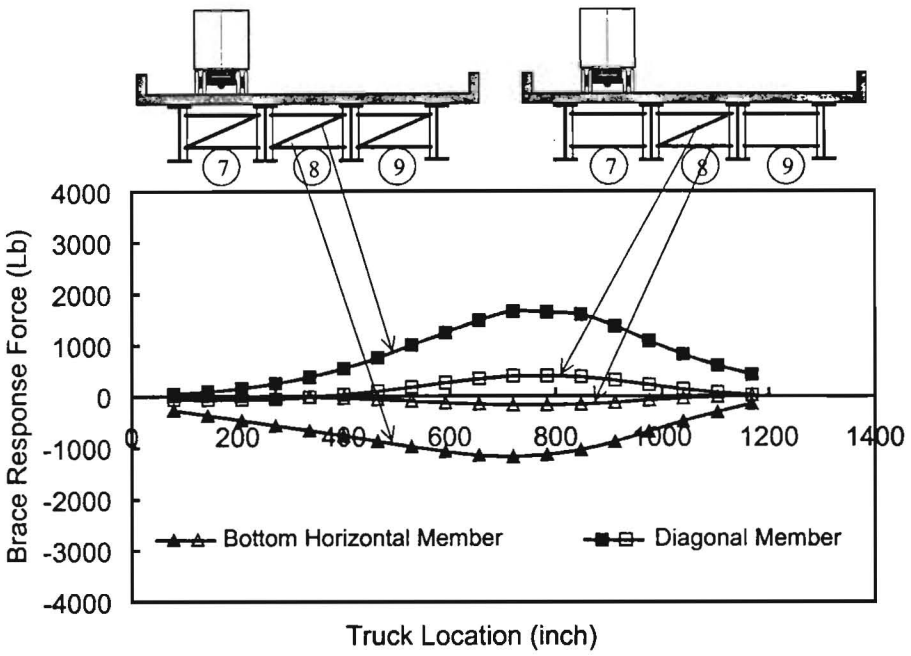

Figure 8.20 (c) Brace Force Response Envelope at Brace Location #8 with Edge Truck Loading - Conventional vs. Lean On Bracing

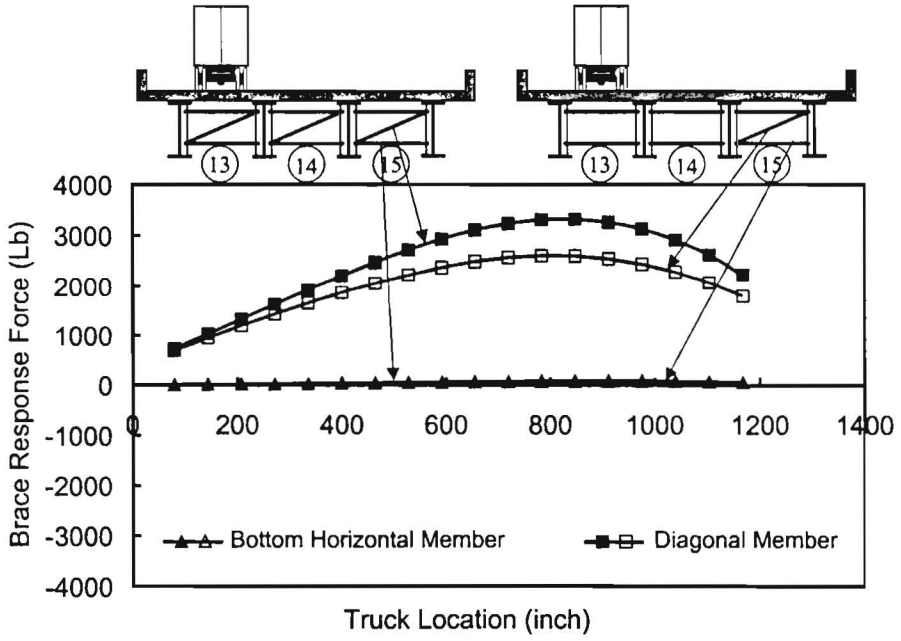

Figure 8.20 (d) Brace Force Response Envelope at Brace Location #15 with Edge Truck Loading - Conventional vs. Lean On Bracing

Figure 8.21 shows some of the cross-frame member forces that resulted with the Case B truck location. For the cross-frames located near midspan, the Case B truck location was the critical truck position with regards to the maximum member forces in the conventional bracing layout. For the cross-frames located near the supports, the Case A truck location was the critical layout. Figure 8.21a shows the resulting forces in Cross-frame #1 with the Case B loading. The member forces are smaller than were observed for the Case A loading. The maximum force values of the lean-on bracing were only approximately 50% of the corresponding values from the conventional layout. Figures 8.21b and 8.21c show the resulting forces for Cross-frames #7 and #8 for the two bracing layouts. The member forces for the conventional layout in these two cross-frames were larger with the Case B truck location than for the Case A location. The corresponding lean-on forces for these two brace locations were substantially lower than with the conventional layout.

In addition to the conventional bracing layout that was shown in Fig. 8.1, additional analyses were also conducted on other layouts that are currently used. Although the parallel layout that was studied in Chapter 6 can be employed for some skewed bridges, the layout is currently limited by the AASHTO Specification for skew angles less than 20 degrees. A cross-frame layout similar to the parallel layout that is sometimes employed consists of staggering the cross-frames along a parallel line. The individual cross-frames are normal to the longitudinal axis of the individual girders, however they are offset along a line parallel to the skew. Figure 8.22 shows a potential staggered cross-frame layout for the 4-girder bridge that has been studied. As with the previous layouts, the cross-frame locations have been numbered from S1 to S15.

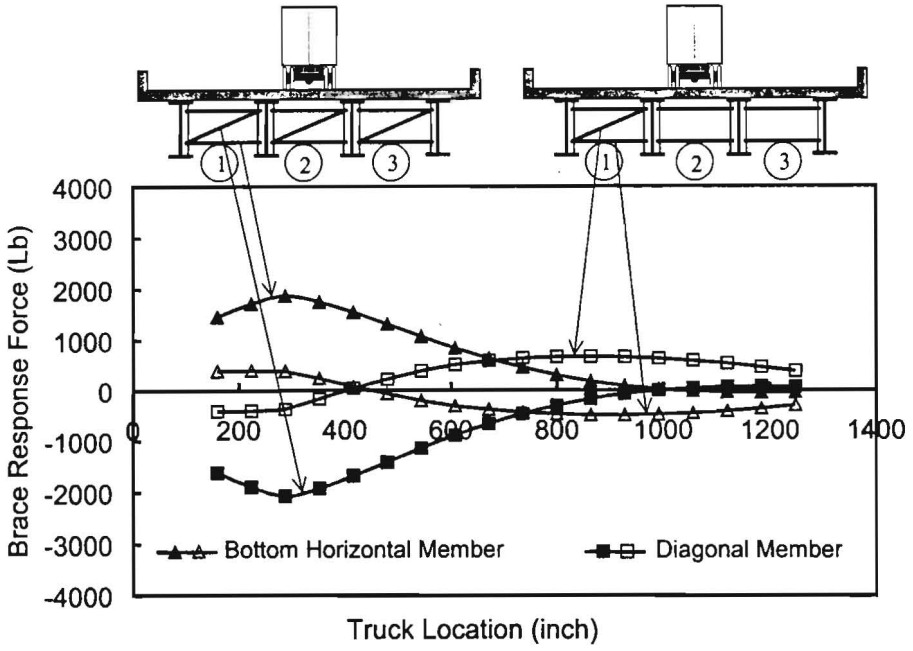

Figure 8.21 (a) Brace Force Response Envelope at Brace Location #1 with Center Truck Loading - Conventional vs. Lean On Bracing

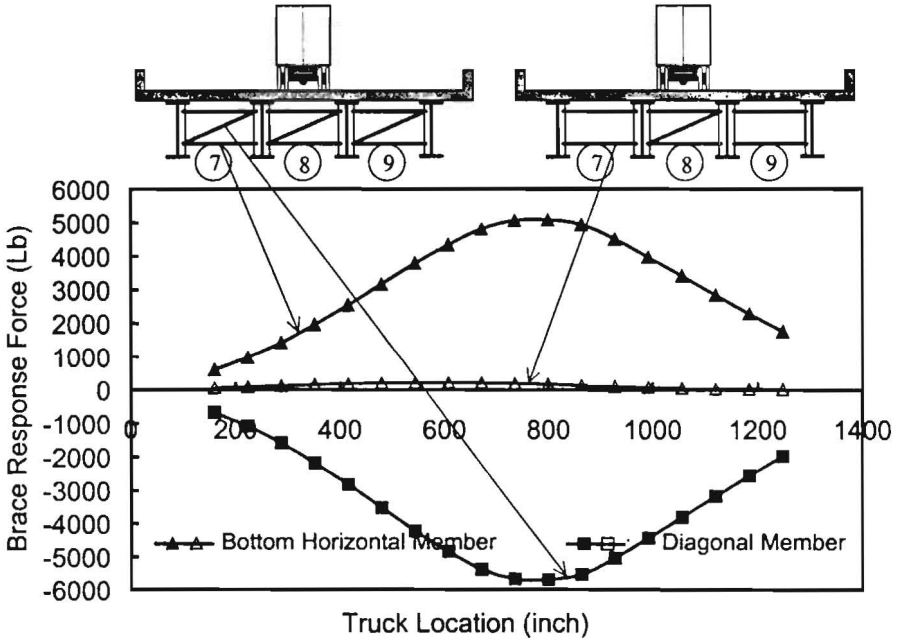

Figure 8.21 (b) Brace Force Response Envelope at Brace Location #7 with Center Truck Loading - Conventional vs. Lean On Bracing

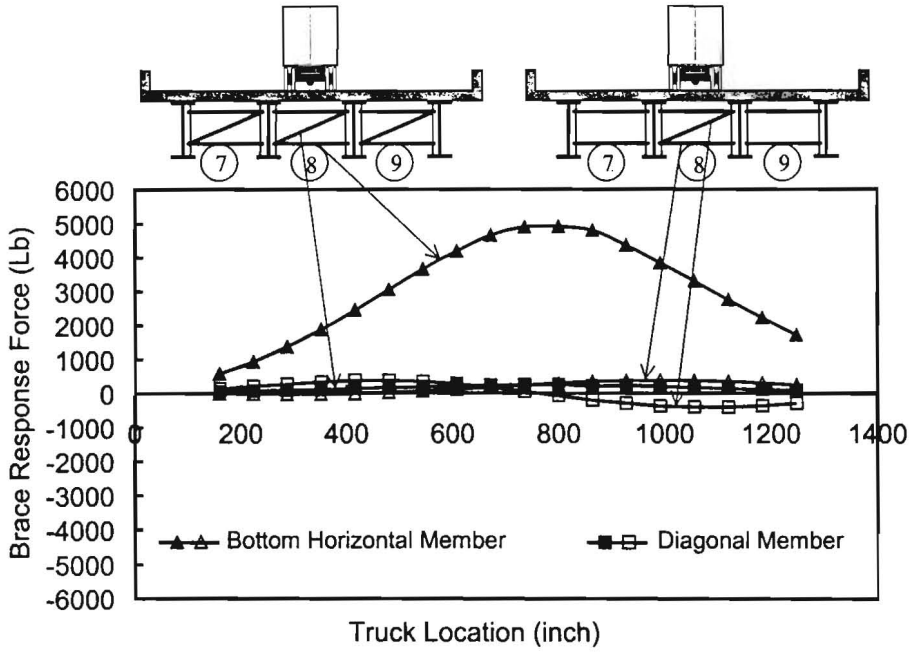

Figure 8.21 (c) Brace Force Response Envelope at Brace Location #8 with Center Truck Loading - Conventional vs. Lean On Bracing

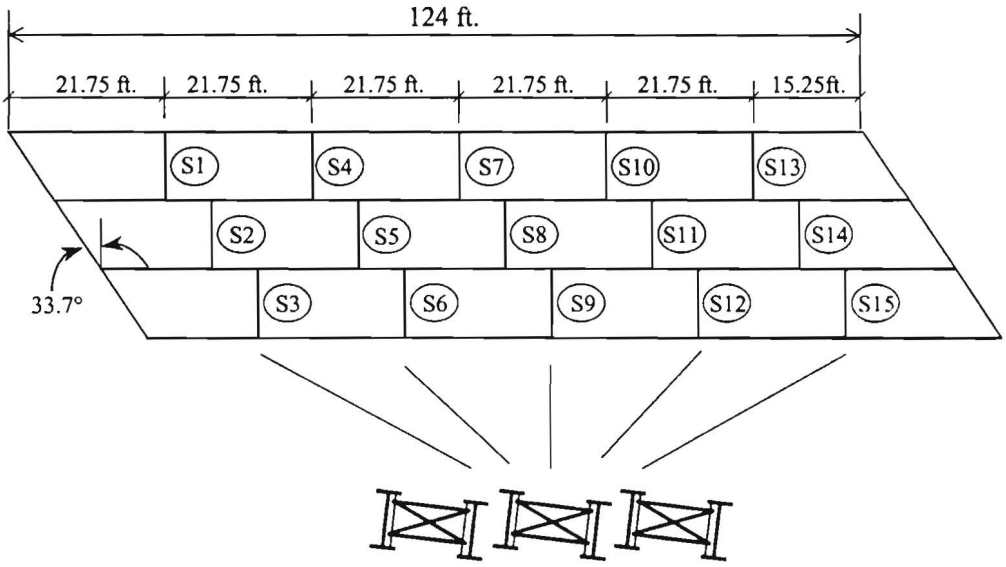

5 intermediate cross-frame lines x 3/line = 15 cross-frames

Figure 8.22 Staggered Cross-Frame Layout.

Figure 8.23 shows a comparison of the brace force response envelopes for the staggered and lean-on cross-frame layouts for some of the cross-frames with edge truck loading. For the first line of cross-frames (1, 2, and 3), there is very little difference between the staggered layout and the lean-on system with edge truck loading. This is demonstrated in Fig. 8.23a, which shows that the lean-on system has slightly higher brace forces for Cross-frame #1 compared to the staggered layout. The envelopes for Cross-frames #2 and #3 are nearly identical with respect to the maximum brace force as illustrated in Fig. 8.23b for Cross-frame #3. At the other support, the lean-on system had higher brace forces than the conventional staggered layout as shown in Fig. 8.23c for edge truck loading. However, aside from the cross-frame lines near the supports, the forces in the lean-on system drop substantially and are considerably smaller than the staggered layout at the other brace lines. The conventional staggered layout still has significant forces at these other cross-frame locations. This is shown in Figs. 8.23d and 8.23e for the respective cross-frames #4 and #8.

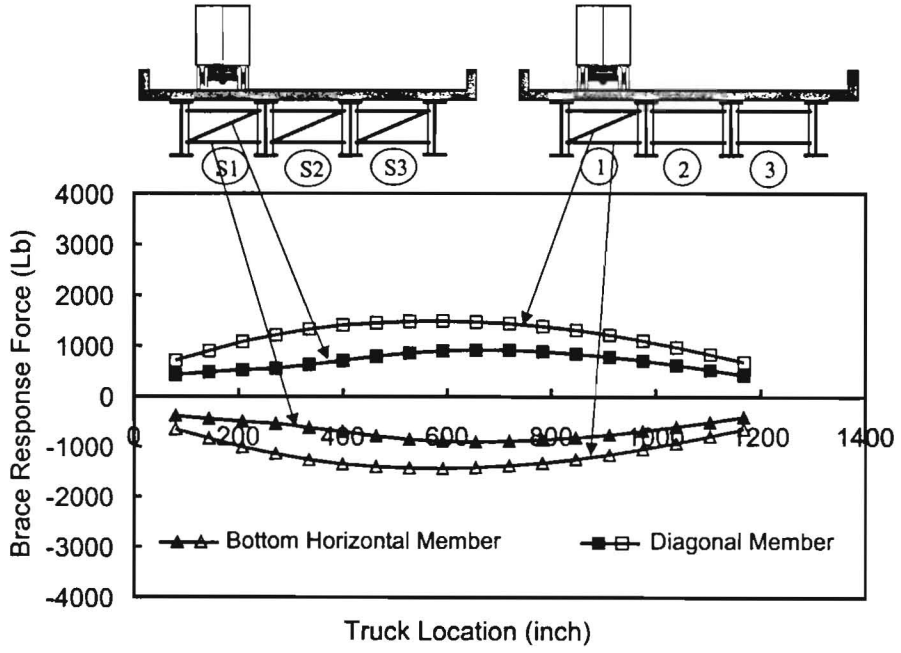

Figure 8.23(a) Brace Force Response Envelope at Brace Location #1 with Edge Truck Loading – Conventional Stagger vs. Lean On Bracing

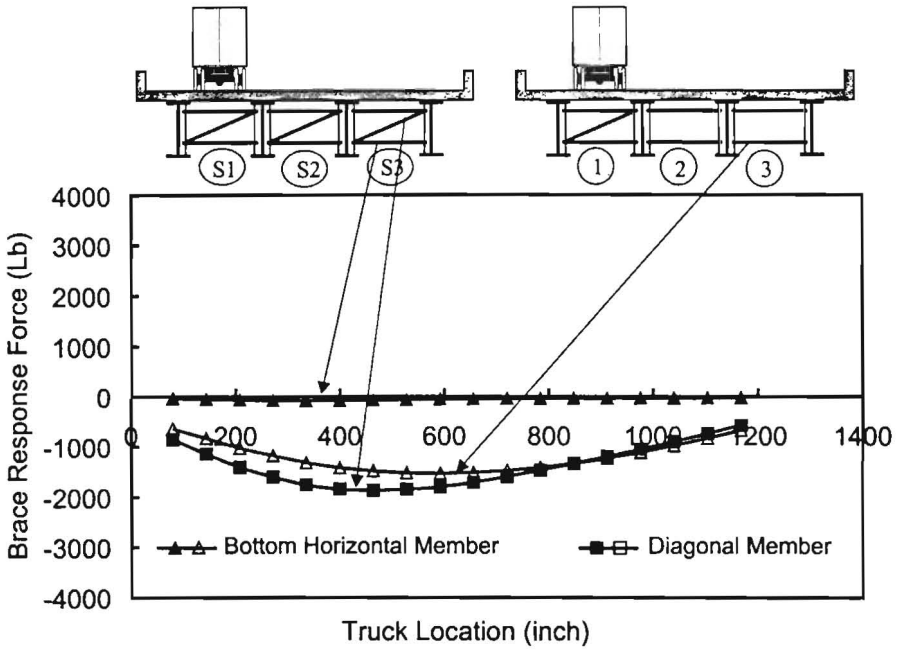

Figure 8.23 (b) Brace Force Response Envelope at Brace Location #3 with Edge Truck Loading – Conventional Stagger vs. Lean On Bracing

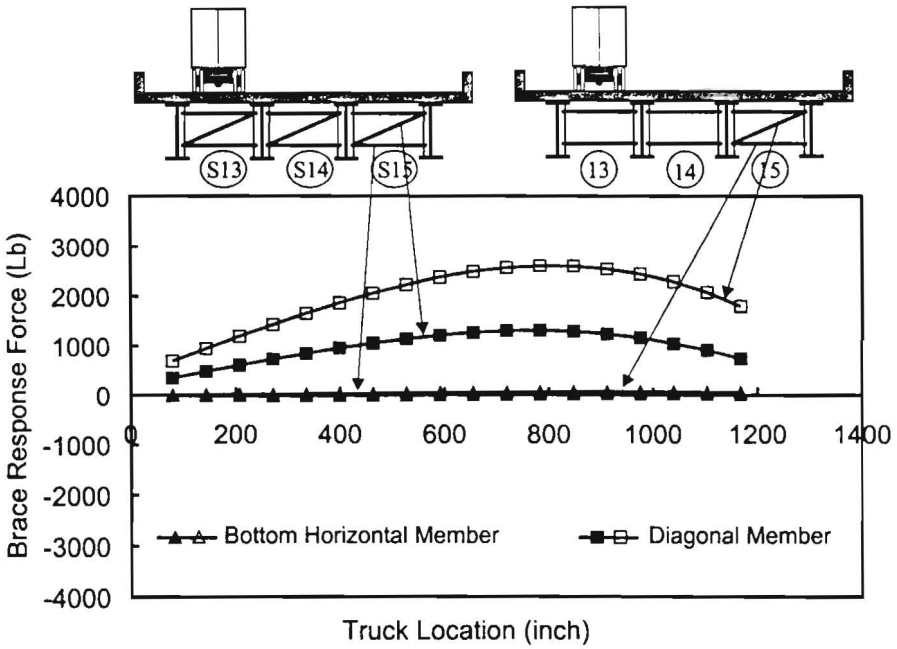

Figure 8.23 (c) Brace Force Response Envelope at Brace Location #15 with Edge Truck Loading – Conventional Stagger vs. Lean-On Bracing

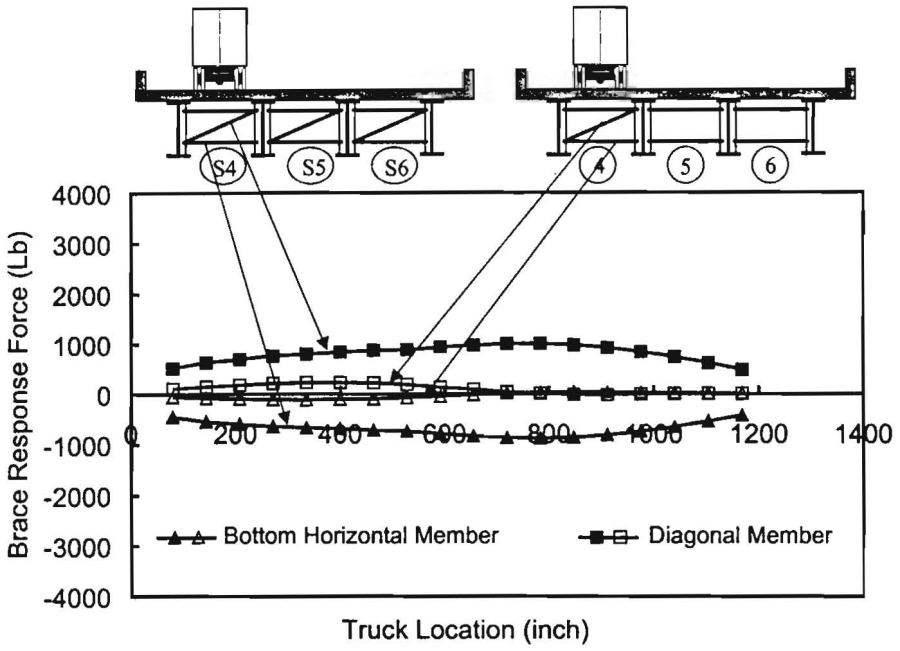

Figure 8.23 (d) Brace Force Response Envelope at Brace Location #4 with Edge Truck Loading – Conventional Stagger vs. Lean-On Bracing

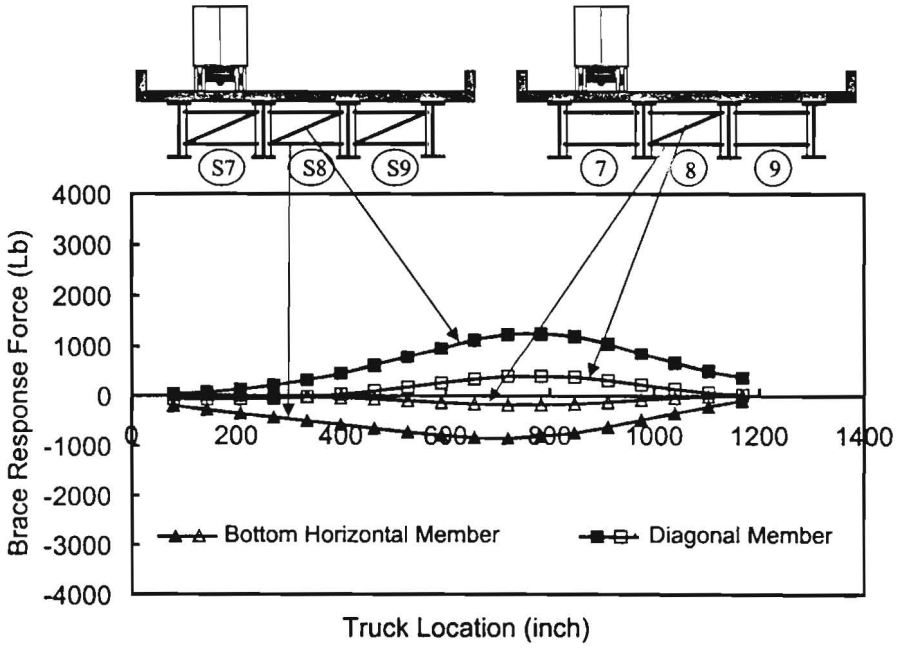

Figure 8.23 (e) Brace Force Response Envelope at Brace Location #8 with Edge Truck Loading – Conventional Stagger vs. Lean-On Bracing

As previously observed, the critical loading for the cross-frame lines near the middle of the bridge was obtained with the center truck position. Figure 8.24 presents some of the comparisons between the conventional staggered layout and the lean-on layout for the cases with center truck loading. The forces in the cross-frame lines near the supports were generally smaller than those near midspan. However with center truck loading, the staggered layout generally experienced larger forces than the lean-on system. This is shown in Figs. 8.24a, 8.24b, and 8.24c for the respective Cross-frame locations #1, #3, and #15. For the cross-frame lines away from the supports, the staggered layout had significantly larger forces than the lean-on system. This is shown or Cross-frames #4 and #8 in Figs. 8.24d and 8.24e, respectively.

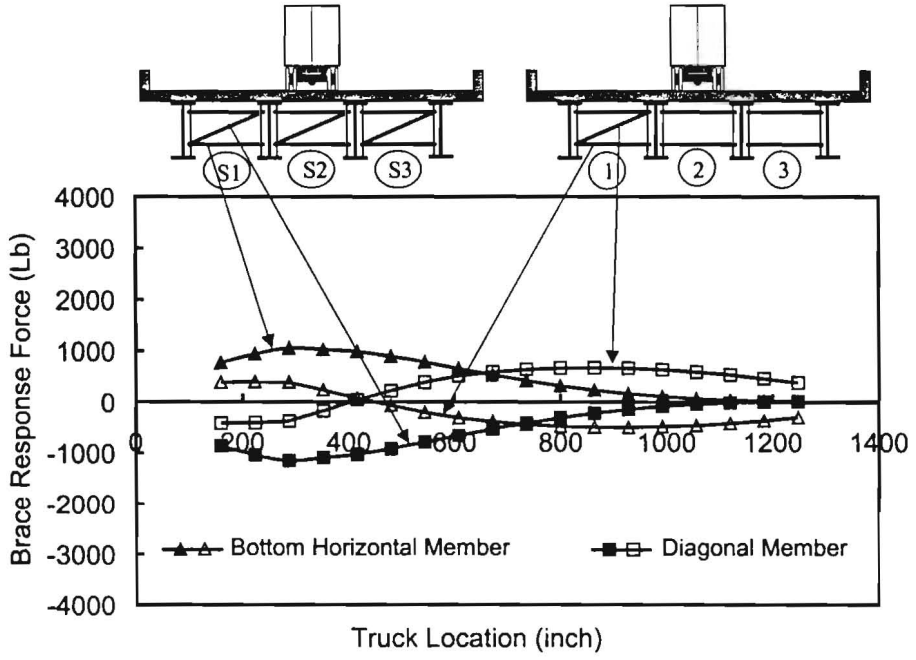

Figure 8.24 (a) Brace Force Response Envelope at Brace Location #1 with Center Truck Loading – Conventional Stagger vs. Lean-On Bracing

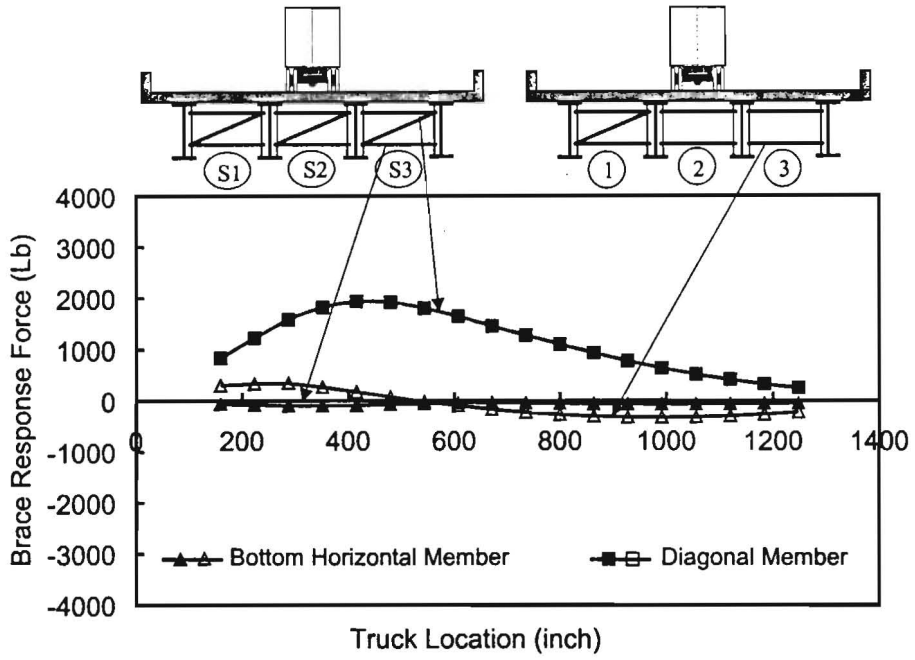

Figure 8.24 (b) Brace Force Response Envelope at Brace Location #3 with Center Truck Loading – Conventional Stagger vs. Lean-On Bracing

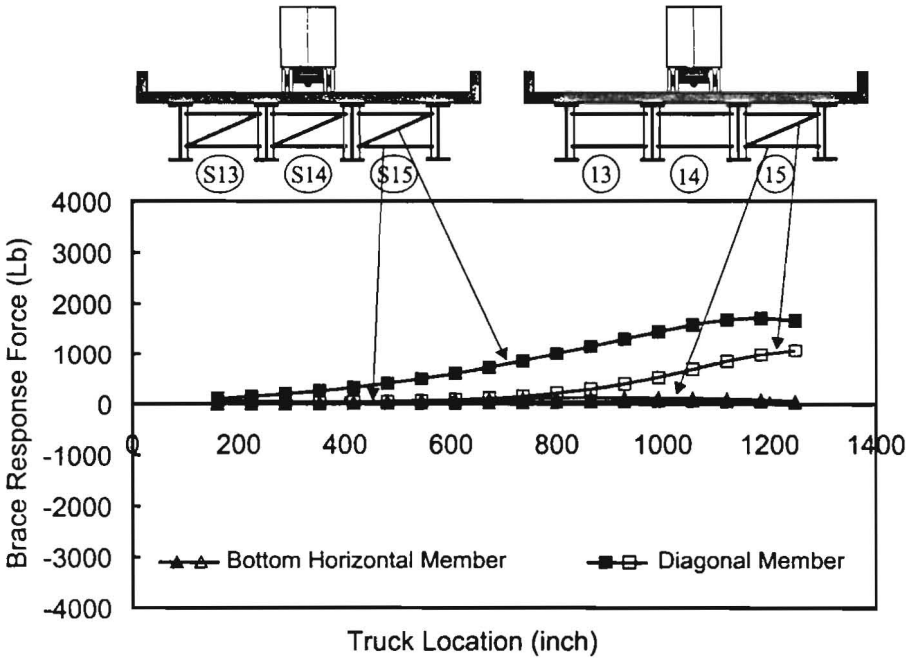

Figure 8.24 (c) Brace Force Response Envelope at Brace Location #15 with Center Truck Loading – Conventional Stagger vs. Lean-On Bracing

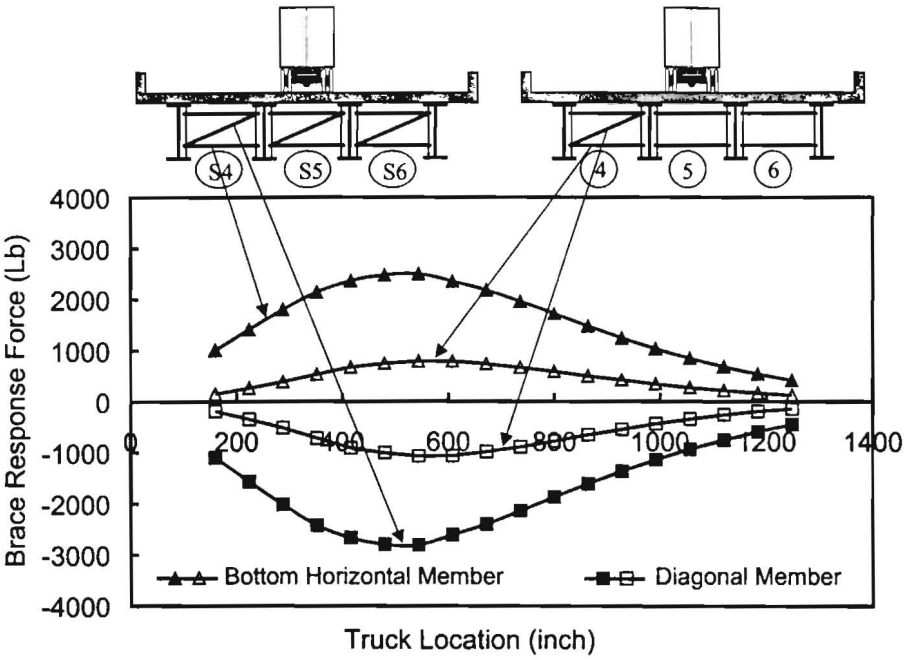

Figure 8.24 (d) Brace Force Response Envelope at Brace Location #4 with Center Truck Loading – Conventional Stagger vs. Lean-On Bracing

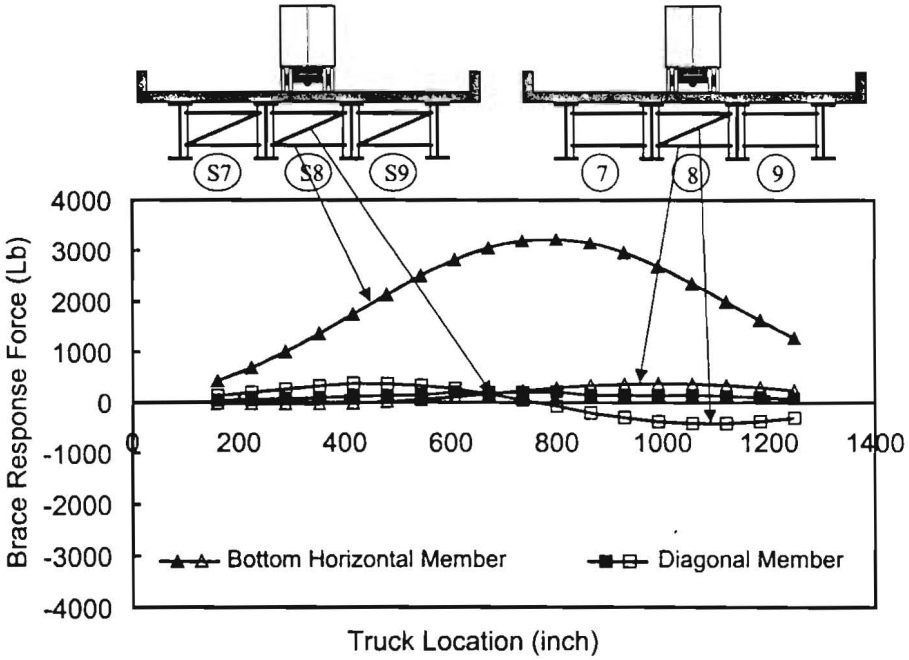

Figure 8.24 (e) Brace Force Response Envelope at Brace Location #8 with Center Truck Loading – Conventional Stagger vs. Lean-On Bracing

The graphs that have been presented have shown the response envelopes when the truck is moving across the bridge. The results presented in this chapter have focused on a few cross-frame locations. The brace force response envelops for all of the cross-frame locations are presented in Appendix D for all three brace layouts. The results presented in this chapter as well as those in the Appendix show that positioning the truck close to the edge of the bridge results in larger brace forces near the supports. Positioning the truck close to the center of the bridge generally leads to larger cross-frame forces near midspan. For most truck positions, the figures show that the forces of the brace members can be significantly reduced at most cross-frame locations when the lean-on bracing system is used, provided that the cross-frame lines do not frame directly into the support. A relatively small offset of 4 or 5 feet will significantly reduce the brace forces when the lean-on system is used.

For conventional normal braces that extend the full width of the bridge, the maximum cross-frame forces for the lean-on system were substantially lower for both truck positions that were considered (edge and center loading). For the conventional staggered layout, with edge truck loading, the lean-on system resulted in similar brace forces for the cross-frame lines near the supports. The cross-frame forces for the lean-on system were actually larger than the staggered layout for a few of the locations. For center truck loading, the staggered layout resulted in significantly larger forces than the lean-on system at all of the cross-frame locations.

Comparisons of the lean-on bracing with the conventional normal and staggered layouts generally show lower forces develop in many of the cross-frames for both truck positions. Therefore, based on the force magnitudes, a ranking of the recommended details would proceed in the following order: 1) lean-on layout, 2) conventional staggered layout, and 3) conventional normal layout. Although this study has not focused on the localized stress concentrations that may occur around the cross-frame to girder connections, the lower forces induced in the cross-frames based upon the recommended details should result in a reduction of potential fatigue damage in the girders due to long-term service truck traffic. In addition, these bridges with fewer cross-frame locations should be easier to inspect than bridges with the conventional layout of cross-frames.

8.5 Summary

This chapter has presented finite element results for girders with skewed supports and different bracing systems. The results have demonstrated the bracing behavior of simplified bracing system during the construction stage and during the truck loading on the completed bridges.

For the lean-on bracing system, expressions for the brace stiffness and girder in-plane stiffness shown in Eqs. 8.5 and 8.8 had good agreement with the FEA results in obtaining the ideal stiffness. Equations presented in Figs. 8.7 and 8.8 can be used to estimate the brace moment for the lean-on cross-frames. FEA analyses showed that the lean-on bracing system

led to significant reductions in the cross-frame member forces induced to by truck loading. Therefore, the use of these details should lead to improved fatigue behavior around cross-frame and diaphragm locations as well as making the bridges easier to inspect.

Chapter 9
Conclusions and Future Work

9.1 Conclusions

The objective of the research outlined in this dissertation is to improve the understanding of the bracing behavior of cross frames and diaphragms in steel bridges with skewed supports. General bracing requirements were developed and new cross-frame and diaphragm details to minimize fatigue problems at bracing locations were proposed. Although the research investigation included both experimental and computational studies, this dissertation has focused on results from the computational studies. In the process of developing a design approach for bracing requirements of bridge girders with skewed supports, the following parameters were considered:

1) Girder System (two to four girder systems were considered)
2) Girder Span (40 feet to 120 feet)
3) Girder Cross Section (Singly and Doubly Symmetric Cross-Sections)
4) Skew Angle (0, 15, 25, 35, and 45 degrees)
5) Brace Orientation (Parallel to Skewed Support or Normal to girders)
6) Loading Condition (Uniform Moment, Concentrated Load, and Uniformly Distributed Load)
7) Number of intermediate braces
8) Shape of Imperfection

A number of conclusions can be made based upon the results presented in this investigation. The conclusions have been categorized based upon the applicable parameters and the bracing systems that were studied. These conclusions will be presented in the subsequent subsections of this chapter.

9.1.1 Imperfections for Torsional Bracing Systems

The magnitudes of the brace moments for torsional bracing of beams are sensitive to the magnitude and distribution of the initial twist of the section. Although pure lateral sweep of the beam or girder can cause moments in the torsional braces, the magnitudes of the resulting moments are much smaller than those caused by initial twist in the beams. The initial imperfection that was utilized in this study consisted of a twist of the cross-section in which the top flange was displaced an amount equal to $L_b/500$, while the bottom flange remained straight. For girder systems with several braces along the girder length and subjected to loads with moment gradient, the forces that develop in the different braces along the girder length are relatively sensitive to the girder moment at the brace location. The imperfection that will generally cause the largest brace force is one in which the maximum initial twist occurs near the brace closest to the point of maximum beam moment with zero twist at adjacent brace points.

9.1.2 Bracing Behavior for Girders with Normal Supports

Several analyses were conducted on girder systems with normal supports. Comparisons between FEA results and solutions that were presented in previous studies for the brace stiffness requirements for steel girders with normal supports showed good agreement. Comparisons between the FEA results and previous equations for the strength requirements showed good agreement for the case when the girders were at moment levels corresponding to buckling between braced points. However these solutions were generally conservative for smaller values of the applied moment. Modifications to these previous solutions provided good agreement with the FEA solutions for the full range of moments up to buckling between the brace points. The modification consisted of simply squaring the moment term, which results in the following expression for the total twist in the girder:

$$\phi_T = \frac{\phi_0}{1 - \frac{\beta_{Ti}}{\beta_T}\left(\frac{M^*}{M_{cr}}\right)^2} \tag{9.1}$$

where: ϕ_T is the total girder twist, ϕ_o is the initial twist of the girder (often taken as $L_b/(500d)$, β_{Ti} is the ideal brace stiffness, β_T is the actual brace stiffness that was provided, M^* is the maximum applied bending moment, and M_{cr} is the buckling capacity of the girder corresponding to buckling between brace points. The resulting brace moment was then found using the following expression:

$$M_{br} = \beta_T (\phi_T - \phi_o) \tag{9.2}$$

where: M_{br} is the resulting torsional brace moment, β_T is the torsional brace stiffness, ϕ_T is the total twist given by Eq. 9.1, and ϕ_o is the initial twist of the girder.

The required brace stiffness is based upon twice the ideal stiffness, which can be evaluated using the following equation:

$$\beta_{T\,Req'd} = \frac{2.4 L M_u^2}{C_{bb}^2 n E I_y} \tag{9.3}$$

For an initial twist $\phi_o = L_b/(500h)$, where L_b is the girder unbraced length and h is the girder depth, Eq. 9.3 can be expressed as follows:

$$M_{br} = \beta_{T\,Req'd}\phi_0 = \frac{2.4 L M_u^2}{C_{bb}^2 n E I_y} \times \frac{L_b}{500h} \tag{9.4}$$

M_{br} is the brace moment based upon providing a brace stiffness corresponding to twice the ideal value ($\beta_{TReq'd}$). For cases when the actual provided brace stiffness, β_{act}, is larger than twice the ideal value ($\beta_{TReq'd}$), the brace moment can be reduced by the following expression:

$$M_{act} = M_{br}\left[\frac{\left(\frac{M_u}{Mcr}\right)^2}{2-\frac{\beta_{T\,\mathrm{Req'd}}}{\beta_{act}}\left(\frac{M_u}{M_{cr}}\right)^2}\right] \tag{9.5}$$

where: M_{br} is the brace moment resulting from Eq. 9.4, M_u is the maximum factored moment, M_{cr} is the moment corresponding to buckling between the brace points, $\beta_{TReq'd}$ corresponds to twice the ideal value, and β_{act} is the actual brace stiffness provided.

Most of the previous bracing solutions were developed for twin-girder systems. For systems with several girders, the bracing is generally more efficient since the effective number of girders that each cross-frame must brace decreases. A simple modification that accounts for the number of cross-frames along the length and width as well as the number of girders across the width was recommended in Chapter 5. The modification had good agreement with the FEA results. Neglecting the modification results in conservative estimates of the bracing requirements.

9.1.3 Bracing Behavior for Girders with Skewed Supports and Parallel Braces

The effectiveness of a brace that is oriented parallel to skewed supports can be substantially reduced compared to normal braces. The reduction in the effectiveness is generally due to the fact that the full stiffness of the brace is not engaged at resisting twist of the girder cross-section due to the angled orientation of the brace. For a skew angle of θ, applying a modification $\cos^2\theta$ to the cross-frame stiffness in the plane of the brace had good agreement with the FEA results. Good agreement was also achieved between the FEA results and the brace moment expressions by simply modifying the strength requirement of the brace by $1/\cos\theta$.

9.1.4 Bracing Behavior for Girders with Skewed Supports and Normal Braces

The skew angle had very little effect on the bracing behavior when the bracing was oriented normal to the girders. For cases with more than one intermediate brace, the bracing requirements for girders with normal supports generally showed good agreement with the results for girders with skewed supports when the bracing was oriented perpendicular to the longitudinal axis of the girders. However for the case of one brace, modifications were required to the original brace requirements that were developed for the case with normal supports. The bracing requirements are based on an equivalent continuous brace stiffness $\overline{\beta_T} = n\beta_T / L$. However for the case of a single brace, the length L in the expression for $\overline{\beta_T}$, is replaced by 0.75L. For beams with skewed supports, however, better agreement was achieved by using the same expression that is used for cases with multiple intermediate

braces. Therefore for all cases the definition for $\overline{\beta_T} = n\beta_T / L$. Using this expression for normal supports or cases with small skew angles will generally be conservative.

9.1.5 Proposed Details for Cross-Frames and Diaphragms

The investigations of the stability bracing behavior of torsional bracing systems has led to an improved understanding of the bracing requirements for girders with relatively general support conditions. Expressions that were originally developed for girders with normal supports were modified to account for the skew angle as outlined in the previous subsections. Therefore, design engineers can effectively design the cross-frames and diaphragms for the actual application. In many situations these provisions will lead to smaller cross-frame members than typically employed. Utilizing smaller cross-frame members will generally lead to smaller brace forces induced by truck loading, thereby reducing the potential for fatigue damage.

In addition to designing the cross-frames for the actual application, one of the goals of this study was to develop recommended details to further minimize fatigue damage. Since relatively small member sizes can satisfy the bracing requirements for several design applications, a number of cross-frames can potentially be eliminated and top and bottom horizontal struts can be provided to lean several girders on a single cross-frame along a brace line. Eliminating cross-frames should make the girders easier to inspect since there are fewer regions complicated by the cross-frame to girder interaction from the truck loading. Finite element studies were done on the girders to investigate the impact on the stability behavior of the lean-on bracing system. Since the demand on each cross-frame is increased by the leaning girders, modifications to the strength and stiffness expressions were necessary. Both the cross-frame stiffness and the in-plane stiffness of the girders needed to be modified to account for the in-plane girders. The modified expressions show good agreement with the FEA results.

In addition to studying the stability behavior of the bracing systems with the steel girders during the construction stage, studies were also conducted on the behavior of the bracing systems and girders with a composite concrete deck. Finite element studies were conducted on the composite girders under truck loading. The behavior of both conventional cross-frame layouts and lean-on systems were studied with HS20-44 truck loading. The conventional cross-frame systems that were considered consisted of cases with cross-frames extending across the full bridge width as well as cases in which normal cross-frames were staggered along a line parallel to the skewed supports. The lean-on systems generally had substantially lower brace forces than observed for many of the conventional bracing systems. Although there were isolated braces in which the lean-on system brace forces were close to the conventional systems, the brace forces in the lean-on system were substantially lower for the majority of the braces in the bridges that were studied.

The results presented show that positioning the truck close to the edge of the bridge results in larger brace forces near the supports. Positioning the truck close to the center of the bridge generally leads to larger cross-frame forces near midspan. For truck positions, the results show that the forces of the brace members can be significantly reduced at most cross-frame locations when the lean-on bracing system is used, provided that the proposed recommendations are followed with respect to the geometrical layout:

1) The first normal line of braces adjacent to the support should not frame directly into the support but should be offset by a small distance. A distance of four feet was used in the FEA studies as shown in Fig. 9.1 for brace lines A and E.

2) In brace lines adjacent to the support, the cross-frame should be placed so as to maximize the distance from the support. Based upon the skewed supports in Fig. 9.1, the cross-frame should be put between the top two girders along brace lines A and B and between the bottom two girders at girder lines D and E.

3) Although each brace line only has one cross-frame, the layout of these cross-frame should be spread out across the width of the bridge as indicated in Fig. 9.1. This provides better overall stability as well as engaging all of the girders in the calculation of the in-plane girder stiffness. With lean-on systems, the effect of the in-plane girder stiffness was reduced by a factor of 2.

9.2 Future Work

In addition to improving the design and detailing procedures for conventional bracing systems such as cross-frame and diaphragm systems for steel bridge girders, other potential bracing systems should also be investigated. A likely bracing element is the permanent metal deck forms (PMDF) that are often used to support the concrete bridge deck during construction. These forms have substantial in-plane stiffness that can help restrain the lateral movement of the top flange of the girders during casting of the concrete deck. Although PMDF in the building industry are routinely relied upon for bracing, these forms are not currently permitted to be relied upon for bracing in the bridge industry. The forms that are used in the bridge industry are actually stronger and stiffer than those used in the building industry, however the method of connecting the forms to the girders substantially reduces the in-plane stiffness of the PMDF. Research is currently underway at the University of Houston to improve the method of connection between the formwork and the girders. The study is also focused on improving the understanding of the behavior of the metal formwork as a bracing element. The resulting bracing system would probably consist of cross-frames and diaphragms provided to support the weight of the steel girders, while the metal deck forms would be used to brace the girders during construction and the placement of the concrete bridge deck.

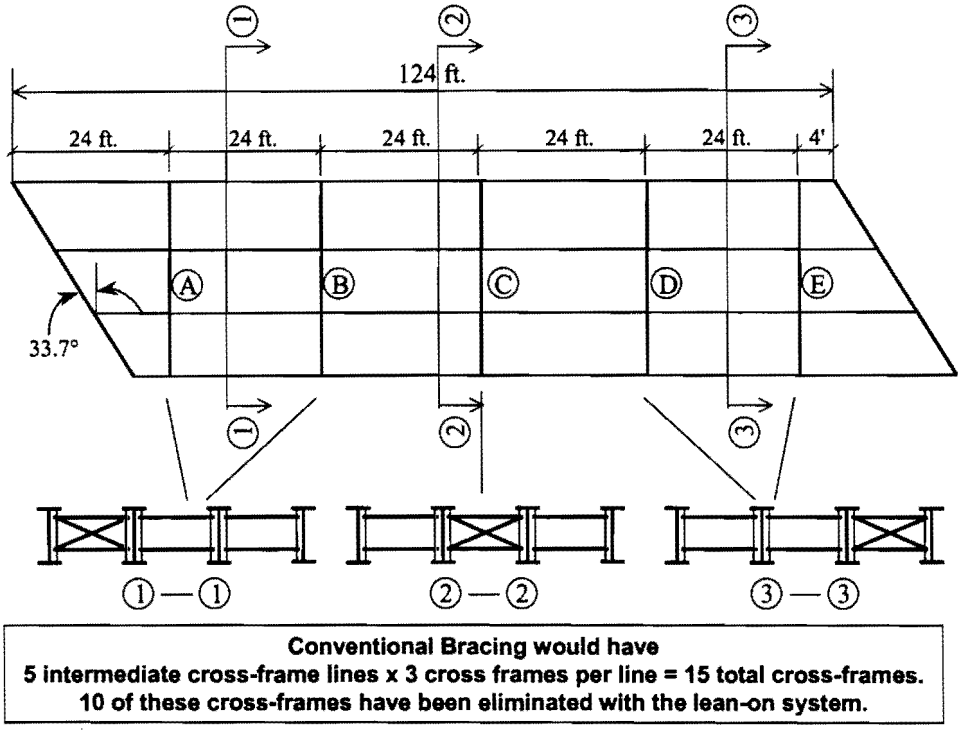

Figure 9.1 Proposed Geometric Layout for Lean-On Bracing System

Appendix A
Supplemental Results for Girders with Normal Supports

As discussed in Chapter 5, for many of the girder cross-sections that were considered in this investigation, comparisons between the FEA results and the equations showed similar trends. In these cases, representative results were presented and discussed in Chapter 5, while additional results for sections with similar behavior are presented in this appendix.

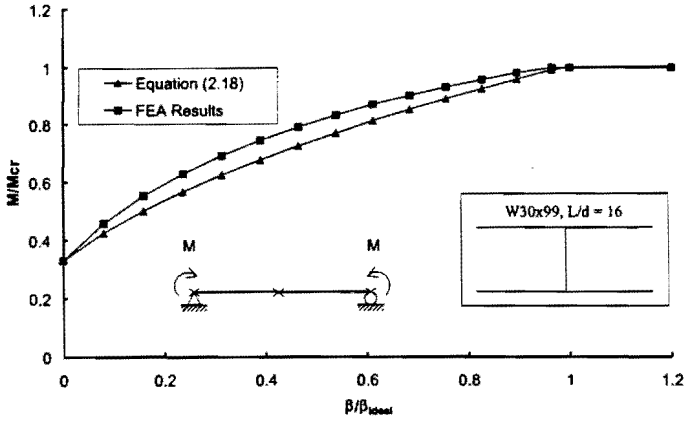

Figure A.1(a) M/M_{cr} versus β/β_{ideal} for a W30x99 Section with Uniform Moment

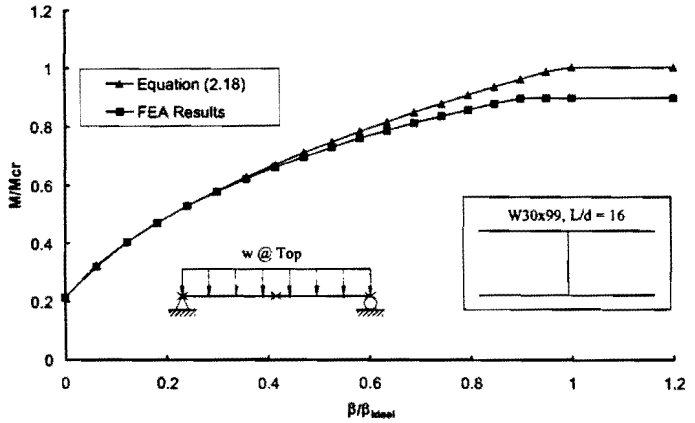

Figure A.1(b) M/M_{cr} versus β/β_{ideal} for a W30x99 Section with Distributed Loads on Top Flange

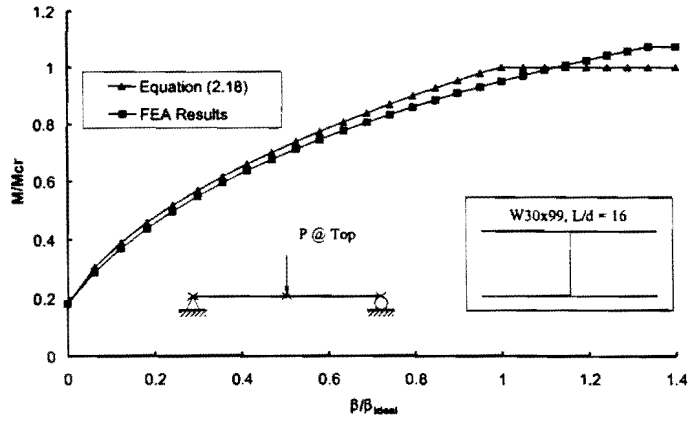

Figure A.1(c) M/M_{cr} versus β/β_{ideal} for a W30x99 Section with Midspan Concentrated Load on Top Flange

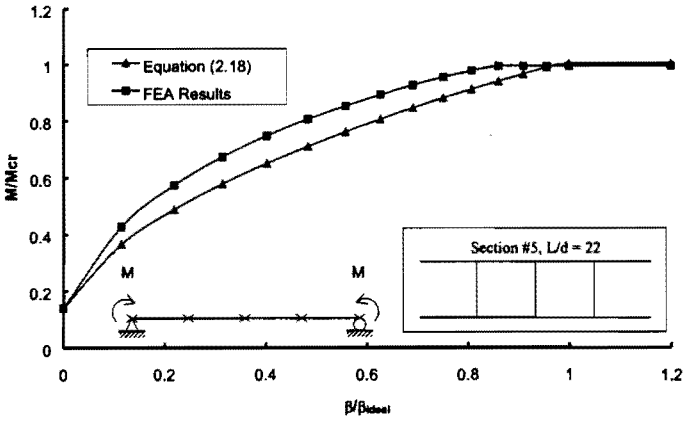

Figure A.2(a) M/M_{cr} versus β/β_{ideal} for Section #5 with Uniform Moment

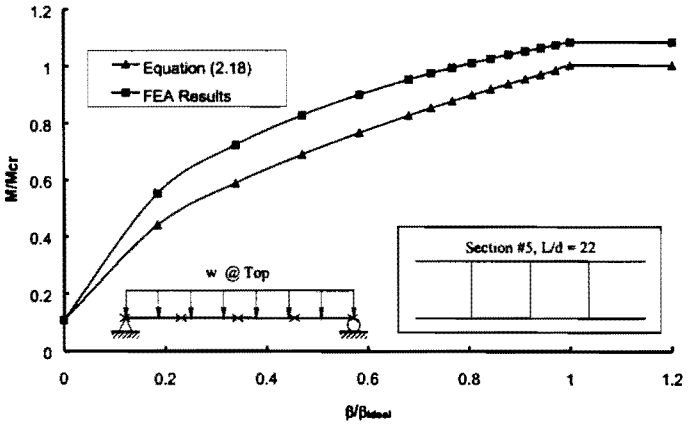

Figure A.2(b) M/M_{cr} versus β/β_{ideal} for Section #5 with Distributed Loads Top Flange

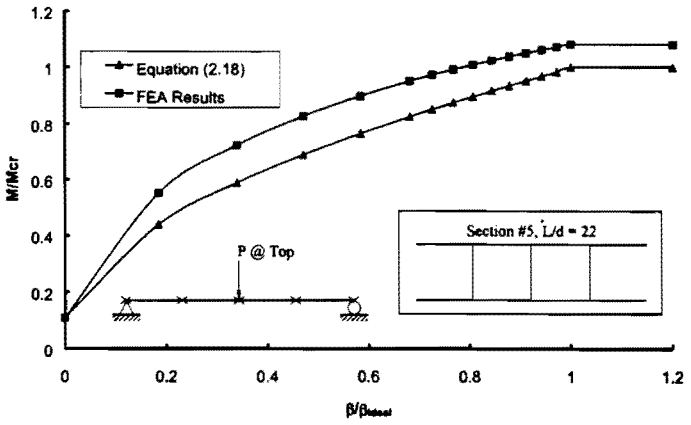

Figure A.2(c) M/M_{cr} versus β/β_{ideal} for Section #5 with Midspan Concentrated Load on Top Flange

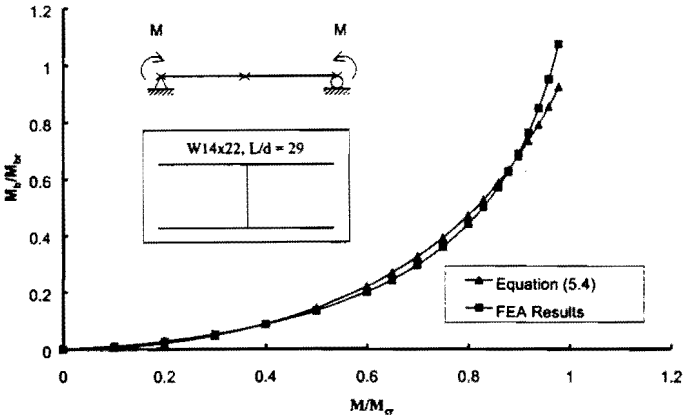

Figure A.3(a) M_b/M_{br} versus M/M_{cr} for a W14x22 Section with Uniform Moment

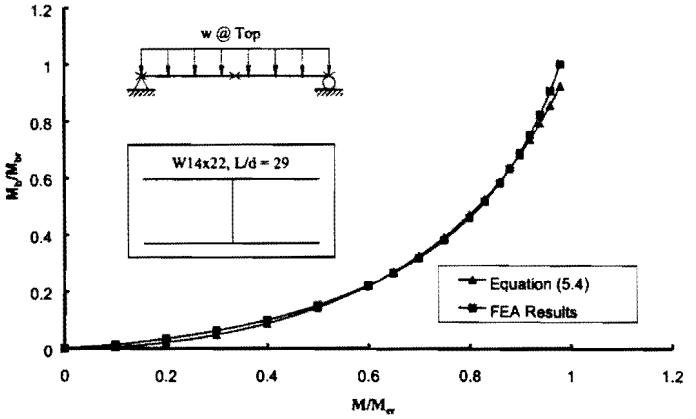

Figure A.3(b) M_b/M_{br} versus M/M_{cr} for a W14x22 Section with Distributed Loads on Top Flange

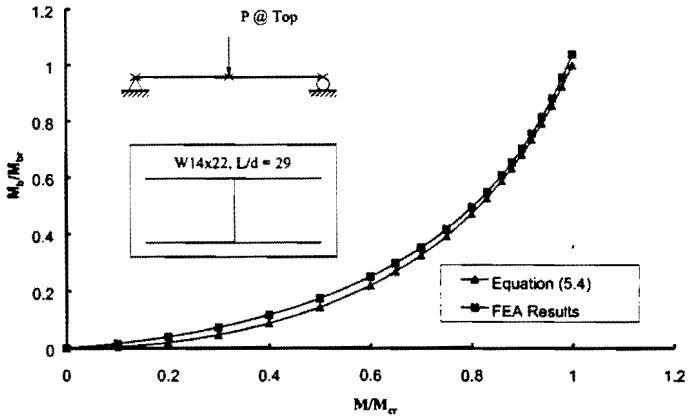

Figure A.3(c) M_b/M_{br} versus M/M_{cr} for a W14x22 Section with Midspan Concentrated Load on Top Flange

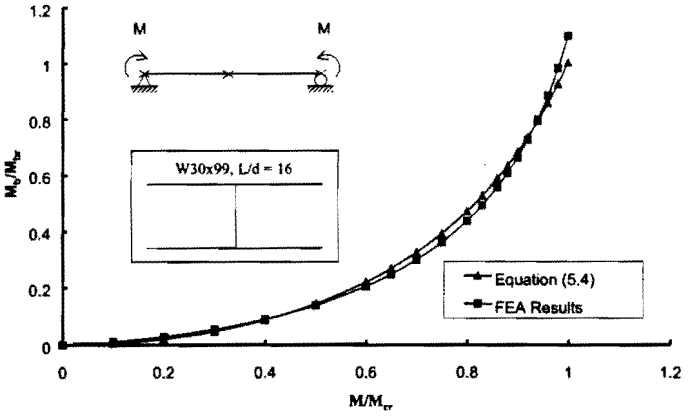

Figure A.4(a) M_b/M_{br} versus M/M_{cr} for a W30x99 Section with Uniform Moment

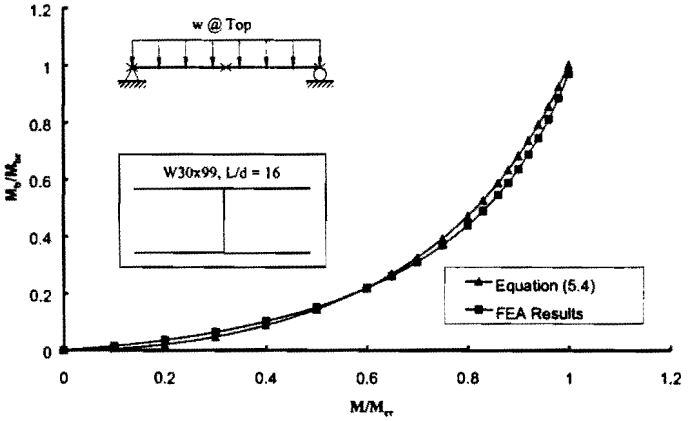

Figure A.4(b) M_b/M_{br} versus M/M_{cr} for a W30x99 Section with Distributed Loads on Top Flange

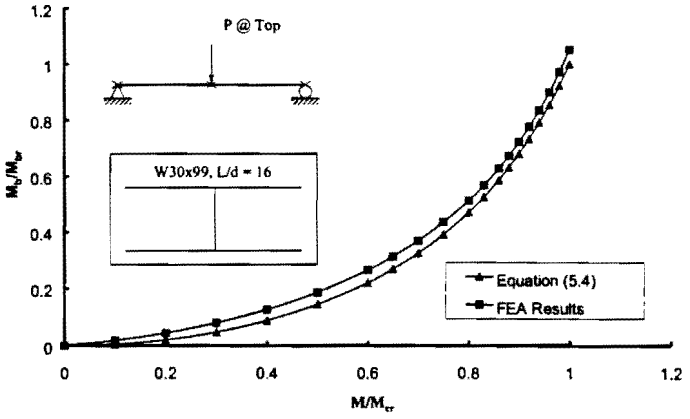

Figure A.4(c) M_b/M_{br} versus M/M_{cr} for a W30x99 Section with Midspan Concentrated Loads on Top Flange

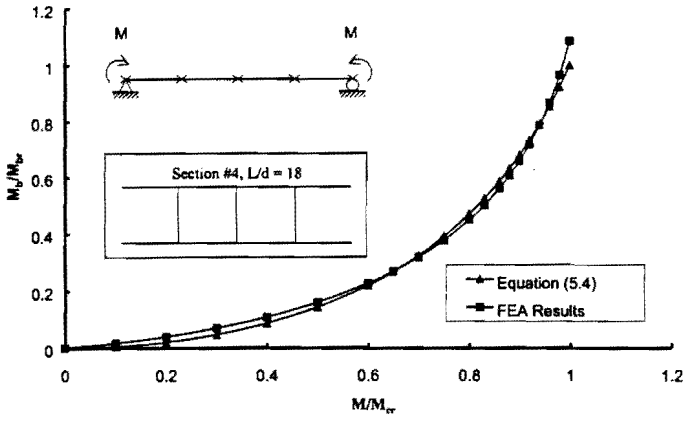

Figure A.5(a) M_b/M_{br} versus M/M_{cr} for Section #4 with Uniform Moment

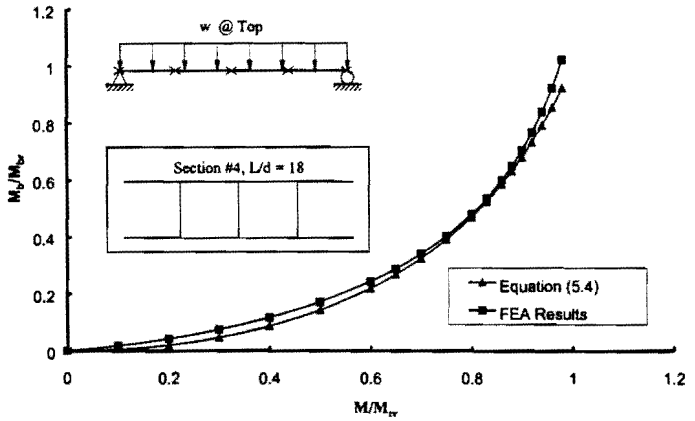

Figure A.5(b) M_b/M_{br} versus M/M_{cr} for Section #4 with Distributed Loads on Top Flange

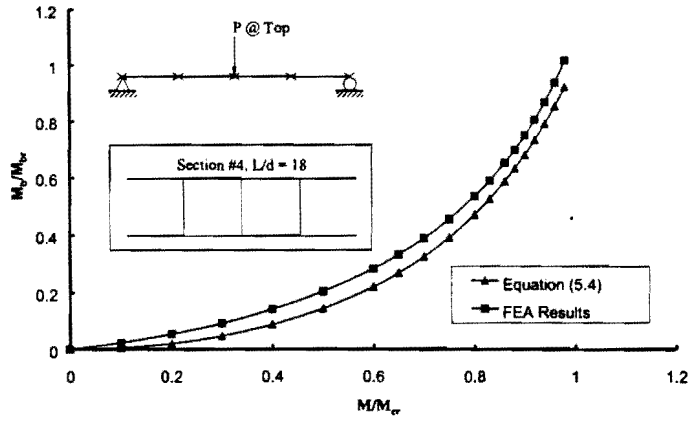

Figure A.5(c) M_b/M_{br} versus M/M_{cr} for Section #4 with Midspan Concentrated Load on Top Flange

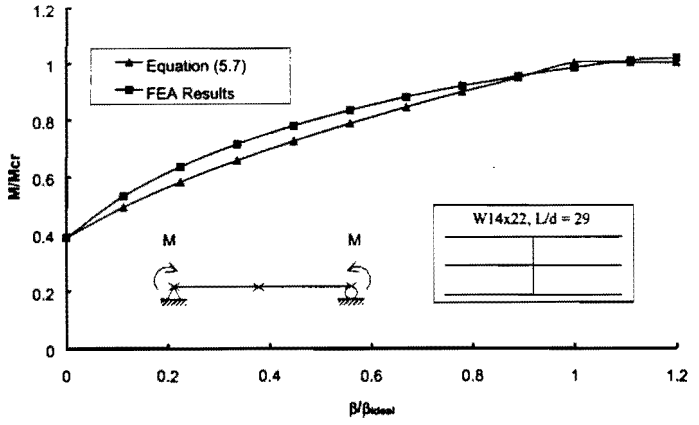

Figure A.6(a) M/M_{cr} versus β/β_{ideal} for a W14x22 Section 3-Girder System with Uniform Moment

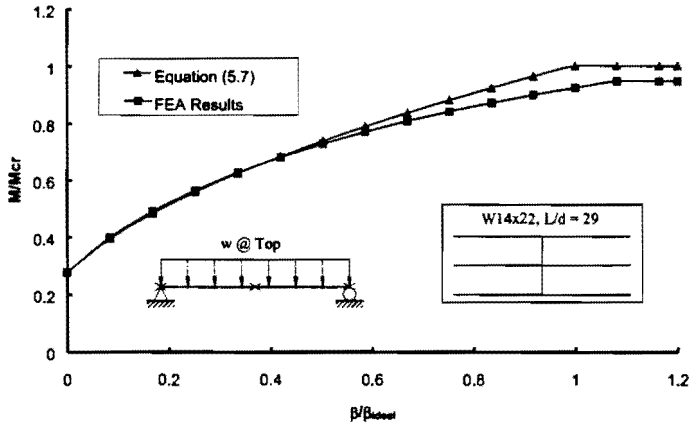

Figure A.6(b) M/M_{cr} versus β/β_{ideal} for a W14x22 Section 3-Girder System with Distributed Loads on Top Flange

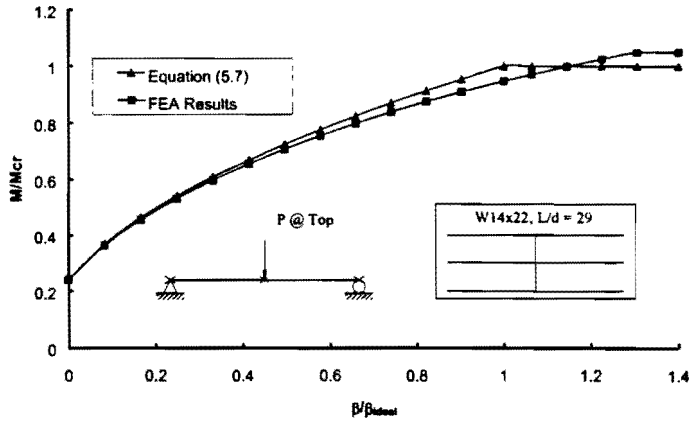

Figure A.6(c) M/M_{cr} versus β/β_{ideal} for a W14x22 Section 3-Girder System with Midspan Concentrated Load on Top Flange

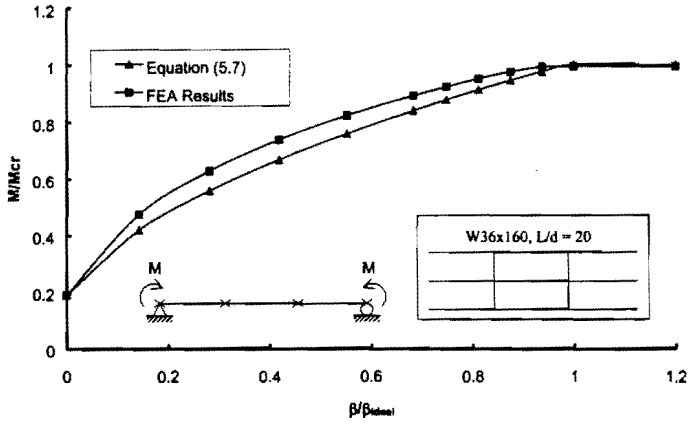

Figure A.7(a) M/M_{cr} versus β/β_{ideal} for a W36x160 Section 3-Girder System with Uniform Moment

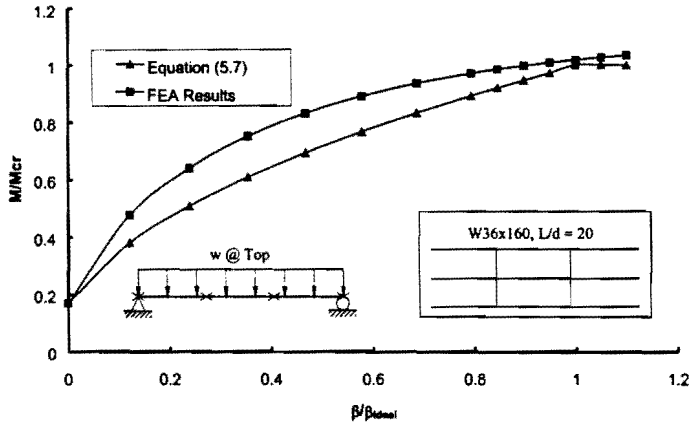

Figure A.7(b) M/M_{cr} versus β/β_{ideal} for a W36x160 Section 3-Girder System with Distributed Loads on Top Flange

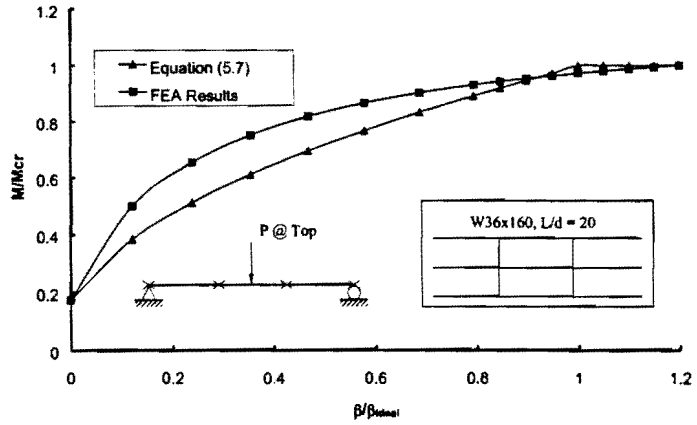

Figure A.7(c) M/M_{cr} versus β/β_{ideal} for a W36x160 Section 3-Girder System with Midspan Concentrated Load on Top Flange

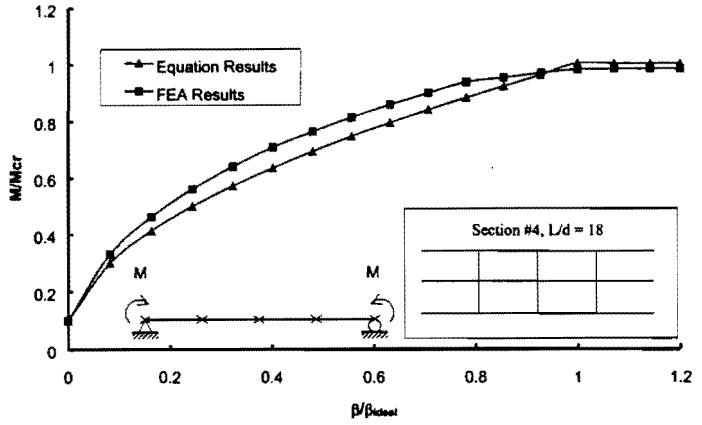

Figure A.8(a) M/M_{cr} versus β/β_{ideal} for Section #4 3-Girder System with Uniform Moment

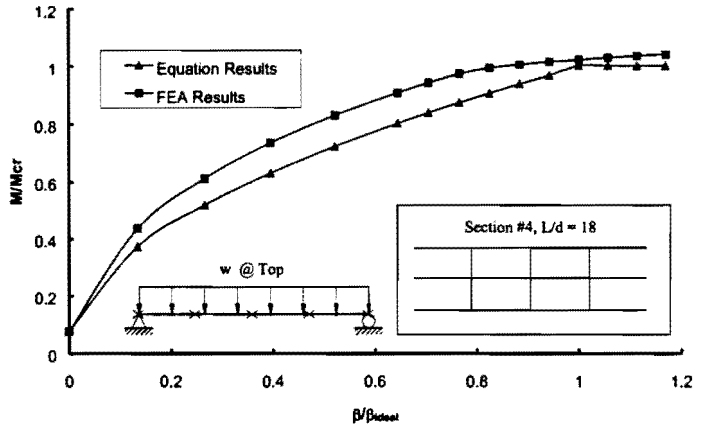

Figure A.8(b) M/M_{cr} versus β/β_{ideal} for Section #4 3-Girder System with Distributed Loads on Top Flange

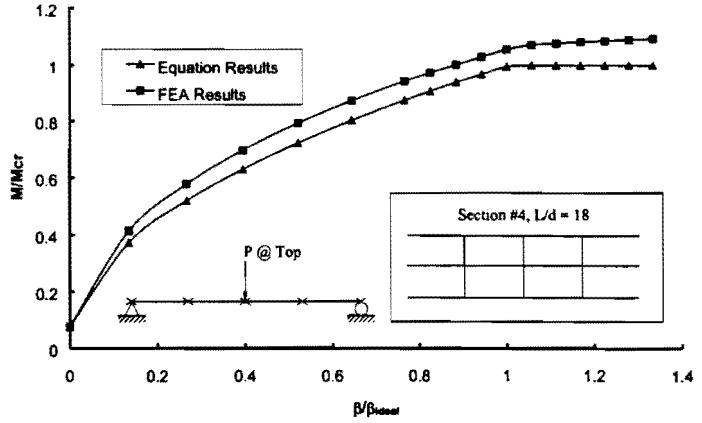

Figure A.8(c) M/M_{cr} versus β/β_{ideal} for Section #4 3-Girder system with Midspan Concentrated load on Top Flange

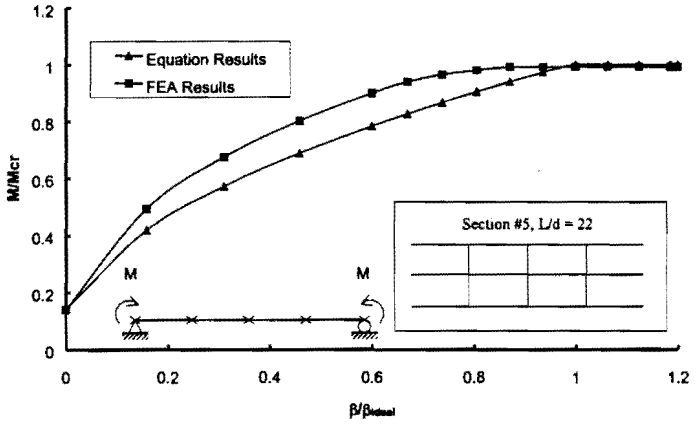

Figure A.9(a) M/M_{cr} versus β/β_{ideal} for Section #5 3-Girder System with Uniform Moment

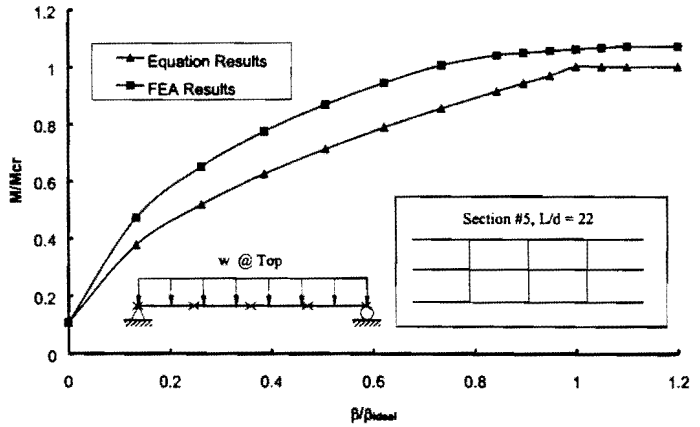

Figure A.9(b) M/M_{cr} versus β/β_{ideal} for Section #5 3-Girder System with Distributed Loads on Top Flange

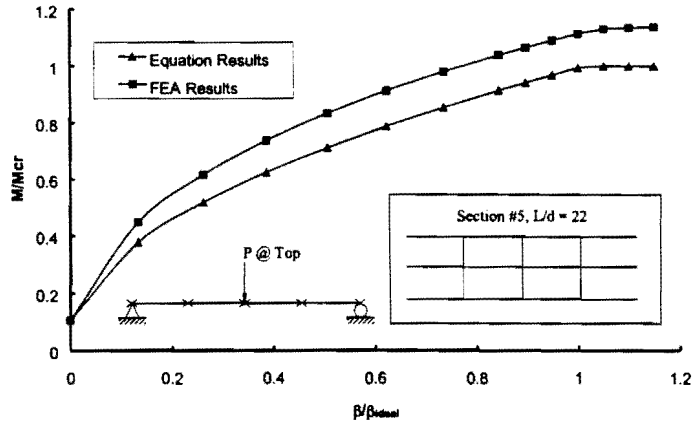

Figure A.9(c) M/M_{cr} versus β/β_{ideal} for Section #5 3-Girder System with Midspan Concentrated Load on Top Flange

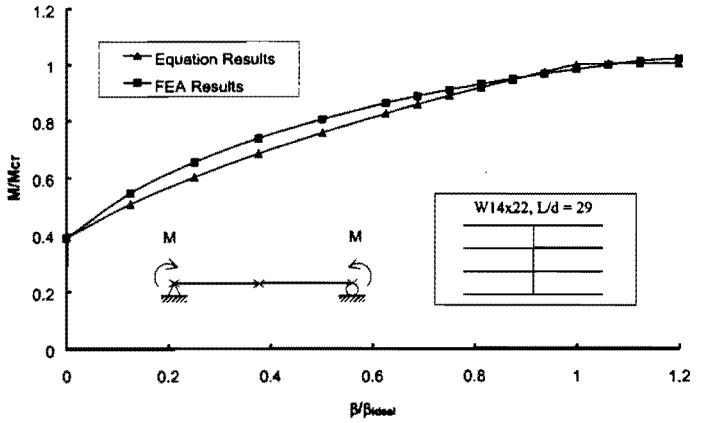

Figure A.10(a) M/M_{cr} versus β/β_{ideal} for a W14x22 Section 4-Girder System with Uniform Moment

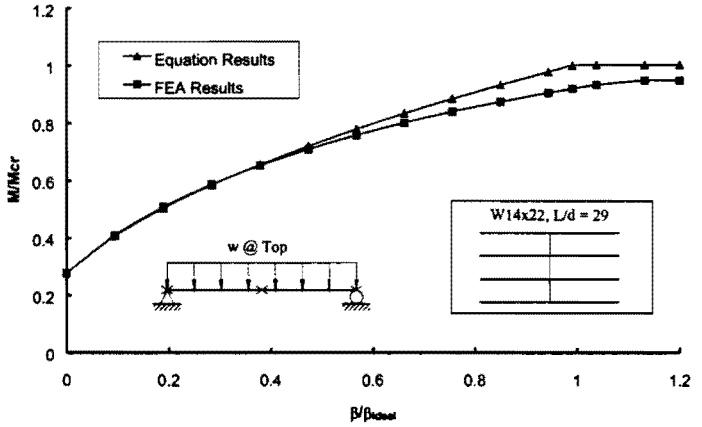

Figure A.10(b) M/M_{cr} versus β/β_{ideal} for a W14x22 Section 4-Girder System with Distributed loads on Top Flange

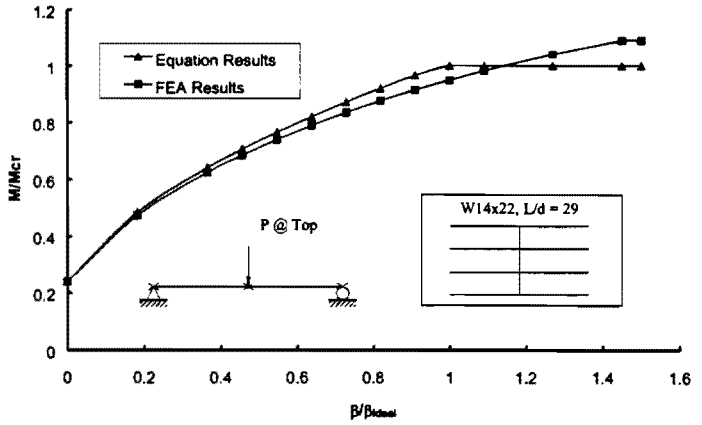

Figure A.10(c) M/M_{cr} versus β/β_{ideal} for a W14x22 Section 4-Girder System with Midspan Concentrated load on Top Flange

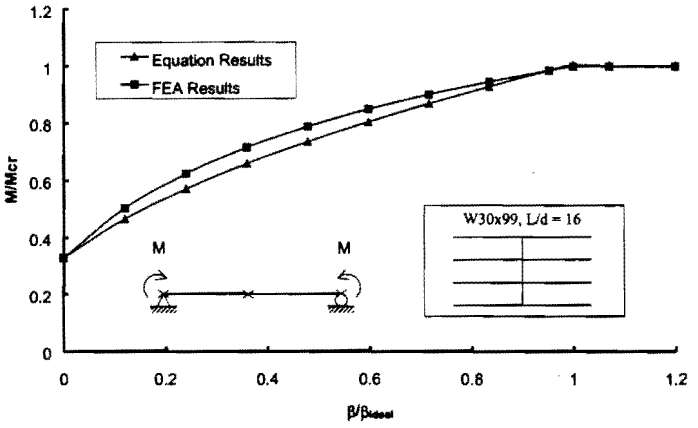

Figure A.11(a) M/M_{cr} versus β/β_{ideal} for a W30x99 Section 4-Girder System with Uniform Moment

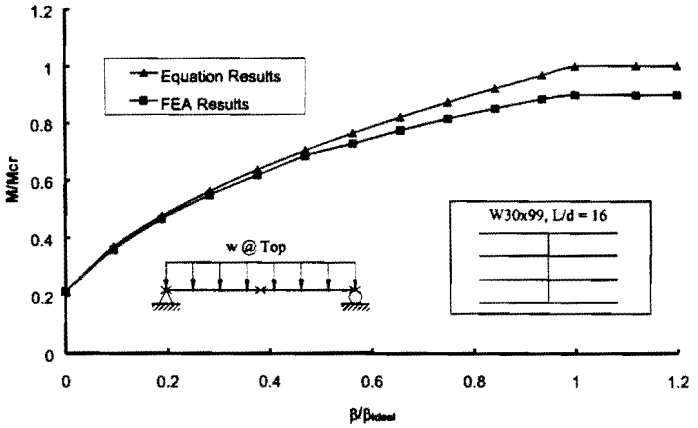

Figure A.11(b) M/M_{cr} versus β/β_{ideal} for a W30x99 Section 4-Girder System with Distributed loads on Top Flange

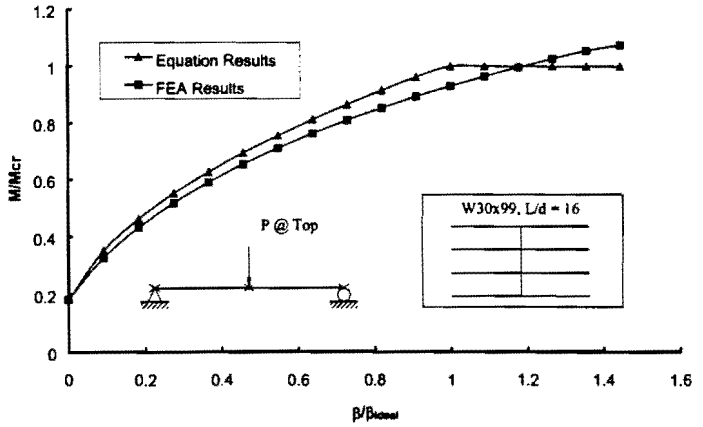

Figure A.11(c) M/M_{cr} versus β/β_{ideal} for a W30x99 Section 4-Girder System with Midspan Concentrated load on Top Flange

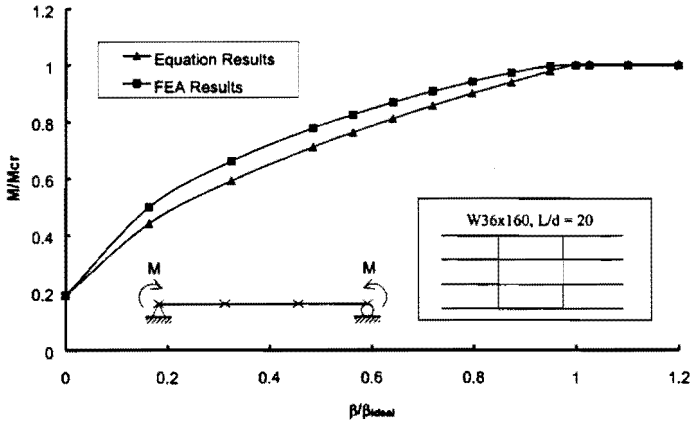

Figure A.12(a) M/M_{cr} versus β/β_{ideal} for a W36x160 Section 4-Girder System with Uniform Moment

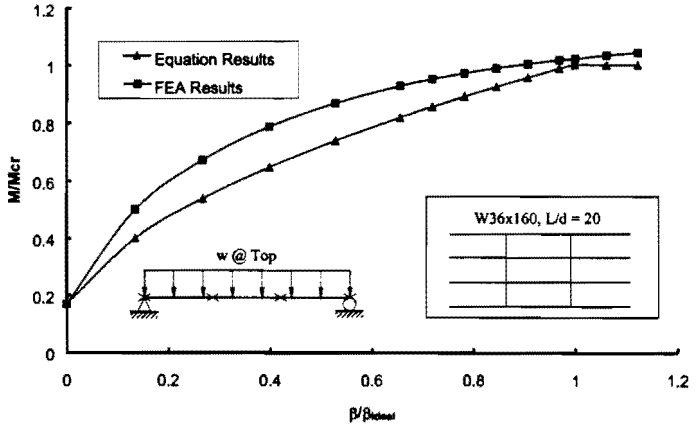

Figure A.12(b) M/M_{cr} versus β/β_{ideal} for a W36x160 Section 4-Girder System with Distributed loads on Top Flange

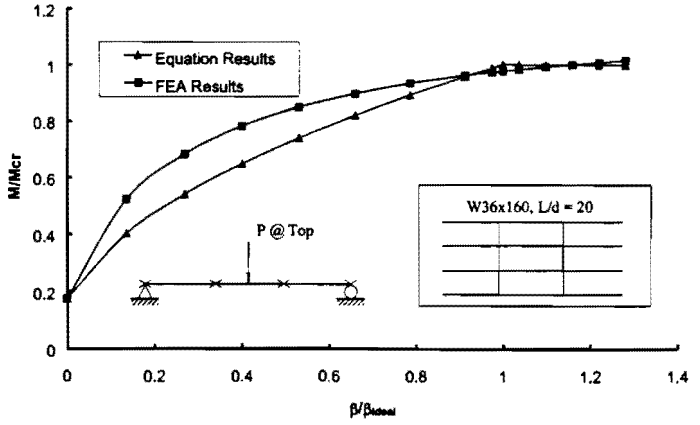

Figure A.12(c) M/M_{cr} versus β/β_{ideal} for a W36x160 Section 4-Girder System with Midspan Concentrated load on Top Flange

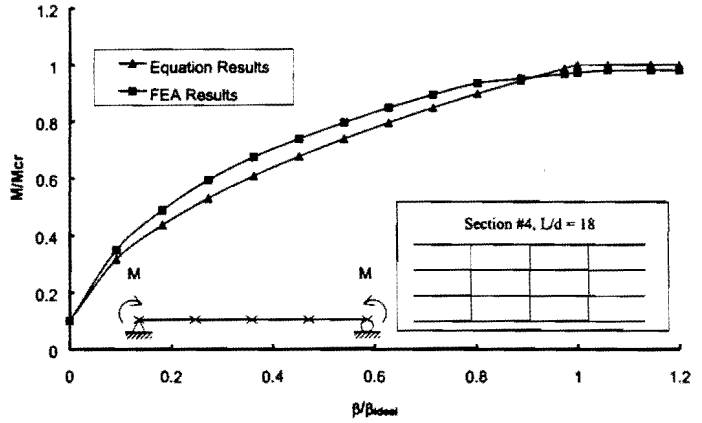

Figure A.13(a) M/M_{cr} versus β/β_{ideal} for Section #4 4-Girder System with Uniform Moment

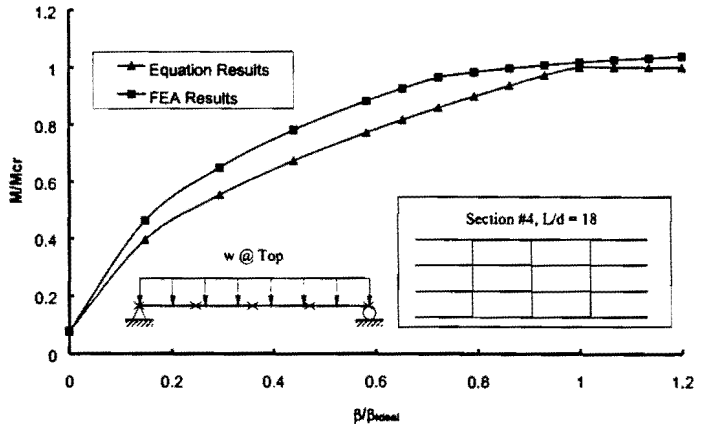

Figure A.13(b) M/M_{cr} versus β/β_{ideal} for Section #4 4-Girder System with Distributed Loads on Top Flange

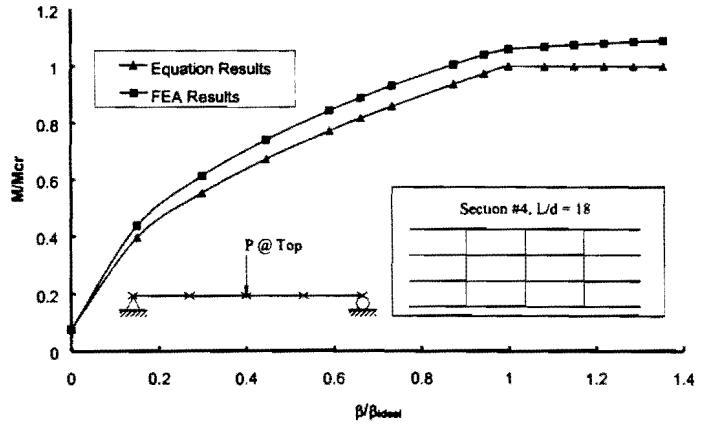

Figure A.13(c) M/M_{cr} versus β/β_{ideal} for Section #4 4-Girder System with Midspan Concentrated load on Top Flange

Appendix B
Supplemental Results for Girders with Skewed Supports and Parallel Braces

As discussed in Chapter 6, for many of the girder cross-sections that were considered in this investigation of girders with skewed supports and braces oriented paralleled to skewed supports, comparisons between the FEA results and the equations showed similar trends. In these cases, representative results were presented and discussed in Chapter 6, while additional results for sections with similar behavior are presented in this appendix.

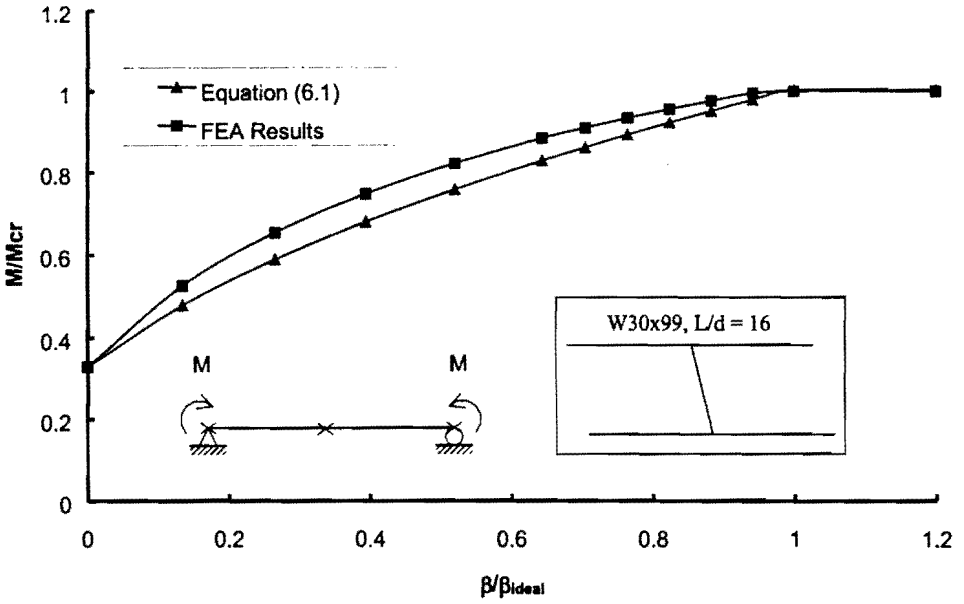

(a) skew angle =10°

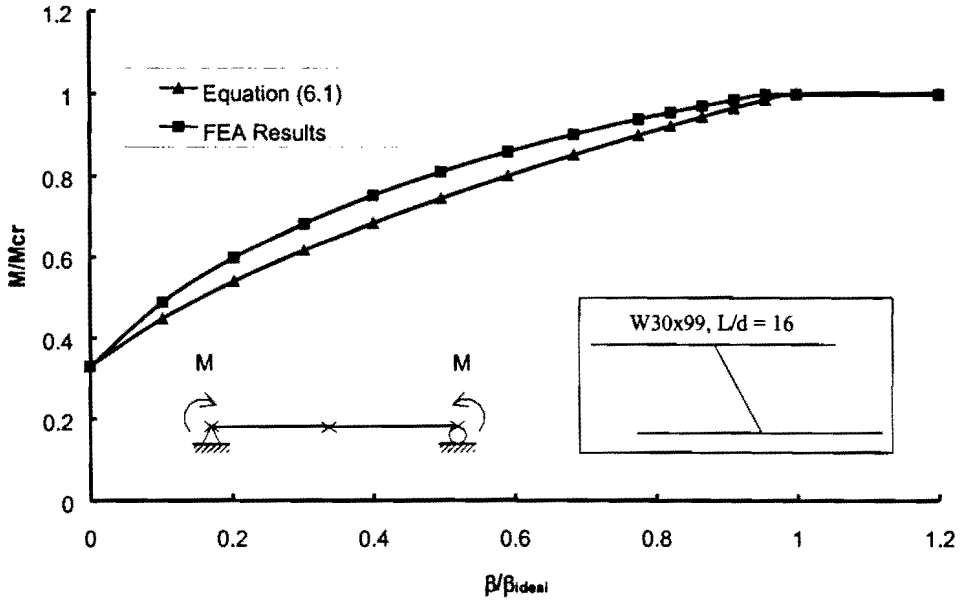

(b) skew angle = 30°

Figure B.1 M/M_{cr} versus β/β_{ideal} for a W30x99 Section with Uniform Moment

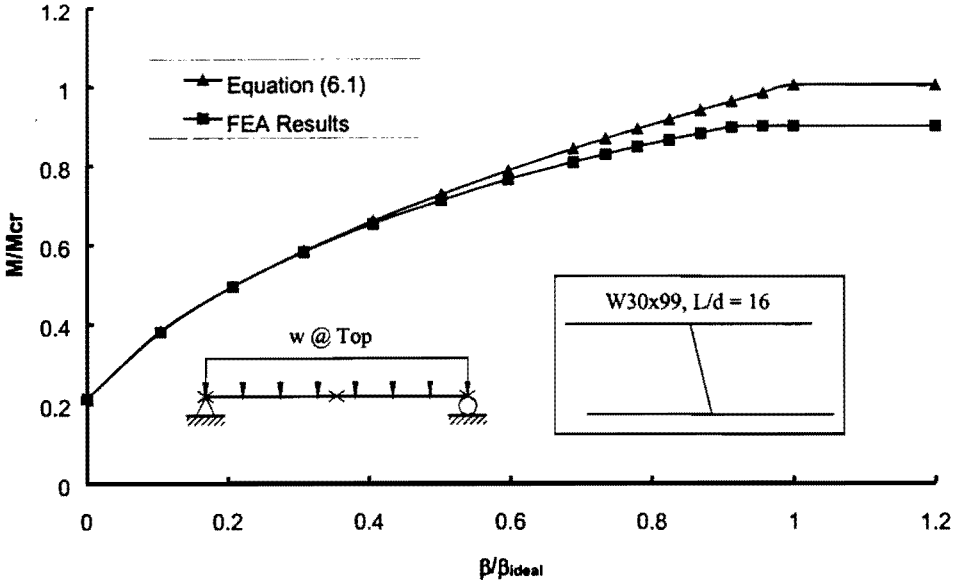

(a) skew angle =10°

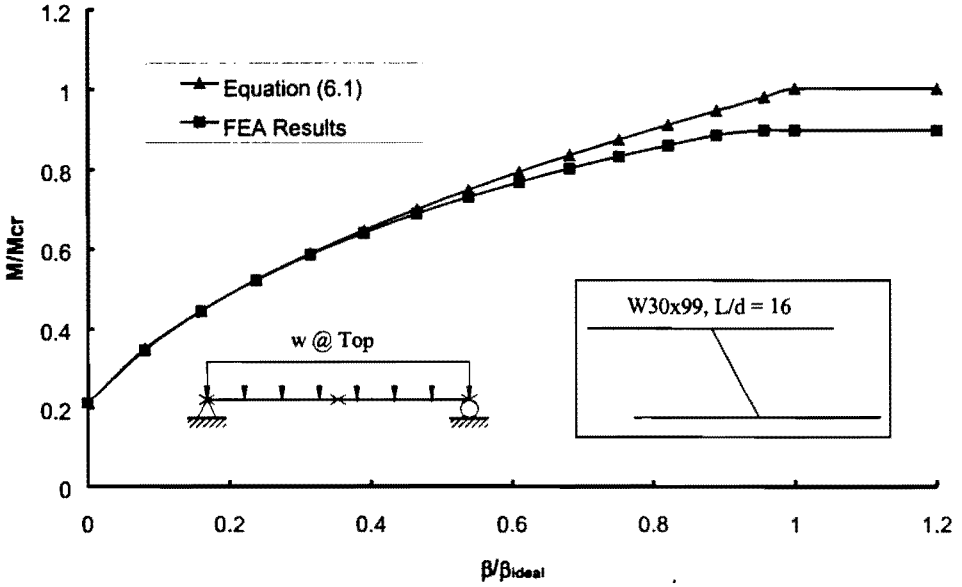

(b) skew angle = 30°

Figure B.2 M/M_{cr} versus β_t/β_{ideal} for a W30x99 Section with Distributed Loads on Top Flange

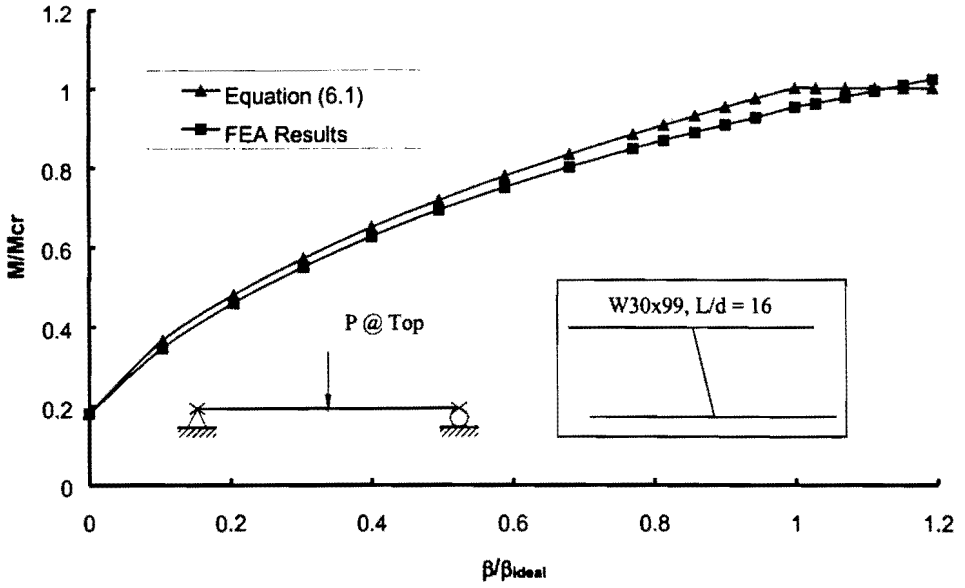

(a) skew angle =10°

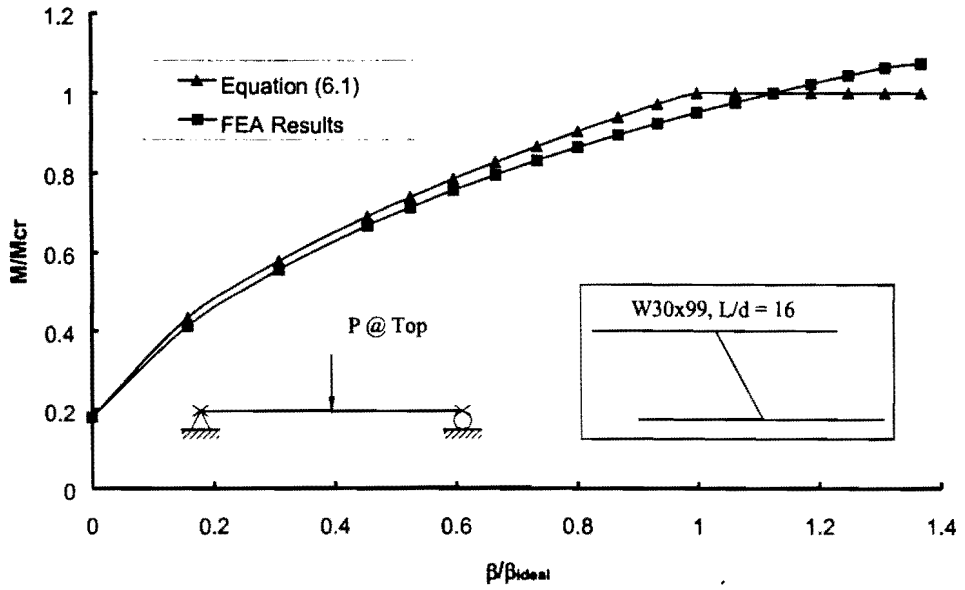

(b) skew angle = 30°

Figure B.3 M/M_{cr} versus β/β_{ideal} for a W30x99 Section with Midspan Concentrated Load on Top Flange

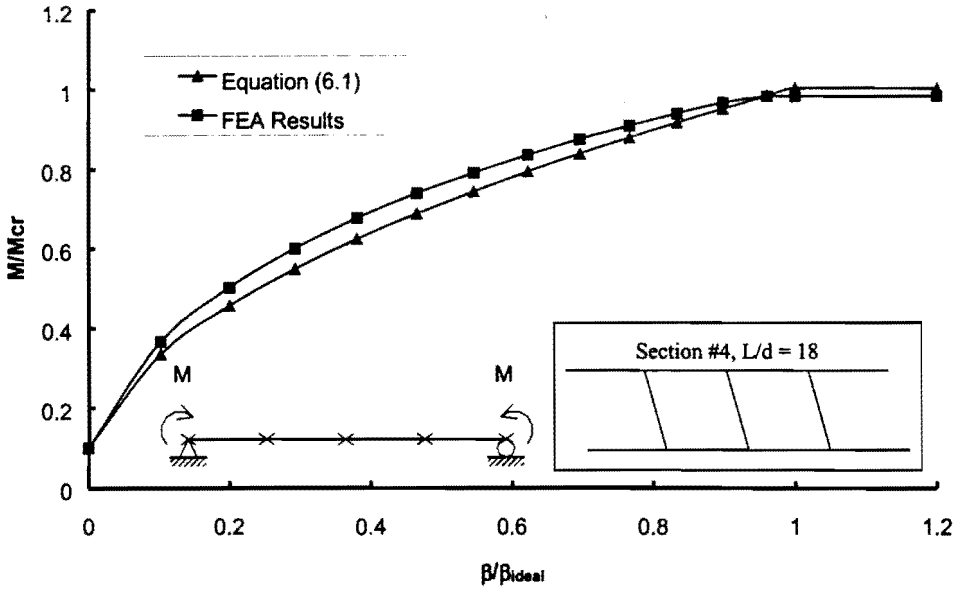

(a) skew angle =20°

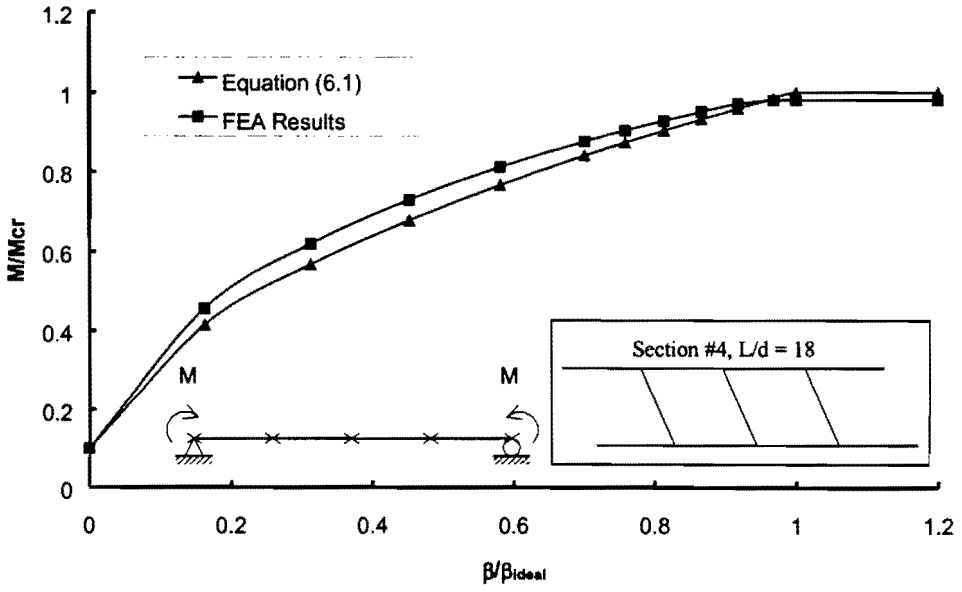

(b) skew angle = 30°

Figure B.4 M/M_{cr} versus β/β_{ideal} for Section #4 with Uniform Moment

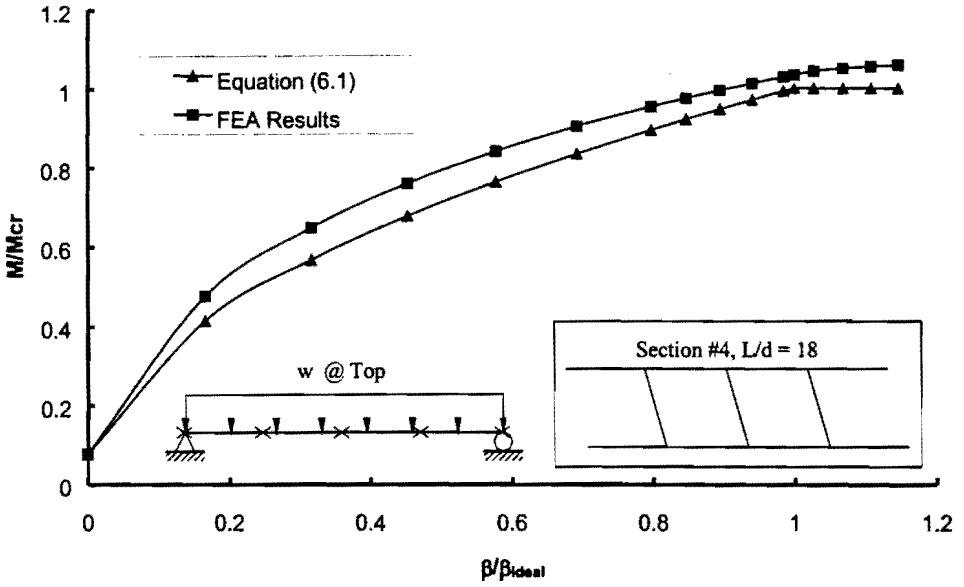

(a) skew angle =20°

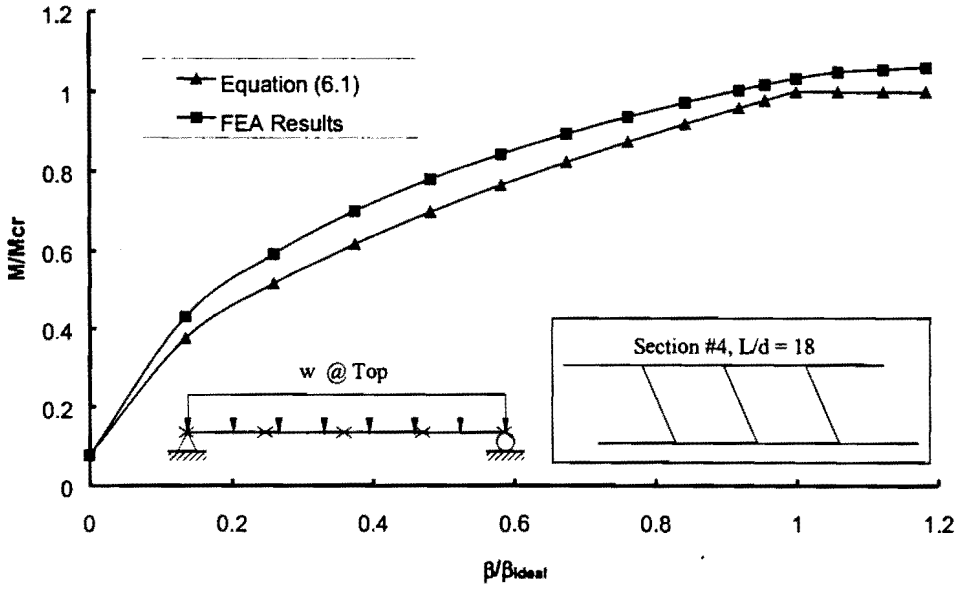

(b) skew angle = 30°

Figure B.5 M/M_{cr} versus β/β_{ideal} for Section #4 with Distributed Loads on Top Flange

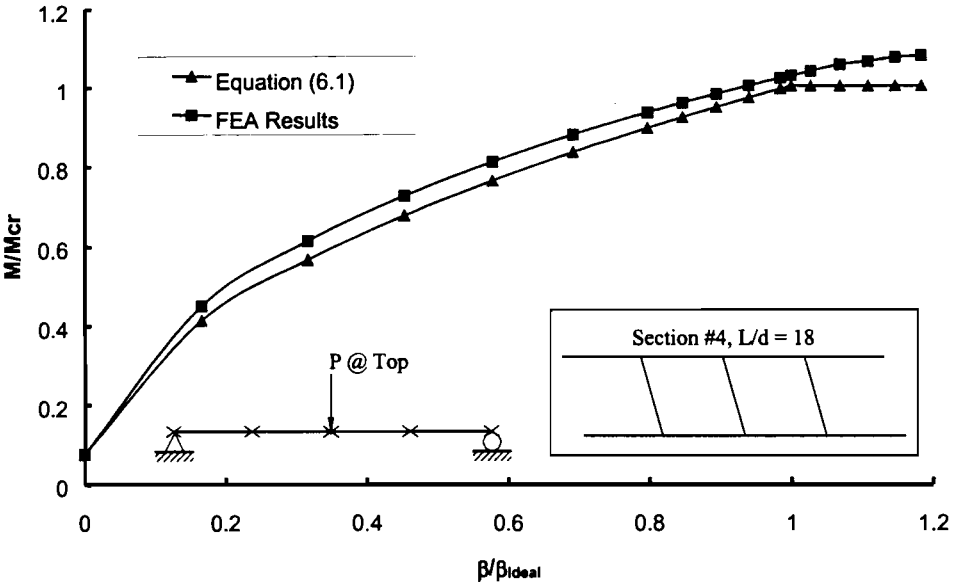

(a) skew angle =20°

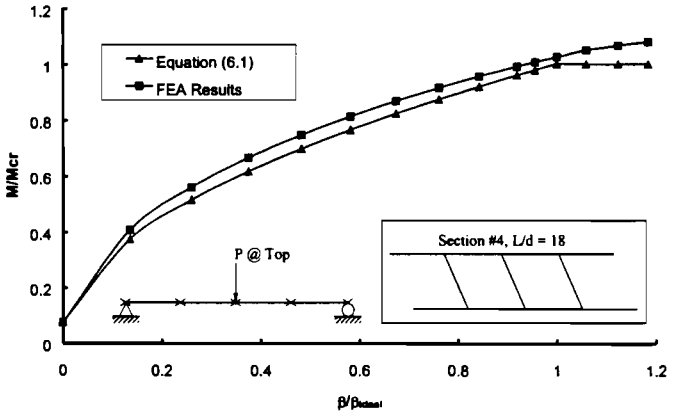

(b) skew angle = 30°

Figure B.6 M/M_{cr} versus β/β_{ideal} for Section #4 with Midspan Concentrated Load on Top Flange

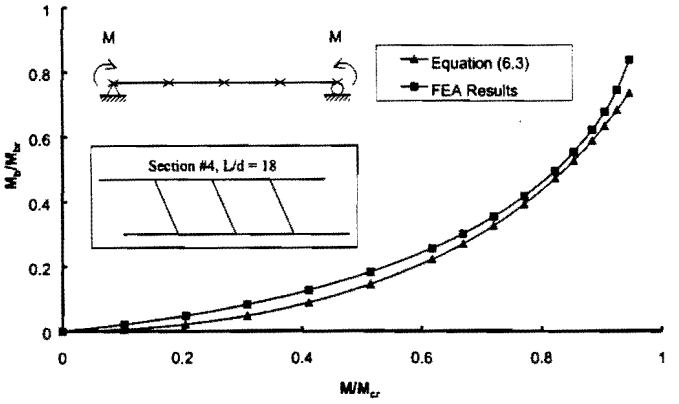

Figure B.7(a) M_b/M_{br} versus M/M_{cr} for Section #4 30° Skew Angle with Uniform Moment, $\beta_T = 2\beta_{ideal}$

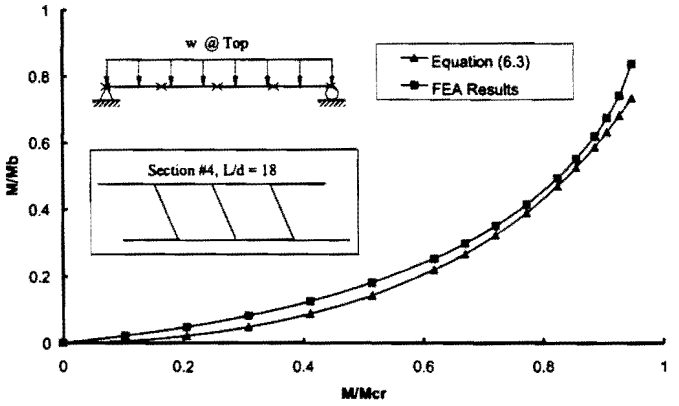

Figure B.7(b) M_b/M_{br} versus M/M_{cr} for Section #4 30° Skew Angle with Distributed Loads on Top Flange, $\beta_T = 2\beta_{ideal}$

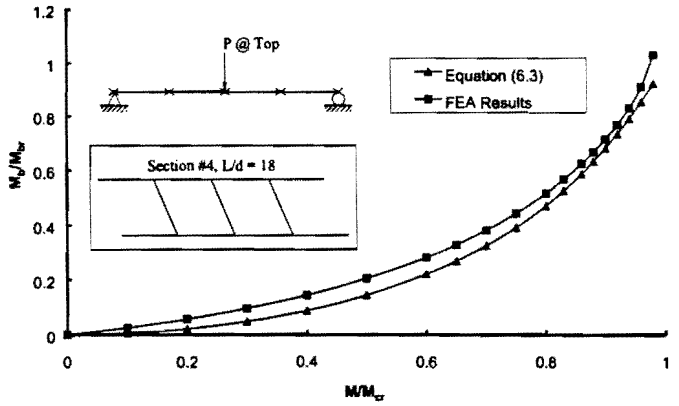

Figure B.7(c) M_b/M_{br} versus M/M_{cr} for Section #4 30° Skew Angle with Midspan Concentrated Load on Top Flange, $\beta_T = 2\beta_{ideal}$

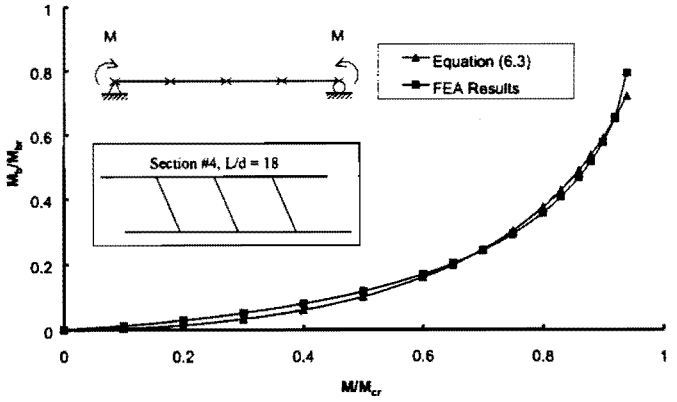

Figure B.8(a) M_b/M_{br} versus M/M_{cr} for Section #4 30° Skew Angle with Uniform Moment, $\beta_T = 1.5\beta_{ideal}$

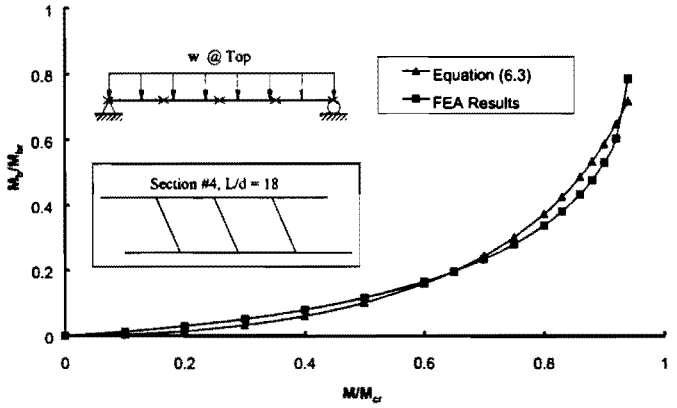

Figure B.8(b) M_b/M_{br} versus M/M_{cr} for Section #4 30° Skew Angle with Distributed Loads on Top Flange, $\beta_T = 1.5\beta_{ideal}$

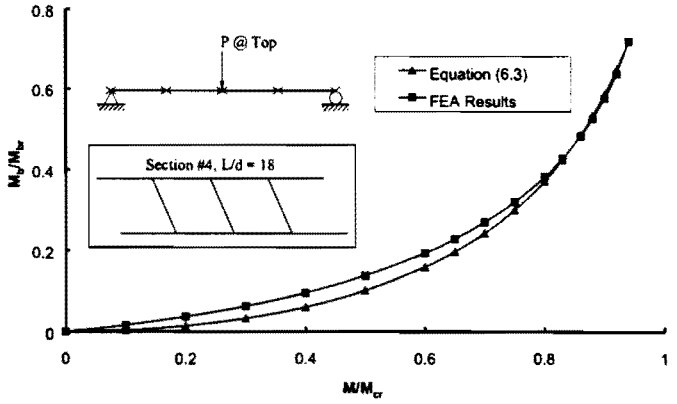

Figure B.8(c) M_b/M_{br} versus M/M_{cr} for Section #4 30° Skew Angle with Mispan Concentrated load on Top Flange, $\beta_T = 1.5\beta_{ideal}$

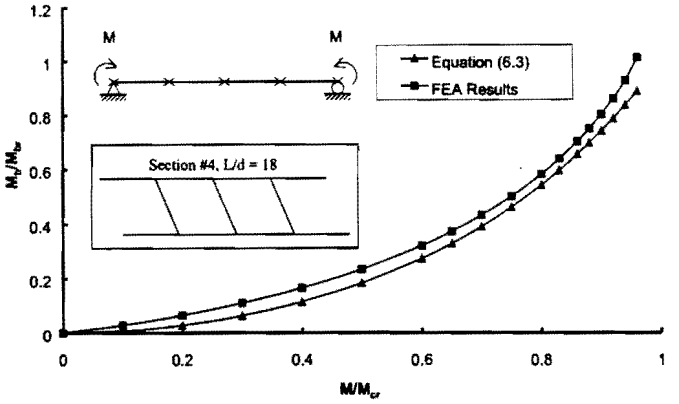

Figure B.9(a) M_b/M_{br} versus M/M_{cr} for Section #4 30° Skew Angle with Uniform Moment, $\beta_T = 3\beta_{ideal}$

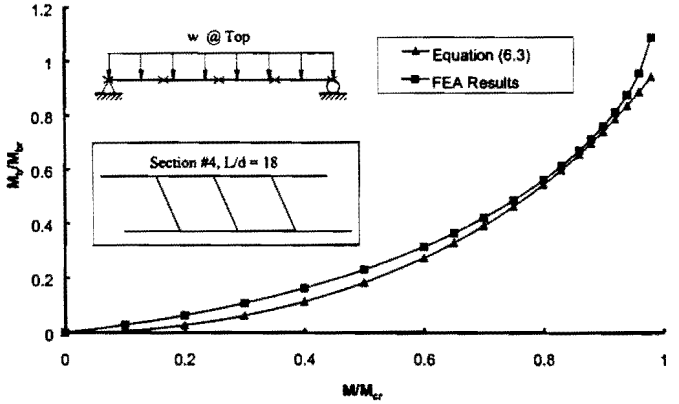

Figure B.9(b) M_b/M_{br} versus M/M_{cr} for Section #4 30° Skew Angle with Distributed Loads on Top Flange, $\beta_T = 3\beta_{ideal}$

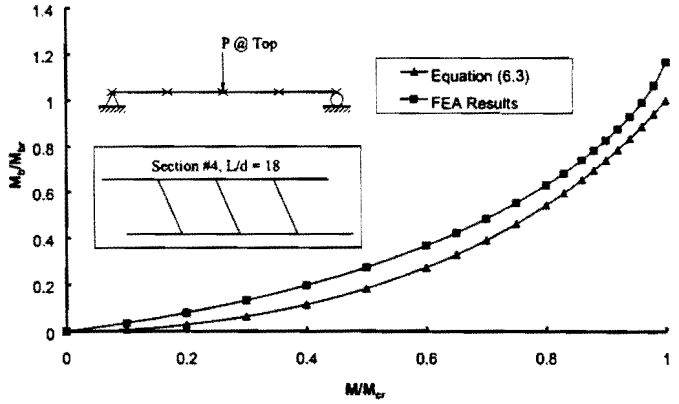

Figure B.9(c) M_b/M_{br} versus M/M_{cr} for Section #4 30° Skew Angle with Midpan Concentrated load on Top Flange, $\beta_T = 3\beta_{ideal}$

Appendix C
Supplemental Results for Girders with Skewed Supports and Normal Braces

As discussed in Chapter 7, for many of the girder cross-sections that were considered in this investigation of girders with skewed supports and braces oriented perpendicular to the girder longitudinal direction, comparisons between the FEA results and the equations showed similar trends. In these cases, representative results were presented and discussed in Chapter 7, while additional results for sections with similar behavior are presented in this appendix.

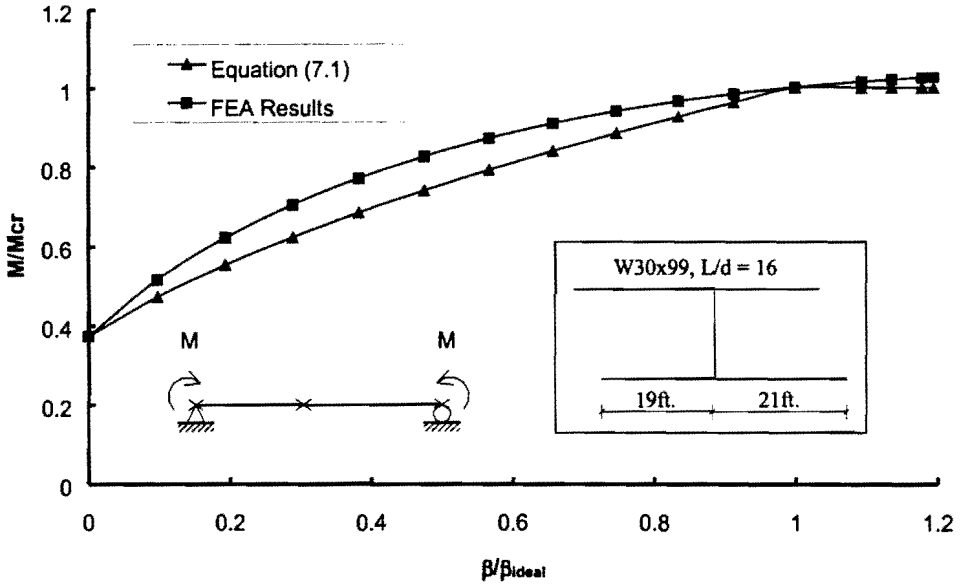

(a) skew angle =10°

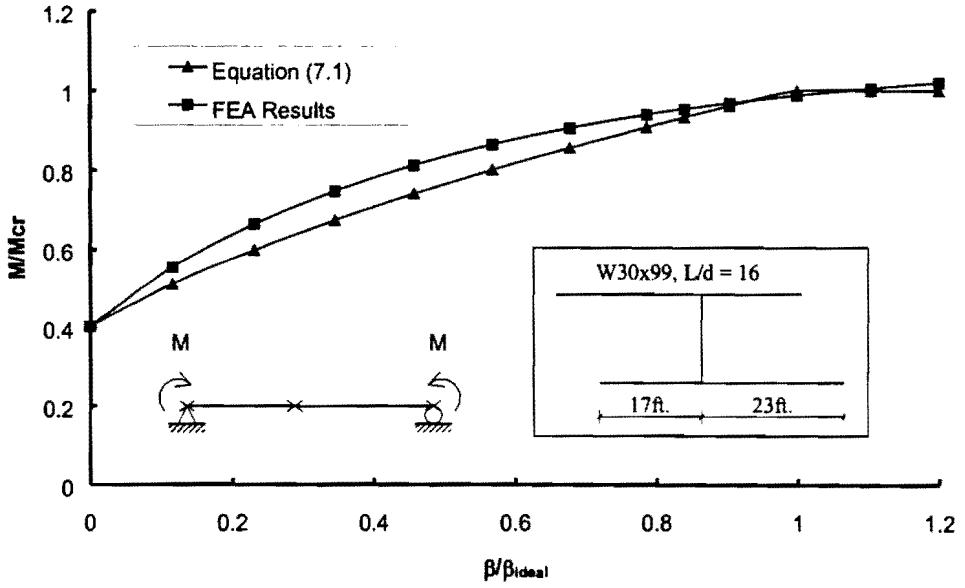

(b) skew angle = 30°

Figure C.1 M/M_{cr} versus β/β_{ideal} for a W30x99 Section with Uniform Moment

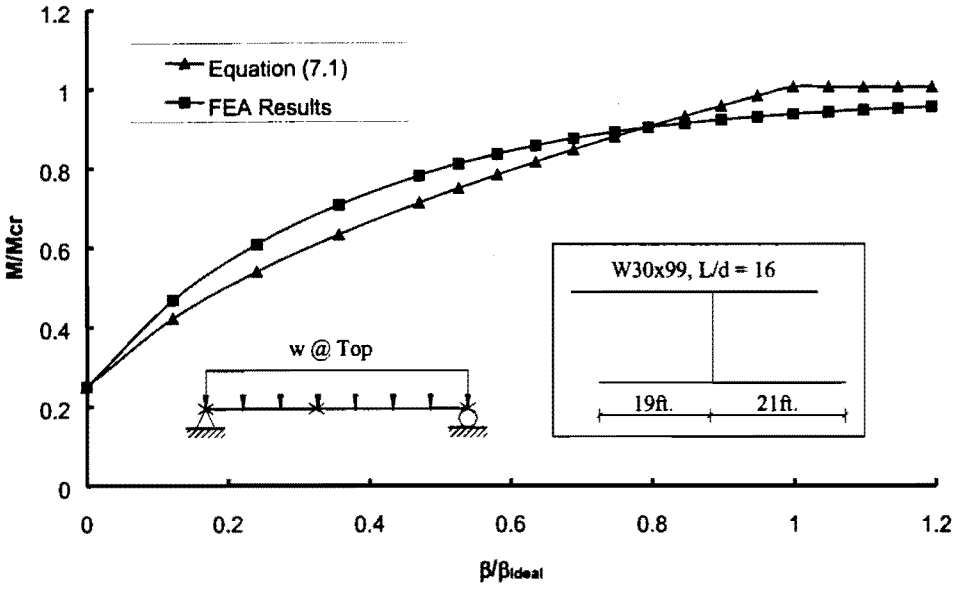

(a) skew angle =10°

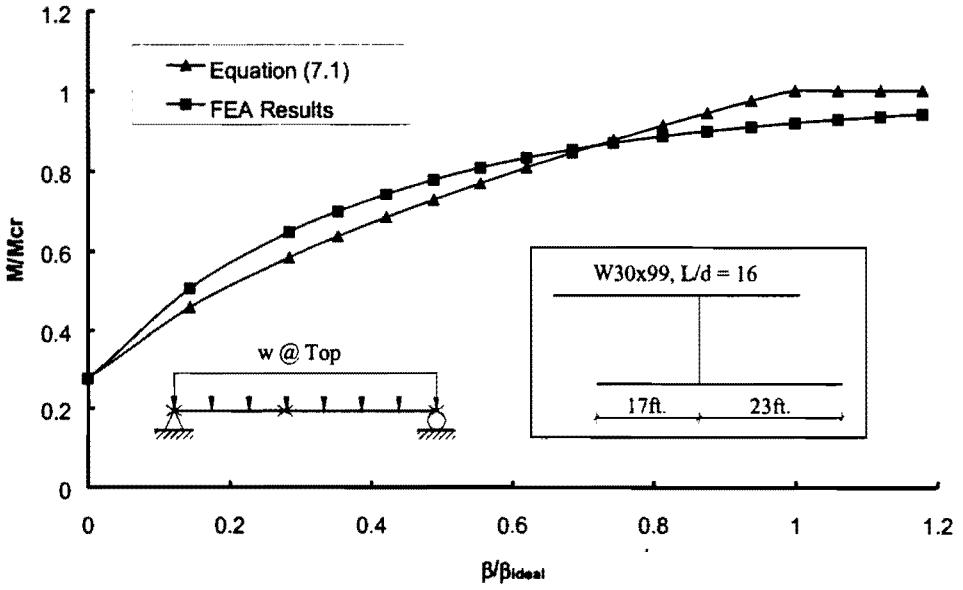

(b) skew angle = 30°

Figure C.2 M/M_{cr} versus β/β_{ideal} for a W30x99 Section with Distributed Loads on Top Flange

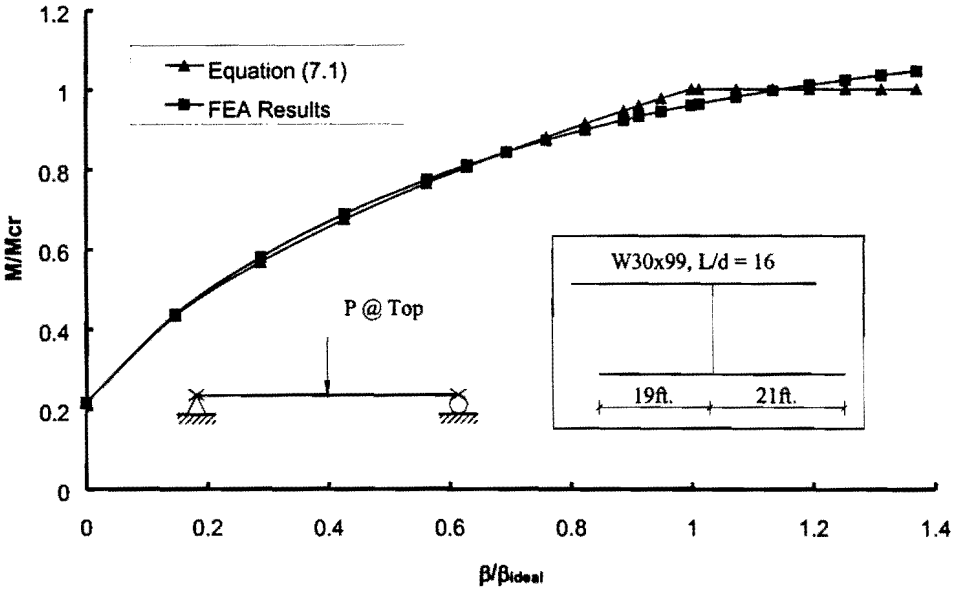

(a) skew angle = 10°

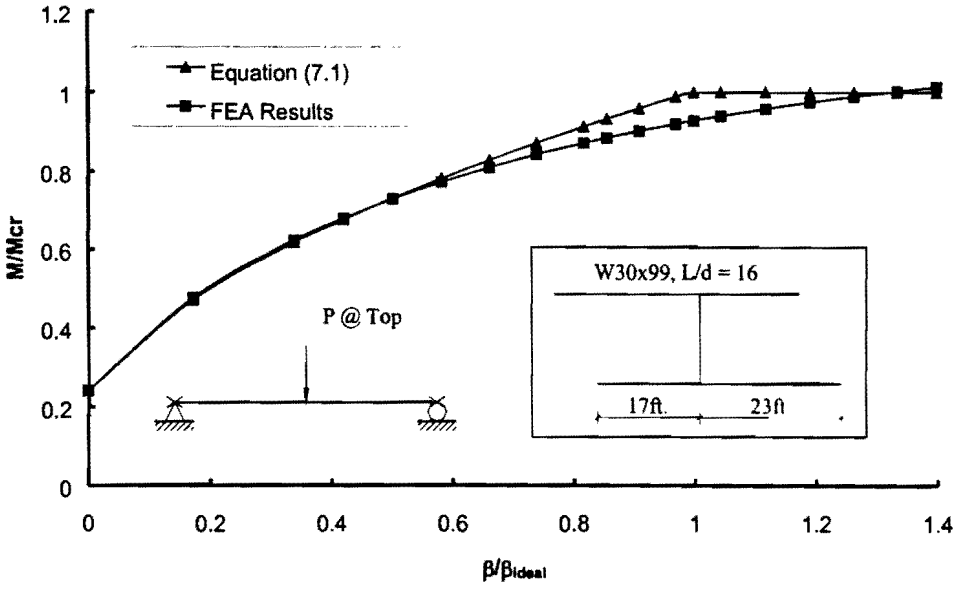

(b) skew angle = 30°

Figure C.3 M/M_{cr} versus β/β_{ideal} for a W30x99 Section with Midspan Concentrated load on Top Flange

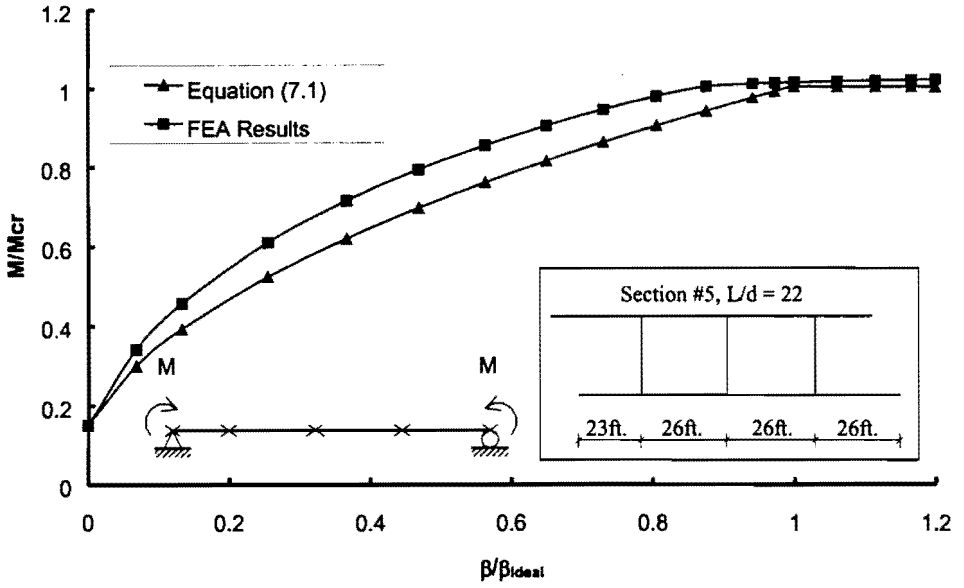

(a) skew angle =20°

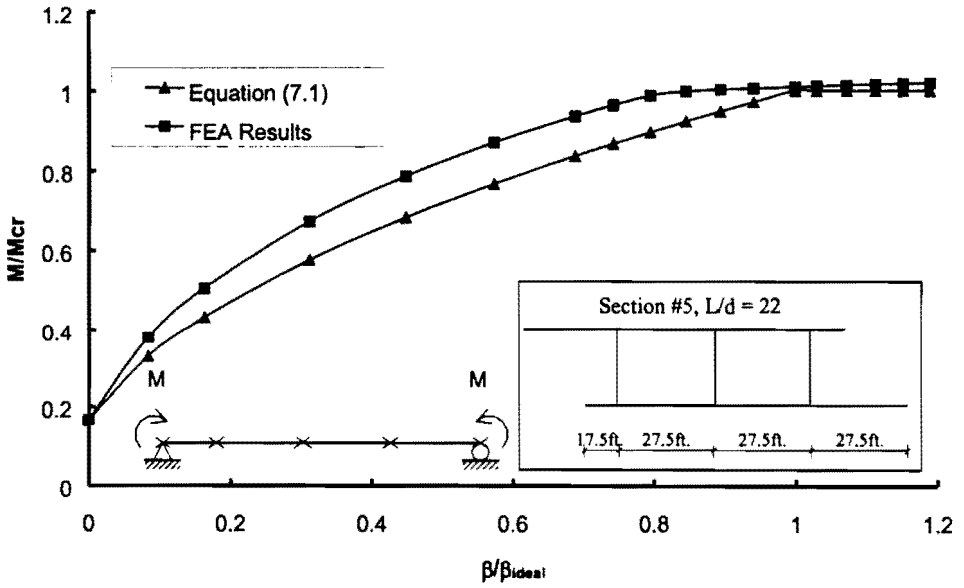

(b) skew angle = 45°

Figure C.4 M/M_{cr} versus β/β_{ideal} for Section #5 with Uniform Moment

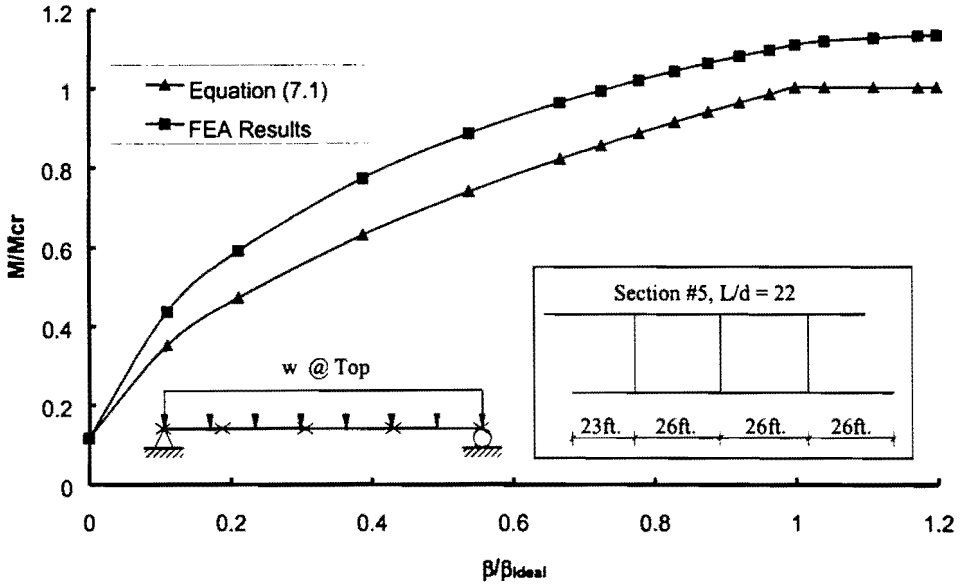

(a) skew angle =20°

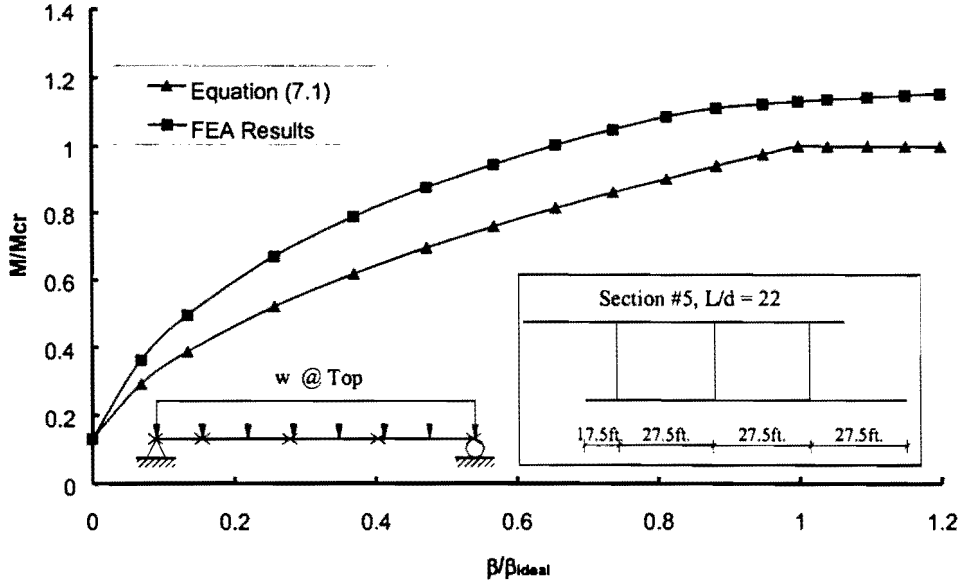

(b) skew angle = 45°

Figure C.5 M/M_{cr} versus β/β_{ideal} for Section #5 with Distributed Loads on Top Flange

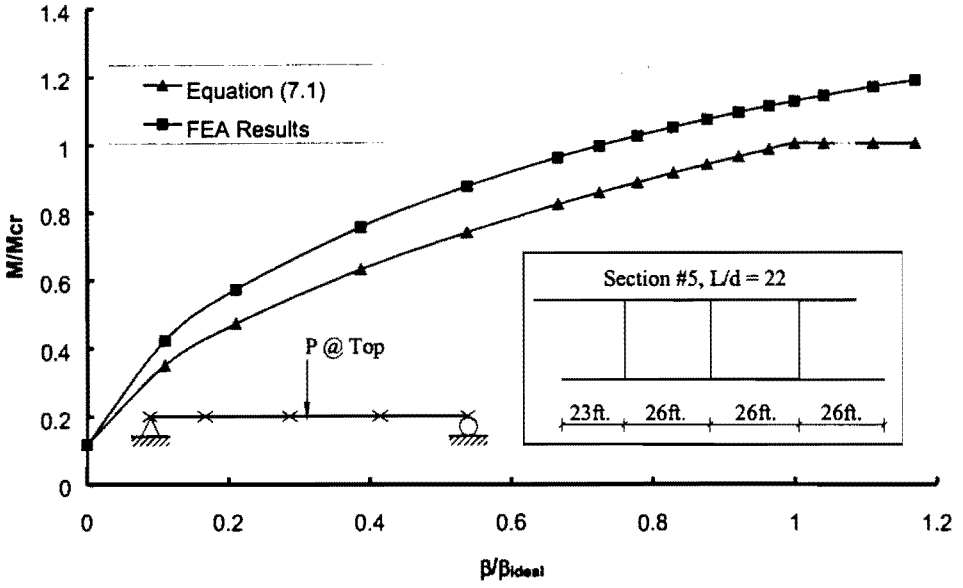

(a) skew angle =20°

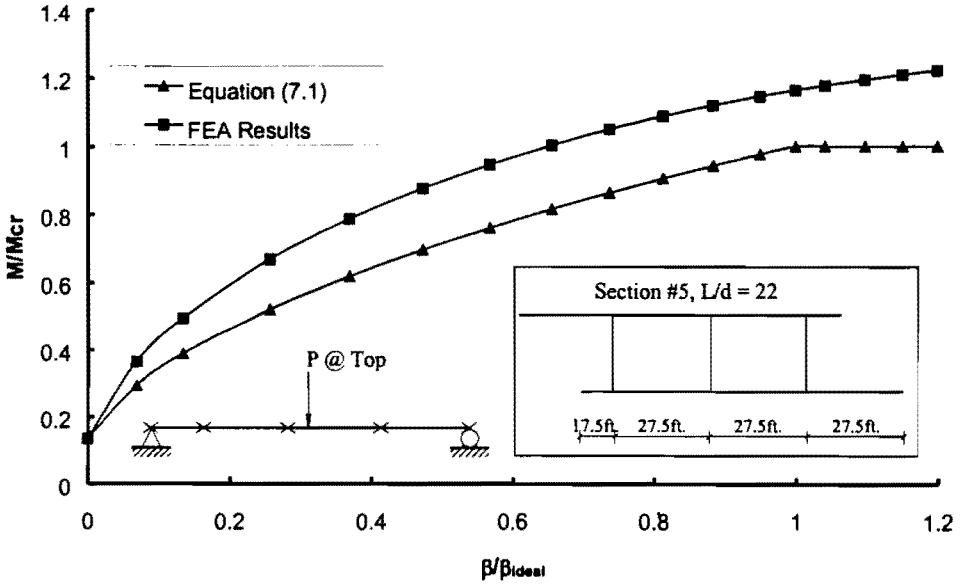

(b) skew angle = 45°

Figure C.6 M/M_{cr} versus β/β_{ideal} for Section #5 with Midspan Concentrated Load on Top Flange

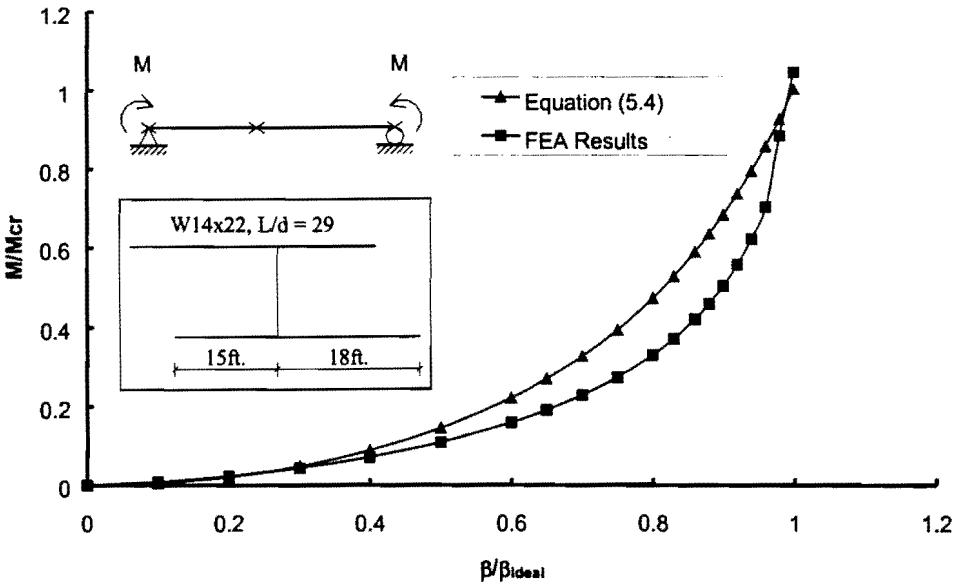

(a) skew angle =26.5°

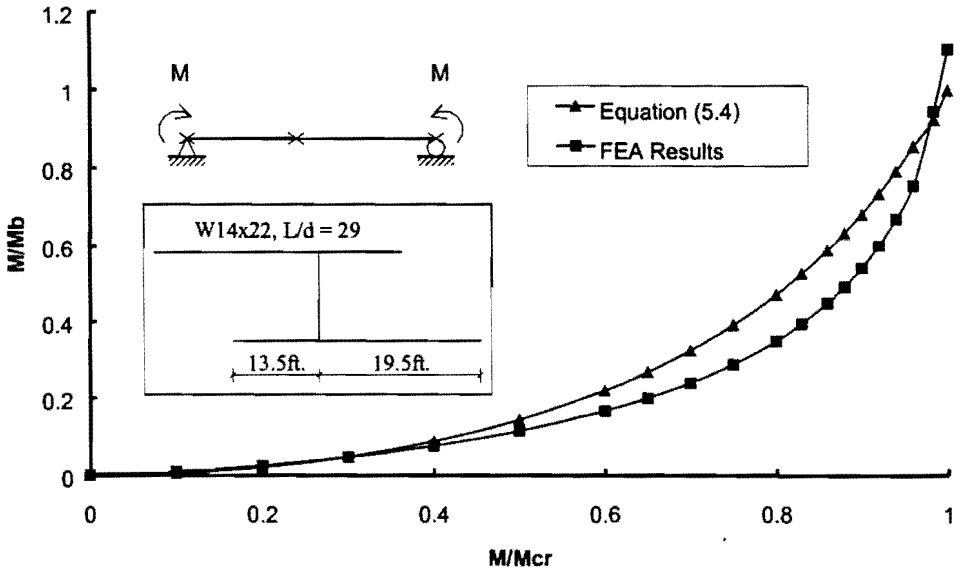

(b) skew angle = 45°

Figure C.7 M_b/M_{br} versus M/M_{cr} for w14x22 Section Twin-Girder System with Uniform Moment, $\beta_T = 2\beta_{ideal}$

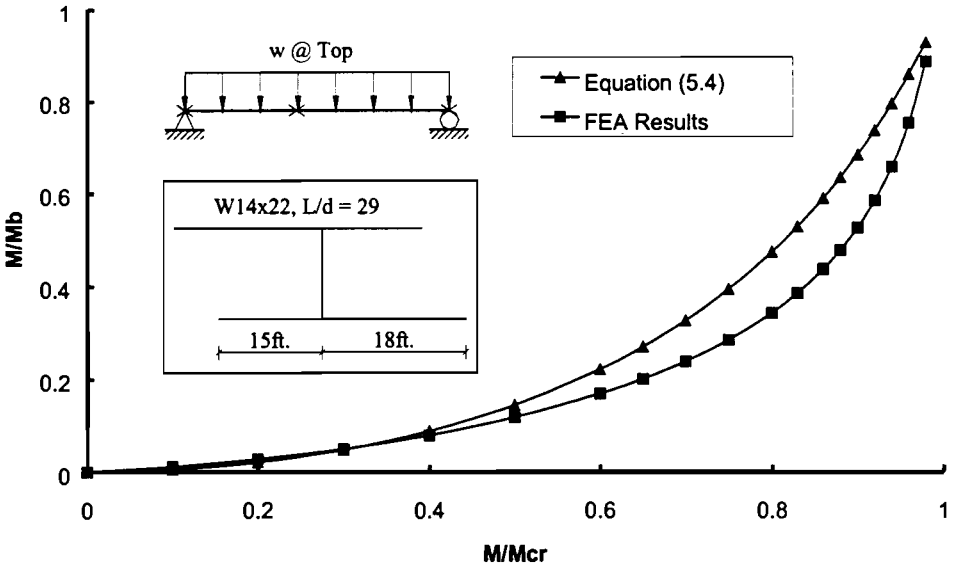

(a) skew angle =20°

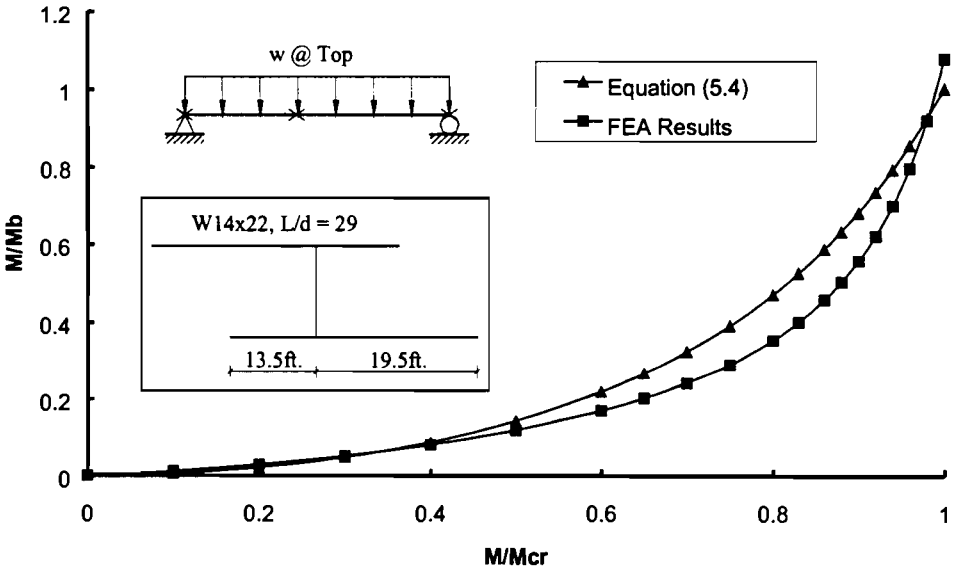

(b) skew angle = 45°

Figure C.8 M_b/M_{br} versus M/M_{cr} M_{cr} for a W14x22 Section Twin-Girder System with Distributed Loads on Top Flange, $\beta_T = 2\beta_{ideal}$

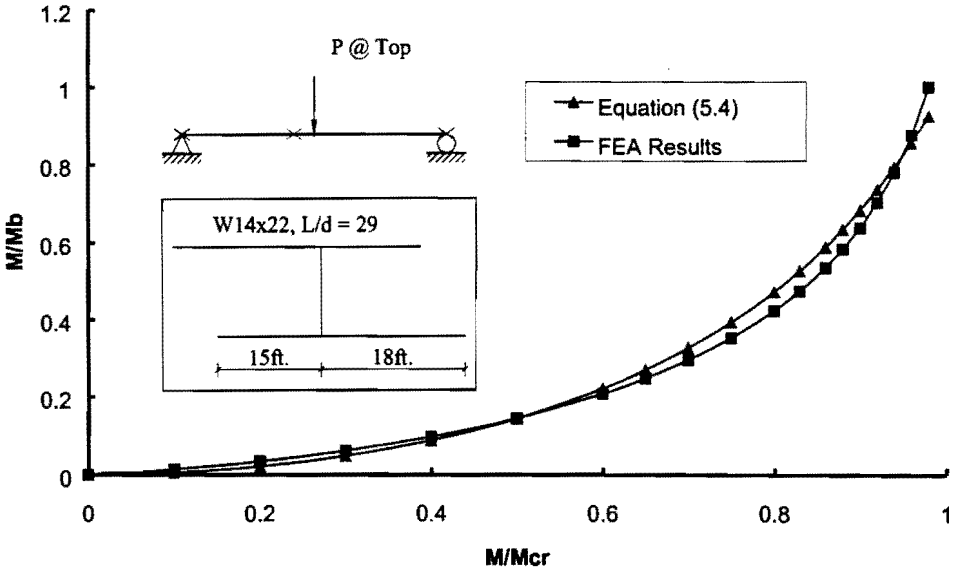

(a) skew angle =20°

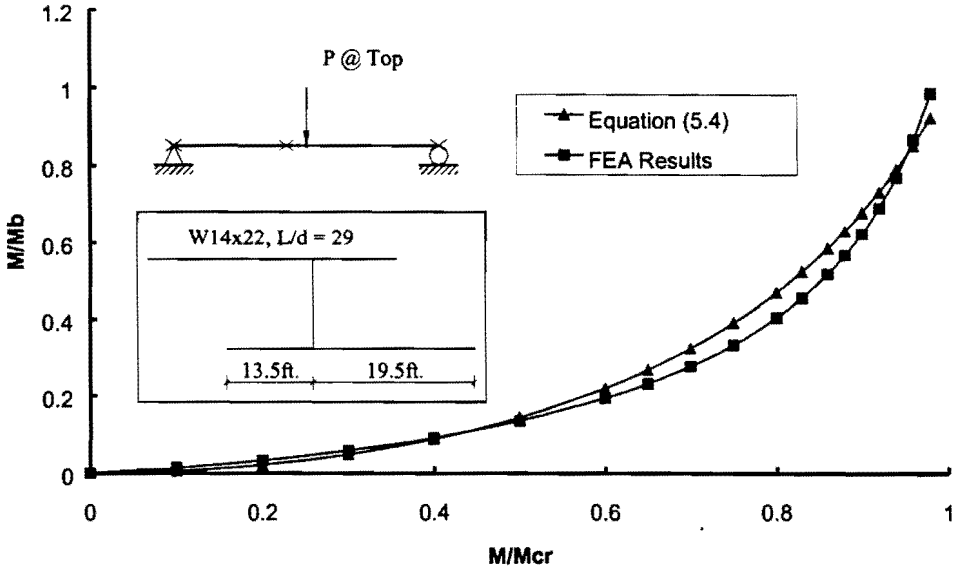

(b) skew angle = 45°

Figure C.9 M_b/M_{br} versus M/M_{cr} for a W14x22 Section Twin-Girder System with Concentrated Load at Midspan, $\beta_T = 2\beta_{ideal}$

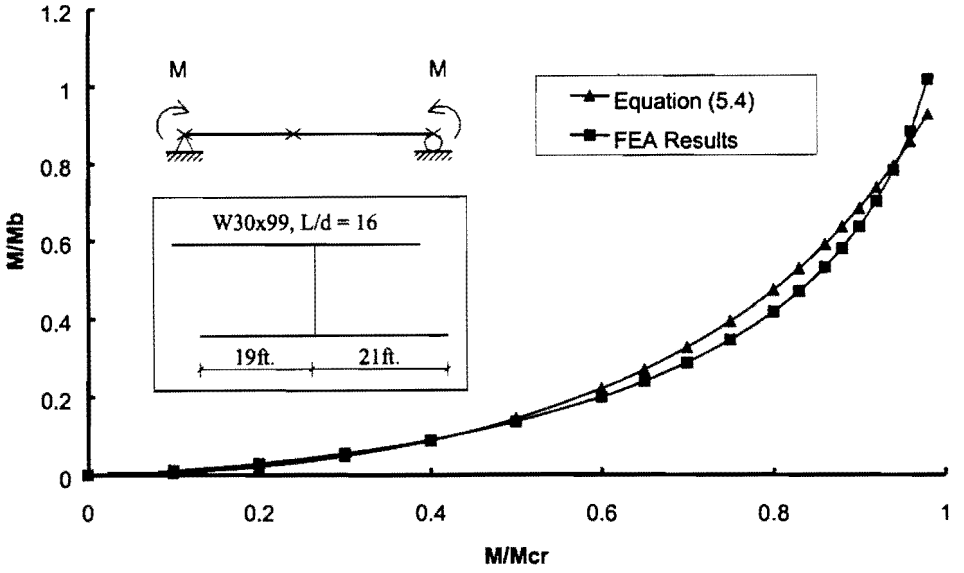

(a) skew angle =10°

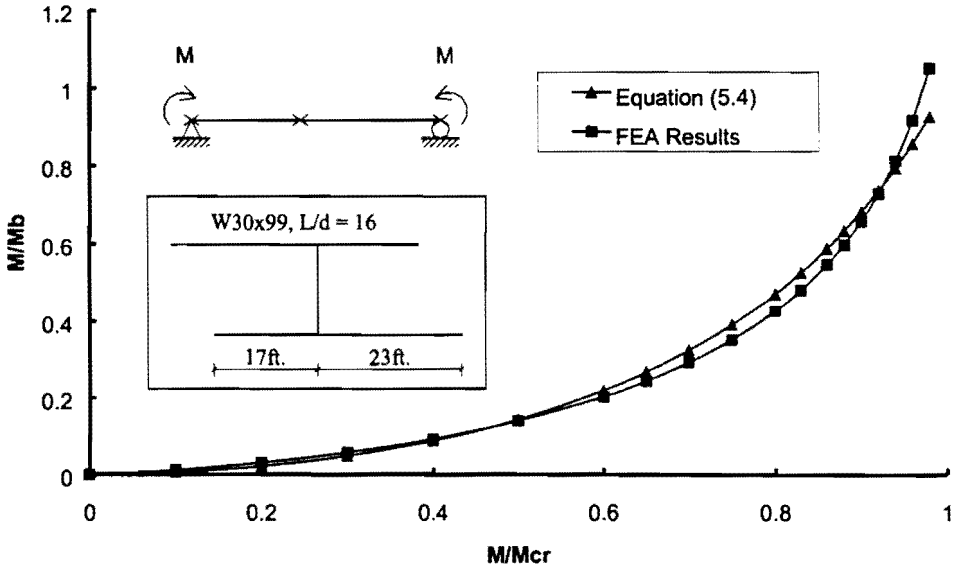

(b) skew angle = 30°

Figure C.10 M_b/M_{br} versus M/M_{cr} for a W30x99 Section Twin-Girder System with Uniform Moment, $\beta_T = 2\beta_{ideal}$

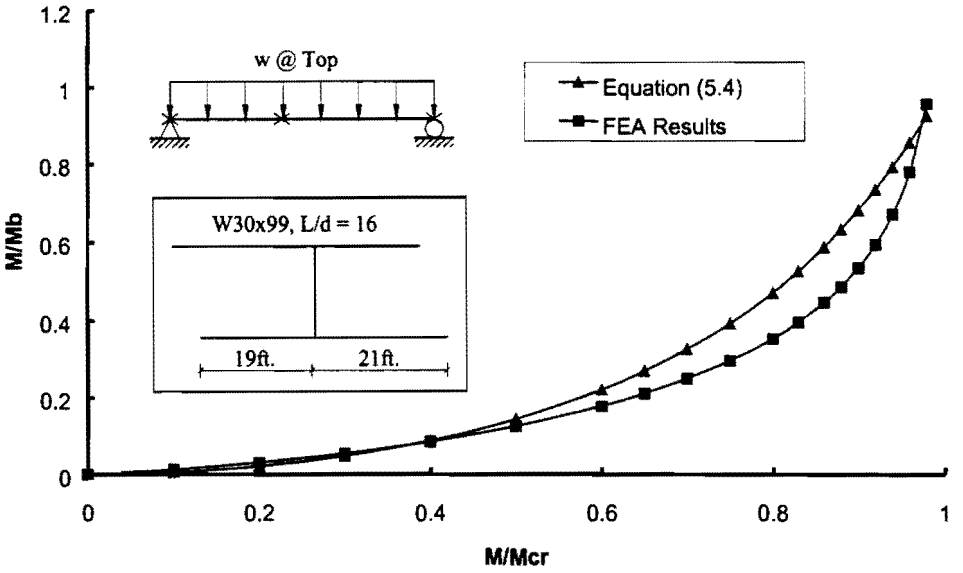

(a) skew angle =10°

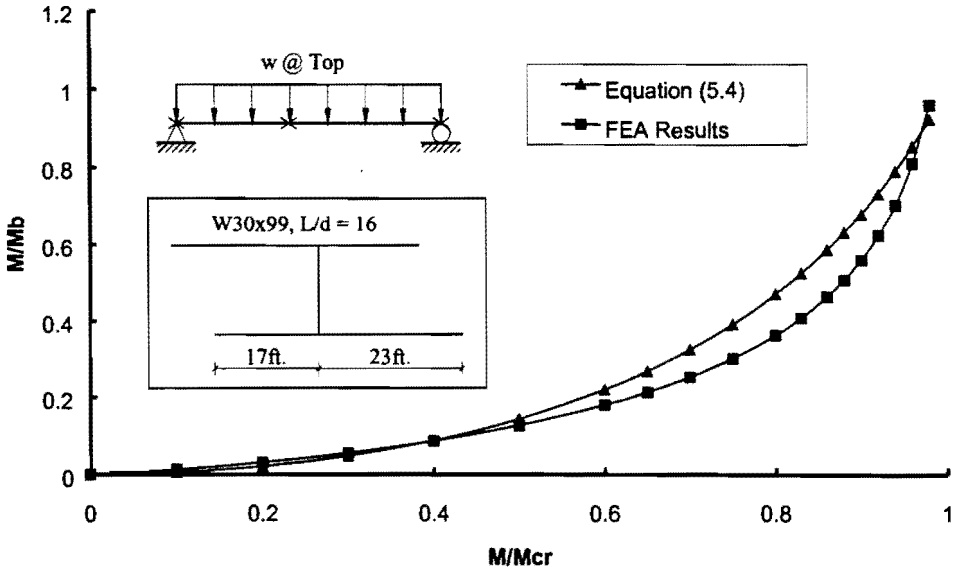

(b) skew angle = 30°

Figure C.11 M_b/M_{br} versus M/M_{cr} for a W30x99 Section Twin-Girder System with Distributed Loads on Top Flange, $\beta_T = 2\beta_{ideal}$

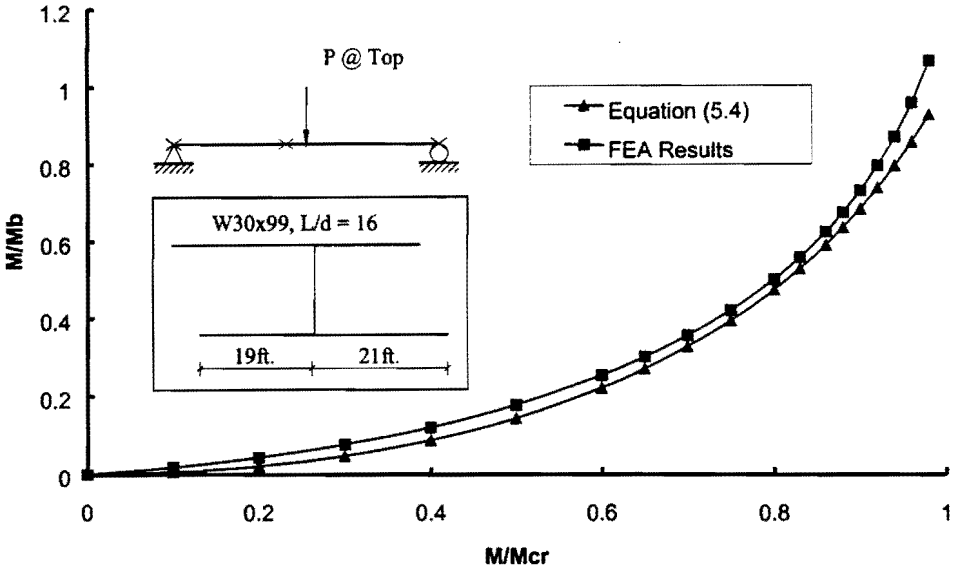

(a) skew angle =10°

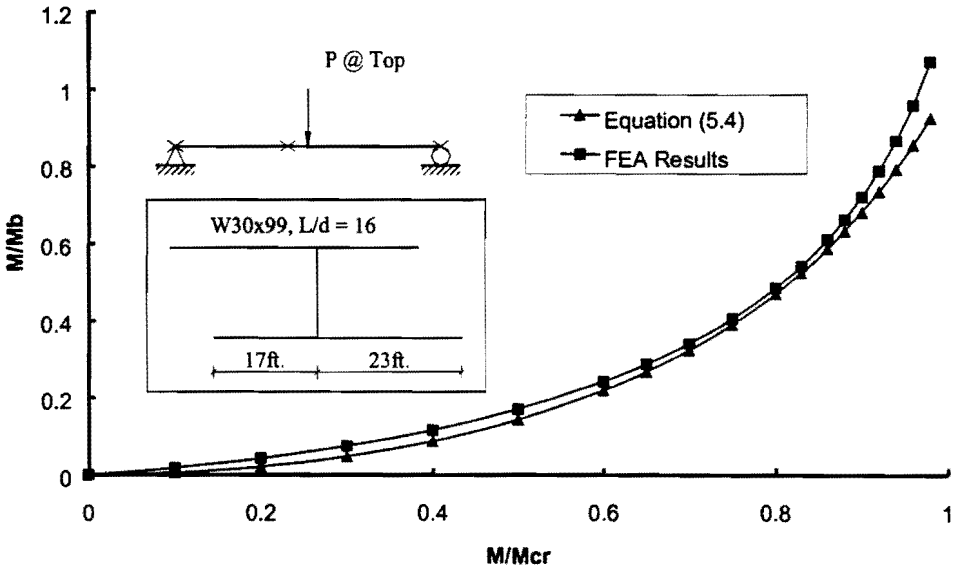

(b) skew angle = 30°

Figure C.12 M_b/M_{br} versus M/M_{cr} for a W30x99 Section Twin-Girder System with Concentrated Load at Midspan, $\beta_T = 2\beta_{ideal}$

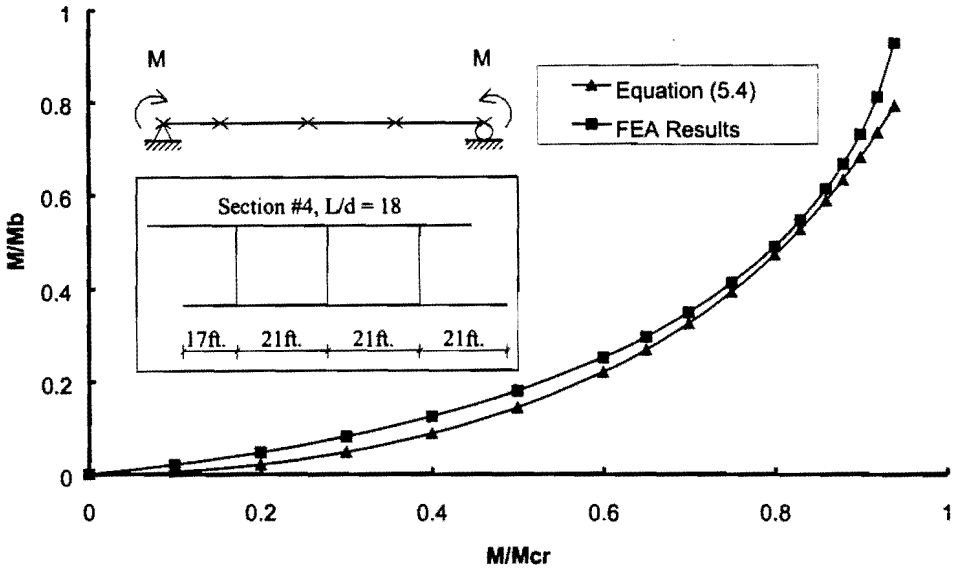

(a) skew angle =20°

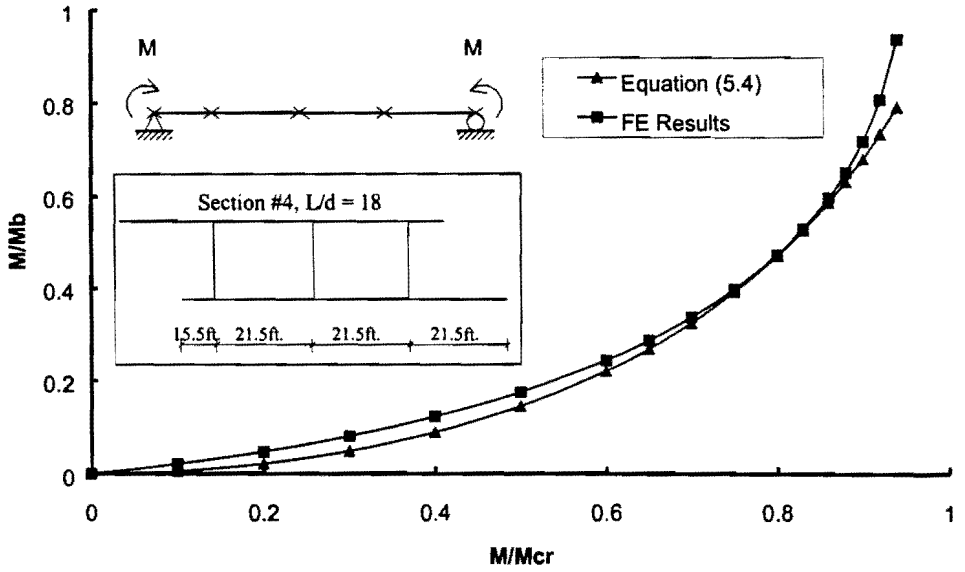

(b) skew angle = 30°

Figure C.13 M_b/M_{br} versus M/M_{cr} for Section #4 Twin-Girder System with Uniform Moment, $\beta_T = 2\beta_{ideal}$

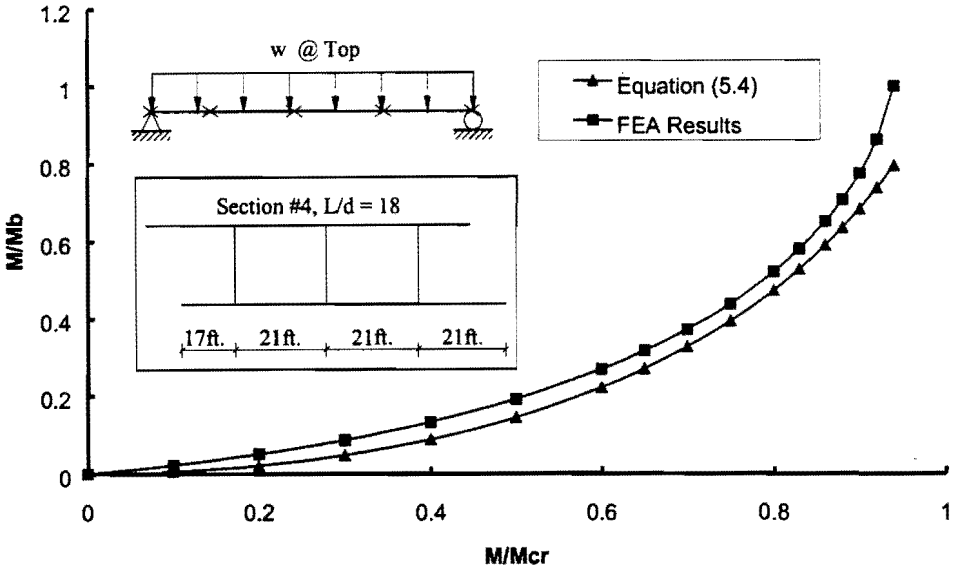

(a) skew angle =20°

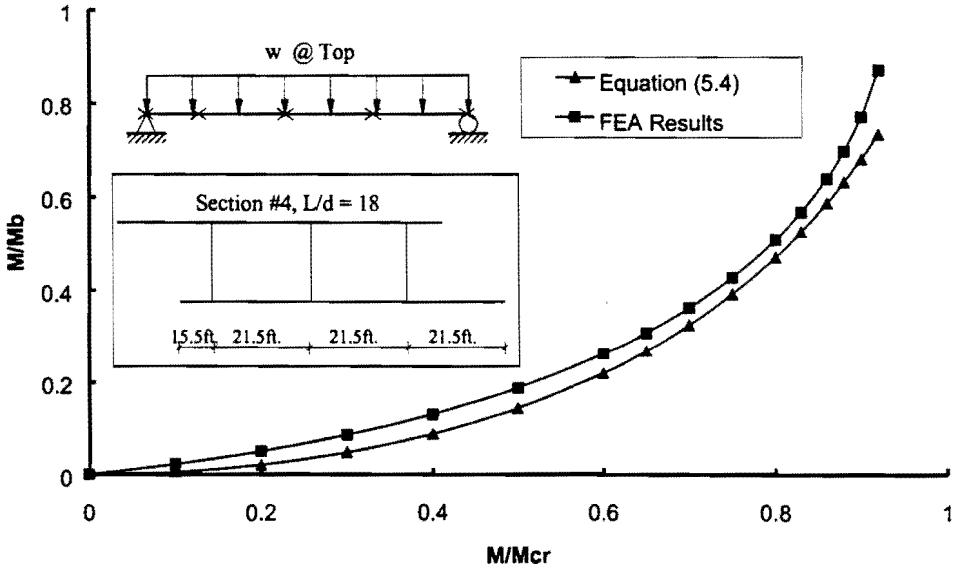

(b) skew angle = 30°

Figure C.14 M_b/M_{br} versus M/M_{cr} for Section #4 Twin-Girder System with Distributed Loads on Top Flange, $\beta_T = 2\beta_{ideal}$

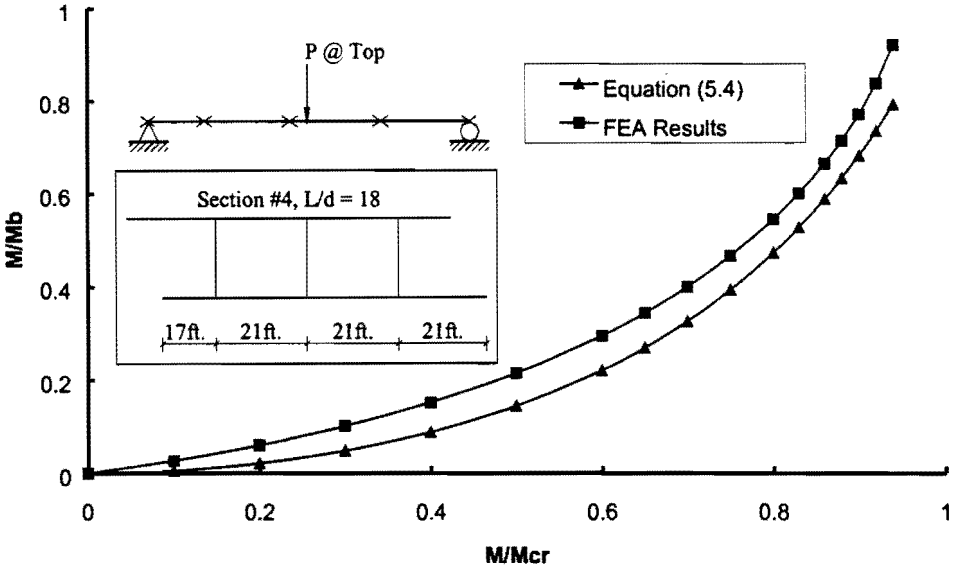

(a) skew angle =20°

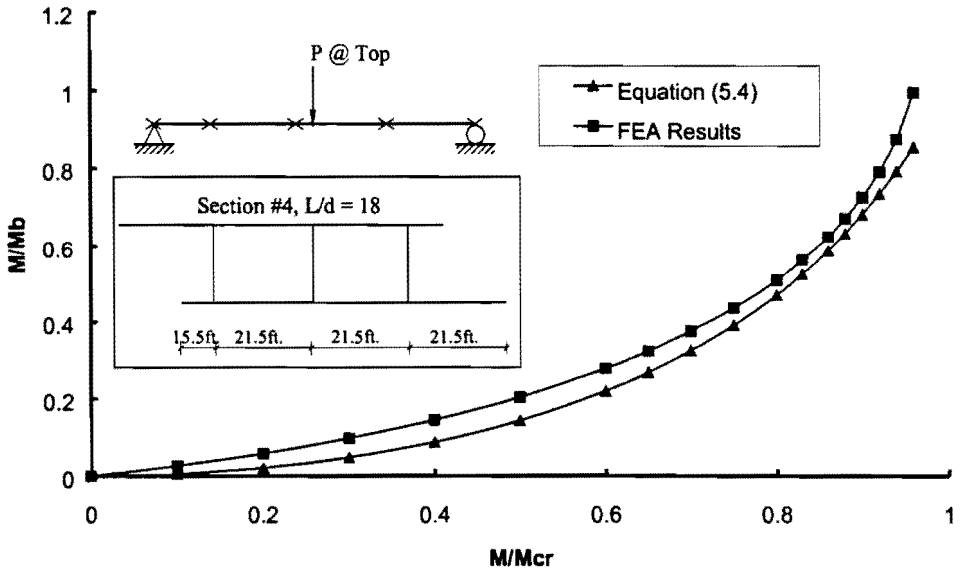

(b) skew angle = 30°

Figure C.15 M_b/M_{br} versus M/M_{cr} for Section #4 Twin-Girder System with Concentrated Load at Midspan, $\beta_T = 2\beta_{ideal}$

Appendix D
Supplemental Results for Bracing Details for Bridges with Skewed Supports

In addition to the derivation of the stiffness and strength equations for cross-frames and diaphragms presented in Chapter 8, complete results of the brace force response envelops for the truck loading is presented in this appendix. The results include three types of brace layouts: conventional brace layout, conventional stagger brace layout, and lean-on brace layout.

Equation for Predicting Brace Moment, $\beta_T = \beta_{T\,Req'd}$

The required brace stiffness that corresponds to twice the ideal brace stiffness is given by the expression:

$$\beta_{T\,Req'd} = \frac{2.4LM_u^2}{nC_{bb}^2 EI_{eff}} \qquad \text{Equation (8.2)}$$

Assuming an initial twist: $\phi_0 = \frac{L_b}{500h}$

The brace moment for girders with brace stiffness equal to $\beta_{T\,Req'd}$: is therefore equal to:

$$M_{br} = \beta_{T\,Req'd}\phi_0 = \frac{2.4LM_u^2}{nC_{bb}^2 EI_{eff}} \times \frac{L_b}{500h}$$

Equation for Predicting Brace Moment, $\beta_T > \beta_{T\,Req'd}$

The brace moment for girders with a brace stiffness larger than $\beta_{T\,Req'd}$: is can be calculated as follows:

$$M_{act} = \beta_{act}(\phi_T - \phi_0) \qquad \text{where:} \qquad \phi_T = \frac{\phi_0}{1 - \frac{\beta_{ideal}}{\beta_{act}}\left(\frac{M^*}{M_{cr}}\right)^2}$$

$$M_{act} = \beta_{act}\phi_0 \times \frac{\frac{\beta_{ideal}}{\beta_{act}}\left(\frac{M^*}{M_{cr}}\right)^2}{1 - \frac{\beta_{ideal}}{\beta_{act}}\left(\frac{M^*}{M_{cr}}\right)^2} = 2\beta_{ideal}\phi_0 \times \frac{\left(\frac{M^*}{M_{cr}}\right)^2}{2 - \frac{2\beta_{ideal}}{\beta_{act}}\left(\frac{M^*}{M_{cr}}\right)^2}$$

$$= M_{br}\left[\frac{\left(\frac{M^*}{M_{cr}}\right)^2}{2 - \frac{\beta_{T\,Req'd}}{\beta_{act}}\left(\frac{M^*}{M_{cr}}\right)^2}\right] \qquad \text{Equation (8.4)}$$

Figure D.1 Brace Moment for Girders with Brace Stiffness Larger than the Required Brace Stiffness

Lean-on System – Cross-Frame Located at Edge

Brace Forces:

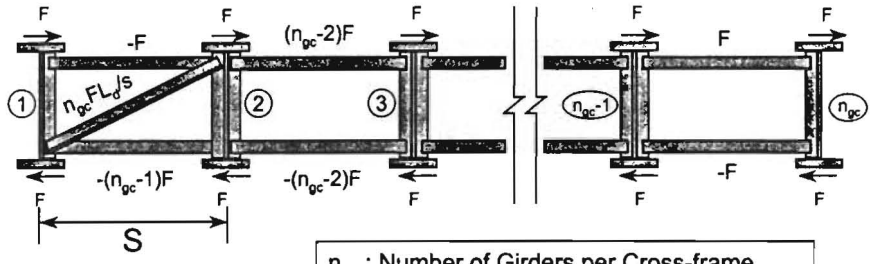

n_{gc} : Number of Girders per Cross-frame
A_d: Area of Diagonal Member of Cross-frame
A_c: Area of Horizontal Struts

Brace Deformations:

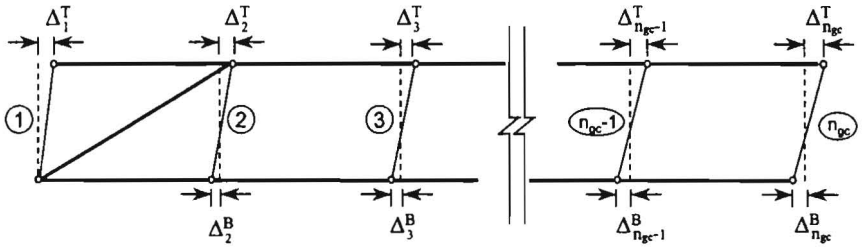

CROSS-FRAME STIFFNESS AND STRENGTH REQUIREMENTS

Brace Stiffness: Girder n_{gc} is Critical for Stiffness

$$\Delta_2^T = \left(\frac{n_{gc} F \times L_d/S \times L_d}{EA_d} \right) \div \left(S/L_d \right) = \frac{n_{gc} F L_d^3}{EA_d S^2} \qquad \Delta_2^B = \frac{(n_{gc}-1)FS}{EA_c}$$

$$\Delta_3^T = \Delta_2^T + \frac{(n_{gc}-2)FS}{EA_c} \qquad \Delta_3^B = \Delta_2^B + \frac{(n_{gc}-2)FS}{EA_c}$$

$$\Delta_{n_{gc}}^T = \Delta_2^T + \underbrace{\frac{(n_{gc}-2)FS}{EA_c} + \frac{(n_{gc}-3)FS}{EA_c} + \ldots + \frac{FS}{EA_c}}$$

$$\Delta_{n_{gc}}^B = \Delta_2^B + \underbrace{\frac{(n_{gc}-2)FS}{EA_c} + \frac{(n_{gc}-3)FS}{EA_c} + \ldots + \frac{FS}{EA_c}}$$

Number of terms $=(n_{gc}-2)$

Figure D.2 Equations for Stiffness and Strength Requirements for Lean-on Braces –Cross-Frame (1/2)

CROSS-FRAME STIFFNESS AND STRENGTH REQUIREMENTS

$$\Delta^T_{n_{gc}} = \frac{n_{gc}FL_d^3}{EA_dS^2} + \frac{FS}{EA_c}\frac{(n_{gc}-2)(n_{gc}-1)}{2} \qquad \Delta^B_{n_{gc}} = \frac{(n_{gc}-1)FS}{EA_c} + \frac{FS}{EA_c}\frac{(n_{gc}-2)(n_{gc}-1)}{2}$$

Relative Displacement between Top and Bottom Flanges:

$$\Delta_{n_{gc}} = \Delta^T_{n_{gc}} + \Delta^B_{n_{gc}} = \frac{n_{gc}FL_d^3}{EA_dS^2} + \frac{FS}{EA_c}(n_{gc}-1) + \frac{FS}{EA_c}(n_{gc}-2)(n_{gc}-1)$$

$$= \frac{n_{gc}FL_d^3}{EA_dS^2} + \frac{FS}{EA_c}(n_{gc}-1)^2$$

$$\beta_b = \frac{M}{\theta} = \frac{Fh_b}{\Delta/h_b} = \frac{Fh_b^2}{\Delta} = \frac{h_b^2}{\frac{n_{gc}L_d^3}{EA_dS^2} + \frac{S}{A_c}(n_{gc}-1)^2}$$

$$= \frac{ES^2h_b^2}{\frac{n_{gc}L_d^3}{A_d} + \frac{S^3}{A_c}(n_{gc}-1)^2}$$

SUMMARY:

Brace Stiffness:

$$\beta_b = \frac{ES^2h_b^2}{\frac{n_{gc}L_d^3}{A_d} + \frac{S^3}{A_c}(n_{gc}-1)^2}$$

Brace Strength:

$$F_d = \frac{n_{gc}FL_d}{S}$$

$$F_s = (n_{gc}-1)F$$

$$F = M_{br}/h_b$$

Figure D.2 Equations for Stiffness and Strength Requirements for Lean-on Braces –Cross-Frame (2/2)

Lean-on System – Diaphragm Located at Edge

Brace Forces:

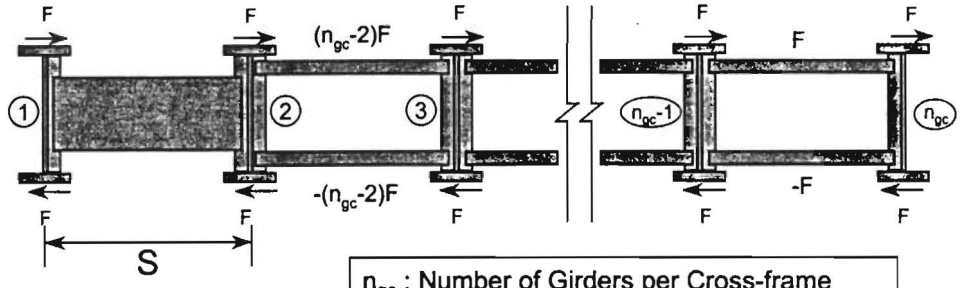

n_{gc} : Number of Girders per Cross-frame
A_d: Area of Diagonal Member of Cross-frame
A_c: Area of Horizontal Struts

Brace Deformations:

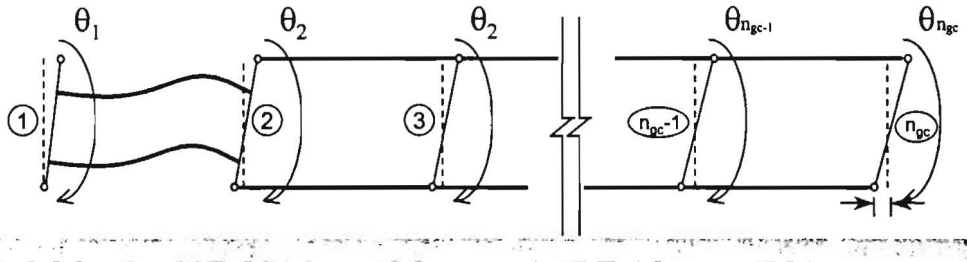

CROSS-FRAME STIFFNESS AND STRENGTH REQUIREMENTS

Moment Diagrams of the Diaphragm :

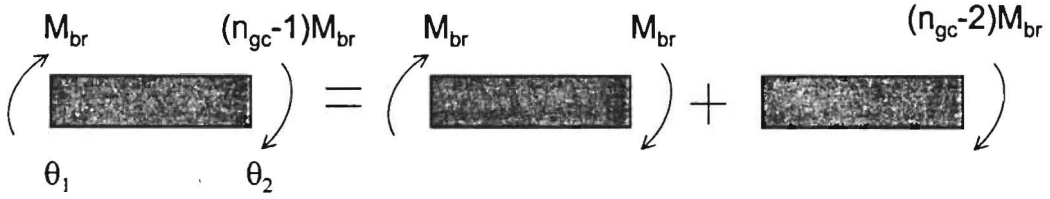

$$\theta_2 = \frac{M_{br}}{6EI_b/S} + \frac{(n_{gc}-2)M_{br}}{3EI_b/S} = \frac{(2n_{gc}-3)M_{br}S}{6EI_b}$$

$$\theta_3 = \theta_2 + \left[\frac{(n_{gc}-2)FS}{EA_c} + \frac{(n_{gc}-2)FS}{EA_c}\right] \Big/ h_b = \theta_2 + \frac{2(n_{gc}-2)FS}{EA_c} \Big/ h_b$$

Figure D.3 Equations for Stiffness and Strength Requirements for Lean-on Braces – Diaphragm (1/2)

CROSS-FRAME STIFFNESS AND STRENGTH REQUIREMENTS

Brace Stiffness: Girder n_{gc} is Critical for Stiffness

$$\theta_{n_{gc}} = \theta_2 + \frac{2FS}{EA_c h_b}\underline{\left[(n_{gc}-2)+(n_{gc}-3)+\ldots+1\right]} \qquad \text{Number of terms} = (n_{gc}-2)$$

$$= \frac{(2n_{gc}-3)M_{br}S}{6EI_b} + \frac{2FS}{EA_c h_b}\frac{\left(n_{gc}-2+1\right)}{2}\left(n_{gc}-2\right)$$

$$= \frac{(2n_{gc}-3)F_{br}h_b S}{6EI_b} + \frac{FS}{EA_c h_b}\left(n_{gc}-1\right)\left(n_{gc}-2\right)$$

$$\beta_b = \frac{M_{br}}{\theta} = \frac{Fh_b}{\theta} = \frac{1}{\frac{(2n_{gc}-3)S}{6EI_b} + \frac{(n_{gc}-1)(n_{gc}-2)S}{EA_c h_b^2}}$$

$$= \frac{E}{\frac{(2n_{gc}-3)S}{6I_b} + \frac{S}{A_c h_b^2}(n_{gc}-1)(n_{gc}-2)}$$

SUMMARY:

Brace Stiffness:

$$\beta_b = \frac{E}{\frac{(2n_{gc}-3)S}{6I_b} + \frac{S}{A_c h_b^2}(n_{gc}-1)(n_{gc}-2)}$$

Brace Strength:

$$F_h = (n_{gc}-2)F$$

$$M = (n_{gc}-1)M_{br}$$

$$\Big\rangle \; F = M_{br}/h_b$$

Figure D.3 Equations for Stiffness and Strength Requirements for Lean-on Braces – Diaphragm (2/2)

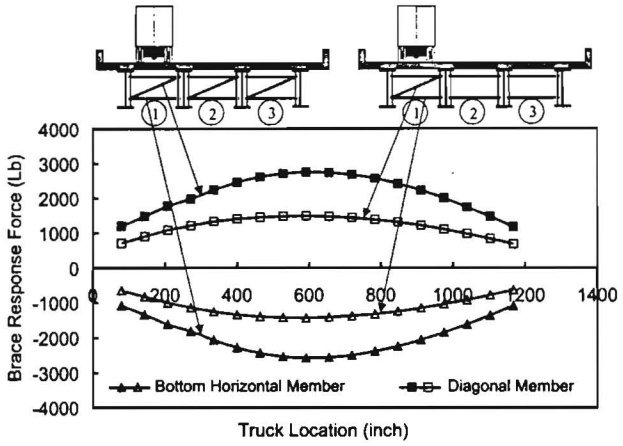

Figure D.4 (a) Brace Force Response Envelope at Brace Location #1, Edge Truck Loading- Conventional vs. Lean On Bracing

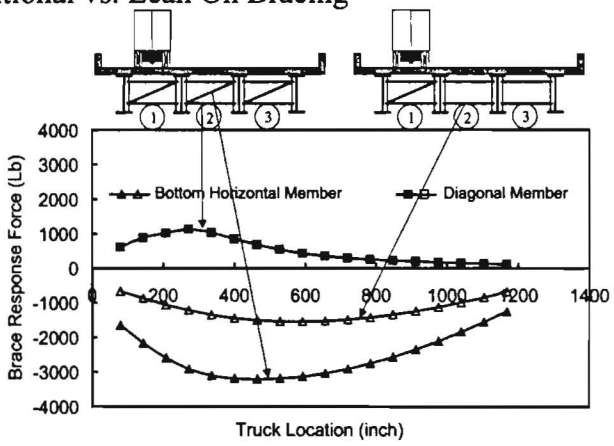

Figure D.4 (b) Brace Force Response Envelope at Brace Location #2, Edge Truck Loading- Conventional vs. Lean On Brace

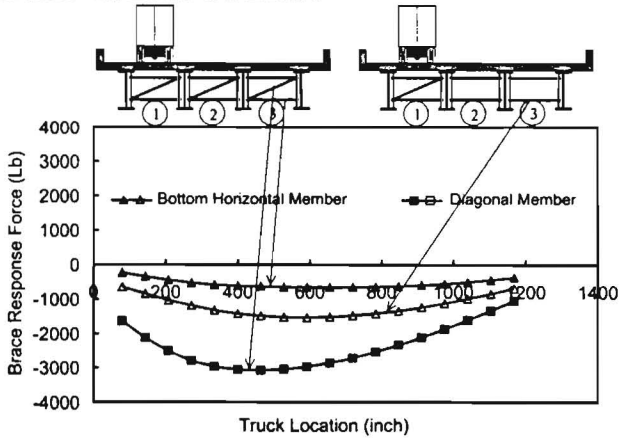

Figure D.4 (c) Brace Force Response Envelope at Brace Location #3, Edge Truck Loading- Conventional vs. Lean On Brace

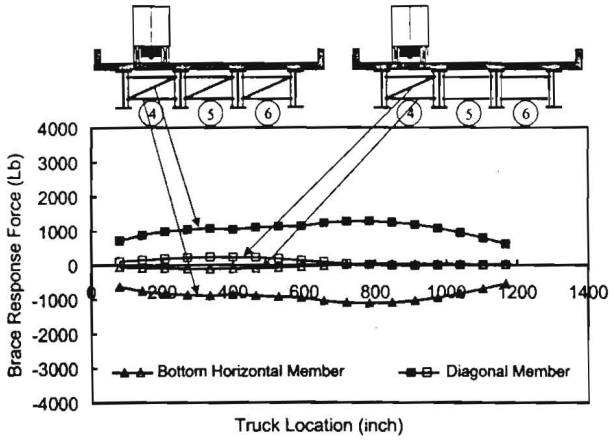

Figure D.4 (d) Brace Force Response Envelope at Brace Location #4 Edge Truck Loading-Conventional vs. Lean On Brace

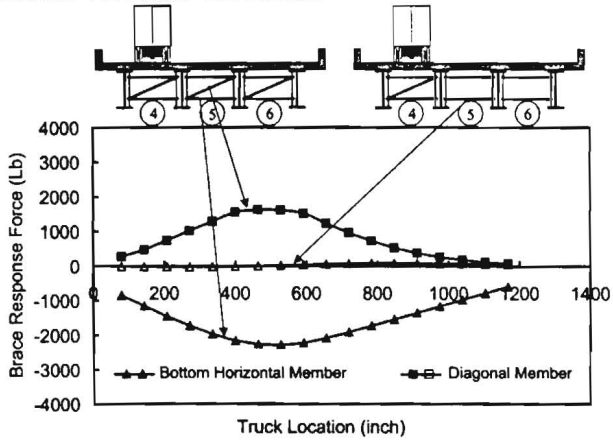

Figure D.4 (e) Brace Force Response Envelope at Brace Location #5 Edge Truck Loading-Conventional vs. Lean On Brace

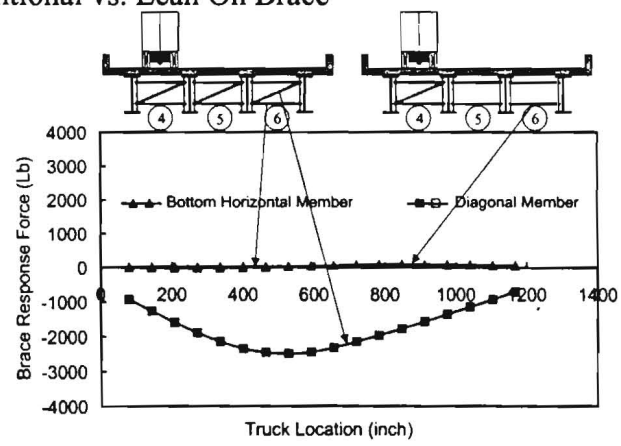

Figure D.4 (f) Brace Force Response Envelope at Brace Location #6 Edge Truck Loading-Conventional vs. Lean On Brace

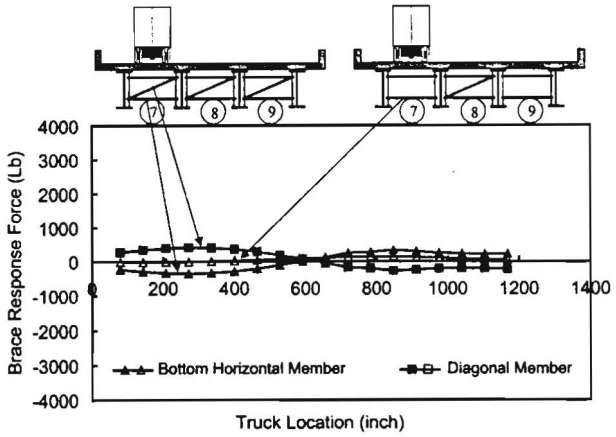

Figure D.4 (g) Brace Force Response Envelope at Brace Location #7, Edge Truck Loading-Conventional vs. Lean On Brace

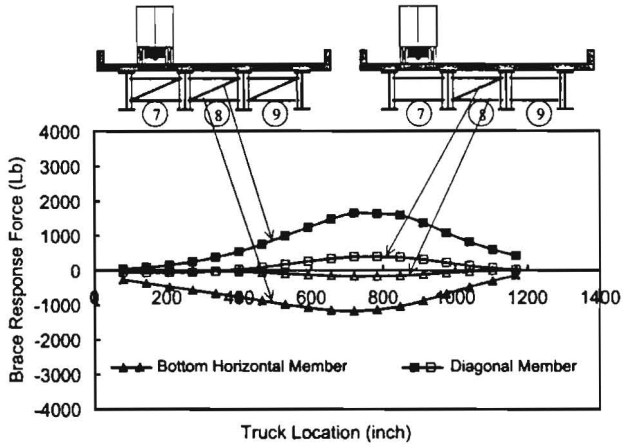

Figure D.4 (h) Brace Force Response Envelope at Brace Location #8Edge Truck Loading-Conventional vs. Lean On Brace

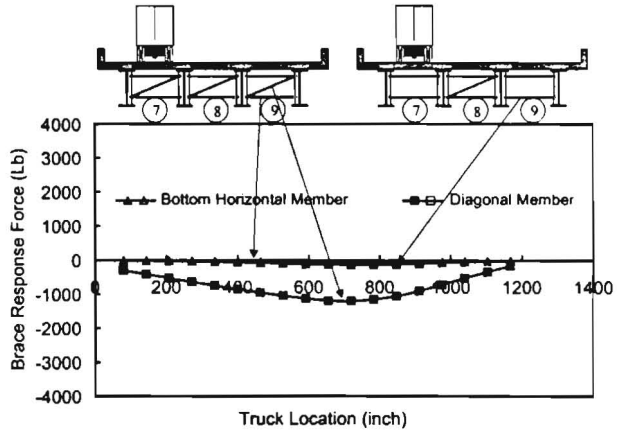

Figure D.4 (i) Brace Force Response Envelope at Brace Location #9Edge Truck Loading-Conventional vs. Lean On Brace

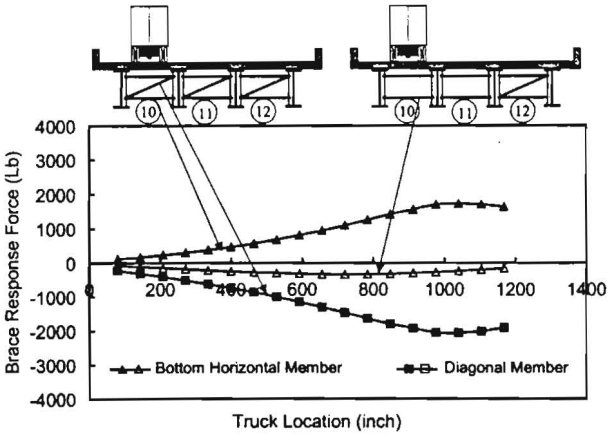

Figure D.4 (j) Brace Force Response Envelope at Brace Location #10, Edge Truck Loading-Conventional vs. Lean On Brace

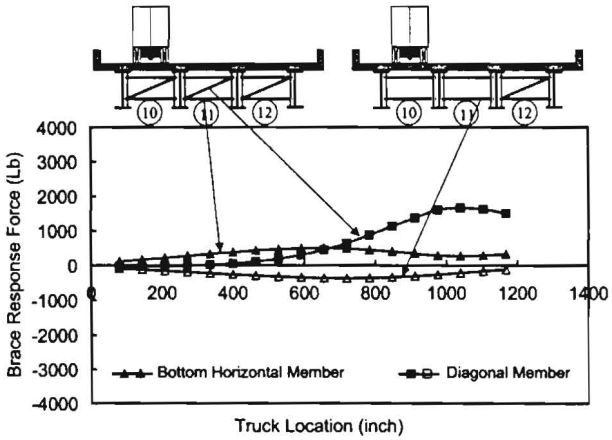

Figure D.4 (k) Brace Force Response Envelope at Brace Location #11, Edge Truck Loading-Conventional vs. Lean On Brace

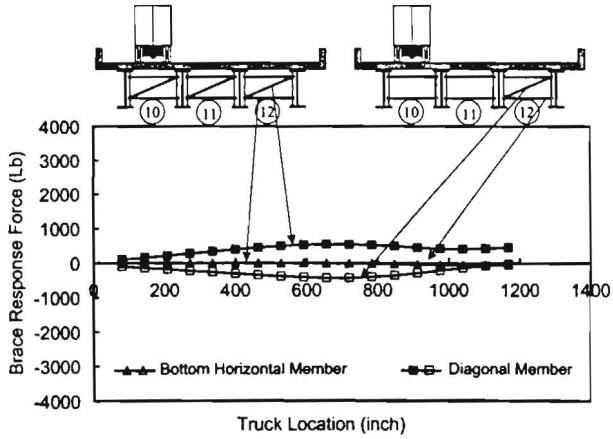

Figure D.4 (l) Brace Force Response Envelope at Brace Location #12, Edge Truck Loading-Conventional vs. Lean On Brace

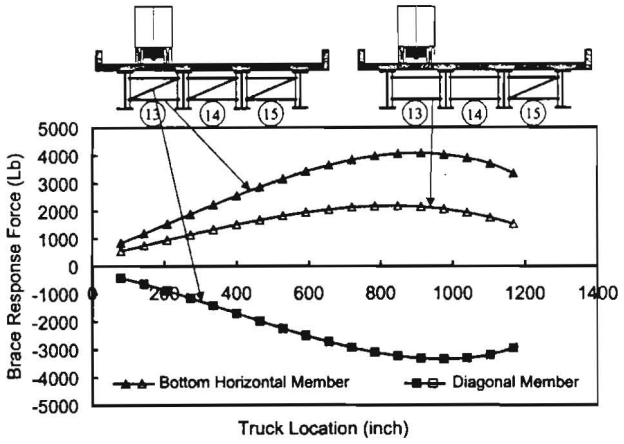

Figure D.4 (m) Brace Force Response Envelope at Brace Location #13, Edge Truck Loading- Conventional vs. Lean On Brace

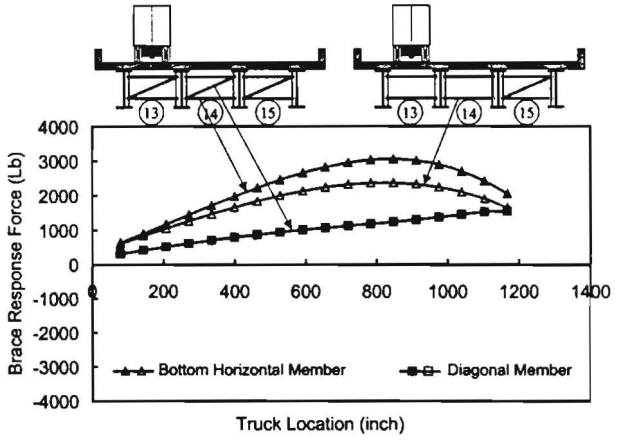

Figure D.4 (n) Brace Force Response Envelope at Brace Location #14, Edge Truck Loading - Conventional vs. Lean On Brace

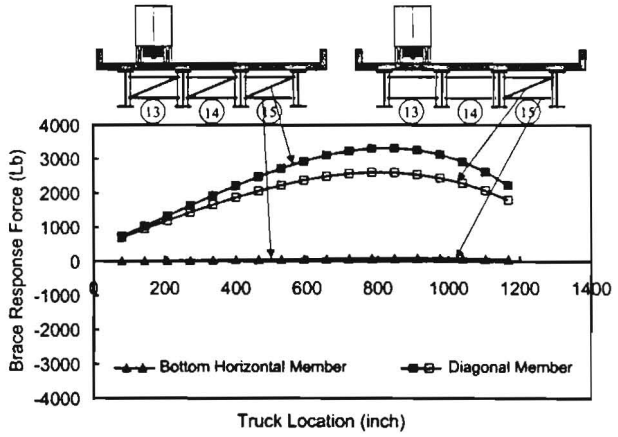

Figure D.4 (o) Brace Force Response Envelope at Brace Location #15, Edge Truck Loading- Conventional vs. Lean On Brace

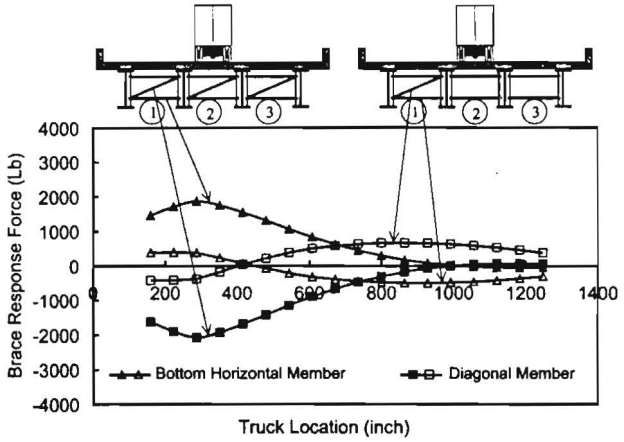

Figure D.5 (a) Brace Force Response Envelope at Brace Location #1, Center Truck Loading-Conventional vs. Lean On Brace

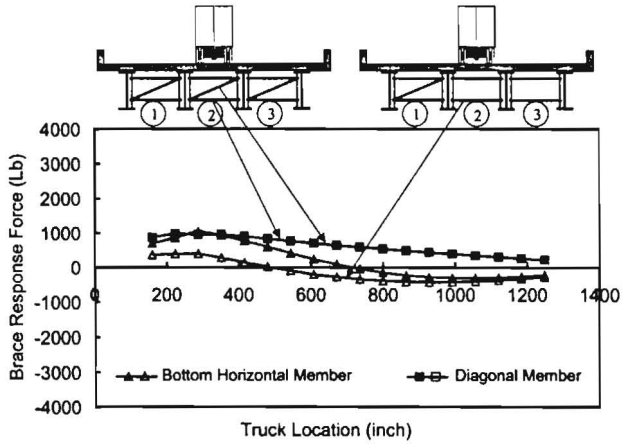

Figure D.5 (b) Brace Force Response Envelope at Brace Location #2, Center Truck Loading-Conventional vs. Lean On Brace

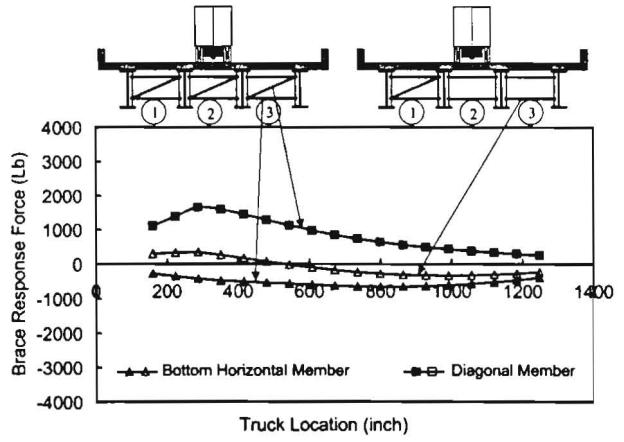

Figure D.5 (c) Brace Force Response Envelope at Brace Location #3, Center Truck Loading-Conventional vs. Lean On Brace

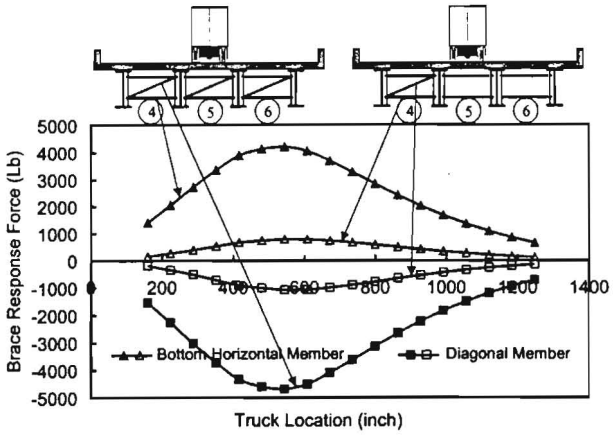

Figure D.5 (d) Brace Force Response Envelope at Brace Location #4, Center Truck Loading-Conventional vs. Lean On Brace

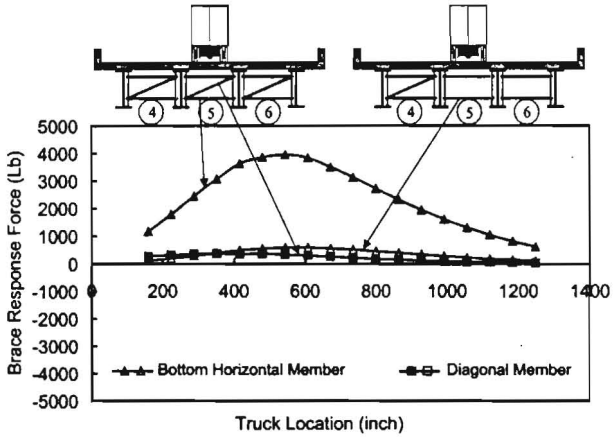

Figure D.5 (e) Brace Force Response Envelope at Brace Location #5, Center Truck Loading-Conventional vs. Lean On Brace

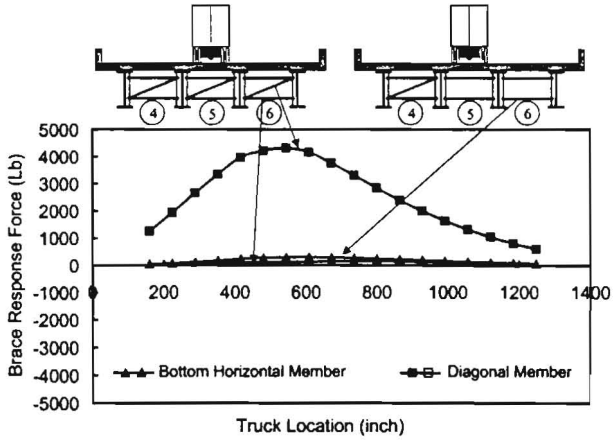

Figure D.5 (f) Brace Force Response Envelope at Brace Location #6, Center Truck Loading-Conventional vs. Lean On Brace

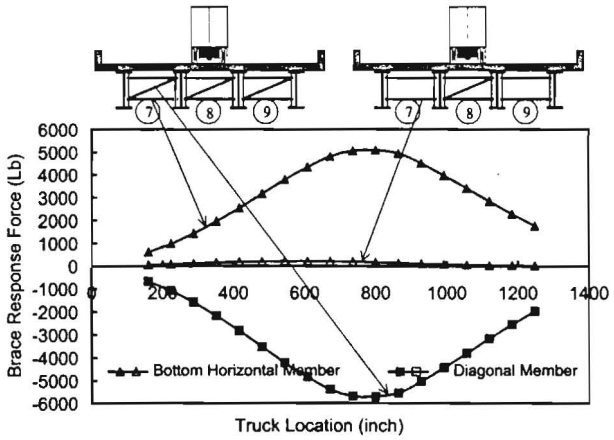

Figure D.5 (g) Brace Force Response Envelope at Brace Location #7, Center Truck Loading-Conventional vs. Lean On Brace

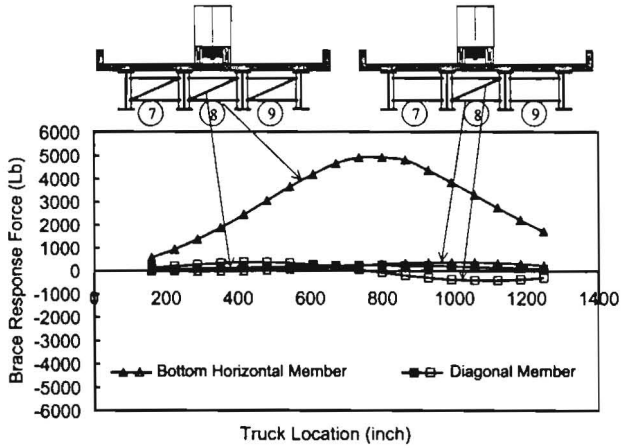

Figure D.5 (h) Brace Force Response Envelope at Brace Location #8, Center Truck Loading-Conventional vs. Lean On Brace

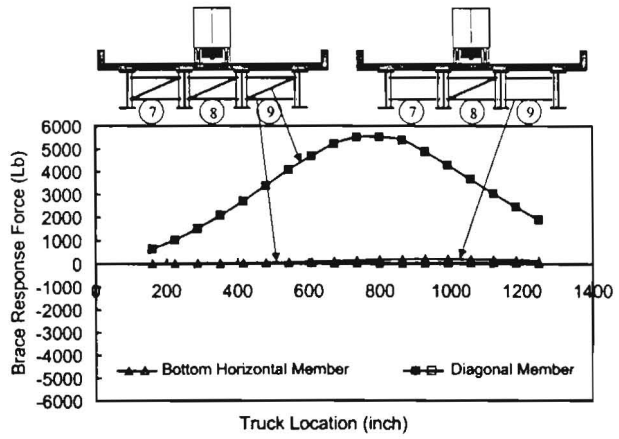

Figure D.5 (i) Brace Force Response Envelope at Brace Location #9, Center Truck Loading-Conventional vs. Lean On Brace

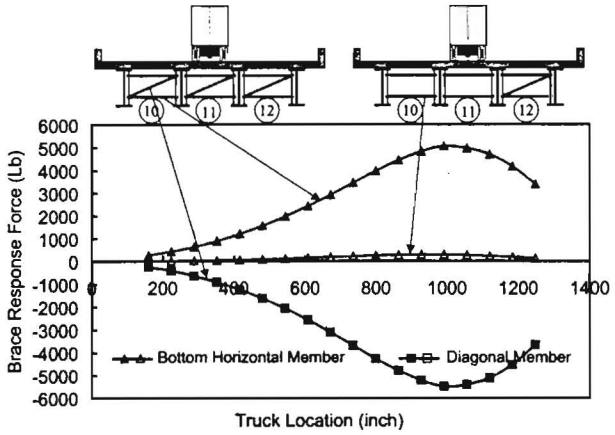

Figure D.5 (j) Brace Force Response Envelope at Brace Location #10, Center Truck Loading- Conventional vs. Lean On Brace

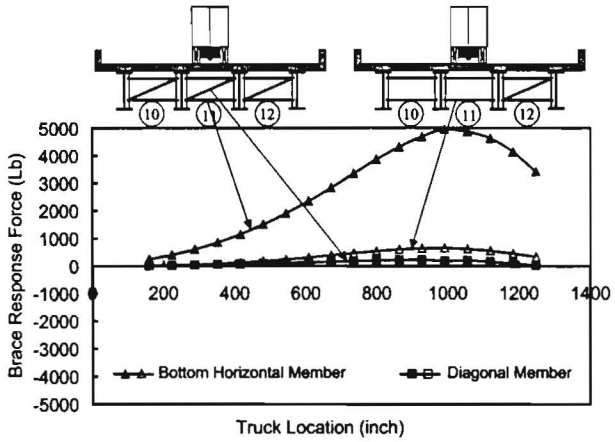

Figure D.5 (k) Brace Force Response Envelope at Brace Location #11, Center Truck Loading- Conventional vs. Lean On Brace

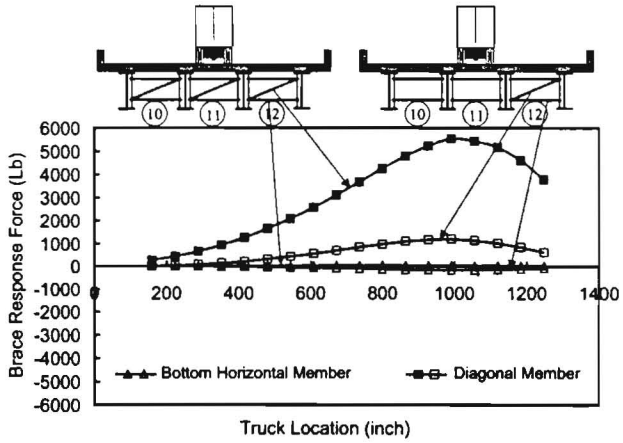

Figure D.5 (l) Brace Force Response Envelope at Brace Location #12, Center Truck Loading- Conventional vs. Lean On Brace

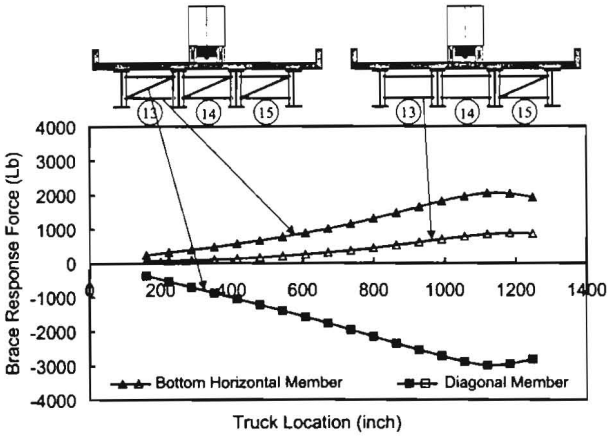

Figure D.5 (m) Brace Force Response Envelope at Brace Location #13, Center Truck Loading - Conventional vs. Lean On Brace

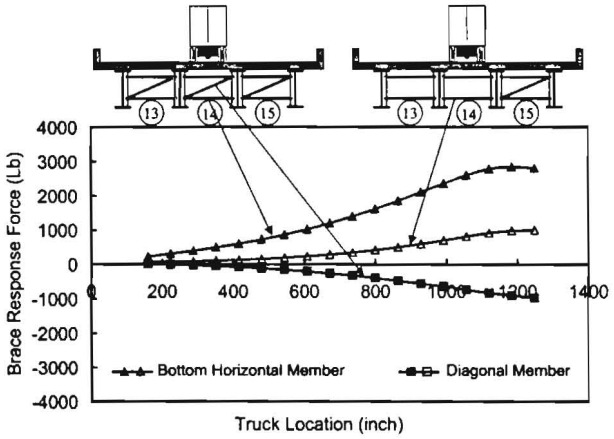

Figure D.5 (n) Brace Force Response Envelope at Brace Location #14, Center Truck Loading- Conventional vs. Lean On Brace

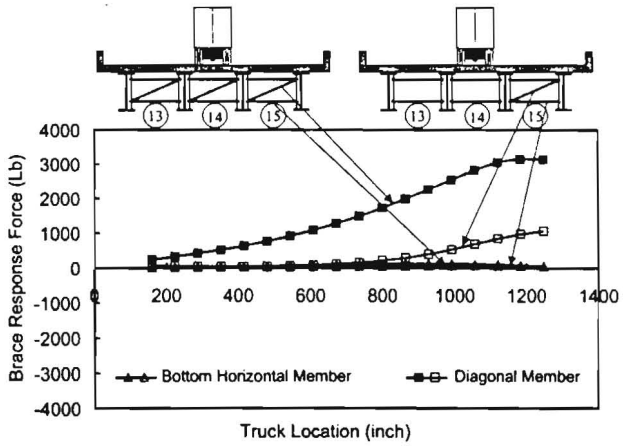

Figure D.5 (o) Brace Force Response Envelope at Brace Location #15, Center Truck Loading- Conventional vs. Lean On Brace

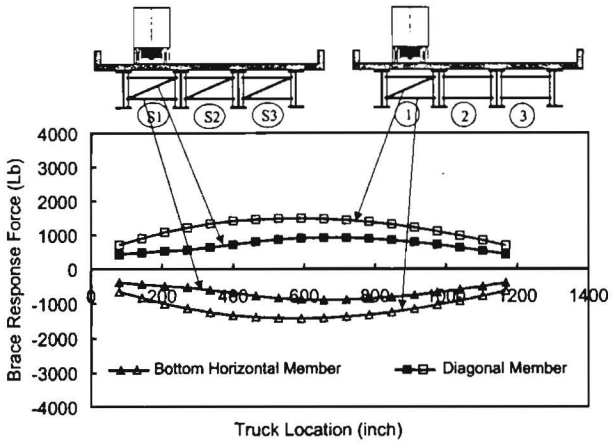

Figure D.6 (a) Brace Force Response Envelope at Brace Location #1, Edge Truck Loading-Conventional Stagger Brace vs. Lean On Brace

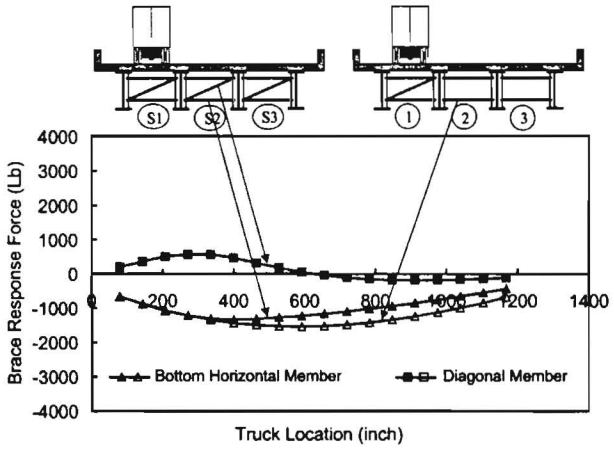

Figure D.6 (b) Brace Force Response Envelope at Brace Location #2, Edge Truck Loading-Conventional Stagger Brace vs. Lean On Brace

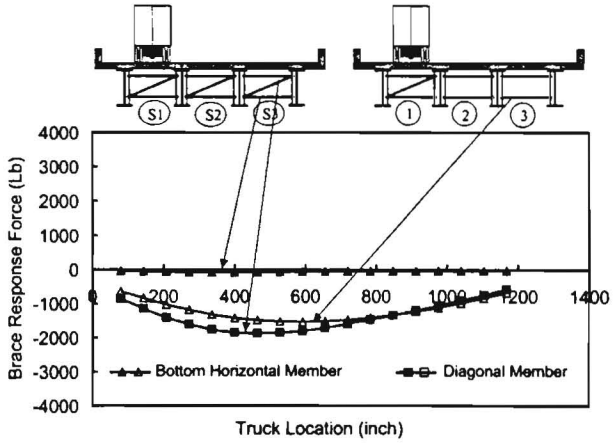

Figure D.6 (c) Brace Force Response Envelope at Brace Location #3, Edge Truck Loading-Conventional Stagger Brace vs. Lean On Brace

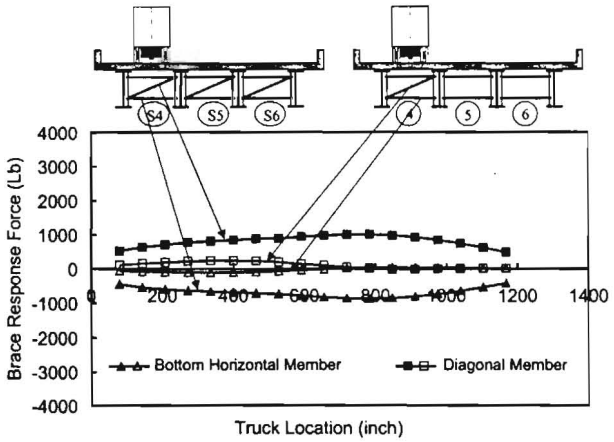

Figure D.6 (d) Brace Force Response Envelope at Brace Location #4, Edge Truck Loading-Conventional Stagger Brace vs. Lean On Brace

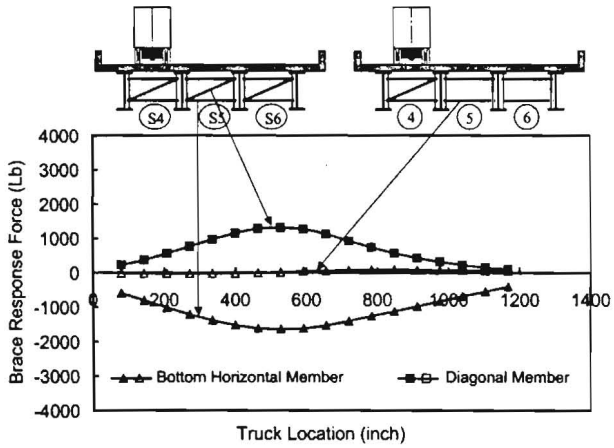

Figure D.6 (e) Brace Force Response Envelope at Brace Location #5, Edge Truck Loading-Conventional Stagger Brace vs. Lean On Brace

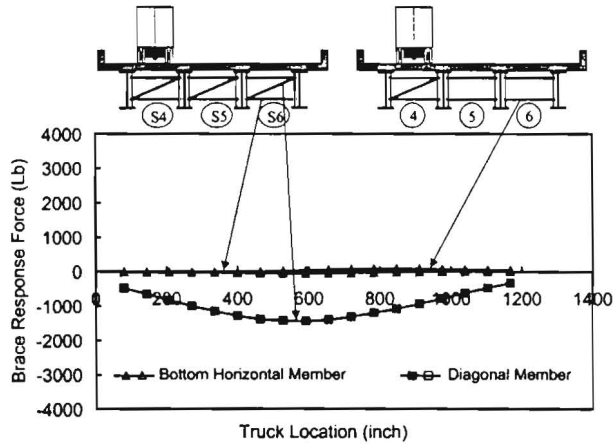

Figure D.6 (f) Brace Force Response Envelope at Brace Location #6, Edge Truck Loading-Conventional Stagger Brace vs. Lean On Brace

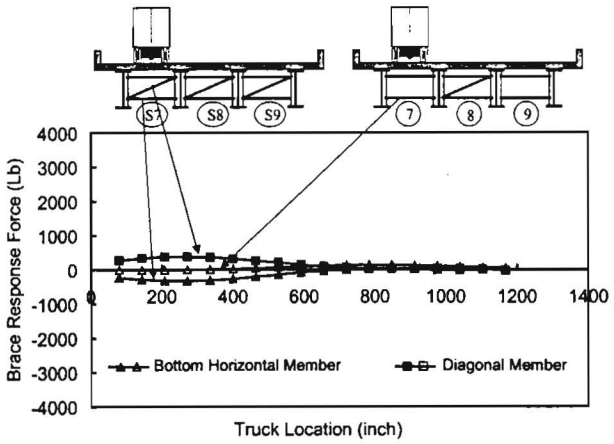

Figure D.6 (g) Brace Force Response Envelope at Brace Location #7, Edge Truck Loading-Conventional Stagger Brace vs. Lean On Brace

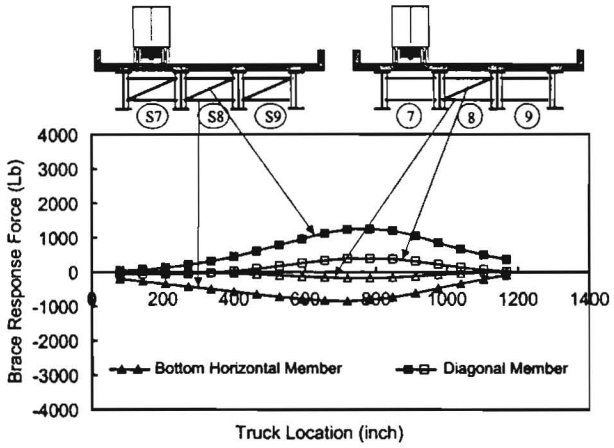

Figure D.6 (h) Brace Force Response Envelope at Brace Location #8, Edge Truck Loading-Conventional Stagger Brace vs. Lean On Brace

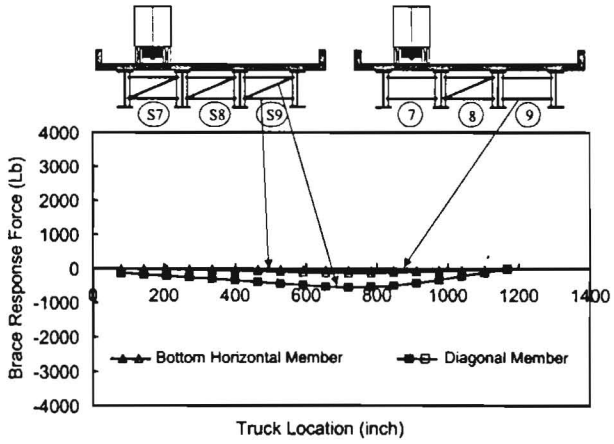

Figure D.6 (i) Brace Force Response Envelope at Brace Location #9, Edge Truck Loading-Conventional Stagger Brace vs. Lean On Brace

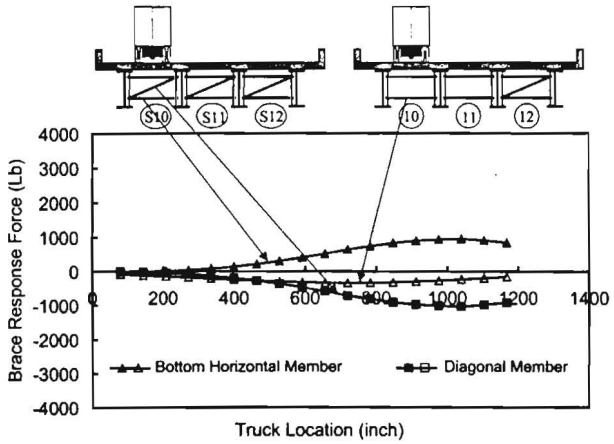

Figure D.6 (j) Brace Force Response Envelope at Brace Location #10, Edge Truck Loading-Conventional Stagger Brace vs. Lean On Brace

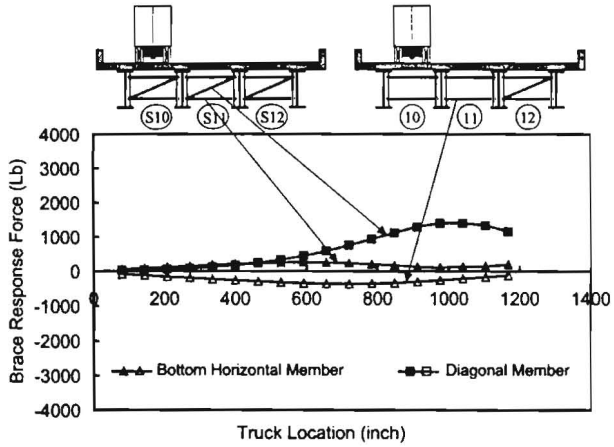

Figure D.6 (k) Brace Force Response Envelope at Brace Location #11, Edge Truck Loading-Conventional Stagger Brace vs. Lean On Brace

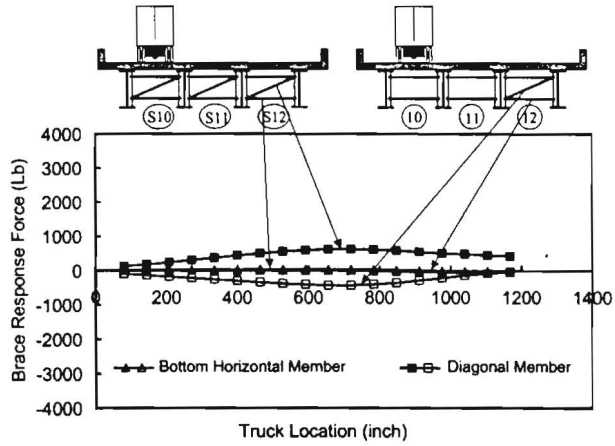

Figure D.6 (l) Brace Force Response Envelope at Brace Location #12, Edge Truck Loading-Conventional Stagger Brace vs. Lean On Brace

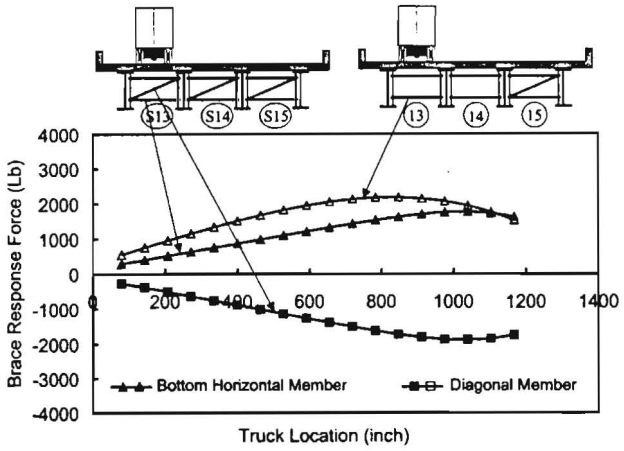

Figure D.6 (m) Brace Force Response Envelope at Brace Location #13, Edge Truck Loading-Conventional Stagger Brace vs. Lean On Brace

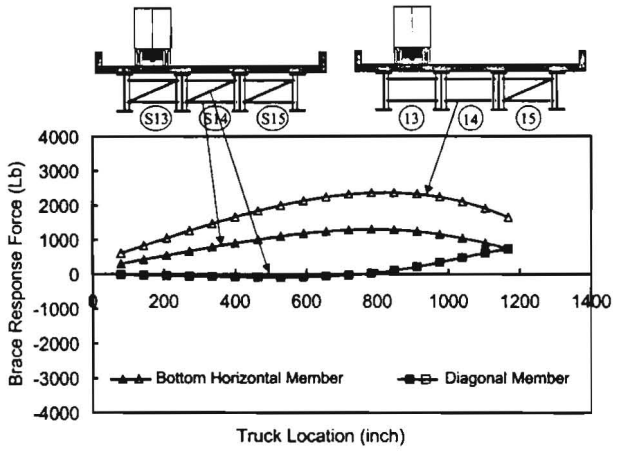

Figure D.6 (n) Brace Force Response Envelope at Brace Location #14, Edge Truck Loading-Conventional Stagger Brace vs. Lean On Brace

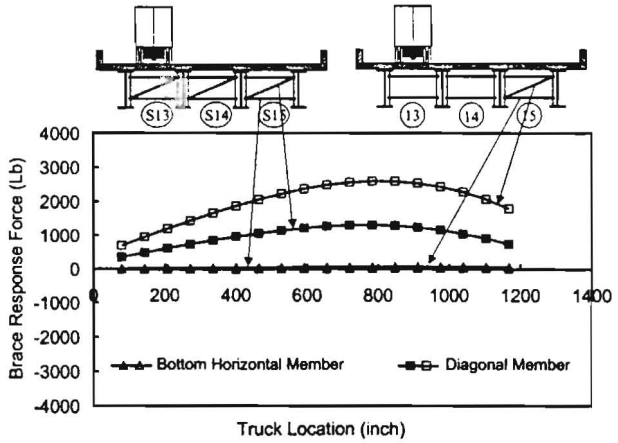

Figure D.6 (o) Brace Force Response Envelope at Brace Location #15, Edge Truck Loading-Conventional Stagger Brace vs. Lean On Brace

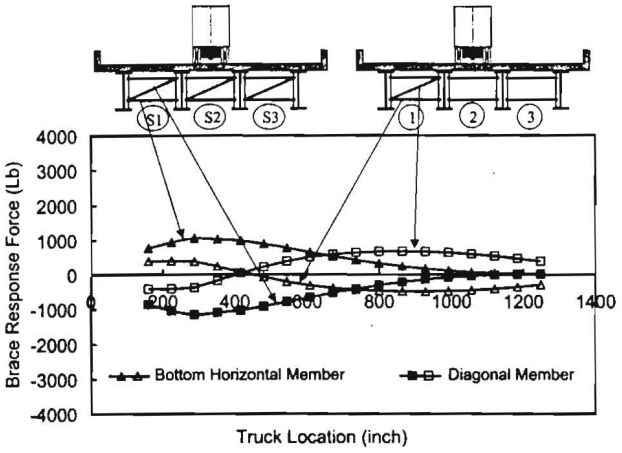

Figure D.7 (a) Brace Force Response Envelope at Brace Location #1, Center Truck Loading-Conventional Stagger Brace vs. Lean On Brace

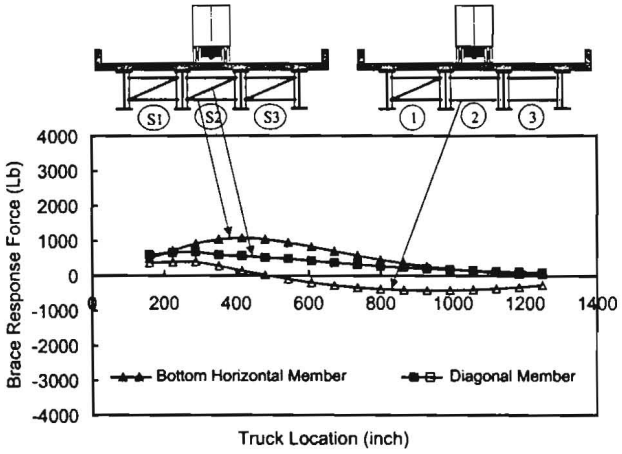

Figure D.7 (b) Brace Force Response Envelope at Brace Location #2, Center Truck Loading-Conventional Stagger Brace vs. Lean On Brace

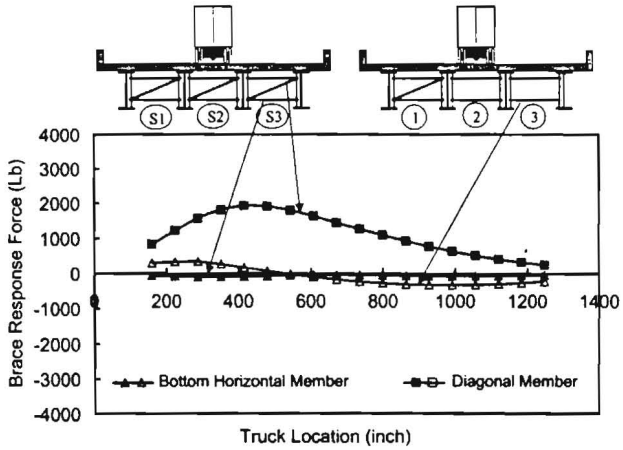

Figure D.7 (c) Brace Force Response Envelope at Brace Location #3, Center Truck Loading-Conventional Stagger Brace vs. Lean On Brace

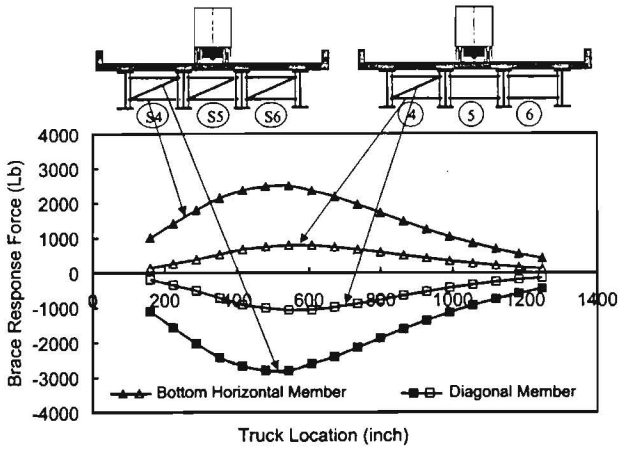

Figure D.7 (d) Brace Force Response Envelope at Brace Location #4, Center Truck Loading-Conventional Stagger Brace vs. Lean On Brace

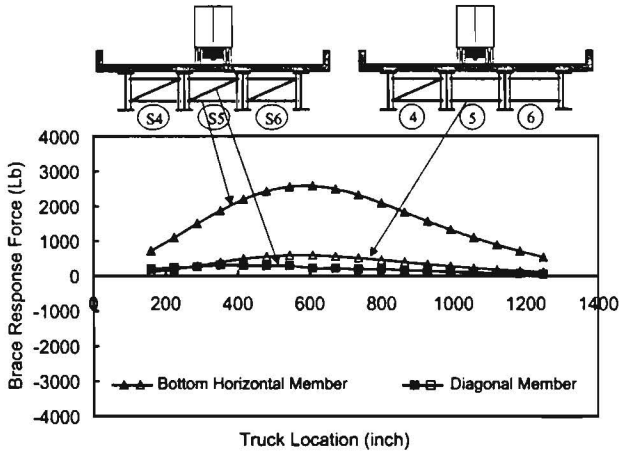

Figure D.7 (e) Brace Force Response Envelope at Brace Location #5, Center Truck Loading-Conventional Stagger Brace vs. Lean On Brace

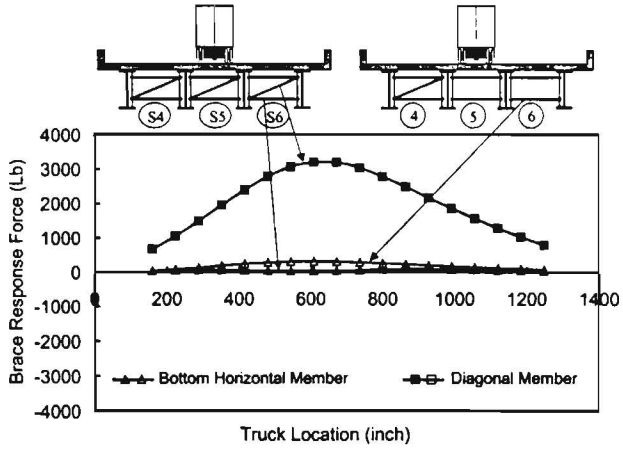

Figure D.7 (f) Brace Force Response Envelope at Brace Location #6, Center Truck Loading-Conventional Stagger Brace vs. Lean On Brace

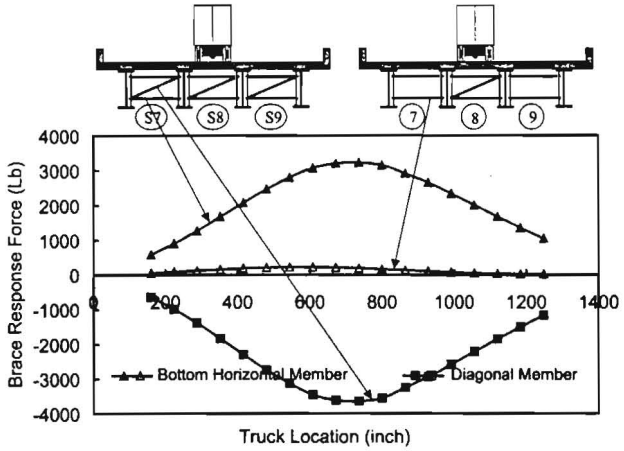

Figure D.7 (g) Brace Force Response Envelope at Brace Location #7, Center Truck Loading-Conventional Stagger Brace vs. Lean On Brace

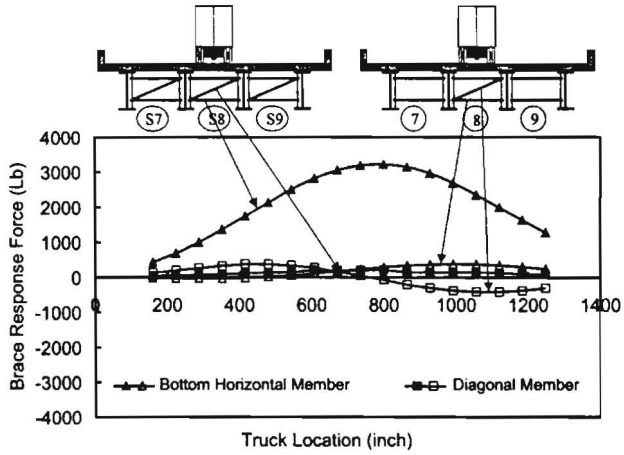

Figure D.7 (h) Brace Force Response Envelope at Brace Location #8, Center Truck Loading-Conventional Stagger Brace vs. Lean On Brace

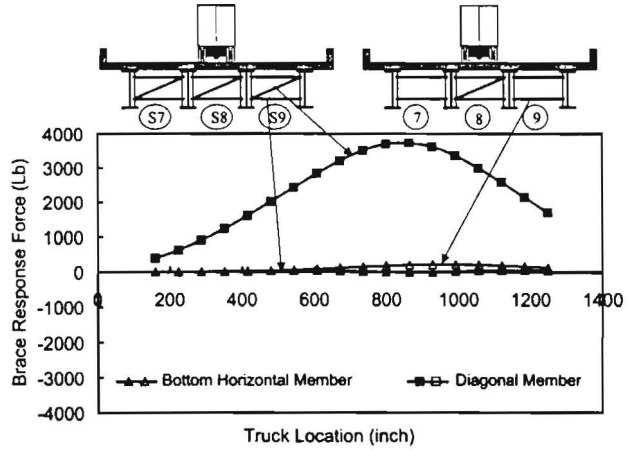

Figure D.7 (i) Brace Force Response Envelope at Brace Location #9, Center Truck Loading-Conventional Stagger Brace vs. Lean On Brace

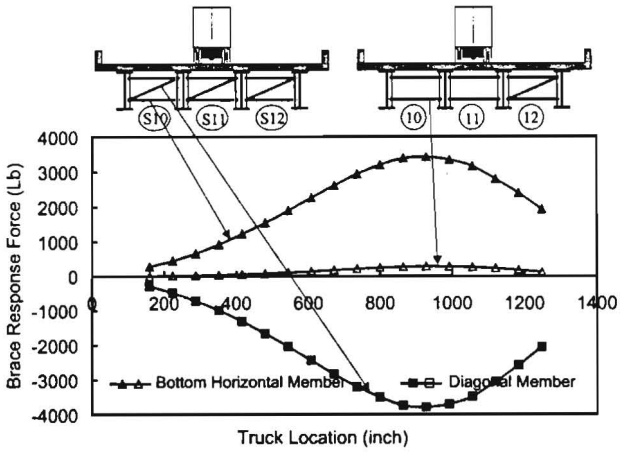

Figure D.7 (j) Brace Force Response Envelope at Brace Location #10, Center Truck Loading- Conventional Stagger Brace vs. Lean On Brace

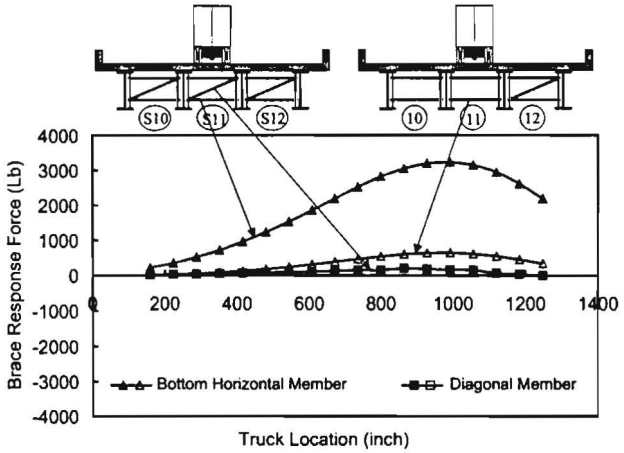

Figure D.7 (k) Brace Force Response Envelope at Brace Location #11, Center Truck Loading- Conventional Stagger Brace vs. Lean On Brace

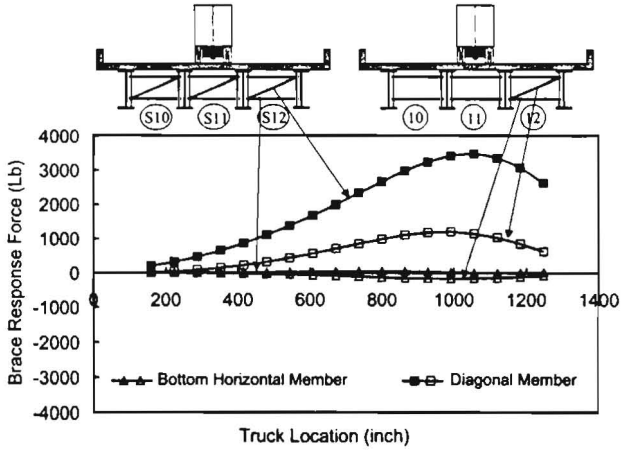

Figure D.7 (l) Brace Force Response Envelope at Brace Location #12, Center Truck Loading- Conventional Stagger Brace vs. Lean On Brace

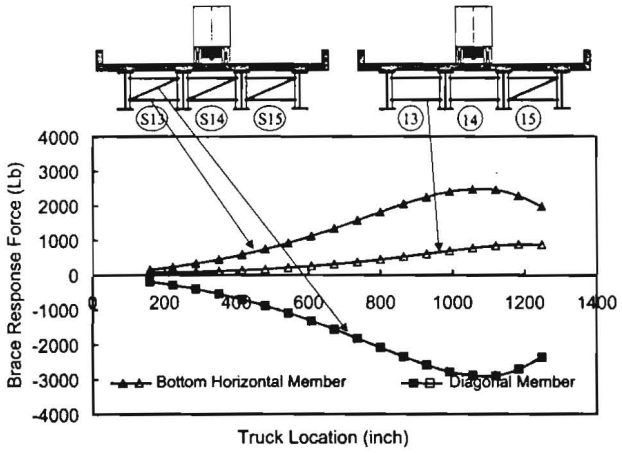

Figure D.7 (m) Brace Force Response Envelope at Brace Location #13, Center Truck Loading - Conventional Stagger Brace vs. Lean On Brace

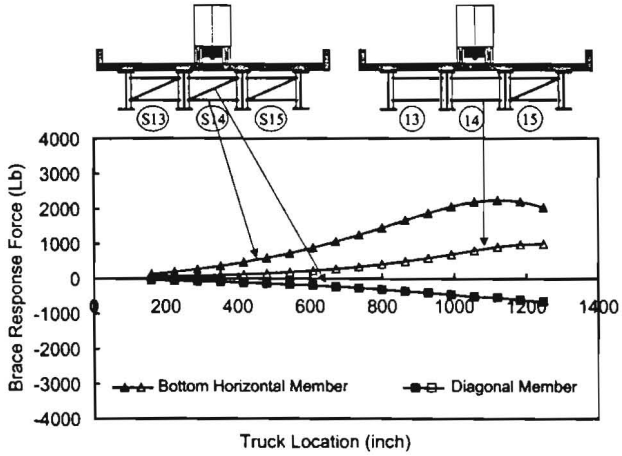

Figure D.7 (n) Brace Force Response Envelope at Brace Location #14, Center Truck Loading- Conventional Stagger Brace vs. Lean On Brace

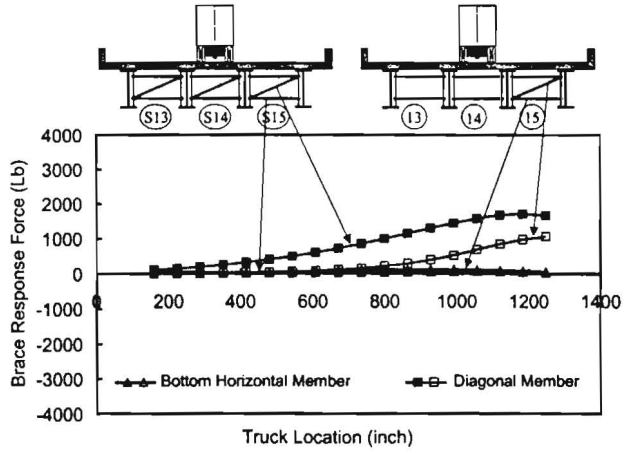

Figure D.7 (o) Brace Force Response Envelope at Brace Location #15, Center Truck Loading- Conventional Stagger Brace vs. Lean On Brace

References

[AASHTO 1992] American Association of State Highway and Transportation Officials, Standard Specifications for Highway Bridges, Fifteenth Edition, Washington, D. C., 1992.

[AASHTO 1996] American Association of State Highway and Transportation Officials, Standard Specifications for Highway Bridges, Load & Resistance Factor Design, First Edition, Washington, D. C., 1996.

[AISC 2001] American Institute of Steel Construction, Manual of Steel Construction, Load & Resistance Factor Design, 2001.

[AISI 1994] American Iron and Steel Institute, AISI Short Span Steel Bridges, 1994.

[Anderson and Trahair 1972] Anderson, J. M., and Trahair, N. S., "Stability of Monosymmetric Beams and Cantilevers," Journal os the Structural Division, ASCE, Vol. 98, No. ST1, Proc. Paper 8648, Jan., 1972, pp. 269-286.

[ANSYS 1996] "Finite Element Program Users Manual, Version 5.0", ANSYS, Inc.

[BASP 1987] Choo, K. M., "Buckling Program BASP for Use on a Microcomputer", M. S. Thesis, Department of Civil Engineering, University of Texas at Austin.

[Bishara and Elmir 1990] Bishara, A. G., and Elmir, W. E., "Interaction between Cross Frames and Girders", Journal of Structural Engineering, ASCE, Vol. 116, No. ST5, May 1990, pp. 1319-1333.

[Brockenbrough 1986] Brockenbrough, R. L., "Distribution Factors for Curved I-Girder Bridges", Journal Structural Engineering, ASCE, Vol.112, No.10, pp. 2200-2215.

[Fan 1999] Fan, Z. F., "Field and Computational Studies of Steel Trapezoidal Box Girder Bridges", Ph. D. Dissertation, Civil and Environmental Engineering Department, University of Houston.

[Flint 1951] Flint, A. R., "The Influence of Restraint on the Stability of Beams," The Structural Engineer, Vol.29, September, 1951, pp.235-246.

[Helwig et al. 1993] Helwig, T. A., Frank, K. H., and Yura, J. A., "Bracing Forces in Diaphragms and Cross Frames", Structural Stability Research Council Conference, April 6-7, 1993, Milwaukee, Wisconsin.

[Helwig 1994] Helwig, T. A., Lateral Bracing of Bridge Girders by metal Deck Forms" Ph. D. Dissertation, Department of Civil Engineering, University of Texas at Austin.

[Helwig et al. 1997] Helwig, T. A., Frank, K. H., and Yura, J. A., "Lateral-torsional Buckling of Singly Symmetric I-beams", Journal of Structural Engineering, ASCE, September, 1997, pp. 1172-1179.

[Keating and Alan 1992] Keating, P. B. and Alan, R. C., Evaluation and Repair of Fatigue Damage to Midland County Bridges (Draft), TX-92/1331-1.

[Kitipornchai and Trahair 1980] Kitipornchai, S., and Trahair, N.S., " Buckling Properties of Monosymmetric I-beams", Journal of the Structural Division, ASCE, No. ST5, May 1980, pp. 941-958.

[Mutton and Trahair 1973] Mutton, B. R., and Trahair, N. S., " Stiffness requirements for Lateral Bracing", Journal of the Structural Division, ASCE, Vol. 99, No. ST10, October 1973, pp. 2167-2181.

[Schmidt 1965] Schmidt, L. C., "Restraints Against Elastic Lateral Buckling," Journal of the engineering Mechanics Division, ASCE, Vol. 91, No. EM6, Proc. Paper 4561, December, 1965, pp. 1-10.

[Shi 1997] Shi, J. H., " Brace Stiffness Requirements of Skewed Bridge Girders", M. S. Thesis, Civil and Environmental Engineering Department, University of Houston.

[SSRC 1988] Structural Stability Research Council, Fourth Edition, John Wiley &Sons, Inc., New York, 1988.

[Tabsh and Sahajwani 1997] Tabsh, S. W., and Sahajwani, K., "Approximate Analysis of Irregular Slab-on-Girder Bridges", Journal of Bridge Engineering, ASCE, Vol.2, No. 1, pp. 11-17.

[Taylor and Ojalvo 1966] Taylor, A. C. Jr., and Ojalvo, M., "Torsional restraint of Lateral Buckling", Journal of the Structural Division, ASCE, Vol. 92, No. ST 2, April 1966, pp. 115-129.

[Timoshenko 1961] Timoshenko, S., and Gere, J., "Theory of Elastic Stability", 2nd edition, McGraw-Hill Book Company, New York, 1961.

[Trahair and Nethercot 1982] Trahair N. S., and Nethercot, D. A., "Bracing Requirements in Thin-Walled Structures", Rhodes and Walker-Ed., Elsevier Applied Science Publishers, 1982.

[Tarhini and Frederick 1992] Tarhini, K. M., and Frederich G. R., "Wheel Load Distribution in I-Girder Highway Bridges", Journal Structural Engineering, ASCE, Vol. 118, No. 5, pp. 1285-1294.

[Winter 1958] Winter, G., "Lateral Bracing of Columns and Beams," Journal of the Structural Division, ASCE, Vol. 84, No. ST2, Proc. Paper 1561, March 1958, pp. 1-22.

[Yura 1992] Yura, J. A., and Phillips, B. A., "Bracing Requirements for Elastic Steel Beams", Report No. 1239-1, Center for Transportation Research, The University of Texas at Austin, May 1992.

[Yura 1992] Yura, J. A., and Phillips, B. A., Raju, S., and Webb, S., "Bracing of Steel Beams in Bridges", Report No. 1239-4F, Center for Transportation Research, The University of Texas at Austin, October 1992.

[Yura 1995] Yura, Joseph A., "Bracing for stability – state of the art." Proc., 13th ASCE Structure Congr., Masoud Sanayei, ed., New York, N. Y., 1995, pp. 88-103.